

INGENIEURFAKULTÄT BAU GEO UMWELT

Lehrstuhl für Verkehrswegebau

The influence of track quality to the performance of vehicle-track interaction

Duo Liu

Vollständiger Abdruck der von der Ingenieur fakultät Bau Geo Umwelt der Technischen Universität München zur Erlangung des akademischen Grades eines

Doktor-Ingenieurs

genehmigten Dissertation.

Vorsitzender: Univ.-Prof. Dr.-Ing. Gebhard Wulfhorst

Prüfer der Dissertation:

1. Univ.-Prof. Dr.-Ing. Stephan Freudenstein
2. Univ.-Prof. Dr.-Ing. Ullrich Martin, Universität Stuttgart
3. Univ.-Prof. Dipl.-Ing. Dr. techn. Peter Veit,
Technische Universität Graz / Österreich

Die Dissertation wurde am 07.04.2015 bei der Technischen Universität München eingereicht und durch die Ingenieur fakultät Bau Geo Umwelt am 12.10.2015 angenommen.

Table of Contents

| | |
|---|-----------|
| Terms and definitions | V |
| Abstract | VI |
| 1. INTRODUCTION | 1 |
| 1.1. Background of the research..... | 1 |
| 1.2. Scope and objectives..... | 2 |
| 2. STATE OF TECHNOLOGY | 4 |
| 2.1. Track geometry (Non-recoverable track settlement) | 4 |
| 2.1.1. Track recording wagon (TRW) | 4 |
| 2.1.2. Linear-Time-Invariant (LTI) analysis ^[06] | 5 |
| 2.1.3. Track irregularity and Power-Spectral-Density function (PSD) ^[09] | 6 |
| 2.2. Track stiffness (recoverable track deflection under loading) | 7 |
| 2.2.1. Load distribution and elastic deflection line (static)..... | 7 |
| 2.2.2. Characteristics of the stiffness and damping behavior along the track | 9 |
| 2.3. Modeling approach for analyzing railway track dynamics..... | 10 |
| 2.3.1. Analytic models and calculation of wheel dynamic load | 11 |
| 2.3.2. Numerical models..... | 12 |
| 2.3.3. Finite-Element-Method (FEM) | 13 |
| 2.3.4. Multi-Body-Simulation (MBS)..... | 14 |
| 2.3.5. Comparisons and co-simulation..... | 15 |
| 3. PILOT SECTIONS AND DESIGN OF FIELD MEASUREMENT | 18 |
| 3.1. Introduction..... | 18 |
| 3.2. Selection of pilot sections..... | 18 |
| 3.3. Test program | 19 |
| 3.3.1. Determination of track geometry (plastic track deformation, unloaded) 20 | |
| 3.3.2. Measurement of elastic rail deflection (quasi-static)..... | 21 |
| 3.3.3. Installation of strain gauges | 23 |

Table of contents

| | | |
|-----------|---|-----------|
| 3.3.4. | Recording the vertical track response under running trains | 24 |
| 3.3.5. | Measurement of vertical acceleration level | 25 |
| 3.4. | Long-term effects..... | 27 |
| 3.5. | Vehicle information..... | 27 |
| 3.5.1. | Vehicle information in sections 1 and 2 (German railway high speed line) 28 | |
| 3.5.2. | Vehicle information in sections 3 and 4 (Austrian railway high speed line) 30 | |
| 4. | FIELD MEASUREMENT AND DATA ANALYSIS | 32 |
| 4.1. | Track geometry and irregularity (plastic settlement)..... | 32 |
| 4.1.1. | Calculation of absolute track geometry..... | 32 |
| 4.1.2. | Statistical analysis of the measured data | 33 |
| 4.1.3. | Calculation of track quality parameters using Power-Spectral-Density function (PSD)..... | 34 |
| 4.2. | Rail deflection under static loading (elastic deflection)..... | 39 |
| 4.3. | Dynamic rail bending behavior | 41 |
| 4.3.1. | Automatic peak finding of the measured dynamic strain | 42 |
| 4.3.2. | Calibration runs with quasi-static loading | 43 |
| 4.3.3. | Rail bending behavior under operational train runs | 45 |
| 4.4. | Test of track vibration level | 51 |
| 4.4.1. | Track vibration level under impact load | 52 |
| 4.4.2. | Track vibration level under operational trains | 53 |
| 4.5. | Data provision for the numerical simulations | 55 |
| 5. | THE NUMERICAL MODELING | 57 |
| 5.1. | Introduction | 57 |
| 5.2. | Model 1 (FEM) – Calibration of the elastic track model based on field side Benkelman measurement..... | 59 |
| 5.2.1. | Introduction and modeling approach | 59 |
| 5.2.2. | Model setup and boundary condition | 60 |
| 5.2.3. | The iterative process..... | 62 |

| | | |
|-----------|---|-----------|
| 5.2.4. | Results and conclusions..... | 66 |
| 5.2.5. | Automation of the iteration methods (Co-Simulation with ANSYS and MATLAB) 68 | |
| 5.3. | Model 2 (MBS) – Dynamic simulation of the vehicle track interaction with pre-defined track excitations | 70 |
| 5.3.1. | Background and introduction | 70 |
| 5.3.2. | Modeling of the vehicle | 70 |
| 5.3.3. | Inclusion of measured track excitation | 72 |
| 5.3.4. | Modeling results..... | 73 |
| 5.4. | Model 3 (Co-simulation with FEM and MBS) – Calibration of the quasi-static wheel rail load under modal represented elastic track from FEM | 75 |
| 5.4.1. | Background and introduction | 75 |
| 5.4.2. | Model condensation and modal analysis..... | 76 |
| 5.4.3. | Adjustment of the vehicle model with contact markers and model calculation 79 | |
| 5.4.4. | Simulation results | 80 |
| 5.5. | Model 4 (Co-simulation with FEM and MBS) – Calculation of the dynamic wheel load under elastic track with irregularities ($V = 160$ km/h)..... | 81 |
| 5.5.1. | Background and introduction | 81 |
| 5.5.2. | Simulation results | 82 |
| 5.6. | Conclusion and outcome | 84 |
| 6. | FEEDBACK BETWEEN VEHICLE AND TRACK UNDER TRACK SIDED EXCITATIONS | 86 |
| 6.1. | The limitation of the existing method on evaluation of the track quality and preliminary studies | 86 |
| 6.2. | The improvement of track quality evaluation method | 88 |
| 6.3. | Variation of the included influence parameters..... | 89 |
| 6.4. | Distribution of dynamic wheel load according to standard track quality factors ($Y = 6$) | 91 |
| 6.5. | Simulation results under purely track geometry variations ($Z = 0$) | 93 |
| 6.6. | Simulation results under purely track stiffness variations ($Y = 0$) | 94 |

Table of contents

6.7. The “hybrid” simulations 95

6.8. ESD analysis and possibilities of improving existing track measures
with track inspection car in high speed lines 99

7. SUMMARY AND CONCLUSIONS 104

7.1. Summary of the workflow 104

7.2. Conclusions 108

SOURCE OF REFERENCE 111

List of Figures 115

List of Tables 117

Appendices 119

Annexes and user instructions 163

Terms and definitions

Track stiffness – Rigidity of track; track resistance against deformation in response to traffic loading (here: vertical direction).

Track damping – Viscosity of track, dependent on the loading speed.

Track irregularity – Track geometrical imperfections (variation of track geometry).

Track recording wagon (TRW) – A pushing track measurement wagon operated under walking speed by human. Sample equipment includes the type CLS from the company Vogel&Ploetscher.

Track inspection car (TIC) – Powered vehicle for continuous acquisition of the track geometry under loaded track with different operational speed. Examples of such vehicles include the OMWE (OberbauMessWagenEinheit) for Germany.

(Fast) Fourier Transformation (FT or FFT) – Frequency representation of a continuous or discrete signal in time or distance domain (the inverse transformation from frequency domain back to time or distance domain is called **iFT or iFFT**).

Power Spectral Density (PSD) – Distribution of the power of a signal by a frequency per unit frequency.

Energy Spectral Density (ESD) – Distribution of the energy of a signal by a frequency per unit frequency.

Vertical spread – Maximum difference of elevation of track geometry over the total evaluated track section in vertical direction with reference to track alignment.

Abstract

The term “track quality” defines the conformance quality of the track, or degree to which the track is built or maintained correctly. Important parameters specifying the general quality level of the track include the track geometry, track stiffness and damping, which can be evaluated by dynamic vehicle-track interaction along real tracks. Running railway vehicles excite the track (with certain track quality level) by exerting repeated dynamic wheel loads on track which will consequently lead to a decrease of track quality (track deterioration). The research presented in this dissertation has practically and numerically analyzed the influence of track quality parameters including track geometry, track stiffness and damping to the performance of vehicle-track interaction by online data from field measurement at various pilot sections and the from measurement data verified co-simulation models of Finite-Element-Method (FEM) and Multi-Body-Simulation (MBS).

Field measurements at preselected pilot sections including ballasted and ballastless tracks were performed under operational trains with various speed levels. Power Spectral Density (PSD) analysis was applied for the evaluation and categorization of the measured 3D track geometry. Classic Benkelman beam method was included for gathering the track stiffness of individual rail seat. Dynamic measurements with strain gauges and accelerometers along the track oriented themselves for an illustration of the time dependent dynamic wheel load along the pilot section (track damping) and their impacts on low frequency track vibration levels in frequency domain.

Varies numerical simulation models including FEM and MBS are constructed for a systematic co-simulation including both vehicle and track. A real time illustration of the vehicle and track interaction is realized for the best view of the counteractive effect from track side parameters to the vehicle, as well as the other way back.

An innovative track quality evaluation method is introduced with the help of Energy Spectral Density (ESD) distribution of the simulated dynamic wheel load. Effects of track geometry, track stiffness and damping to the performance of vehicle track interaction can be now separately analyzed and evaluated. Determination of the dynamic loading factors for modern locomotives running on ballastless track can lead to reduced dynamic factors applied for ballastless track design.

1. INTRODUCTION

1.1. Background of the research

Train runs excite the track through the wheel - rail contact mechanisms. Under certain conditions of track, by uneven track settlement or change of stiffness, the load coming from the train could be significantly higher than the static value. Also, the vehicle itself contributes to dynamic loads e.g. by wheel flats (not focus of this research). If the static load of a wheel is F_0 , then the actual force of this wheel acting on the track (F_{dyn}) is calculated as follows:

$$F_{dyn} = F_0 + F_{exc}$$

where F_{dyn} – dynamic load

F_0 – static load

F_{exc} – excitation load

The excitation load F_{exc} is a form of time function, which makes the F_{dyn} to vary in the time domain. Moreover, from the track side analysis, the excitation load F_{exc} depends mostly on the stiffness and the geometrical excitation (track irregularity).

Normally, the most important factors determining the capacity of tracks to handle excitation loading is track stiffness and damping factors. For optimizing the track structural design, solutions were developed, such as implementation of high elastic rail fastening systems, etc.

There is also interaction between the track performance in terms of stiffness and the track quality in terms of geometry. The appearance of track irregularity along the new track shows stochastic distributions, which are highly dependent on the initial condition and the traffic loading. However, when certain track irregularities are spotted, the

deterioration of the track quality (conventional, ballasted tracks) according to the traffic loads is related to the overall track stiffness, which is one of the most determinant factors from the track side on the level of the excitation load. It is intuitively that higher track deterioration rate should appear in the location where higher vehicle excitation load is activated.

In order to get a further view on the quasi-static and the dynamic behavior of the system, numerical models would be necessary for the simulation of the modification of the system behavior after years of operation. These numerical procedures focus on the quasi-static and dynamic performance of the track superstructure, as well as the track foundation. As the vehicle track interaction is a key element which cannot be ignored, a complicated train-track interaction model should be generated. Possible numerical simulation models here include the Finite-Element-Method (FEM) and the Multi-Body-Simulation (MBS).

1.2.Scope and objectives

In the current economic environment, it is important for railway organizations to be as competitive as possible. The major task for the railway track engineer often is to determine the economic effect or allowable limit to increase axle loads and vehicle speeds on existing tracks. By analyzing the railway track structure using realistic track simulation models, more informed design decisions can be made. The research presented in this report aims to the relationship between the track sided stiffness, the irregularity parameters and the performance of the vehicle track interaction with modern numerical modeling strategies.

The overall scope of the research presented in this report includes:

- Quality of track stiffness;
- Stochastic distribution of track irregularities and its representation using Power-Spectral-Density function (PSD);

- Identification and verification of railway dynamic analysis models (Finite Element Method and Multi-Body Simulation);
- Analysis and evaluation of the test results;
- Conclusions and perspectives.

The overall work plan for the research work includes:

- Feasibility study (Literature review and methodologies);
- Development of suitable simulation tools based on Multi-Body-Simulation in combination with Finite Element Models;
- The selection and field side measurements on given pilot sections (including ballasted and ballastless tracks);
- Verification of the model with measurement results;
- Analysis and conclusions.

2. STATE OF TECHNOLOGY

2.1.Track geometry (Non-recoverable track settlement)

The track geometry level is decisive for the track quality. Track geometrical imperfections (track irregularity) could cause enormous consequences which leads to a lower quality of the vehicle track interaction and again counteract on the track quality degradation. For this research, the wave length defining the overall track irregularity was set between 0.5 m and 100 m.

The characteristic of the track irregularity normally shows a wide banded spectral distribution, which makes the rebuild and categorization complicated. Therefore, digital signal processing techniques are required to provide the best ways of rebuilding the signal in an identical quality level. Many methodologies were studied and investigated on the representation of the track irregularity via Fast-Fourier-Transform (FFT) and Linear-Time-Invariant (LTI) analysis.

2.1.1. Track recording wagon (TRW)

The measurement of the track irregularity is normally included in the track inspection car (TIC). These measurements are conducted under the travel of the train. Their recording (especially in vertical direction) of the track irregularity is under the loaded track condition.

Nonetheless, track recording wagon is found to be better for recording the track irregularity levels for this study. Those wagons were normally weighted less than 1 t so their eigen loads can be neglected. By doing so, the measured track irregularity refers to the unloaded track condition which is identical to the plastic track settlement. There are various products available in the market which can be easily operated by human.

2.1.2. Linear-Time-Invariant (LTI) analysis ^[06]

Due to the fact that the values measured by the TRW are normally indirect and require further processing, various methods of transferring those measured data into the realistic track irregularity distribution were developed. The following paragraphs focus on one of the best analysis methods, the Linear Time Invariant (LTI) analysis.

The LTI system theory can be applied to analyze the response of a linear and time-invariant system to an arbitrary signal. The basic theory and the applied Fourier Transformation is found in the literature ^[07]. Recording of the raw data normally succeeds through time cursor, but for the distance application of relevant measurements, the LTI system can also have trajectories in spatial dimensions. The general work flow of the LTI analysis is shown in Figure 1:

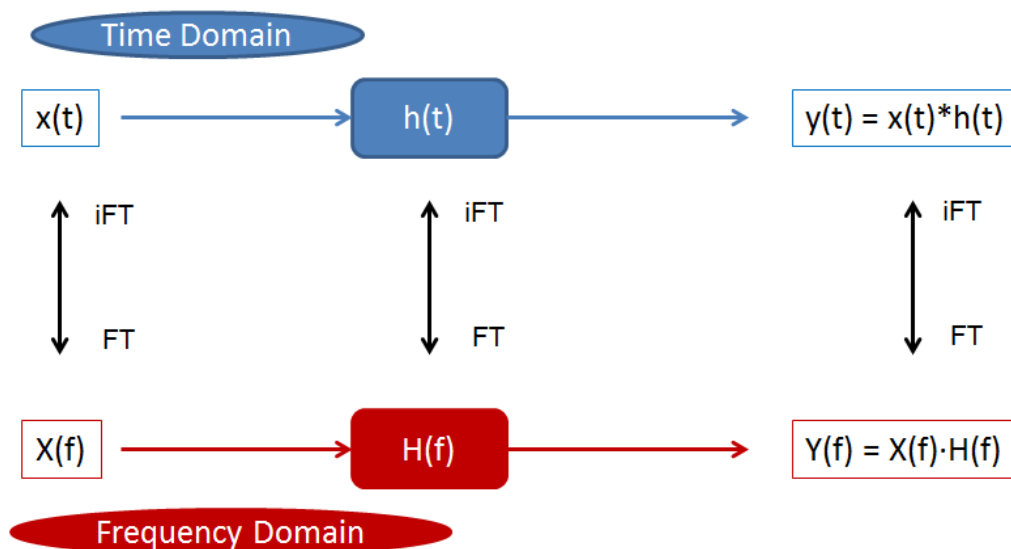


Figure 1 Principle of the LTI system ^[07]

The raw data for the application of the LTI analysis should fulfill the following two prerequisites, the Linearity and the Time invariance. The calculation of the transfer

function relies on the dirac-delta function ^[08]. After applying the Fourier Transformation (FT) on the output signal $y(t)$ into $Y(j\omega)$, the input signal in frequency domain could be calculated using the $Y(j\omega)$ and $H(j\omega)$, as shown above. The calculated $X(j\omega)$ can be then converted back to distance signal by applying the Inverse Fourier Transformation (iFT).

According to the measured raw data from the track recording wagon, it is obvious that the calculation of absolute track geometry should be only applied in the vertical and lateral direction (see Chapter 2.1.1 and 2.1.2).

2.1.3. Track irregularity and Power-Spectral-Density function (PSD) ^[09]

Spectral analysis can be applied on many diverse fields. There are two broad approaches to spectral analysis, namely the Energy-Spectral-Density of deterministic signals and Power-Spectral-Density of random signals ^[09].

The characteristic of the track excitation is that the variation outside the measured section is uncertain. It is only possible to estimate the statements of the variation. The method describes how the power of a signal or time series is distributed within frequency. The convenience is that the power could be here adjusted to the required target variable, which in this case, is the track excitation. The accuracy of the prediction of the further track excitations can be increased through the enlargement of the number of characteristic frequency super-positions.

The PSD function utilizes a pre-defined “Auto-Correlation-Function” (also called “Transfer function”) and calculates the respective PSD function by Fourier transform of the transfer function. There are also respective regulations (known as the ORE B176 ^[10], also called “ERRI”) that define the respective parameters, which were obtained from a number of measurements carried out by the European railway operators.

2.2.Track stiffness (recoverable track deflection under loading)

The quality of rail transport has a strong relation to the track quality. Wheel load distribution, within rail track structure, and wheel guidance are characterized by the overall track design, but particularly by geometrical and elastic properties. The above mentioned elastic properties usually refer to resilient rail pads, under sleeper pads, sub ballast mat, etc. ^[01]. Figure 2 shows a normal railway superstructure together with all the optional elastic elements (marked in red).

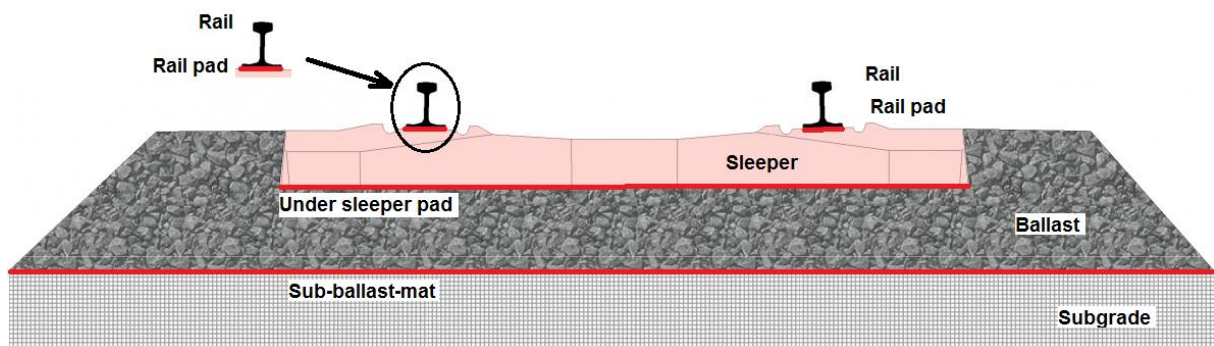


Figure 2 Typical railway superstructure and optional elastic elements

2.2.1. Load distribution and elastic deflection line (static)

Determining the wheel load distribution, within the track superstructure, under given train loads is always the first step to analyze the overall performance of rail track.

The theory of Winkler and Zimmermann (Winkler, 1867; Zimmermann, 1888) is still frequently used because it allows a precise calculation of the essential parameters, which are the rail deflection and the bending moment. It considers the rail as an infinitely long beam continuously supported by an elastic foundation. This is based on the assumption that the reaction forces of the foundation are proportional to the deflection of the beam at every point. This assumption was first introduced by E.

Winkler (WINKLER 1867) and formed the basis of H. Zimmermann’s classical work on the railroad track in Berlin (ZIMMERMANN 1888)^[02]. The actual soil stress distribution along the load axis based on the half space theory can be also calculated. Sample deflection lines and stress distribution under typical soft (pad stiffness 40 kN/mm) and stiff (pad stiffness 500 kN/mm) supports are calculated and shown in Table 1, Figure 3 and Figure 4:

Table 1: Theoretical calculation with Zimmermann theory (Rail type 60E2)

| Item | Symbol | Soft pad | Stiff pad |
|---|----------------|----------|-----------|
| Pad stiffness (kN/mm) | c pad | 40 | 500 |
| Ballast stiffness (kN/mm) | c ballast | 125 | |
| System stiffness (kN/mm) | c | 30.3 | 100 |
| Static load (kN) | Q | 100 | |
| Contact area B70 (mm ²) | F | 546000 | |
| maximum rail deflection (mm) | y ₀ | 1.17 | 0.48 |
| Max. rail seat support load (kN) | S | 35.5 | 47.9 |
| Ballast surface pressure (N/mm ²) | p | 0.13 | 0.18 |
| σ_z at bottom of 30 cm ballast(N/mm ²) | σ_z | 0.06 | 0.09 |

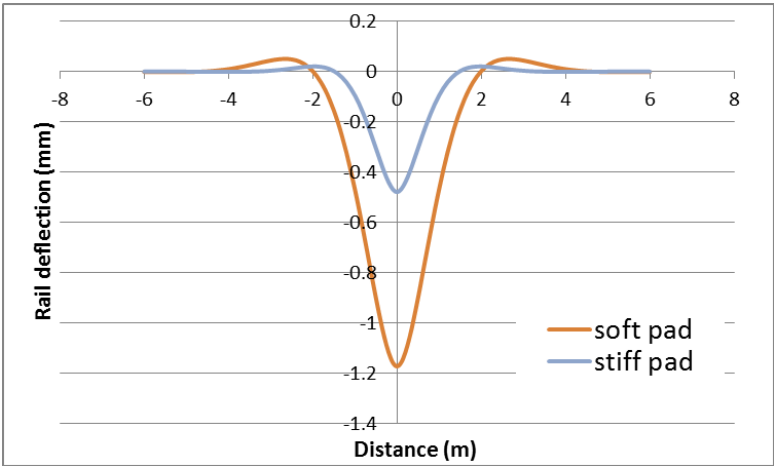


Figure 3 Typical deflection line calculated by Zimmermann Theory

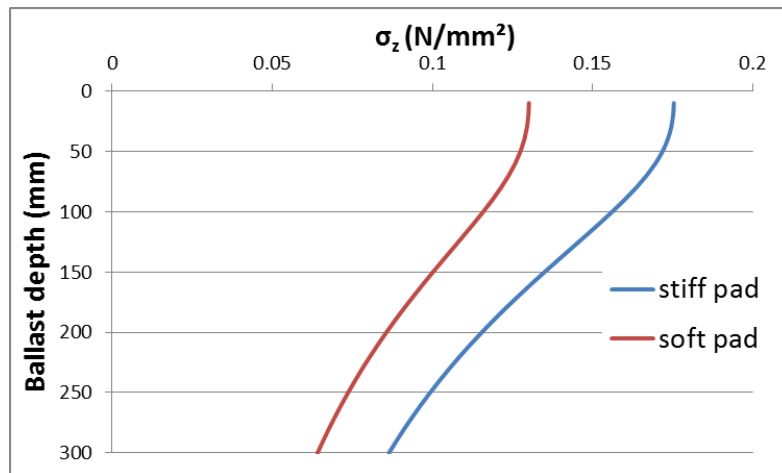


Figure 4 Distribution of ballast pressure under soft and stiff pad allocations

The inclusion of soft pad can significantly reduce the ballast pressure by enlarging the load distribution length, which emphasizes the advantage of achieving better load distribution in the ballast and substructure layers leading to the reduction of the track settlement.

2.2.2. Characteristics of the stiffness and damping behavior along the track

The dynamic properties of the elastic elements in railway superstructure can be described in terms of the dynamic stiffness and damping. These parameters are dependent usually on the following properties; materials, design, temperature, preload, loading frequency, thickness, effective area and roughness of the contact surface. In practice, the initial value of the dynamic stiffness and damping may change with time due to aging, weathering and fatigue ^[03].

It was commented by Knothe and Grassie (1993) that the load/deflection behavior of the fastening system is non-linear ^[04]; however since its behavior, when loaded by one wheel, is of the greatest interest, some linearization of the load/deflection behavior can be justified. For vertical vibration an elastic element is usually modeled as a spring and viscous damper in parallel. Elements are mainly loaded in compression, permanently

by the fastening system, the eigen load and/or repetitively by the traffic. By taking elastic rail pad as examples, in two dimensional models a pad can be represented by a pointed support under the rail foot; however for three dimensional models a visco-elastic layer across the rail foot is often considered (Kumaran, 2003) ^[05].

The classic methods can provide accurate results, but due to too many idealized parameter settings, the realistic rail seat deflection and load distribution can never be simply calculated by applying classic formulas. Firstly, the elastic elements, usually made from rubber or polymeric compound materials, show normally a nonlinear elastic behavior under loading. This will make the classic calculation with formulas at higher deflection rates uncertain. Secondly, the rail seat can have individual elastic behavior and have a variation of the stiffness even between the neighboring rail seats. This variation can be caused by different parameters including the initial condition of the construction and time dependent settlements. Track irregularity with respect to geometry is affecting the individual performance of rail seats (fastening system) and therefore the track stiffness quality along the track. Application of the modern numerical methods for a systematic study of realistic parameter variation is needed.

2.3. Modeling approach for analyzing railway track dynamics

Railway system components can be classified on the basis of their principal properties, either mass or elastic properties, or both. Together with the geometrical design (layout) of a track structure, a mechanical design or a model can be described. Such a model is basically formed by a set of relationships between all components, with inertia properties. These relationships are influenced by both elastic properties and dimensions of the components. The set of relationships defines a mechanical model, suitable for the analysis of the track structural behavior. De Man (2002) comments that in order to combine properties and dimensions into models, two modeling methods may be used, the analytical and the numerical modeling ^[11].

2.3.1. Analytic models and calculation of wheel dynamic load

Analytical models are preferably based on homogenous situations. For instance, continuous conditions are applied to support a limited number of connections and load positions. Examples for analytical models are the mathematical solutions of an infinite beam on an elastic foundation by Zimmermann (1888), Euler, Bernoulli (1736) and Timoshenko (1926).

It was released by the Deutsche Bundesbahn, in 1993, for the track superstructure calculation concerning the calculation of dynamic wheel load based on track sided influencing parameters ^[12]. The calculation of the maximum possible dynamic wheel load is realized as follows:

$$\max Q = Q_{mean} * (1 + t * \bar{s}) = Q_{mean} * (1 + t * n * \varphi)$$

Where Q_{mean} – static load of the wheel

t – Factor, dependent on confidence level ($t = 3$ for confidence of 99.7 %)

n – Track quality factor

φ – Speed factor

The following Table 2 shows the determination of the factors n and φ with reference to different operational situations. $t = 3$ is used for check of rail stresses and thickness design of slabs/pavements for ballastless track. 0.15% of loads may exceed Q_{max}

Table 2: Determination of factors n and φ [12]

| Track quality factor “n” | | |
|------------------------------|---|------|
| Track quality | Typical tracks | n |
| Very good | New main lines; Rehabilitated main lines | 0.10 |
| Good /moderate | Trunk lines; Commuter lines | 0.15 |
| Bad | Other main lines | 0.20 |
| Very bad | Other tracks, local tracks | 0.25 |
| Speed fact “φ” (V > 60 km/h) | | |
| Passenger train | $\phi = 1 + \frac{V - 60}{380}$ (V – vehicle speed in km/h) | |
| Freight train | $\phi = 1 + \frac{V - 60}{160}$ (V – vehicle speed in km/h) | |

A passenger train with static wheel load of 105 kN under the speed of 160 km/h and 300 km/h in new or rehabilitated main line track returns a “max Q” of 144.8 kN and 156.4 kN. Since the modern ballastless track can achieve better track quality, the calculated “max Q” will be even smaller. These values are already able to provide a rough guideline for the estimation of the dynamic loading.

2.3.2. Numerical models

Numerical models are typically used for more accurate stress analysis of track components and where the retrieval of solutions with analytical models is difficult. Instead of finding a solution in a continuous input range, numerical methods search for the solution by comprising nodes, connecting elements and boundary conditions. All the component properties and the model restrictions have to be embedded in the definition of this numerical model. Examples for numerical models are the Finite Element Method (FEM) and the Multi-Body Simulation (MBS).

Generally, the working processes for both FEM and MBS can be split in six steps [13]. The six steps and the targets are shown in Table 3:

Table 3: General working process of FEM and MBS

| Name | Description |
|---|--|
| 1, Problem Definition | Finding the exact specifications of the model |
| 2, Development of a model | Dividing the mechanical structure into model specified bodies and elements (Structural analysis) |
| 3, Provision of the physical parameters | Providing the physical information to the respective bodies and elements |
| 4, Pre-Processing | Input of the pre-defined information in Step 1-3 into the software; Model setup |
| 5, Problem solution | Calculation of the solution based on the given information using differential equations |
| 6, Post-Processing | Numerical or graphical representation of the results |

It has to be clarified that only the steps 4 to 6 are handled by the respective simulation software, while the steps 1 to 3 are related to the feasibility study and the structural analysis of the system.

2.3.3. Finite-Element-Method (FEM)

As summarized from Madenci and Guven (2006); Suvo and Khemani (2010); Liu and Quek (2003); and Moaveni (1999) concerning the Finite-Element-Method (FEM) or Finite-Element-Analysis (FEA), Courant (1943) has been credited with being as the first person who developed the FEM in his paper related to the investigation of torsion problems by using piecewise polynomial interpolation over triangular sub-regions. Nowadays, the FEM is known as a dominant discretization technique in structural mechanics, which means the subdivision of the mathematical model into disjoint components with a predefined geometry, called finite elements. Afterwards, for each element, finite degrees of freedom will be assigned, characterized by special functions or expressions ^[14].

The exact work flow which is performed by FEM simulation software is:

- Pre-processing: definition of geometry, materials, and element types and generation of finite-element grids (meshing).
- Problem solution: definition of analysis type, boundary conditions and constraints, application of loads and calculation of solution by intern defined calculation mechanisms.
- Post-processing: Visualization of the analysis results (usually time-independent).

The FEM software, chosen for this research is named ANSYS. It provides general solutions to the practical problems for universal purposes. The first version was released in 1971.

2.3.4. Multi-Body-Simulation (MBS)

Multi-Body Simulation is a newly developed modeling approach in railway engineering field. Such kinds of simulation software (e.g. SIMPACK) are already widely used in the design of automobiles or locomotives ^[15]. On MBS systems, the structural parts or bodies are often connected using complex joints (complex suspension joints, for example), with complicated force elements acting between these bodies. Often in such systems, the bodies themselves can be considered as rigid, as the relative deflection of the bodies is small in comparison to the rigid body motion. MBS software has allowed the modelling of these types of dynamic systems, where previously was not possible. A sample model done at SIMPACK is shown in Figure 5:

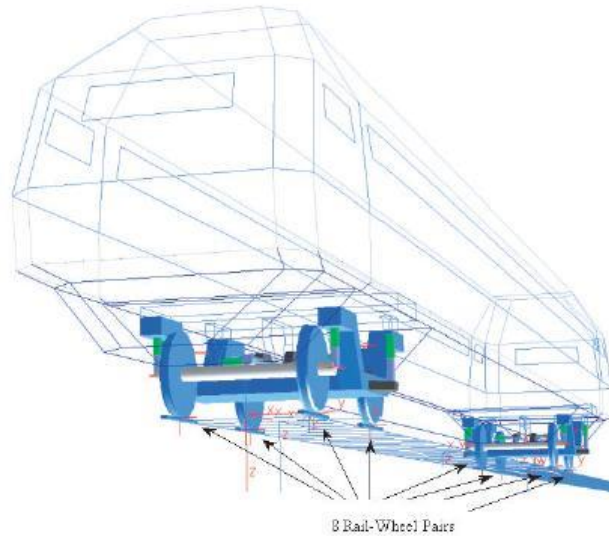


Figure 5 Sample SIMPACK Model for railway vehicle [15]

2.3.5. Comparisons and co-simulation

When comparing MBS software to Finite Element (FE) software, the differences between them become clear. The FE software, which focuses on the elastic body itself, requires all bodies to be defined as elastic, whereas MBS software, requiring mostly rigid bodies, focuses more on the complex interaction between them. Table 4 shows a comparison of the modeling approaches.

Table 4: Comparison of FEM and MBS approach

| | FEM Finite-Element-Method | MBS Multi-Body-Simulation |
|---------------------------|--|--|
| System characteristics | System with 2D/ 3D Elements | System with 3D bodies |
| Basic elements | Elastic elements (Material properties, Element types) | Rigid bodies (Mass, CoG, Inertia Tensor, etc.) |
| Formulation of the system | Elements are connected by nodes | Connection of bodies with idealistic joints |
| Type of analysis | Static analysis | Kinematic and dynamic analysis |
| Output results | Calculated Deflections, Strain, Stress | Calculated Force, Speed, Acceleration |
| Degrees of Freedoms | System with many Degrees of Freedoms | System with limited Degrees of Freedoms (Condensation) |
| Representative software | ANSYS, SoFisTIK ... | Simpack, Adams... |

The FEM gains advantages in the representation of element stiffness, whereas MBS can easily handle 4D systems with time-dependent dynamic analysis. Considering the complexity of the vehicle track dynamic system, both approaches have to be utilized in the most efficient way. The FEM allows the sufficient approximation of the track flexibility, while the vehicles' motion, including its complex wheel-rail interface, is produced within the appropriate MBS system. Therefore, a joint use of both, named "Co-simulation", is one of the best solutions [16]. Co-simulation means that both FEM and MBS programs simulate their respective parts separately on a superior artificial discretized time-scheme and interchange the conjunctive data at the thus defined points of time.

The MBS software SIMPACK provides the possibility to preform co-simulation with FEM software ANSYS by integrating the FEM model into the MBS interface. Nevertheless, the FEM model should be firstly condensed before such integration. This condensation is achieved through the modal approach, which calculates a large number of eigen modes to represent the track stiffness and damping characteristics.

The FEM model should be condensed, since it originally contains too many variables. The way of condensing the FEM model is to specially define some nodes as so called “Master nodes”, whereas the other nodes are controversially “Slave nodes”. By doing so, the master nodes will still hold independent equations, but the results of the slave nodes will be the linear combination from the results of neighboring master nodes. In other words, slave nodes will not hold independent variables any longer. By carefully selection of master nodes, the number of independent variables is significantly reduced without neglecting the general model characteristics. This calculation is called “Substructuring analysis”, in ANSYS.

The eigen modes of the FEM system provide the most important information for the MBS environment, which is how the stiffness and damping of the track should be represented. The eigen modes of the FEM system are calculated by the so called “Modal analysis” based on the condensed FEM model. The eigen modes of the elastic structure represent both its dynamic response and its local deformation, due to the interfaces loads.

3. PILOT SECTIONS AND DESIGN OF FIELD MEASUREMENT

3.1. Introduction

Field measurements are always the best and most direct way to gather actual information about the track. Experiences from previous research works about the track quality evaluations can be utilized. Various field measurements were reviewed in order to find out the best way of gathering field side data related to this research work.

3.2. Selection of pilot sections

To guarantee comparable situations of the test sections, in order to be able to focus only on the track quality, the following boundaries for the selection procedure, of the track sections, have been fixed:

- straight alignment to exclude additional centrifugal forces by the cant deficiency or centripetal forces due to the cant excess,
- no or moderate longitudinal slope,
- no changes in substructure,
- modern high speed railway lines as the best suitable pilot sections and
- the initial condition of the section should be measured.

A systematic understanding of the vehicle-track interaction relies on both vehicle and track sided inputs. Since this interaction is generally increased by increasing the speed level, modern high speed railway lines with different type of superstructure are the best scenarios for the research work.

An important reason for the variance of the track quality is the initial condition, meaning how “perfectly” the tracks are built. Modern construction technologies could handle those construction works without major difficulties, but small variances of the track

sided parameters can never be fully eliminated. Those variances are the key reasons to provide guidelines for the general deterioration level of the overall track quality.

In total four different measurement sections were selected. General information about these sections can be seen in Table 5. Clearly, the maximum design speed of 250 or 300 km/h and ballasted or ballastless track system are examined.

Table 5: Selection of measurement sections

| Section number | Location between | Type of track | Max. design speed (km/h) |
|----------------|-----------------------------------|--|--------------------------|
| 1 | Nuremberg and Ingolstadt, Germany | Ballastless track Type1 | 300 |
| 2 | Nuremberg and Ingolstadt, Germany | Ballastless track Type2 | 300 |
| 3 | Salzburg and Vienna, Austria | Ballasted track | 250 |
| 4 | Salzburg and Vienna, Austria | Ballasted track partially with sub-ballast-mat | 250 |

The detailed section plan, including the position of all the measurement sensors and general information about the alignment and the superstructure installations, is found in appendices 1 to 4.

3.3. Test program

Various activities on the field can be conducted with the focus on different targets. When talking about the research on vehicle-track interaction and the respective track quality, the necessary measurement parameters should include the elastic track deflection, the vertical track geometry and the dynamic track behavior.

3.3.1. Determination of track geometry (plastic track deformation, unloaded)

The determination of track geometry in the representation of plastic track deformation was done previously only in the vertical direction. However, for a better understanding of the influence of the track irregularity to the behavior of the wheel-rail interaction, there is the necessity to continuously record the track geometry in 3 dimensions.

Track geometry in the representation of plastic track settlement is the direct source influencing the vehicle-track interactions. By increasing the travel speed, a longer influence section should be inspected.

The design of modern passenger coach (with air-spring as secondary suspension) always follows the principle, that an eigen frequency of approximately 1 Hz should be achieved ^[17], which means that the calm down time for single impulse could be up to 1 s long (This eigen frequency for locomotives and freight wagons are normally higher due to the installation of coil springs for secondary suspension). This defines the minimum wave length which should be included in the calculation of track geometry. From the previous experiences of the institute, this wave length must have at least 8 repeats in each measurement. Table 6 shows the speed, the respective wave length and required measurement length.

Table 6: Calculation of the minimum measurement length for geometry measurement

| Speed (km/h) | Wave length (m) | Minimum Length for geometry measurement (m) |
|--------------|-----------------|---|
| 160 | 44.4 | 350 |
| 250 | 69.4 | 550 |
| 300 | 83.3 | 650 |

New track recording wagon was introduced and applied in this research work. The wagon was manufactured by the company Vogel & Plötscher with a type series called “MessReg CLS” ^[18]. It can record the respective track parameters continuously along the line by just pulling the wagon with walking speed. The reader is referred to Figure 6 and Table 7 for the handled parameters, as well as the accuracies.

Table 7: Performance data of movable track recording wagon
(Type CLS from company V&P) ^[18]

| Measured parameters | Range from (mm) | Range to (mm) | Accuracy (mm) |
|---------------------|-----------------|---------------|---------------|
| Gauge | 1415 | 1500 | 0.005 |
| Versed sine | -230 | +230 | 0.005 |
| Gradient | -100 | +100 | 0.3 |
| Cant | ± 170 | | 0.001° |
| Distance | Continuous | | 2 |



Figure 6 Movable track recording wagon (Type CLS from company V&P) ^[18]

It is essential to mention that the under sleeper gap actually is another phenomenon of track plastic deformation in vertical direction. These deformations could only be detected by the loaded track; therefore the gaps are measured by other measurement methods.

3.3.2. Measurement of elastic rail deflection (quasi-static)

In order to check the uniformity of the vertical load distribution of the track by rail deflection, it is required to perform static rail deflection measurements at a certain amount of rail seats (sleepers) within each test section. Rail deflection is influenced by all the elastic components within the railway sub- and superstructure, as well as by potential gaps between the sleepers and the ballast. A minimum number of 100 rail

seats (50 continuous on each rail) should be measured at each pilot section for statistical reasons.

Rail deflection measurements on successive rail seats can be performed using the track movable, modified Benkelman-beam, which gives the overall rail deflection under a given quasi-static axle load, as well as the shape of the deflection bowl of one rail during the approach of the loaded wheel. The quasi-static loading is given by a ballast bulk wagon with a single axle load. A loco was used to push and pull the wagon with walking speed within a regular stop to stop distance of about 10 m. In Figure 7 the design of the Benkelman measurement wagon is shown.



Figure 7 Benkelman beam for the measurement of track elastic deflection

For the analysis purposes, the deflection line should be calculated based on the measured influence line. The values of the deflection line for each rail seat could not be directly taken from the measurement data, because the specification for the deflection line requires stable load (while during the Benkelman measurement, the load train was moving while the data were measured). Therefore, an interpolation is carried out, which functions as follows:

- The rail seat i , where the deflection line will be drawn, is chosen.
- The deflection at the load point (max. deflection) is read from the measurement i , under the position of $s = 0$ m
- The deflection at $x = x_0$ m (x_0 is sleeper spacing) is read from the measurement $i-1$, under the position of $s = x_0$ m (which is the exact deflection of $x = x_0$ m when the load is on the rail seat i)
- The deflection at $x = 2 \cdot x_0, 3 \cdot x_0, 4 \cdot x_0$ etc. can be similarly calculated.

3.3.3. Installation of strain gauges

Strain gauges are installed on the rail and within the length of the sleeper spacing. Particularly, the strain gauges with length of 6 mm were located at the rail foot middle point, between the sleepers, and could record the strain changes caused by the wheel load of the vehicle. The maximum allowable channels for a synchronized measurement are 64, so when rail foot stress between every two rail seats are measured, the total length is limited to approximately 20 m, which is too short to measure dynamic effects. Therefore, the following modifications are made:

- Most of the strain gauges should be installed inside the area of the Benkelman beam measurement;
- A difference of installation density should be realized for higher efficiency;
- The total number of installed strain gauges should be slightly higher than the maximum allowable channels to prevent possible failures.

The strain gauges were installed in three different densities named 'Fine', 'Middle' and 'Rough'. The allocation of the strain gauges follows the following principles:


1. The dynamic strain / stress caused by the four wheels of one bogie should be recorded at the same time;

2. The change of the strain / stress in time sequence should be recorded at least for one cycle with possible fine step size (area ‘fine’);
3. Middle and rough stepped measurement should be located after the ‘fine’ area for concluding the change of strain / stress during the passage of the train; (area ‘middle’ and ‘rough’)
4. A sufficient length of the measurement section should be provided for gathering the decay / amplification rate between different cycles.

3.3.4. Recording the vertical track response under running trains

For data recording, the QuantumX is used which measures up to 8 channels at the same time. Through fire-wire connection, more units can be connected and measured with synchronized time axis (See Table 8 for hardware information).

Table 8: Data amplifier QuantumX

| | |
|--|---|
|  | |
| 24 bit A/D conversion for synchronous, parallel measurements | Sample rate: up to 19.2 kHz/channel, configurable |
| Filters: Bessel, Butterworth 0.01 Hz to 3.2 kHz (-1 dB) | Electrically isolated inputs |
| Power supply for active transducers | Permissible cable length up to 100 m |

This equipment supports a maximum measurement frequency of 19 kHz. Thus a train running with up 300 km/h, within a distance of 4 mm of the train’s movement one set of data is recorded. This is required to precisely identify the peak values of the rail foot

strain influence lines. Concerning the evaluation, the strain values were used to determine the respective rail foot stress, retrieved from the formula $\sigma = \varepsilon \cdot E$, while the Young's modulus E was set equal to $2.1 \cdot 10^5$ N/mm².

The test should be conducted under normal operational train runs. It must be taken into account that the measurement data for analysis and evaluation are thus affected by the respective train speed (fixed according to operational or actual, random conditions) and train type (axle loads and axle spacing, suspension system), as well as by load deviations and conditions of the individual axles (potential wheel flats) even when the train type is identical.

3.3.5. Measurement of vertical acceleration level

Accelerometers are placed on the rail and the sleepers, measuring the vertical vibration level of the track. The measured raw acceleration level of the track was used to analyze the track quality and the respective vibration level.

The track side acceleration is often recorded by special made acceleration sensors (also called accelerometers, see Figure 8). Those sensors utilize the gyroscope theory to the physically sense in the real-time acceleration level and represent these levels in a certain type of electric signals.

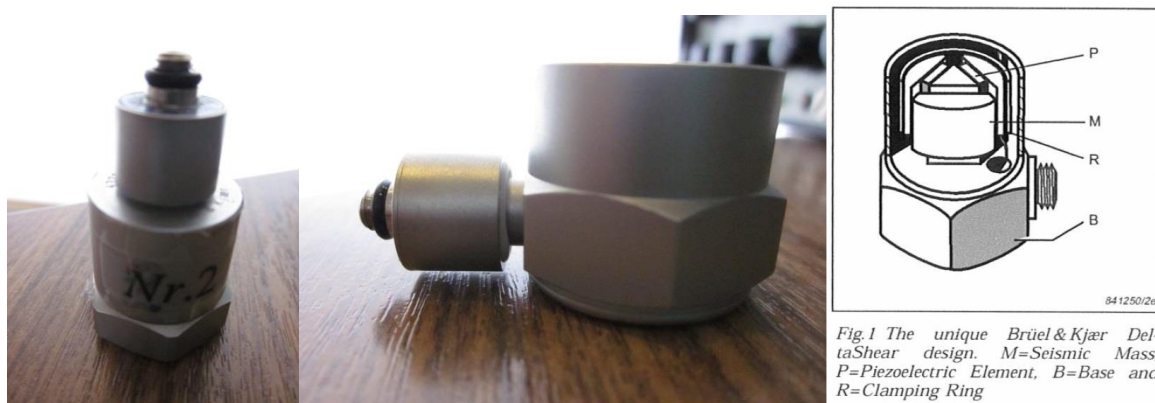


Figure 8: Typical accelerometers and its internal design

The above Figure 8 shows the internal design of a typical accelerometer. This type of sensor is also called piezoelectric accelerometer. It records and converts the physical acceleration into electronic signal. For specific rail and track problems, the included sensor for data recording is from the company Brüel&Kjaer with upper frequency limit at 4.5 kHz.

The electric signals of the transducers were transmitted to a signal amplifier by B&K. An impulse hammer with a head mass of 5.44 kg was also used to extract a standard impulse load on the rail head in order to calibrate the track vibration behavior.

Allocation of more accelerometers on the rail, the sleepers and in the ballast bed provides the exact information regarding the elements which are excited the most. In total, 8 accelerometers are installed in each test section. Their locations are marked with numbers 1 to 8. A sketch of the sensors allocation and moreover, a picture of the exact positions of the sensors 3, 4, 7 and 8 and the impulse locations of A and B in the field, can be found in Figure 9. The locations A and B are the impact points for the impulse hammer.

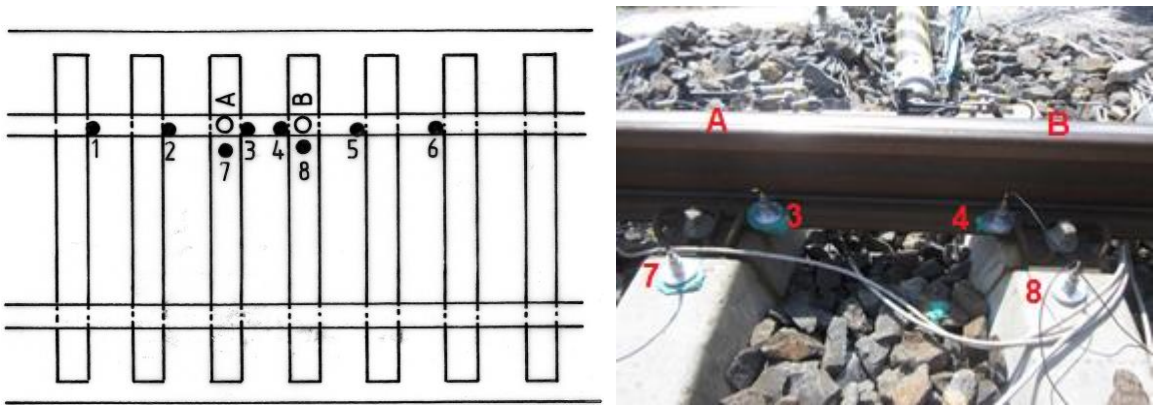


Figure 9: Allocation of the measurement sensors

The acceleration of the system under the hammer impulse and the operational train passages is measured. The amplified signals were sent to a 16 bit PC DAQ-Card of National Instruments, in a laptop. The digital, raw signals were then analyzed and evaluated using the software MEDA 2013 from Wölfel.

The accelerometers measure the vibration acceleration level (m/s^2) and the impact hammer measures the impact load (N). The analysis of the measured signals firstly

demands the division of the acceleration channel to the respective load channel in order to determine the acceleration under the unit loading. This was performed to eliminate the difference of the hammer excitation load. In the next step, the vibration speed is determined by integrating the acceleration signal in the time domain. The calculation of the spectrum distribution relies on the Fast Fourier Transformation (FFT) of the processed time signal with a band width of $\Delta f = 1.25$ Hz and a rectangular window with 50 % overlap whilst linear average determination of the spectrum distribution within a time frame of $T = 4$ s. Finally, the vibration speed spectrum is illustrated in frequency domain under Terz distribution from 8 Hz to 6.3 kHz (dependent on the setup of band width in the measurement). The analysis of the data partially fulfills the requirements written in DIN 45672-2 [19].

It should be noticed that the effect of high speed train runs is more sensible to local imperfections, and thus the vibration level could be amplified to a higher level even under very limited track disturbances. These measurements are quite useful to understand the effect of small track irregularities to the vehicle track interaction. All the analyses are accomplished in the software program MEDA 2013.

3.4. Long-term effects

The change of track quality in relationship to the operational parameters is always one of the most determinant factors to specify the general track maintenance strategy. This especially concerns the newly assembled ballasted tracks due to possible adjustment effects. Therefore, repeated measurements in sections 3 and 4 were planned within the time span of approximately 1 year. The change of track sided parameters between both measurements is particularly interesting for this research topic.


3.5. Vehicle information

Different types of vehicles were measured during the train run tests. As the evaluation of the measurement data is highly dependent on the design of the vehicles (axle load, suspension design, etc.), an overview of the measured locomotive and multiple units were collected and shown in the following sections.

3.5.1. Vehicle information in sections 1 and 2 (German railway high speed line)


The general information of the locomotive and multiple units can be seen in Table 9 to Table 11:

Table 9: Inter-City-Express, ICE 1 / ICE 2 (D-DB)

| | |
|---|--------------------------|
|  | |
| ICE 1 (D-DB BR 401) / ICE 2 (D-DB BR 402) | |
| Type of vehicle | EMU |
| Formation | M + 12T + M / M + 6T + L |
| Max. speed (km/h) | 280 |
| Weight (t) | 849 / 412 |
| Max. axle load (t) | 19.5 |
| Axle formation (locomotive) | Bo'Bo' |
| Axle spacing (locomotive, m) | 3.0 |

*) Pic source: Wikipedia

Table 10: Inter-City-Express, ICE 3 / ICE T (D-DB)

| | |
|--|---------------------|
|  | |
| ICE 3 (D-DB BR 403) / ICE T (D-DB BR 411) | |
| Type of vehicle | EMU |
| Formation | 4M4T / 4M3T |
| Max. speed (km/h) | 330 / 230 |
| Weight (t) | 409 / 368 |
| Max. axle load (t) | 17.0 / 15.5 |
| Axle formation (motor car) | Bo'Bo' / (1A)'(A1)' |
| Axle spacing (m) | 2.5 |

*) Pic source: Wikipedia

Table 11: The express trains IC / RE (D-DB)


| | |
|--|--------------------|
|  | |
| Type 101 (D-DB BR 101) / Passenger wagon | |
| Type of vehicle | Locomotive / wagon |
| Formation | - |
| Max. speed (km/h) | 220 / 200 |
| Weight (t) | 84 / 55-60 |
| Max. axle load (t) | 21.7 / 14-15 |
| Axle formation | Bo'Bo' |
| Axle spacing (m) | 2.65 / 2.50 |

*) Pic source: Wikipedia

3.5.2. Vehicle information in sections 3 and 4 (Austrian railway high speed line)

General information of the locomotive and the multiple units is provided in Table 12 to Table 14. The Type ICE-T (D-DB BR 411) was already introduced in subsection 3.5.1.

Table 12: Electric Multiple Units KISS (A-ÖBB)

| | |
|--|--------|
|  | |
| Type KISS, Version Westbahn (A-ÖBB BR 4010) | |
| Type of vehicle | EMU |
| Formation | 2M4T |
| Max. speed (km/h) | 200 |
| Weight (t) | 310 |
| Max. axle load (t) | 17.0 |
| Axle formation (motor car) | Bo'Bo' |
| Axle spacing (m) | 2.5 |


*) Pic source: Wikipedia

Table 13: Electric locomotives (A-ÖBB)

| | |
|--|-------------|
|  | |
| Type 1116 (A-ÖBB BR 1116) / Type 1144 (A-ÖBB BR 1144) | |
| Type of vehicle | Locomotive |
| Formation | - |
| Max. speed (km/h) | 230 / 160 |
| Weight (t) | 85 / 84 |
| Max. axle load (t) | 21.5 / 21.0 |
| Axle formation | Bo'Bo' |
| Axle spacing (m) | 3.0 |

*) Pic source: Wikipedia

Table 14: Passenger wagons (A-ÖBB)

| | |
|--|-----------|
|  | |
| Passenger wagons for IC / RJ | |
| Type of vehicle | Wagon |
| Formation | - |
| Max. speed (km/h) | 200 / 250 |
| Weight (t) | 55-60 |
| Max. axle load (t) | 14-15 |
| Axle formation | Bo'Bo' |
| Axle spacing (m) | 2.5 |

*) Pic source: Wikipedia

4. FIELD MEASUREMENT AND DATA ANALYSIS

This chapter documents the measurements conducted for all the pilot sections. The sequence of the chapter is according to measurement components. It is manually defined, that specific strain gauge is located at 0 m and the rail on the left side of the travel direction, with increasing number of points, is called 'Left rail' (refer to appendices 1 to 4 for detailed position information). This definition is used through all the following figures and tables in this chapter. Pictures from the measurement activities can be found in Annexes 1 to 6.

4.1.Track geometry and irregularity (plastic settlement)

4.1.1. Calculation of absolute track geometry

As introduced in chapter 2, an automatic calculation of the absolute track geometry under the guideline of Linear-Time-Invariant theory (LTI) should be firstly applied for the measured raw data. This was achieved by the self-developed Matlab program. A Graphical-User-Interface (GUI) was also created for easier processing and is shown in Figure 10, the user specification and instructions could be found in User Instruction manual 1.

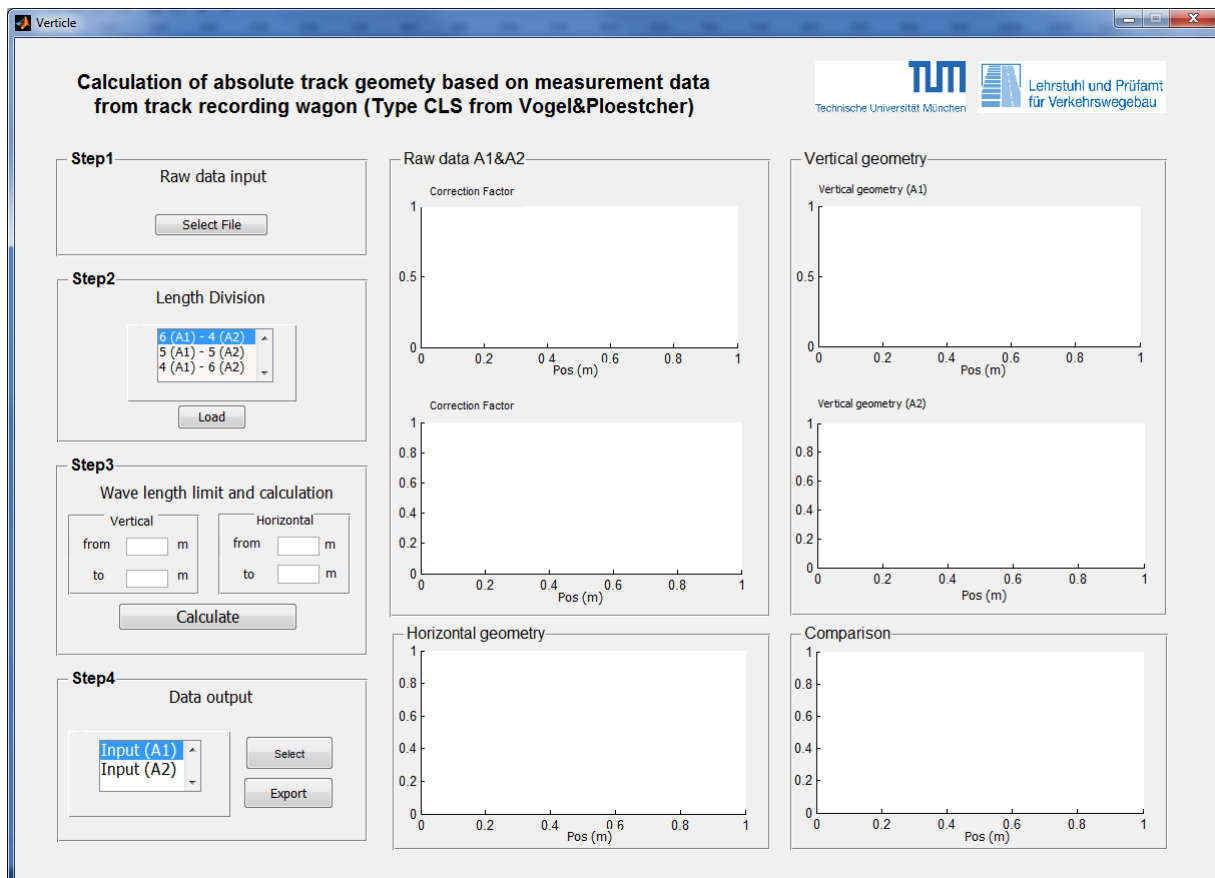


Figure 10: The processing of track geometry (GUI interface)

The processed irregularities of all the measurement sections can be found in appendices 5 to 10. The wave length for vertical irregularity is set between 0.5 m and 50 m.

4.1.2. Statistical analysis of the measured data

The following Table 15 collected the statistical analysis of the vertical track geometry for all the measurement sections.

Table 15: Statistical analysis of vertical track geometry

| | Measurement section number | | | | | |
|------------------------------------|----------------------------|---------------------|------|------|------|------|
| | 1 | 2 | 3 | 4 | 3 | 4 |
| Year of measurement | 2013 | | 2012 | | 2014 | |
| Year of operation begin | 2006 | | 2013 | | | |
| Length of measurement (m) | 1234 | 834 | 531 | 600 | 527 | 561 |
| Vertical spread (mm) ^{*)} | 1.51 | 6.93 ^{**)} | 2.89 | 5.96 | 2.68 | 6.34 |
| Standard deviation (mm) | 0.24 | 1.11 ^{*)} | 0.74 | 0.86 | 0.90 | 1.08 |

^{*)}: Calculated by subtracting the maximum value from the minimum value

^{**)}: Change of track geometry quality due to level compensation work (see Annex 7)

It is shown, that the track quality, on behalf of track geometry, is better for ballastless track sections 1 than for ballasted track sections 3 and 4 (excluding section 2 due to the applied level compensation against irregular settlement, see Annex 7), even compared to the initial operation of the ballasted track sections. Comparing the results from 2012 and 2014 of sections 3 and 4, the terms “Vertical spread” and “standard deviation” became greater with the increase of load cycles.

4.1.3. Calculation of track quality parameters using Power-Spectral-Density function (PSD)

According to subsection 2.2.2, the calculation of Power-Spectral-Density function provides general information about the track quality level on behalf of the track geometry. Therefore, for the clarification of the measured track geometry in the vertical direction, the power-spectral-density distribution is calculated.

Based on large amount of tests of track geometry, German Railway (Deutsche Bahn AG) specified guidelines concerning the calculation and categorization of PSD into two levels: high irregularity and low irregularity. The result is documented in the standard ORE B 176 (named as “ERRI”) ^[10] and the valid wave length varies from 3 m to 100 m (distance frequency between 0.01 m^{-1} and 0.33 m^{-1}). The values outside this interval were derived without confident values from measurements.

For analysis of vertical track geometry, special guidelines by the German Railway specify the values of PSD especially for the ballastless track. Those values were documented in the “Anforderungskatalog zum Bau der Festen Fahrbahn – 4. Überarbeitete Auflage” [20] (named later as AKFF). This guideline is valid for the characteristic wave length between 1.0 m and 66.7 m (distance frequency between 0.015 m^{-1} and 1.0 m^{-1}). Figure 11 shows the guideline curves of the standard (vertical direction, free factor = 1.0):

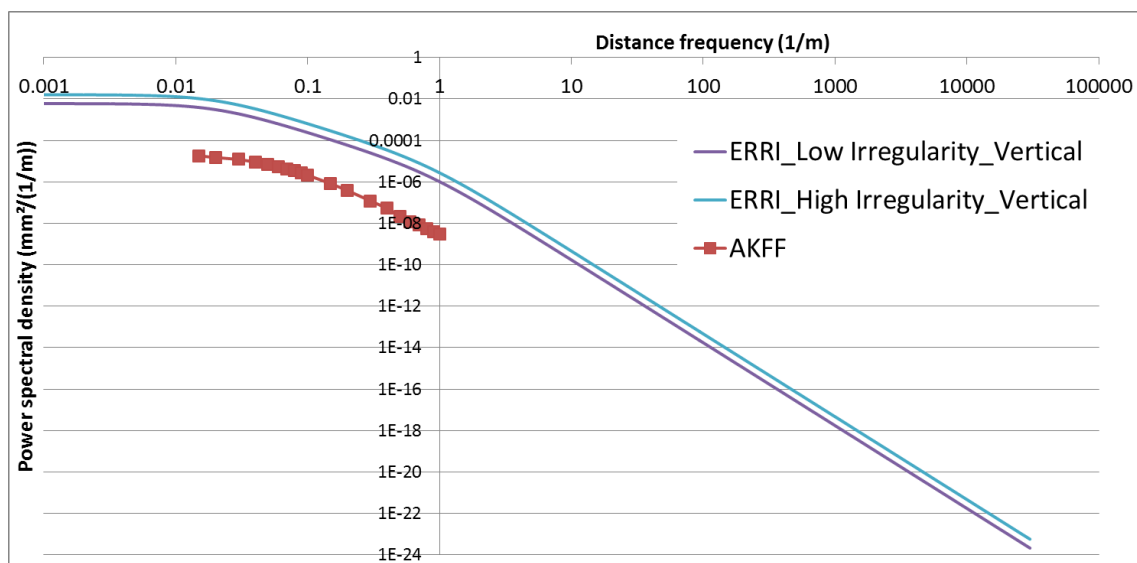


Figure 11: Sample PSD distribution in vertical direction (values derived from “ERRI” and “AKFF”)

According to the calculation procedure, the PSD distributions of all the four measurement sections in vertical direction are calculated. It can be noticed that the cut off frequencies of the measurement is always fixed between 0.02 m^{-1} and 2.0 m^{-1} . Figure 12 and Figure 15 show the results of all the four sections. The guideline are also attached.

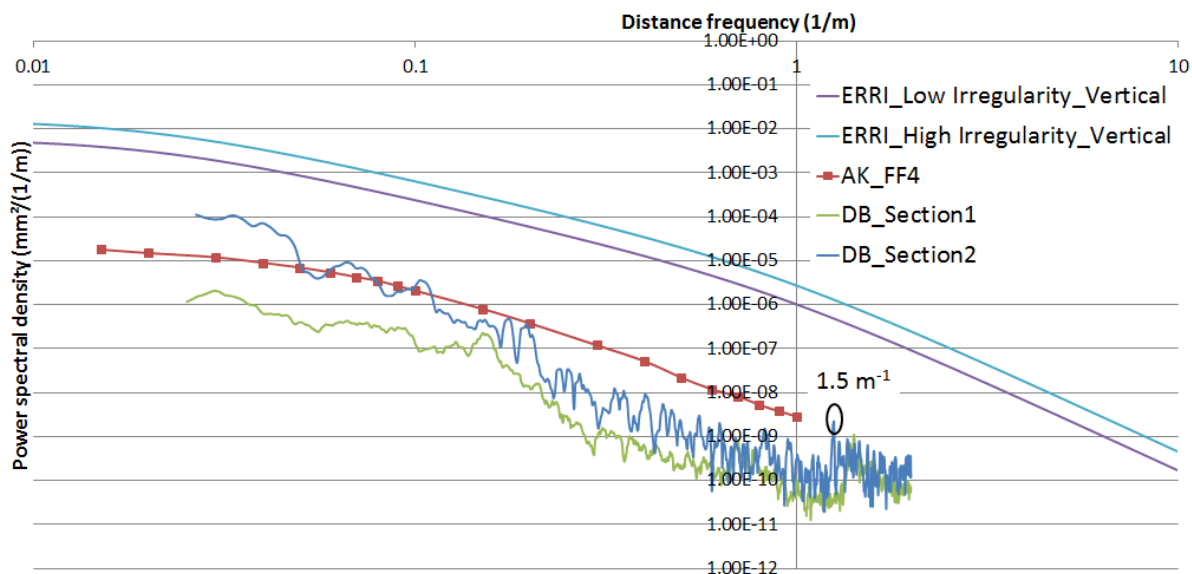


Figure 12: PSD analysis of measurement sections 1 and 2 (vertical direction)

The measured peaks at around 1.5 m^{-1} are due to the rail seat spacing of 0.65 m . It is clear from Figure 12, that the PSD line of the section 2 is partially higher than the guideline from AKFF. Nevertheless, the derivation of the guidelines values from the mentioned literature are calculated based on the *loaded track geometry* data captured by the track inspection car (TIC) and the calculated PSD lines of all the four measurement sections were based on the *unloaded track geometry* captured by the track recording wagon (TRW). Therefore, the aforementioned literature guidelines [20] should not be seen as a standard line, but only as a reference for understanding the approximate track quality level. The higher PSD values of the section 2, compared to section 1 are also explained, by the performance of level compensation due to irregular track settlement (see Annex 7). It could also be indirectly concluded, that the track settlement (as well as the maintenance work) could cause much more intensive increase of track irregularity level in low frequency range (long wave length), which can be proved by the large offset of both curves of sections 1 and 2 (one with settlement and one without) in small frequency area but quite overlapped in high frequency area.

For measurement section 4, in Figure 13, firstly shows the overlapped measured vertical track geometry in 2012 and 2014. It can be seen, that the measurement section

contained a section with sub-ballast-mat of about 250 m. Therefore, the calculation of PSD of the section 4 contained two variations: "Section 4" and "Section 4_USM".

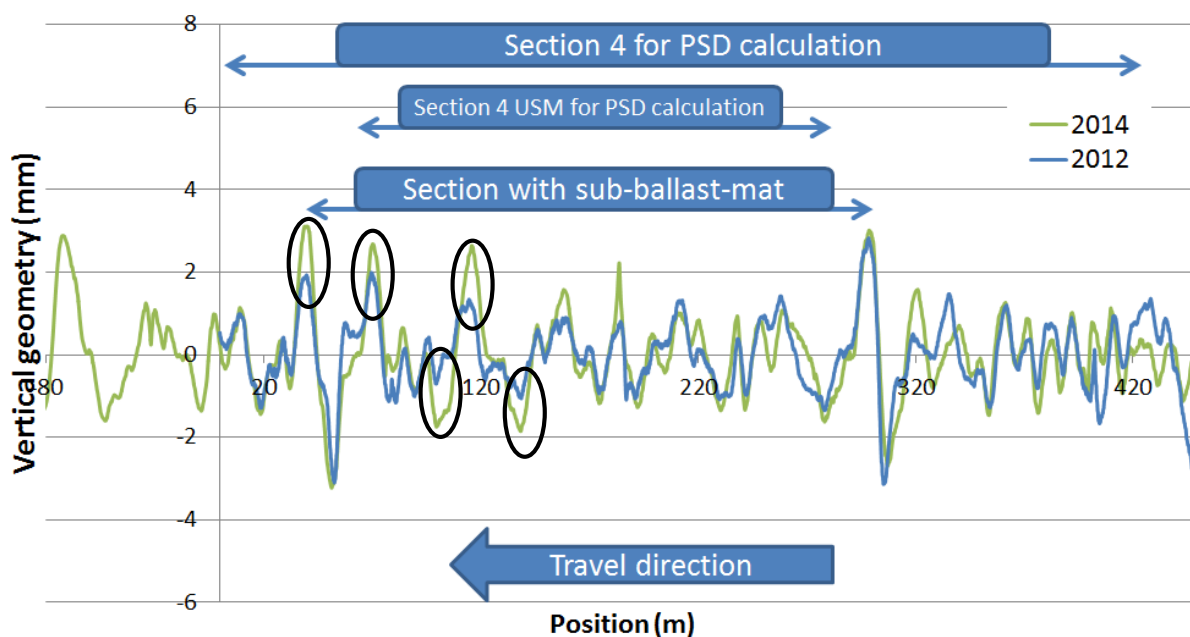


Figure 13: Illustration of the analysis interval of section 4 (vertical direction)

Firstly, the track geometry quality is decreased in 2014 compared to 2012, with obvious increase of vertical spread (marked with circle) inside the section (about 1 mm). Another important observation is that the obvious deterioration is exclusively located at the area with sub-ballast-mat and at the transition to normal track area. This shows that the initial ballast condition inside the area with sub-ballast-mat (due to the energy subtraction from the sub-ballast-mat during tamping) was less compact than at the normal section, which potentially leads to faster deterioration of track geometry by operations.

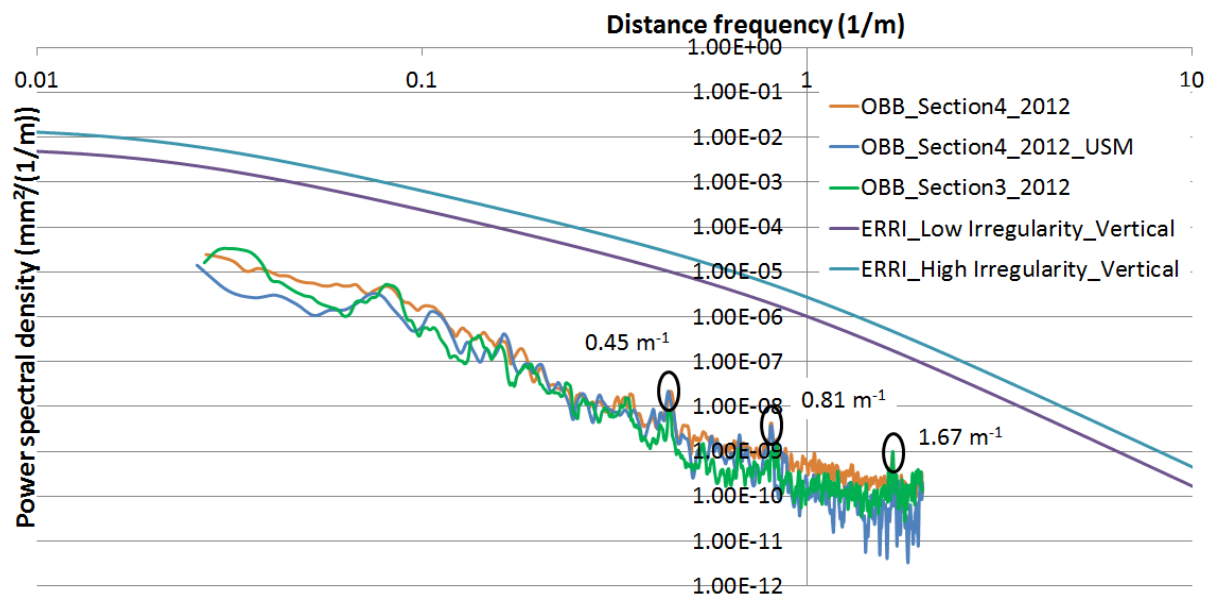


Figure 14: PSD analysis of measurement sections 3 and 4 (vertical direction)

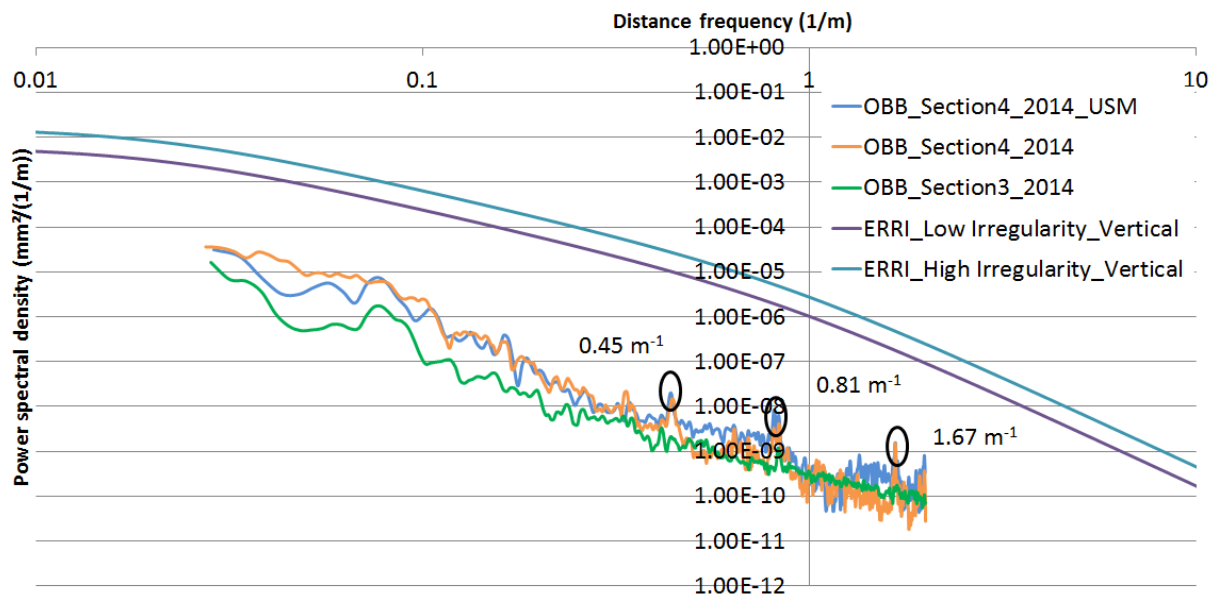


Figure 15: PSD analysis of measurement sections 3 and 4 (vertical direction)

Moreover, the overlapped curves of section 4 indicate that both have similar PSD values expect for the low frequency range, which proves that the track irregularity level near the transition between the normal section and the section with sub-ballast-mat have a normal wave length of longer than 10 m.

Two marked distance frequencies of the both curves indicate the wave length of 0.6 m and 1.2 m, which obviously are identical to 1 and 2 times the sleeper spacing. The reason for the peak at 0.45 m^{-1} is analyzed in chapter 6.5 (peak appeared due to vehicle sided eigen frequency excitation).

For operational and technical reasons, the section 3 in 2012 and 2014 could only hold an overlapped length of approximately 100 m (the total evaluated length was 500 m) and therefore there is not direct comparison for the track geometry at this section.

4.2.Rail deflection under static loading (elastic deflection)

The measurement of track elastic deflection was conducted by the Benkelman-beam method with a ballast wagon of around 20.0 t axle load. The static track behavior of sections 1 and 2 has been initially measured in November of 2005 by the Technische Universität München^[21]. Additionally, the figures of the overlap of the maximum rail and slab deflection can be found in appendices 11 to 12, whereas the statistical analyses of the measurement results are shown in Table 16 to Table 17.

Table 16: Statistical analysis of rail seat deflection at sections 1 and 2 *)

| Side of the measurement | Section 1 (Ballastless track type 1) | | Section 2 (Ballastless track type 2) | | |
|---------------------------------|---|-------------|---|-------------|------|
| | Field side rail | Inside rail | Field side rail | Inside rail | |
| Time of measurement | 2005 | 2013 | 2013 | 2013 | 2005 |
| Number of measurements | 49 | 60 | 60 | 50 | 50 |
| Served wheel load (kN) | 90 | 105 | 95 | 105 | 90 |
| Maximum (mm) | 1.46 | 1.62 | 1.27 | 1.69 **) | 1.46 |
| Minimum (mm) | 1.23 | 1.18 | 1.02 | 1.19 **) | 1.22 |
| Mean value (mm) | 1.35 | 1.44 | 1.15 | 1.39 **) | 1.33 |
| Standard deviation (mm) | 0.06 | 0.07 | 0.06 | 0.12 **) | 0.06 |
| Coefficient of variation (%) | 4.4 | 4.9 | 5.2 | 8.7 **) | 4.4 |

*) : deflected rail shows positive value

**): Change of track stiffness quality due to level compensation work (see Annex 7)

Table 17: Statistical analysis of rail seat deflection at sections 3 and 4 *)

| Sub-ballast-mat | Section 3 | | Section 4 | | | |
|---------------------------------|-------------------------|-----------------|----------------------|-----------------|--------------------|----------------|
| | without sub-ballast-mat | | with sub-ballast-mat | | | |
| Time of measurement | 2012 | | | | | |
| Side of the measurement | Field side rail | Insid e rail | Field side rail | Insid e rail | Field side rail | Inside rail |
| Number of measurements | 75 | 75 | 43 | 23 | 7 | 7 |
| Served wheel load (kN) | 100 | 85 | 100 | 85 | 100 | 85 |
| Maximum (mm) | 1.25 | 1.05 | 1.29 | 1.10 | 2.33 | 2.10 |
| Minimum (mm) | 0.86 | 0.77 | 0.91 | 0.89 | 2.10 | 1.90 |
| Mean value (mm) | 1.05 | 0.90 | 1.03 | 0.99 | 2.21 | 2.00 |
| Standard deviation (mm) | 0.08 | 0.07 | 0.09 | 0.07 | 0.08 | 0.08 |
| Coefficient of variation (%) | 7.8 | 7.9 | 8.4 | 7.2 | 3.4 | 3.7 |

*) : deflected rail shows positive value

According to Table 16, the general track quality, specified by the term “coefficient of variation” (CV), is indicating the advantage of the modern ballastless track in maintaining the track stiffness index. It is also clear that there are no major differences between the values measured in 2005 and 2013, for section 1. Due to the applied level compensation at the section 2 against irregular settlement (see Annex 7), the CV is increased in 2013 compared to the value in 2005.

According to Table 17, due to the partial installation of sub-ballast-mat at the test section 4, the data are analyzed separately. In general the rail deflection is determined by the stiffness of the fastening system, the deflection behavior of the sleepers within the ballast as well as by the deflection of the ballast, of the base layers at the superstructure and of the sub-grade. It is concluded that the actual track quality is on a very good level and the track stiffness varies insignificantly.

Moreover, the introduction of sub-ballast-mat can generally improve the quality of the dynamic vehicle-track interaction and hence, these sections have limited CV. Nonetheless, the general idea of evaluating the track quality based on the analysis of CV might be critical here. The reason being is the different number of measurement points as well as, the unsmooth transition between the two sections. Therefore, the quality of vehicle-track interaction should be analyzed through modern numerical simulation technologies while aiming at a real-time calculation method.

Additionally, the maximum deflection value is influenced not only by the elastic properties of single rail seat, but also by the rail seats nearby. Therefore, it would be useful if the deflection line for each rail seat is given. Appendices 13 to 16 show a typical deflection distribution for each rail seat (sections 3 and 4, each with 9 values, rail seats 1 – 8 have less values because there are no measurement data for interpolation). The different colors specify the measurement source of the data. These data are used as reference values at the FEM model verifications.

4.3.Dynamic rail bending behavior

Various dynamic measurements under quasi-static test runs and operational train runs were performed at each section.

4.3.1. Automatic peak finding of the measured dynamic strain

Due to the huge amount of raw data of each single measurement, the task of retrieving the strain peaks is time consuming. In order to achieve a higher efficiency of data processing, a MATLAB program was developed. The program automates the peak selection even in the case when a certain amount of measurement channels contains electronic disturbances. A Graphical User Interface (GUI) was also established. Moreover, the automatic program also overlaps the selected peak values with the raw data by showing a green dot at the respective location. All the measured raw data together with the retrieved peaks are illustrated as graphics after each calculation, which ensures an easy inspection. The GUI interface is shown in Figure 16. Sample graphical output of raw data sets and the retrieved peaks (green points) can be found in appendices 17 to 18. User's specifications and instructions are provided in [User Instruction manual 2](#).

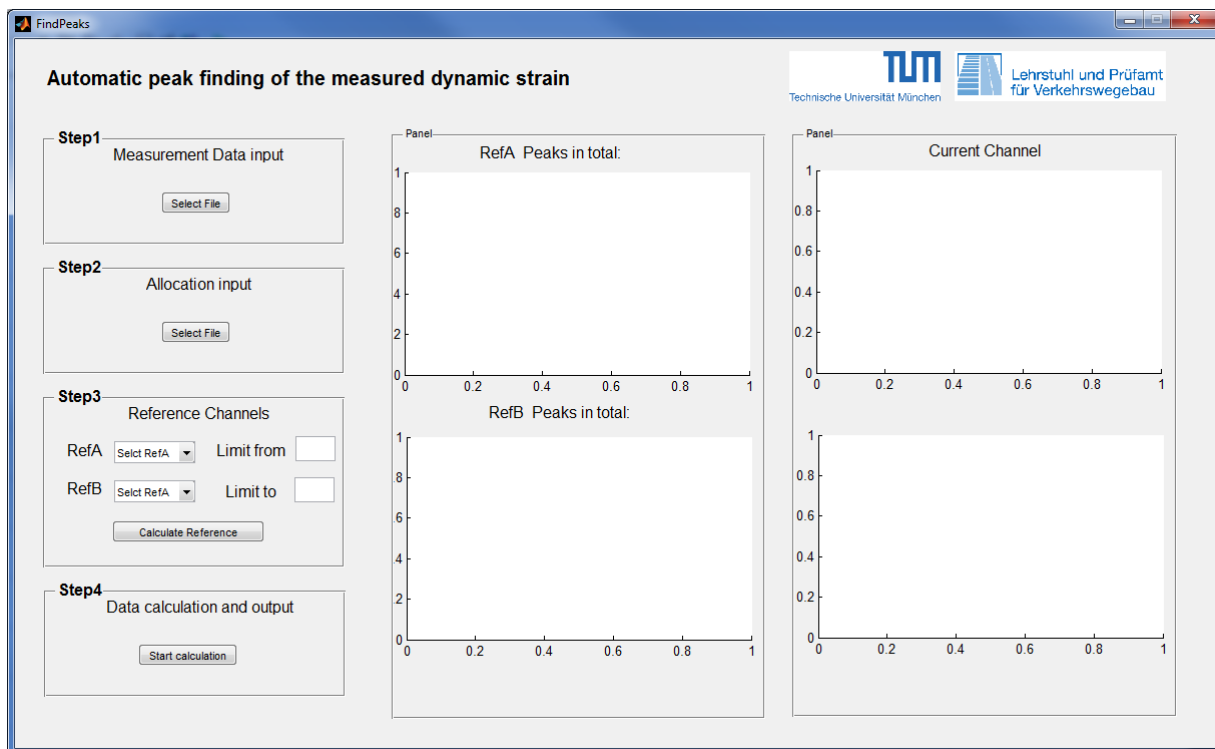


Figure 16: Automatic peak selection (GUI interface)

4.3.2. Calibration runs with quasi-static loading

Quasi-static runs ($V < 15$ km/h) were recorded with the ballast wagon used for the Benkelman beam test at sections 2, 3 and 4, each with 5 to 10 runs. A statistical analysis of the measured values of the ballast wagon provides a good reference of the track quality on behalf of the track stiffness distributions, since the dynamic effect due to irregularity can be neglected under quasi-static runs. Table 18 shows the statistical analysis of the test runs. The same type of ballast wagon was used at all the sections.

Table 18: Statistical analysis of rail foot bending stress of the quasi-static test runs

| | Section 2 | | Section 3 | | Section 4 | | | |
|---|--------------------------|------|---|------|-----------|--------------------------------------|------|------|
| Axle number | 1 | 2 | 1 | 2 | 1 | 2 | 1 | 2 |
| Track structure | Ballastless track type 2 | | Ballasted track without Sub-ballast-mat | | | Ballasted track with sub-ballast-mat | | |
| Time of operation | 2005 | | 2013 | | | | | |
| Time of measurement | 2013 | | 2012 | | | | | |
| Number of measured points | 8 | | 29 | | 30 | | | |
| Axle load (t) | 21 | 20 | 20 | 17 | 20 | 17 | 20 | 17 |
| Mean value (N/mm ²) | 60.3 | 59.3 | 52.5 | 44.1 | 52.4 | 50.2 | 64.8 | 62.4 |
| Standard deviation (N/mm ²) | 7.97 ^{*)} | 7.03 | 3.21 | 3.29 | 3.89 | 3.82 | 2.63 | 2.79 |
| Coefficient of variation (%) | 13.2 ^{*)} | 11.8 | 6.1 | 7.5 | 7.4 | 7.6 | 4.1 | 4.5 |

^{*)}: Appearance of higher values due to level compensation work (see Annex 7)

The analysis excludes the section 2 due to the applied level of compensation (see Annex 7). The Section 4, with sub-ballast-mat, achieves a better track quality (smaller CV), showing generally smaller values than in similar sections without sub-ballast-mat.

No detailed discussions are made because the values shown above cannot generally provide any guidelines related to the behavior under dynamic runs, since the travel speed is limited. Another important effect is that modern passenger trains have much better dynamic performance than the conventional ballast freight wagon.

By referring to the previous statistical results of the Benkelman beam measurement, a very good correlation of the coefficient of variation in both sections 3 and 4 is found, which again proves that the travel behavior under quasi-static runs is dominantly decided by the track stiffness distribution.

4.3.3. Rail bending behavior under operational train runs

The allowable passage speed for each type of train in each section varies; therefore a first overview of the normal passage speed for each train is shown in Table 19:

Table 19: Frequent measured passage speed of all the train types

| Measurement sections 1 & 2 | | Measurement sections 3 & 4 | |
|----------------------------|---------------------|----------------------------|---------------------|
| Train type | Normal speed (km/h) | Train type | Normal speed (km/h) |
| IC / RE | 200 | Railjet / IC (RJ / IC) | 160 – 180 |
| ICE T | 230 | ICE T | 160 – 180 |
| ICE 3 | 300 | WB | 160 – 180 |
| ICE 1 / ICE 2 | 250 | OIC | 120 |
| | | Freight | 80 |

The train type ICE-T was recorded at all measurement sections. Besides, the types IC / RE and the RJ / IC have similar design approach and axle loading. Hence, the aforementioned train types provide a “bridge” for the horizontal comparison among all the measurement sections.

Due to operational variations, ICE-T had too few examples in the measurement sections 1 and 2. Therefore, the attention is drawn into the type “IC” at all the measurement sections. The locomotive and the passenger wagons are excluded from the analysis needs since they carry different axle loads. The following Table 20 shows the statistical analysis results for the locomotive of type “IC” in all the sections. This locomotive holds a static axle load of 21.5 t.

Table 20: Statistical analysis of the dynamic rail foot bending stress of the measured locomotive of type “IC” (static axle load of 21.5 t)

| | | Section 1 | Section 2 | Section 3 | | Section 4 | |
|--|---------|-----------|-----------|-----------|-------------------|-----------|-------------------|
| Year of measurement | | 2013 | 2013 | 2013 | 2014 | 2013 | 2014 |
| Speed of passage (km/h) | | 200 | 200 | 160 | 180 ^{*)} | 160 | 180 ^{*)} |
| Mean value (N/mm ²) | Average | 62.8 | 64.2 | 58.9 | 56.8 | 61.8 | 58.1 |
| | Max | 84.9 | 83.5 | 78.5 | 83.6 | 83.4 | 87.8 |
| Standard deviation (N/mm ²) | Average | 3.48 | 2.78 | 3.91 | 4.87 | 4.82 | 4.89 |
| | Max | 6.18 | 5.54 | 8.63 | 8.06 | 11.21 | 12.28 |
| Coefficient of variation (%) | Average | 5.52 | 4.31 | 6.65 | 8.77 | 7.99 | 9.32 |
| | Max | 9.06 | 8.87 | 12.42 | 15.02 | 17.62 | 20.04 |

^{*)}: measured trains with passage speed between 160 and 180 km/h

The “Coefficient of Variation” (CV) is found to be the best parameter to assess the overall quality of the dynamic vehicle track interaction. The general dynamic increase of the wheel load is approximately concluded from those CV values. Therefore, all the recorded runs with selected locomotive type “IC” were assembled together and the analysis of the CV value, dependent on the location, was made.

Figure 17 to

Figure 20 show the distribution of the points for all the measurement sections. Measurement sections 1 and 2 are packed together due to similar distribution of the value. The curves of the measurement sections 3 and 4 contain the value measured in 2013 and in 2014.

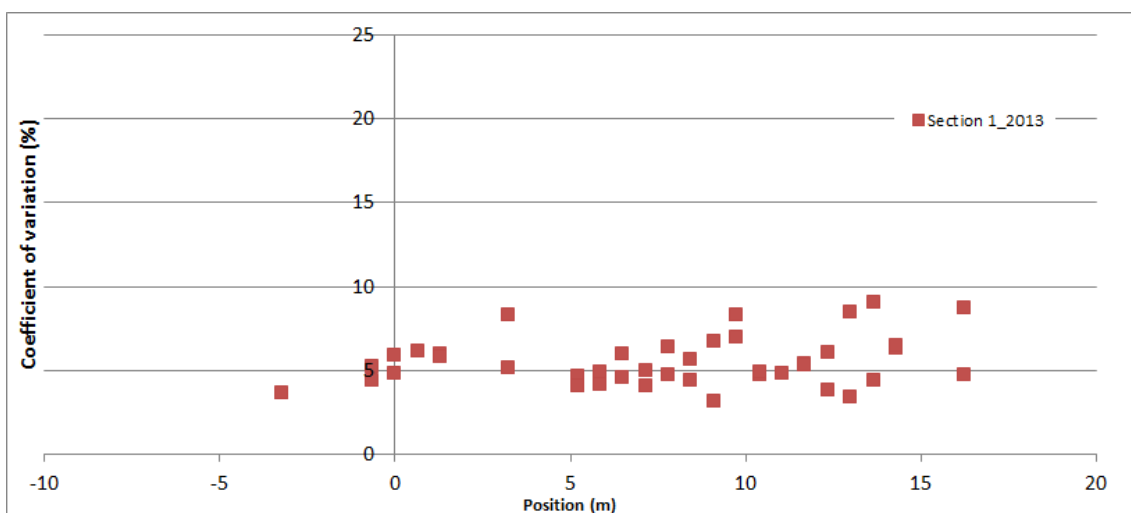


Figure 17: CV of locomotive – Section 1 (passage speed of 200 ± 10 km/h)

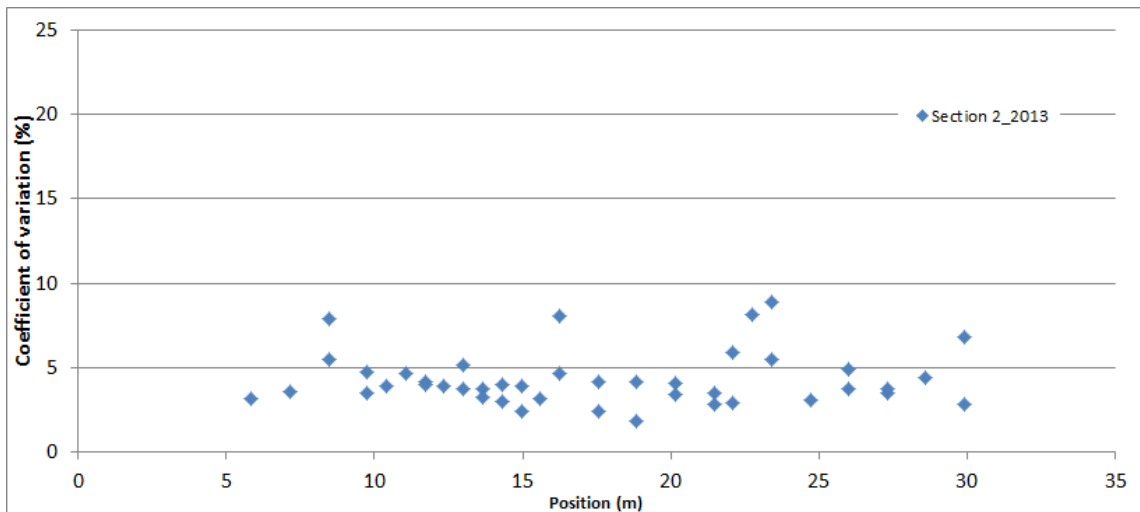


Figure 18: CV of locomotive – Section 2 (passage speed of 200 ± 10 km/h)

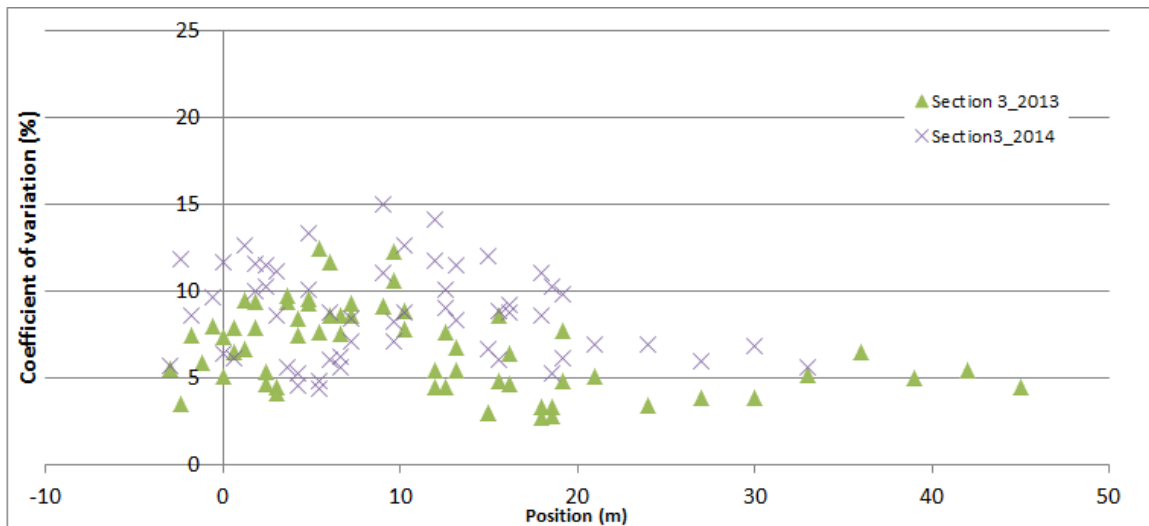


Figure 19: CV of locomotive – Section 3 (passage speed of 160 ± 10 km/h)

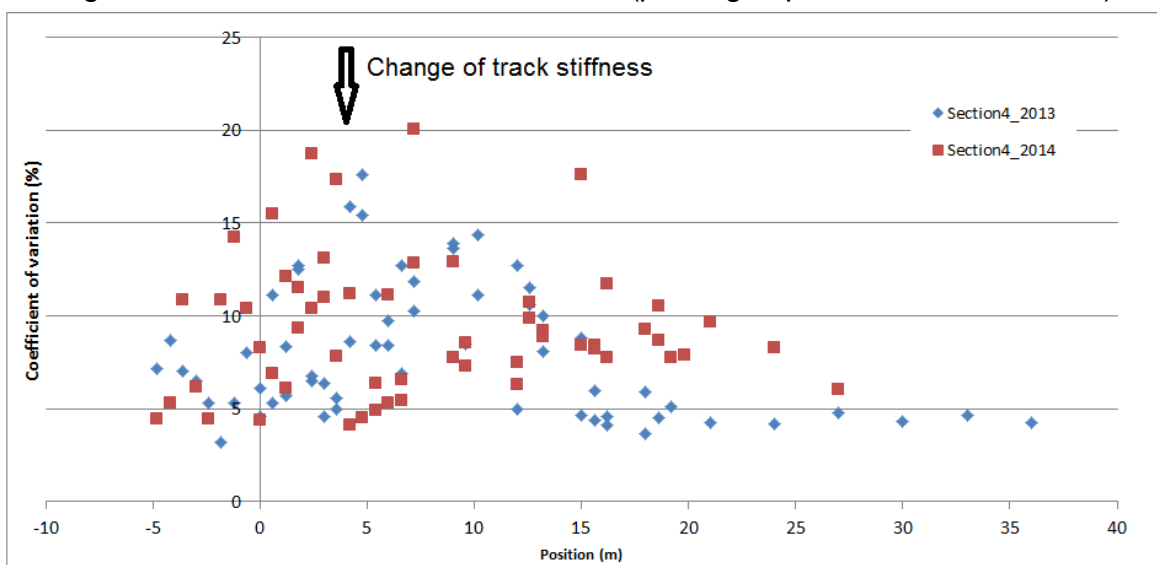


Figure 20: CV of IC locomotive – Section 4 (passage speed of 160 ± 10 km/h)

The values of sections 3 and 4 are generally higher than for sections 1 and 2 even when those values were measured under a lower speed level. By refereeing to the longer operational period of sections 1 and 2, the advantage of ballastless track in maintaining good track quality is again concluded (even in section 2 with applied level compensation work against irregular settlement, see Annex 7). The values of sections 1 and 2 are all below 10.0 %. Nevertheless, for section 2, there were only 2 runs (12 data sets) measured, since the section is located in a station with side track.

At sections 3 and 4, there is an area where the CV values are much higher than at other areas (for section 3 between 0 and 18 m and for section 4 between -5 and 20 m). In order to gain a better understanding on the reasons for this increase, the Table 21 and Figure 21 show the measured elastic deflection only within this area. Hence, the reason behind the increase of CV values remains within limited length, where significant change of track geometry occurs, and in other words, higher curvature. Therefore, those aforementioned areas are already determinant for the overall track quality indexes.

Table 21: Change of vertical track geometry in sections 3 and 4

| | | Section 3 | Section 4 |
|----------|-----------------------|-----------|-----------|
| Geometry | Height change (mm) | 3.0 | 6.0 |
| | Within the length (m) | 10 | 10 |

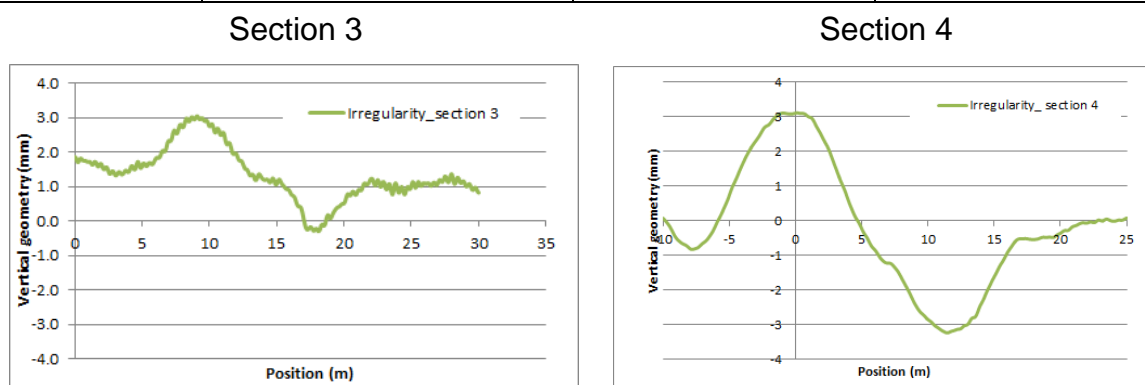


Figure 21: Change of vertical track geometry in sections 3 and 4 (selection)

The other values measured at sections 3 and 4 should be able to provide the guideline of track quality for modern high speed ballasted tracks. A maximum CV value of 10.0 % is set, showing a relative comfortable and safe track. The values measured in 2014 were slightly higher than those measured in 2013, possibly due to the increase of

speed from 160 to 180 km/h, rather than the change of track quality parameters. This observation could be also true for the values measured in section 4.

At the location of stiffness change in section 4 ($x = 4.2$ m), the CV on the measured dynamic rail foot stress achieves the highest value. By combining the values measured in section 3, the effect of the increase of the dynamic wheel load at about a generally extra 5 – 10 %, is expected, due to this stiffness change. Moreover, the change of travel speed affects the length of the influence area (between 0 and 15 m in 2013 and between -5 and 20 m in 2014). Therefore, the assumption of a longer influence area with the increase of passage speed is verified.

The average of the characteristic CV values for the three categories “Passenger wagon”, “Locomotive” and “Electrical Multiple Units (EMU)”, shown in Table 22, illustrate the influence of the vehicle to the dynamic vehicle track interaction. Detailed analysis and graphical documentations can be found in appendices 19 to 21.

Table 22: Average and Max of CV of max rail bending stress for selected train types

| | Section 1 | Section 2 | Section 3 | | Section 4 | |
|---------------------|------------------------------|-----------|--------------------------------|-------|-----------|-------|
| Year of measurement | 2013 | | 2013 | 2014 | 2013 | 2014 |
| | Coefficient of variation (%) | | | | | |
| Type and speed | BR 101 (200 km/h) | | BR 1116 (160 km/h) | | | |
| Average | 5.52 | 4.31 | 6.65 | 8.77 | 7.99 | 9.32 |
| Max | 9.06 | 8.87 | 12.42 | 15.02 | 17.62 | 20.04 |
| Type and speed | IC Wagon (200km/h) | | IC wagon (160 km/h) | | | |
| Average | 13.05 | 11.60 | 6.91 | 8.50 | 8.35 | 8.54 |
| Max | 15.41 | 14.76 | 9.71 | 11.63 | 11.00 | 15.78 |
| Type and speed | ICE-T (230 km/h) | | ICE-T (160 km/h) | | | |
| Average | - | 6.47 | 7.66 | 8.93 | 7.65 | 8.17 |
| Max | - | 7.64 | 9.69 | 12.5 | 9.82 | 13.13 |
| Type and speed | ICE1/2 Loco (250 km/h) | | | | | |
| Average | 6.2 | 7.87 | - | - | - | - |
| Max | 8.84 | 9.35 | - | - | - | - |
| Type and speed | ICE1/2 Wagon (250 km/h) | | Railjet wagon (160 - 180 km/h) | | | |
| Average | 6.44 | 8.93 | 8.32 | 9.35 | 7.42 | 9.09 |
| Max | 9.72 | 11.42 | 11.48 | 13.35 | 11.58 | 13.33 |
| Type and speed | ICE 3 (300 km/h) | | | | | |
| Average | 8.65 | 9.21 | - | - | - | - |
| Max | 11.14 | 12.56 | - | - | - | - |

The average and the maximum CV for ICE-T at section 2 is smaller than at sections 3 and 4, again indicating that the track quality at section 2 is better, due to the implementation of modern ballastless track (even under the applied level compensation at section 2 against irregular settlement, see Annex 7). This is also the case for the locomotives in both sections.

The “IC wagon” for all the sections has the same maximum design speed of 200 km/h. The CV values at sections 1 and 2 are higher than at sections 3 and 4, mostly due to the difference on passage speed. Although, the maximum values are similar, the average values are quite different. This shows the reduction of travel quality while approaching the maximum design speed.

Since the passenger wagons for “Railjet” have design speed of 250 km/h, these values are compared with the wagons from “ICE 1/2”, which generally hold the same specifications. Under this base, although the values from both types are similar, the recorded values at sections 1 and 2 have much higher passage speed, which once more leads to the same conclusion concerning the track quality between the sections.

The ICE 3 with passage speed of 300 km/h could cause smaller dynamic effects in comparison to the IC passenger wagon passing with 200 km/h, since the speed of 200 km/h has already achieved the maximum allowable speed for this wagon. It can be therefore concluded, that the vehicle design is also an important factor influencing the dynamic vehicle track interaction and there is no evidence that a vehicle running at higher speed causes higher dynamic loading. This is proven even from the test runs at same location. This could best indicate that the research of dynamic vehicle track interaction must rely on real-time virtual and numerical simulation programs.

4.4. Test of track vibration level

Understanding the track vibration behavior under train runs is one of the most important aspects in the research of dynamic vehicle-track interactions. Those vibrations are a real-time reflection of the counteractive effect related to the elastic and damping behavior of the track and vehicle.

Track vibration is the output of all the key parameters which interact during a train passage. The important parameters are the dynamic wheel load, the track geometry, the track stiffness and damping, the vehicle design, etc.

In order to separate the influence on the track or on the vehicle, a track-oriented calibration with impact hammer is performed in advance. By simplifying the impact load on the track in a form as dirac delta function ^[8], an intuitive comparison of track sided parameters is achieved. By retrieving this information related to the track sided behavior, the vehicle sided influence under dynamic train runs can also be efficiently analyzed.

Sample raw measurement data and processed data can be found in appendices 22 to 23.

4.4.1. Track vibration level under impact load

Attention should be drawn to the overall behavior of different systems according to the applied impact loading. Therefore, the measurement results from sections 1 and 2 as well as from 3 and 4 are averaged. Figure 22 to Figure 23 show the measured average vibration velocity at the rail and sleeper / track block.

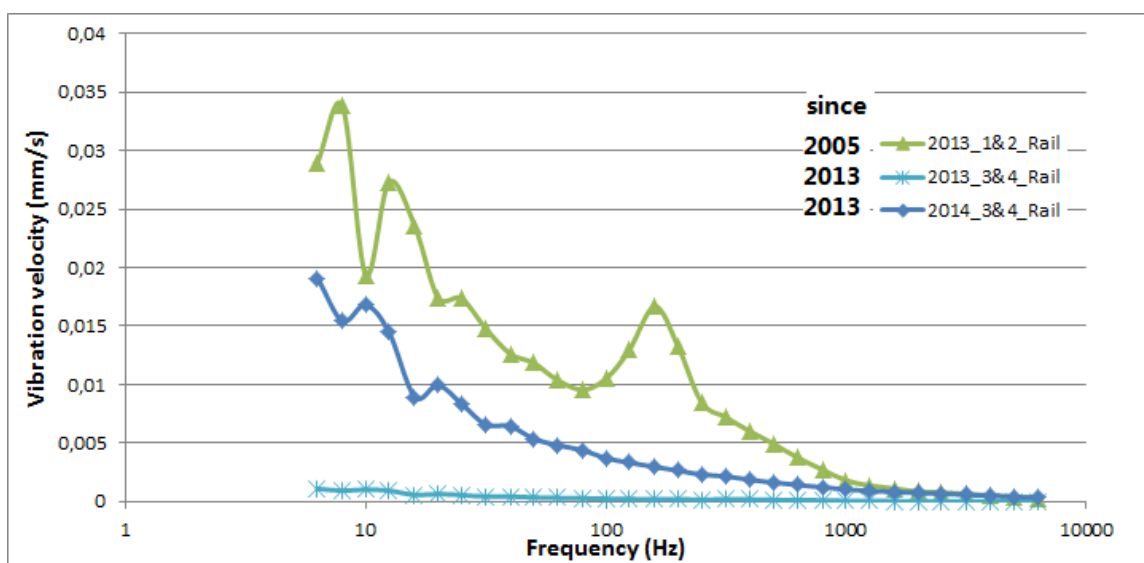


Figure 22: Vibration velocity on rail under hammer excitation

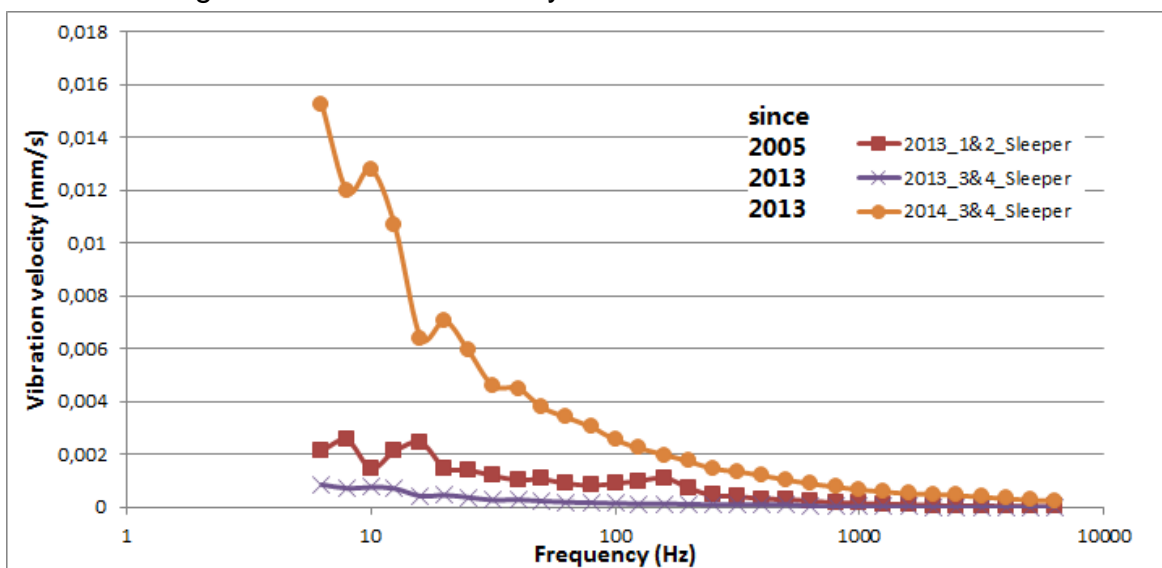


Figure 23: Vibration velocity on sleeper under hammer excitation

It can be seen from Figure 22 that the vibration velocity on rail, in the case of the ballastless track, is generally higher compared to ballasted track, due to the softer design of the rail fastenings, which provides on the other hand very good vibration protection at the slab. By also taking into account the initial operation year, the advantage of ballastless track system to maintain the track quality and to regulate the settlement is obvious.

The shape of the spectrum distribution of rail foot of the ballastless track (1&2) is different from the distribution of the ballasted track (3&4). A clear peak value at 160 Hz for the rail is easily found for ballastless track systems, but not for ballasted tracks. The ballastless track has a damped vibration velocity at around 10 Hz at the rail, while a small amplification for ballasted track is observed.

Shown by Figure 23, it could be found that the average vibration velocity of sleeper for sections 3 and 4, measured in 2014, is increased compared to 2013. Particularly, for the sensors on sleeper, the vibration velocity under low frequencies is increased at about 10 times. This might be due to the weaker support of the surface ballast at the sleeper contact area. In other words, the sleeper becomes more “flexible”.

4.4.2. Track vibration level under operational trains

Useful information provided by the impulse load test is the illustration of track vibration under the same unit load, which can explain the track vibration problems under operational trains.

The vibration level under operational trains in rail and sleeper is strongly dependent on the individual contact quality between the wheel and the rail, the so-called wheel flat. The trains with wheel flat cause a very high vibration level at rail and sleeper. Sample illustration of this effect is illustrated in Figure 24. This is especially critical for the low frequency vibrations. Therefore, all the analyses in this chapter exclude the trains with local wheel flat.

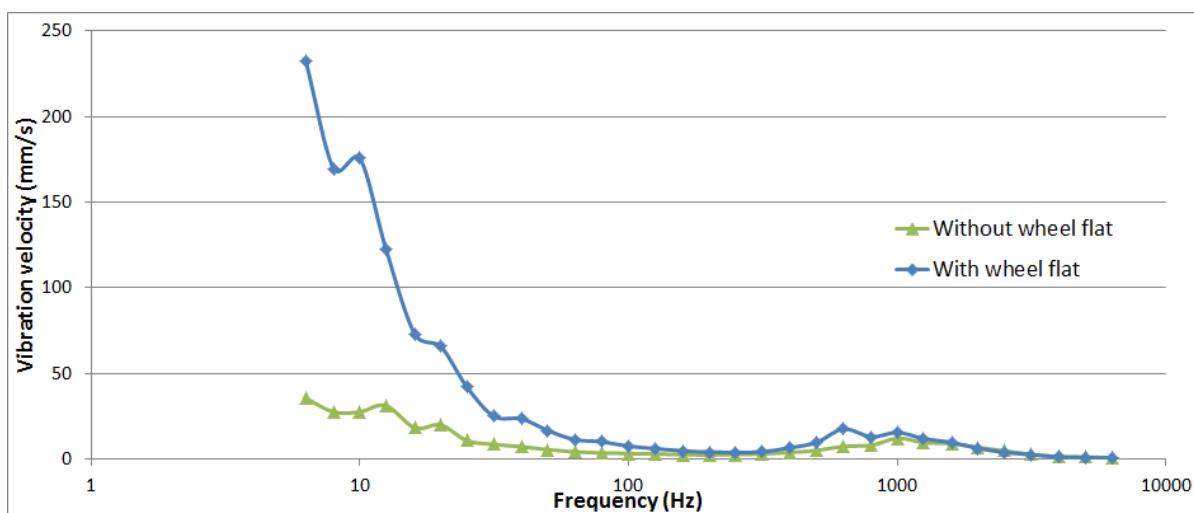


Figure 24: Effect of trains with wheel flat (passage speed of approximately 80 km/h)

The major interests for this part lay on the comparative behavior of the track for sections 3 and 4 measured in 2013 and in 2014. Since similar distribution of vibration velocity, the train type “InterCity” was selected due to the good amount of measured samples. Figure 25 shows the analyzed vibration velocity distribution (all included data sets exclude the wheel flat).

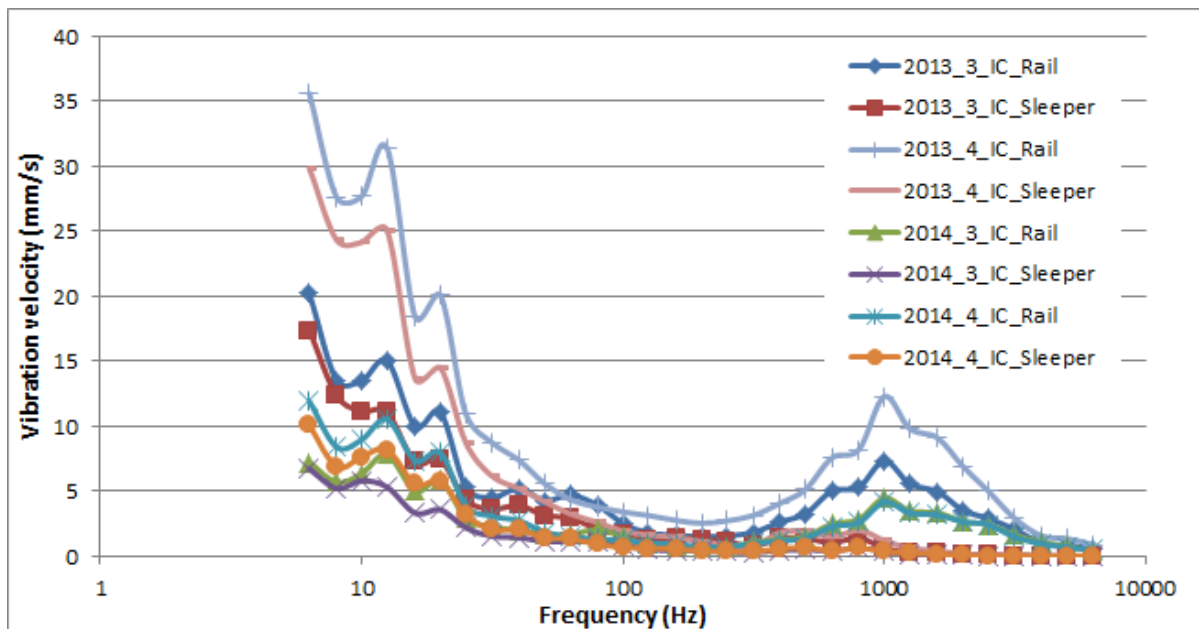


Figure 25: Distribution of vibration velocity – train type IC (V = 160 km/h)

The vibration velocity measured in 2014 is generally smaller than in 2013, for all the measured channels, possibly due to adjustment effect of track superstructure.

Due to the introduction of sub-ballast-mat in section 4, the vibration at rail and sleeper is also higher than in section 3. But it should be considered that the true function of the sub-ballast-mat is to provide better isolation of the track sided vibrations to the substructure. Therefore, it can be assumed that the ground vibration will be smaller in section 4 than in section 3 due to the appearance of the sub-ballast-mat. Since the scope of this research does not include the functionality study of the sub-ballast-mat, no further measurements in ballast and surrounded structure were made.

Comparing the channels “Rail” and “Sleeper” for each group, it can be observed that higher rail vibration is always correlated to higher sleeper vibration and thus, the support under the sleeper is the source of all the changes in the behavior. Similarly, it can be stated that the ballast is the most determinant layer specifying the general track quality for ballasted track system and hence, no obvious change at the quality of the rail fastening systems should be expected.

Similar tendencies are found for the other train types. These analyses are provided in appendices 24 to 25.

4.5.Data provision for the numerical simulations

The track measurement methodologies can be categorized according to the aim of the track assessment as follows (see Table 23). The data that are used for the further numerical simulation models were also shown to illustrate the way the measured values are used in the models:

Table 23: The measurement items and their functionalities for the numerical models

| Item | Location | Parameters measured | Data provision for numerical models | |
|-----------------------------|----------------------|---------------------------|-------------------------------------|--|
| Geometry | rail head | plastic track deformation | MBS (Input) | Track irregularity input |
| Displacement (quasi-static) | rail absolute | Elastic track deformation | FEM (Input) | Track stiffness input |
| Strain / stress | rail foot | Dynamic wheel load | FEM + MBS (Output) | Dynamic wheel rail interaction |
| Acceleration | Rail foot or sleeper | Track vibration level | MBS (Output) | Vibration of the track according to train runs |

Clearly, for a systematic understanding of the track behavior under running trains, both FEM and MBS methodologies are necessary. The written ‘Input’ is referring to the parameters which are needed at the model’s calibrations, while the written ‘Output’ is referring to the parameters which are the results of the simulations.

It should be mentioned that for FEM and MBS, more parameters including the profiles and design parameters should be also provided. However, these are not parameters retrieved from the measurements and they were not listed in the table above.

A detailed application of the modeling strategies is given in Chapter 5.

5. THE NUMERICAL MODELING

5.1. Introduction

As revealed in Chapter 2, a more detailed understanding of the track behavior concerning the vehicle-track interaction can be achieved through numerical models. Various modeling approaches are applied in order to better accomplish the requirement, including the FEM (Finite-Element-Method) and MBS (Multi-Body-Simulation).

A numerical model concentrates only on a part of object's behavior in reality and simplifies the others. In this chapter, various kinds of models based on the field measurement are introduced. These models are developed with different objectives. Imaginary data, as well as experience data, are also used to define parameters of the models. These models utilize FEM and MBS approaches to solve the problems.

The general structural tree of utilizing measurement data for different modeling strategies is shown in Figure 26. The colored circles on the top right of each step symbolize the respective applied technology (refer to section 2.3.5 for software version information). The step 2.2 (model 1), which refers to the FEM modeling on behalf of track stiffness, is firstly performed. The step 3.1 (model 2) reads the input of the vehicle design and measured track irregularity to calculate the dynamic output of the vehicle track interaction. By condensing the FEM model with substructuring and modal analysis, the real-time response of elastic track due to passing train loads is able to be calculated (step 3.2, model 3). The final step – step 4.1 (model 4) – is the result of MBS calculation, which includes the wheel-rail contact, the track irregularity and track stiffness (coming from the condensed FEM model).

All the included software programs and their versions can be found in Table 24.

Table 24: Comparison of FEM and MBS approach

| Type of software | Name of Software | Symbol | Version / valid since |
|-----------------------|------------------|--------|-----------------------|
| Data processing | EXCEL (VBA) | ● | 2010 / 2011 |
| Data calculation | MATLAB | ● | 2012a / 2012 |
| Data measurement | CATMAN | ● | AP / 2010 |
| Acceleration analysis | MEDA | ● | 2013-1 / 2013 |
| FEM | ANSYS | ● | 14.0 / 2013 |
| MBS | SIMPACK | ● | 9.7 / 2014 |

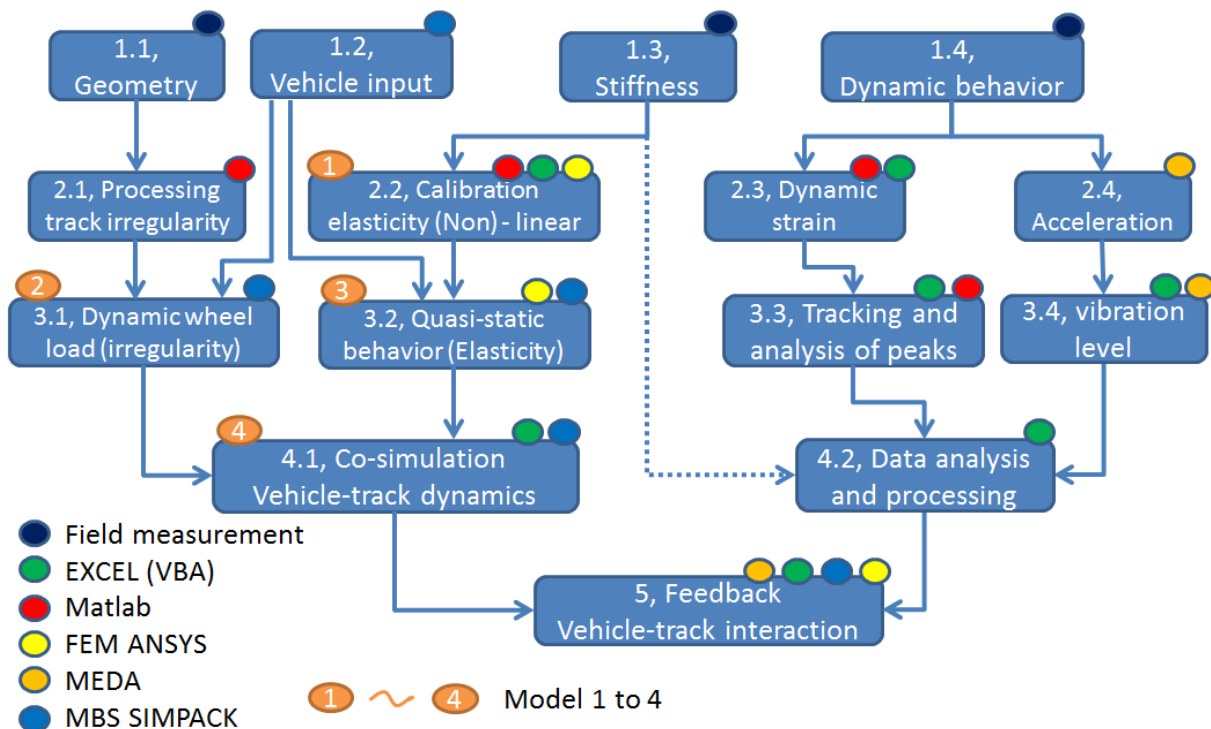


Figure 26 General modeling process

The ballasted track with stiffness change in measurement section 4 (right rail) is used as illustration for all the introduced models, because it is the most challenged case due to intermediated change of stiffness. The simulation results of other measurement sections can be found in chapter 6. The definition of motion directions are found in Table 25.

Table 25: Directions of motion for numerical models

| | X | Y | Z | α | β | γ |
|-----------|--------------|---------|----------|----------|---------|----------|
| Direction | Longitudinal | Lateral | Vertical | Sway | Yaw | Pitch |

5.2. Model 1 (FEM) – Calibration of the elastic track model based on field side Benkelman measurement

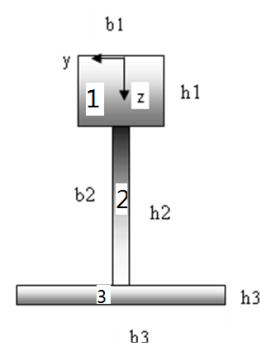
5.2.1. Introduction and modeling approach

The Finite-Element-Method program ANSYS is included for a deeper understanding of the measurement results. Simplified rail profile is used with the same physical parameters with the original profile required for calculation [22]. Table 26 shows the geometry and the parameters of the simplified model.

Table 26: Parameters of the simplified rail model [22]

| | h_i (mm) | b_i (mm) | A_i (mm ²) | Z_i (mm) | Z_s (mm) |
|---|------------|------------|--------------------------|------------|------------|
| 1 | 48.3 | 73.5 | 3550.05 | 24.15 | 83.5 |
| 2 | 114 | 19 | 2166 | 105.3 | |
| 3 | 12.8 | 150 | 1920 | 168.7 | |

With A_i – Area of the body i
 Z_i – Center of gravity of body i
 Z_s – Center of gravity of the whole system



The whole measurement section of 95 rail seats is built at ANSYS software with 75 rail seats with variable stiffness and 10 on each side with assumed values for achieving a reasonable load support at the end rail seats. The mechanism of the FEM model is shown in Figure 27. The substructure layer is integrated into the ballast layer, since there is no change in the substructure design along single section. Three elastic layers naming 'Pad' and 'Ballast + Substructure' are given with predefined unique values for each rail seat.

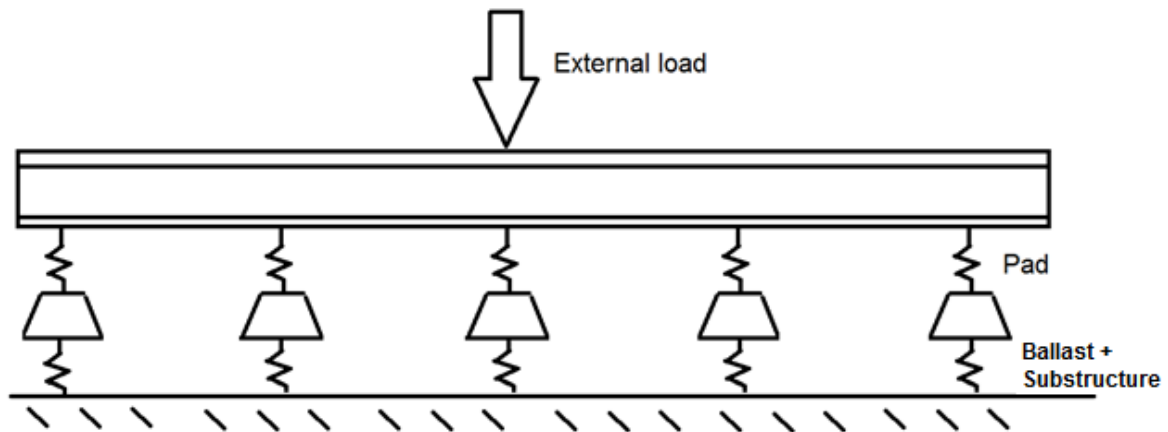


Figure 27 Principle of the FEM model

The modeling structure of pad and ballast relies on the volume element input from the FE code. It requires the Young's Modulus and Poisson number, as material input and length, width and thickness, as geometrical input. Ballast is modeled as a volume element, for simplification, because the stiffness of the ballast, and not the single ballast stone, is the most important factor for this model. A value of 30 cm thickness of ballast is given. The Young's modulus of the ballast layer is set as variable and the modulus is calculated based on measurement data. The iteration strategy is the further developed version based on the master thesis written by Mr. Hongchao MA ^[23].

5.2.2. Model setup and boundary condition

The FEM software ANSYS is used for generating the model. The Figure 28 to Figure 29 show the modeled single element and the assembled system of both ballasted and ballastless track. Different colors of substructure layers symbolize the border of different materials. Irregular meshing is used to achieve higher efficiency, as well as higher accuracy, in the model computation. The variable element is "ballast" for ballasted track and "elastic pad" for ballastless track.

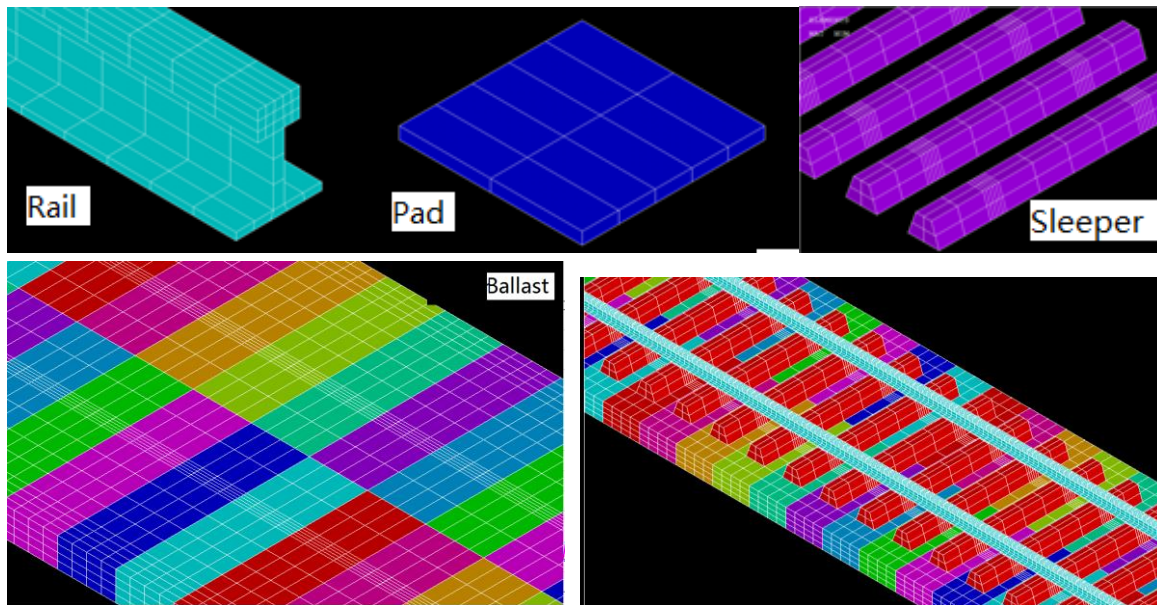


Figure 28 Graphical representation of elements and system (ballasted track)

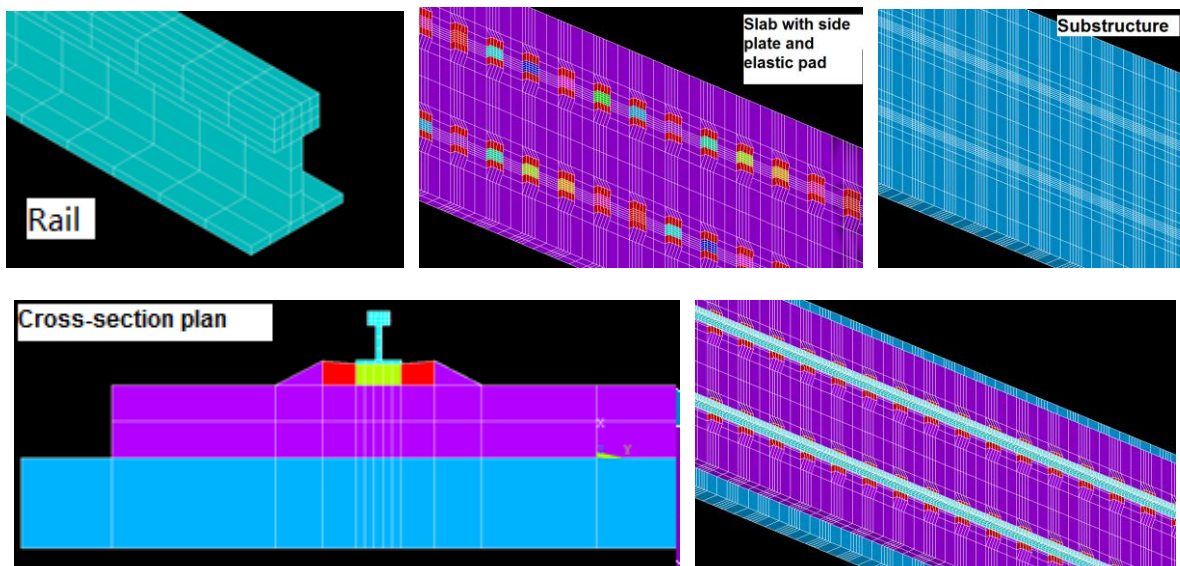


Figure 29 Graphical representation of elements and system (ballastless track)

The ballasted track system is only built by linear elastic materials, without damping input. For the ballastless track scenario, due to the implementation of high elastic rail fastenings, non-linear elastic pad model should be considered. Important reasons for this design include:

- Linear elastic approach provides very good accuracy level for standard ballasted track already;

- Significant saving of computation time in comparison with nonlinear models;
- For further requirements of other computational analyses (like modal analysis).

The application of boundary conditions mainly is according to the actual situation. The nodes from bottom side of the substructure layer on open track and transition are given 0 degrees of freedom (0 DoF).

The calibration of the model utilizes an innovative iterative approach, which is described in subsections 5.2.3 to 5.2.5. The design of the approach is according to the general process: Initial condition, iteration procedure and boundary condition. A calibration of non-linear elastic materials for elastic pad used in ballastless track is also possible.

5.2.3. The iterative process

The initial condition is firstly defined in order to examine the starting point by fixing a unique value for all Young's modulus of ballast (symbolized as E_0). A static wheel load is extracted on one rail seat, which is identical to the wheel load from the Benkelman beam measurement. The maximum deflection is calculated for the pre-defined E_0 of ballast. An exponential regression of the calculated data points is made, which can be described by the following formula:

$$E = a * S^{-b} \quad 5.1)$$

Where E – Young's modulus; S – max. rail deflection

a, b – constants which are only dependent on the model parameters

The initial parameter of Young's modulus for the substructure under each rail seat ($E_{x,0}$) can be calculated by inputting the measured maximum deflection at the rail seat $S_{x,0}$

into the formula 1. The calculated $E_{x,0}$ is imported into the software for calculating the respective rail seat deflection line.

It is clear that, there must exist a small difference (called “error”) between the measured and the simulated deflection line under certain rail seats due to possible different Young’s Modulus of the neighboring rail seats. Sample results from error analysis are shown in Table 27 ($A_{x,0}$). All errors which are bigger than 0.05 mm, are marked in yellow and the maximum value are marked in red. Sample measurement and calculation curves are shown in Figure 30. The number “0A10” represents the results after 0th iteration (initial condition) and rail seat number 10 (5th rail seat on right rail). The number “Z12” represents the rail seat deflection line calculated according to the measurement results at the rail seat 12 (6th rail seat on right rail).

Table 27: Error analysis after initial condition *)

| | RS i | RS i+1 | RS i+2 | RS i+3 | RS i+4 | Measured max. deflection (mm) |
|------|------|--------|--------|--------|--------|-------------------------------|
| | 0 m | 0.6 m | 1.2 m | 1.8 m | 2.4 m | |
| 0A10 | 0.26 | 0.47 | 0.21 | 0.07 | 0.06 | 2.04 |
| 0A12 | 0.36 | 0.31 | 0.14 | 0.08 | 0.02 | 2.10 |
| 0A14 | 0.45 | 0.18 | 0.07 | 0.00 | 0.00 | 1.98 |
| 0A16 | 0.27 | 0.01 | 0.01 | 0.00 | -0.02 | 1.44 |
| 0A18 | 0.00 | 0.00 | 0.00 | 0.00 | 0.00 | 0.84 |
| 0A20 | 0.01 | 0.00 | 0.04 | 0.00 | 0.01 | 0.74 |

*) : calculated by “Measurement – Simulation”

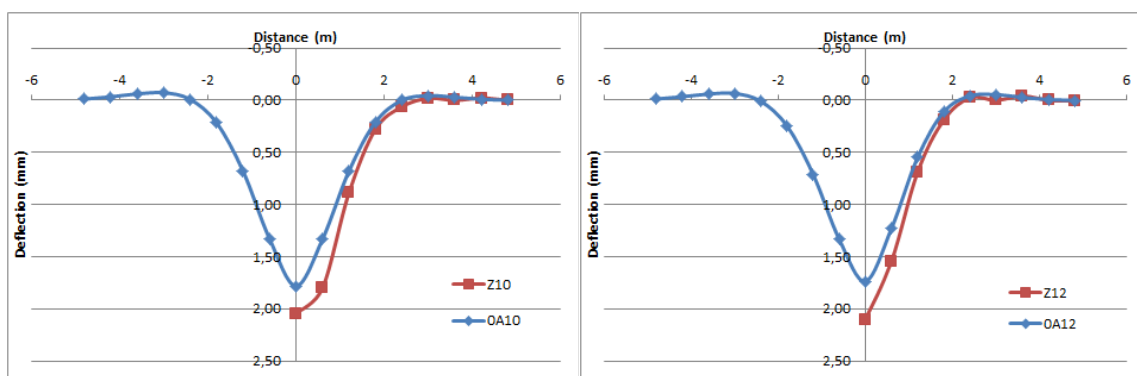


Figure 30 Sample measurement and calculation results (Rail seats 10 and 12)

Another parameter, called “weighting factor”, is also calculated by assessing the average percentage of the deflection of the neighboring rail seats to the loaded one.

In other words, the errors at the neighboring rail seats are less decisive than the errors at the loaded rail seats. This is an important factor for the definition of the new deflection value for the next iteration. To the factor is given the symbol F_i , where i from 0 to 8 representing the factor of rail seat number i . Table 28 shows the calculated factors of right rail, in section 4.

Table 28: Illustration of weighting factor

| | F1 | F2 | F3 | F4 | F5 – F8 |
|------------------|------|------|------|------|---------|
| Weighting factor | 1.00 | 0.73 | 0.38 | 0.12 | 0.00 |

A recalculation of the Young’s modulus of the ballast is required for all rail seats. This is recalculated by the so called “iteration procedure”. It utilizes the results from the last calculation and set them as the pre-conditions for the next calculation round. The recalculation of the Young’s modulus is based on the results of the error analysis from the last calculation. The new maximum deflection of the rail seat ($S_{x,n}$) is calculated by the following formula:

$$\begin{bmatrix} S_{1,n} \\ \vdots \\ S_{x,n} \end{bmatrix} = \begin{bmatrix} S_{1,n-1} \\ \vdots \\ S_{x,n-1} \end{bmatrix} + \begin{bmatrix} A_{1,1} & \cdots & A_{1,i} \\ \vdots & \ddots & \vdots \\ A_{x,1} & \cdots & A_{x,i} \end{bmatrix} * \begin{bmatrix} F_1 \\ \vdots \\ F_i \end{bmatrix} \quad 5.2)$$

with $A_{x,i}$ representing error calculated after iteration step $n - 1$

Where

$S_{x,n}$ – Calculated target deflection for rail seat x before iteration i

$A_{x,j}$ – Error “Measurement – Calculation” at rail seat x (mm)

F_i – weighting factor calculated in the initial condition (See Table 28)

n – Iteration number ($n \geq 1$)

i – Rail seat number ($i = 0$ for the loaded rail seat)

x – Loaded rail seat number

The $S_{x,n}$ is again used to calculate the $E_{x,n}$ according to formula 5.1. Then the model is again calculated for the $n+1^{\text{th}}$ iteration.

It is important to define the boundary conditions to end the iteration process. Principally the iteration should stop when the results from the n^{th} and $n-1^{\text{th}}$ iteration returns similar results (Difference < 0.01 mm). This holds the meaning that, the $n+1^{\text{th}}$ iteration will not make any further change. The boundary condition is concluded in the following formula:

$$S_{x,n} - S_{x,n-1} < 0.01 \quad (5.3)$$

with $S_{x,n}$ including all the measured neighboring rail seats i

Following this principle, the result after 6th iteration already fulfills the criterion (see Table 29):

Table 29: Boundary condition; Diff. Deflection [mm], Iteration 6 – 5 (rounding applied)

| | RS i | RS i+1 | RS i+2 | RS i+3 | RS i+4 | RS i+5 | RS i+6 | RS i+7 | RS i+8 |
|-----|------|--------|--------|--------|--------|--------|--------|--------|--------|
| | 0 m | 0.6 m | 1.2 m | 1.8 m | 2.4 m | 0 m | 0.6 m | 1.2 m | 1.8 m |
| Z10 | 0.00 | -0.01 | 0.00 | 0.00 | 0.00 | 0.00 | 0.00 | 0.00 | 0.00 |
| Z12 | 0.00 | 0.00 | 0.00 | 0.00 | 0.00 | 0.00 | 0.00 | 0.00 | 0.00 |
| Z14 | 0.01 | 0.01 | 0.00 | 0.00 | 0.00 | 0.00 | 0.00 | 0.00 | 0.00 |
| Z16 | 0.01 | 0.01 | 0.01 | 0.00 | 0.00 | 0.00 | 0.00 | 0.00 | 0.00 |
| Z18 | 0.01 | 0.01 | 0.01 | 0.00 | 0.00 | 0.01 | 0.01 | 0.01 | 0.01 |
| Z20 | 0.00 | 0.01 | 0.01 | 0.00 | 0.00 | 0.01 | 0.01 | 0.01 | 0.01 |

Table 30 shows the number of differences bigger than the limitation (0.01 mm, rounding applied) after each calculation. It can be concluded that, the iteration procedure can achieve a very quick convergence without many iteration steps. The calculation on left rail is also attached:

Table 30: Number of difference over limitation

| Between iterations | Number of difference bigger than 0.01 mm | |
|--------------------|--|------------|
| | Left rail | Right rail |
| 1 and 0 | 335 | 243 |
| 2 and 1 | 269 | 131 |
| 3 and 2 | 192 | 83 |
| 4 and 3 | 103 | 69 |
| 5 and 4 | 17 | 12 |
| 6 and 5 | 0 | 0 |
| Total numbers | 450 | 450 |

5.2.4. Results and conclusions

It is clear that when this method is applied for the track section, six iteration steps can already give a converged result. Very good identification can be found between the measurement and simulation results. Table 31 and Figure 31 show the error analysis and the final result after the 6th iteration. It can be seen, that the error is significantly reduced in comparison with the first result, before iteration (shown in Table 27 and Figure 30).

Table 31: Error analysis after 6th iteration step *)

| | RS i | RS i+1 | RS i+2 | RS i+3 | RS i+4 | RS i+5 | RS i+6 | RS i+7 | RS i+8 |
|------|-------|--------|--------|--------|--------|--------|--------|--------|--------|
| | 0 m | 0.6 m | 1.2 m | 1.8 m | 2.4 m | 0 m | 0.6 m | 1.2 m | 1.8 m |
| 6A10 | -0.04 | 0.17 | -0.04 | -0.08 | 0.01 | 0.03 | 0.00 | 0.00 | 0.00 |
| 6A12 | -0.01 | -0.05 | -0.10 | -0.01 | 0.02 | 0.00 | 0.01 | 0.00 | 0.01 |
| 6A14 | 0.05 | -0.11 | -0.04 | 0.00 | 0.00 | -0.01 | 0.00 | 0.01 | 0.00 |
| 6A16 | 0.05 | -0.07 | 0.01 | 0.00 | 0.00 | 0.00 | 0.01 | 0.00 | 0.00 |
| 6A18 | -0.01 | 0.01 | 0.00 | 0.00 | 0.00 | 0.01 | 0.00 | 0.00 | 0.00 |
| 6A20 | 0.00 | 0.00 | -0.01 | 0.00 | 0.01 | 0.00 | 0.02 | 0.00 | 0.00 |

*) : calculated by "Measurement – Simulation"

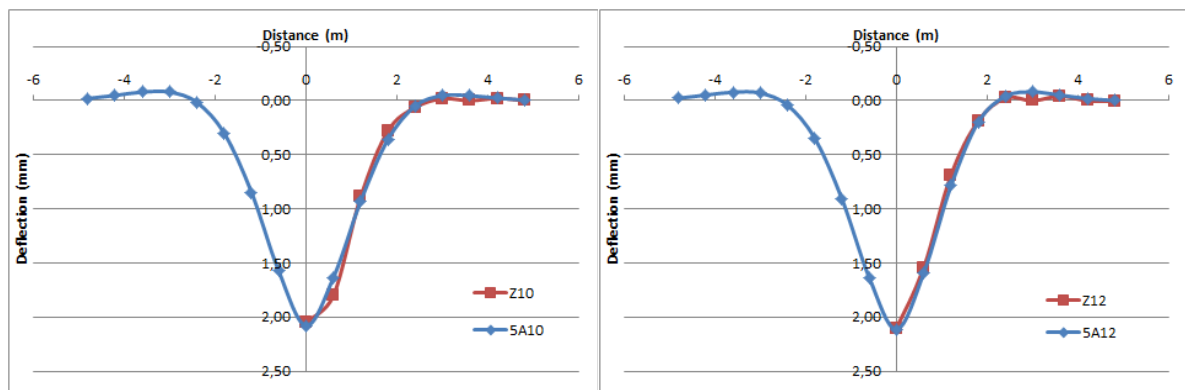


Figure 31 Measurement and calculation result after 6th iteration (Rail seats 10 and 12)

The advantage of the robust defining of the boundary condition is to provide the possibility to find the potential measurement errors at certain location. It can be further seen that the reason for 2nd value at rail seat 10, with a remaining error bigger than 0.1 mm is due to the measurement error at this location. It should be stated that a confident conclusion of the location of measurement error still requires other measurement results.

Following conclusions and perspectives can then be stated:

- The FEM program can satisfactorily rebuild the test section on behalf of elastic rail deflections;
- An innovative iteration process for calibrating the stiffness under each rail seat is developed and found to be suitable to solve the task;
- The simulation results provide a good evidence that concerning the ‘perfect overlapped’ curve, no significant measurement errors should exist.
- The simulation result can provide evidences to define measurement errors on site;
- The calibrated model can be used for further analysis requirements.

5.2.5. Automation of the iteration methods (Co-Simulation with ANSYS and MATLAB)

For smoother application and calibration of the FEM model, the iterative process is translated into the program MATLAB to automatically calibrate the model. This, so called “co-simulation” approach, replaces all the workflow which was previously executed by MS EXCEL, and decides intelligently, whether a new iteration step is required, as well the new input parameters by defining all the regulations by MATLAB based sentences. In other words, the new MATLAB command is written to control the simulation works executed by ANSYS. The principle of the structure can be found in Figure 32. The detailed program, as well as other application scenarios, can be found the internship report by L. DING [24].

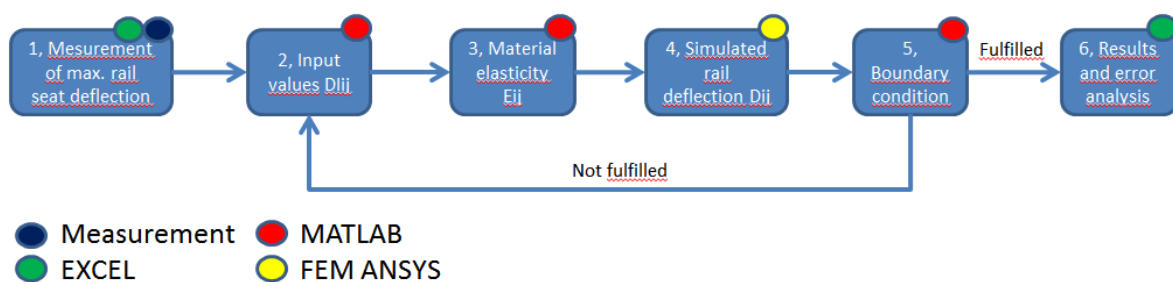


Figure 32: Structure of the co-simulation program

In order to make the program also available for regular users, as well as for easier processing of similar data sets, a Graphical User Interface (GUI) is also established. The user only needs to provide with certain input parameters at the developed MATLAB GUI interface. The calibration of the model is fully automated by the software even without the user getting contact to the ANSYS interface. All the measured and calculated curves after each iteration step automatically are output for further inspection requirements. A list of the required input parameters and comparisons of the computation time for sample data sets with EXCEL and MATLAB approaches are shown in Table 32. The GUI interface can be seen in Figure 33. The user specification and instructions can be found in [User Instruction manual 3](#).

Table 32: Comparison of the calculation time with Excel and Matlab (Model 1)

| Data sets *) | ME3 | EE2 | EE3 |
|--|--------|--------|---------|
| Standard deviation of measured data (mm) | 0.08 | 0.20 | 0.75 |
| Iterations needed | 4 | 6 | 16 |
| Time needed for EXCEL processing (min) **) | 120/45 | 180/65 | 480/165 |
| Time needed for MATLAB (min) **) | 120/4 | 180/6 | 480/16 |
| Time saving by data processing (%) | > 90 % | | |

*): “ME” for measurement section from this work; “EE” for external data

**): The first value for calculation time with ANSYS; the second value for data processing for next iteration

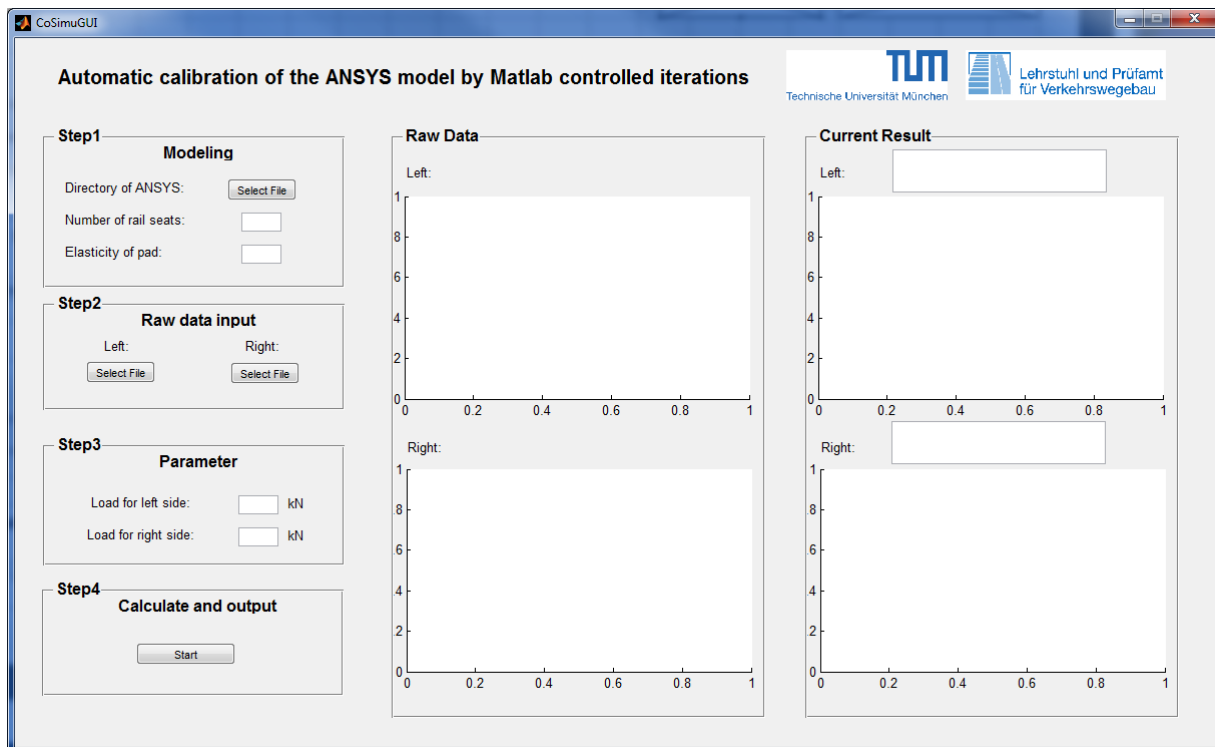


Figure 33: Automatic calibration of ANSYS model (GUI interface)

It can be easily seen, that by introducing the automated calculation software, not only the personal work but also the processing time saved is up to 90 %. This is the time saving during reading the previous calculated results and calculation of the new input parameters for the next iteration with ANSYS. Considering that those iterations can

now be performed without personal interference in between, it is extremely useful for handling large amount of data sets.

5.3.Model 2 (MBS) – Dynamic simulation of the vehicle track interaction with pre-defined track excitations

5.3.1. Background and introduction

The simulation of dynamic vehicle track interaction in a MBS system requires inputs from both vehicle and track sides. The vehicle relative data are typically the mass and suspension design, whereas the input from the track side is for this model mainly the track excitation (irregularity) without track stiffness inputs. In this model, the input factors from both vehicle and track are illustrated.

5.3.2. Modeling of the vehicle

Despite the fact that the vehicle modelling is not a critical issue for this thesis, a detailed vehicle modeling with best possible representation of reality is still necessary, because vehicles, and especially their dynamic performances, are the source of impact. Therefore, a detailed simulation of the “Mass-spring-damper” behavior of the vehicle is required. The modern E-locomotive with an axle load of around 21.5 t is selected, which holds the heaviest axle load, where the most significant dynamic wheel loading is expected.

The modelling of the locomotive is principally according to the mechanisms described in Manchester Benchmarks ^[25] with modifications of detailed values. A detailed list of modelling parameters can be found in appendix 26 (with adjusted values from master’s thesis from K. Pandey ^[26]). The basic topology of the vehicle can be found in Figure 34.

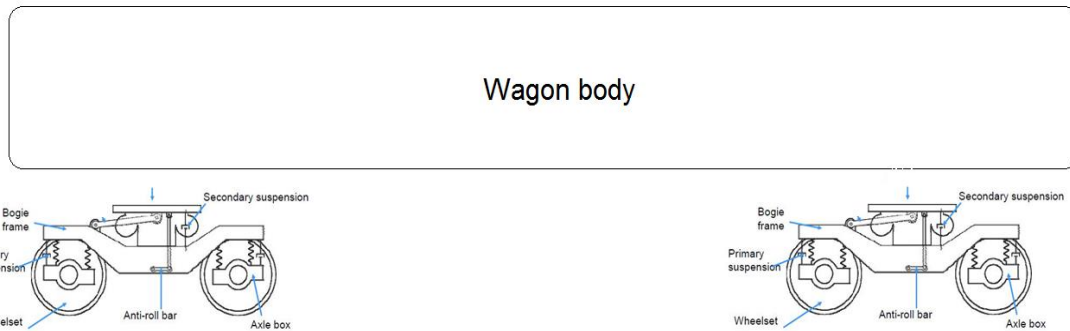


Figure 34 Topology of the vehicle with two layers of suspensions

Figure 35 shows the detailed visualization and eigen frequency analysis of the modeled bogie and vehicle.

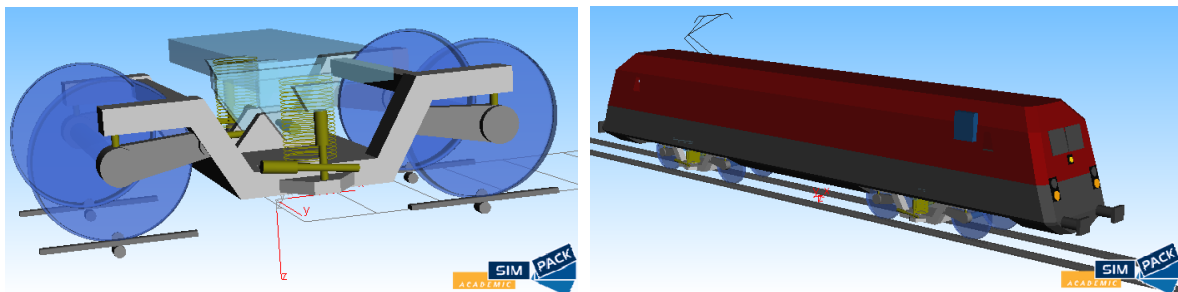


Figure 35 Modeled bogie and vehicle in Simpack

The eigen values of the rigid car body and bogie frame modes for stable simulation results are given below. They symbolize the vehicle sided characteristic vibrations. Only the bounce and yaw modes are included because those modes are determinant for the vertical vehicle behavior. The motion of vibration and their eigen frequencies are shown in Figure 36 and Table 33. The bounce and yaw motion of the bogie frame especially is significant, influencing the overall dynamic behavior of the vehicle track interaction, since this is only suspended with one layer of spring.

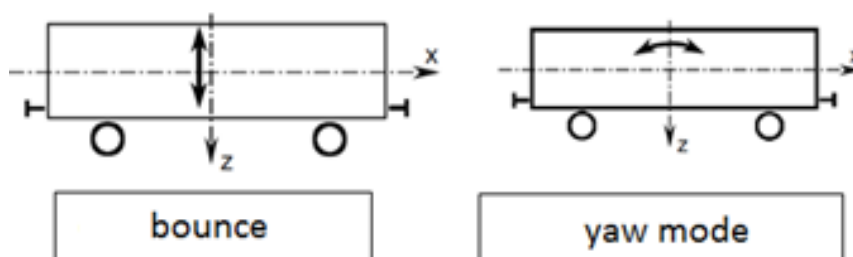


Figure 36 Important eigen modes for vertical vehicle behavior

Table 33: The eigen values of selected motion

| Rigid body motion | Direction of motion | Natural frequency (Hz) | Natural damping (%) |
|--------------------|---------------------|------------------------|---------------------|
| Car body bounce | Z | 2.36 ^{*)} | 3.22 |
| Car body yaw | β | 1.65 | 2.87 |
| Bogie frame bounce | Z | 20.38 | 4.94 |
| Bogie frame yaw | β | 4.57 | 2.84 |

^{*)}: The eigen frequency of car body bounce is bigger than 2 Hz due to the coil spring design of the secondary suspension

The advantage of Simpack is the fully consideration of wheel-rail contact mechanism including both profiles. Therefore, an exact modeling of rail head profile is required in the FEM model. A graphical illustration of the contact between wheel and rail is shown in Figure 37. The blue lines between the wheel and rail profile specify all the possible contact paths. The classic Kalker contact theory (Method “FASTSIM”) [27] is utilized for processing of wheel-rail contact force.

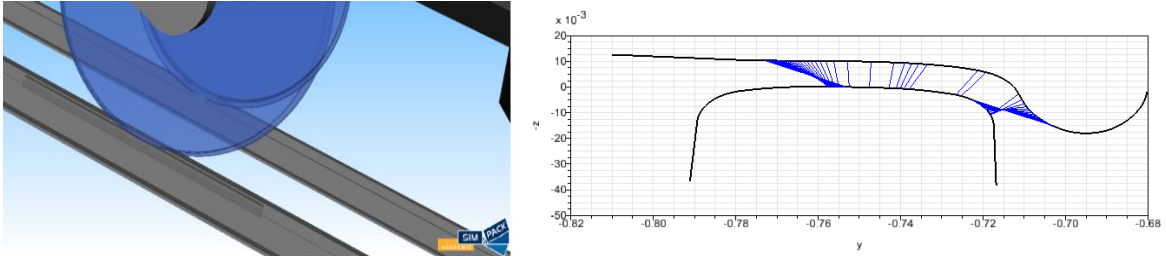


Figure 37 Contact between wheel and rail (Profile S1002 and 60E1)

The speed of the vehicle is fixed at 160 km/h, because this is the most frequently appeared passage speed along the measurement section.

5.3.3. Inclusion of measured track excitation

Noticing that the lateral and longitudinal irregularities can also influence the vehicle track contact behavior, the measured track geometry (documented in chapter 4.2) is

processed to fit the requirements of Simpack. Figure 38 shows the way to define a 3D track excitation, which is divided into 4 independent subjects:

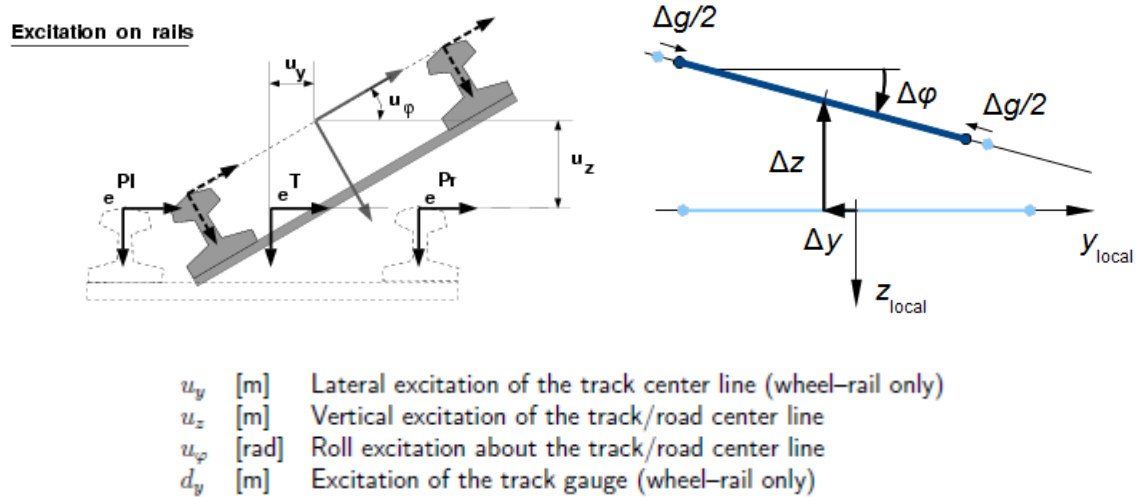


Figure 38 The definition of 3D track excitation in MBS system [28][29]

The both measured track geometry in 2012 and in 2014 is included in the simulation. An overlapped measurement section of 350 m is selected to compare the track quality due to the increased passage loads.

5.3.4. Modeling results

The calculated dynamic wheel load along the selected section is the best output parameter to specify the overall vehicle track interaction behavior. For determining the dynamic load, which is more decisive for the general deterioration rate of the track, the simulated dynamic wheel load should be filtered with a low pass filter of 20 Hz, according to the European railway standard EN 14363:2005 [30]. Under this type of filtering, the excitation load due to wheel or rail roughness is not included since they tend to excite the system at higher frequencies. This filter is also applied to the entire calculated dynamic wheel load in the following models.

Since the time dependent curve shows stochastic behavior (documented in appendix 27), advanced statistical analysis is applied to clarify these values. Table 34 documents the results from classical statistical analysis. It is already confirmed in subchapter 4.1 that the track quality deteriorates in 2014 compared to 2012, due to passage axle loads. This effect on the distribution of dynamic wheel load is then clear.

Table 34: Simulated dynamic wheel loads under track geometry variations(wheel load of 105 kN)

| | Track geometry measured in | | Difference (%) |
|---|----------------------------|-------|----------------|
| | 2012 | 2014 | |
| Minimum (kN) | 84.4 | 83.0 | -1.66 |
| Maximum (kN) | 121.4 | 122.5 | 0.91 |
| Mean (kN) | 103.8 | 104.0 | 0.19 |
| Standard deviation (kN) | 6.25 | 7.80 | 24.8 |
| Coefficient of variation (%) | 6.0 | 7.5 | 25.0 |
| Dynamic load factor (%) | 17.0 | 17.8 | 4.71 |
| Track geometry (data copied from chapter 4.1.2) | | | |
| Standard deviation (mm) | 0.74 | 0.86 | 16.2 |

A deeper understanding of the effect of track deterioration to the change of vehicle track interaction (here dynamic wheel load) should be achieved. A drawing of the “Frequency distribution” is the best illustration. The x-axis represents the dynamic wheel load and the y-axis represents the percentage of measured axle load in this interval. Figure 39 shows the processed curve.

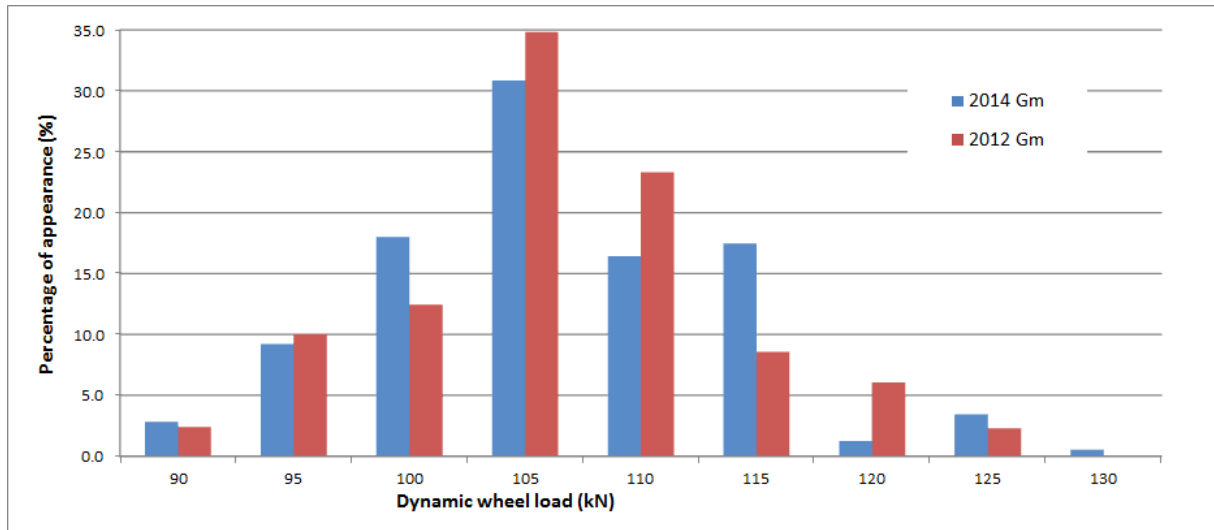


Figure 39 The statistical frequency distribution analysis of dynamic load (Section 4)

It can be clearly observed that the deterioration of the track quality leads to a decrease of appearance in the middle area, close to the static wheel load, and to an increase of appearance in both surrounding areas. In other words, the level of significance of the variation of the dynamic load is numerically shown.

5.4. Model 3 (Co-simulation with FEM and MBS) – Calibration of the quasi-static wheel rail load under modal represented elastic track from FEM

5.4.1. Background and introduction

The variation of track stiffness is also an important factor influencing the overall track dynamics. For sound track without special design specifications, the stiffness of the track significantly varies in comparison with track irregularity characteristics and this part was usually neglected.

This cannot be the case for this research, since the track stiffness, which is one of the both important track sided parameters, influences vehicle track interaction behaviors. By repeated train load, those variations of track stiffness have counterproductive effect to the track geometry. In other words, the appearance of track irregularity is normally the consequence of the “spots” in track stiffness.

Generally, it is suggested to generate track stiffness model in FEM system, since the materials of the single element can be determined and the simulation of complex deflection behavior can be ensured. The disadvantage of this approach is the requirement of complex discretization of the geometry model into small and fine elements, due to which the model should normally orient itself in time-independent analysis.

The co-simulation strategy is used to solve the problem. There exists the contact marker in Simpack, which fully supports the moving contact between rigid and flexible body ^[31]. Therefore, the model should be able to utilize information from both FEM and MBS and to combine them together for the solution. Since MBS is designed to accomplish time dependent simulations, the FEM model is condensed and utilized as the prerequisite of the MBS model. This model condensation can be achieved by the modal analysis approach ^[32].

5.4.2. Model condensation and modal analysis

The reason for the time-intensive simulation of a FEM model remains at the finite element meshing of the geometrical model, which creates huge number of independent formulas. This accuracy is required for the best representation of the bending behavior of the structure.

A group of generated elements, whose internal behavior is not required to be analyzed in detail, can be defined as a “Substructure” in FEM model, with pre-defined “Master

nodes” still holding independent formulas and the other nodes, so called “Slave nodes”, being interpolated from the behavior of the neighboring “Master nodes”.

Other simulations on the Substructuring and modal analysis of an existing FEM model are already documented in the master thesis by KL, CHEN [33] and SMART rail report [34]. The FEM model 1 described in subchapter 5.2 is used as input. Realistic density of each material is set to fulfill the calculation needs. According to chapter 2, the “Master node” in ANSYS should be defined, which is later defined as “Marker” in Simpack. Those markers are able to define the behavior of the track under vehicle loads. Therefore, one node on top of each rail seat is defined as “Master node” (see Figure 40). The rail is extended for provision of sufficient running time on the elastic track. The extended rail is fixed at the bottom without extra provision of stiffness, equally to a quasi-rigid body in this case. The fixation of the model remains the same as before. This analysis is called “Substructuring/CMS” in ANSYS software.

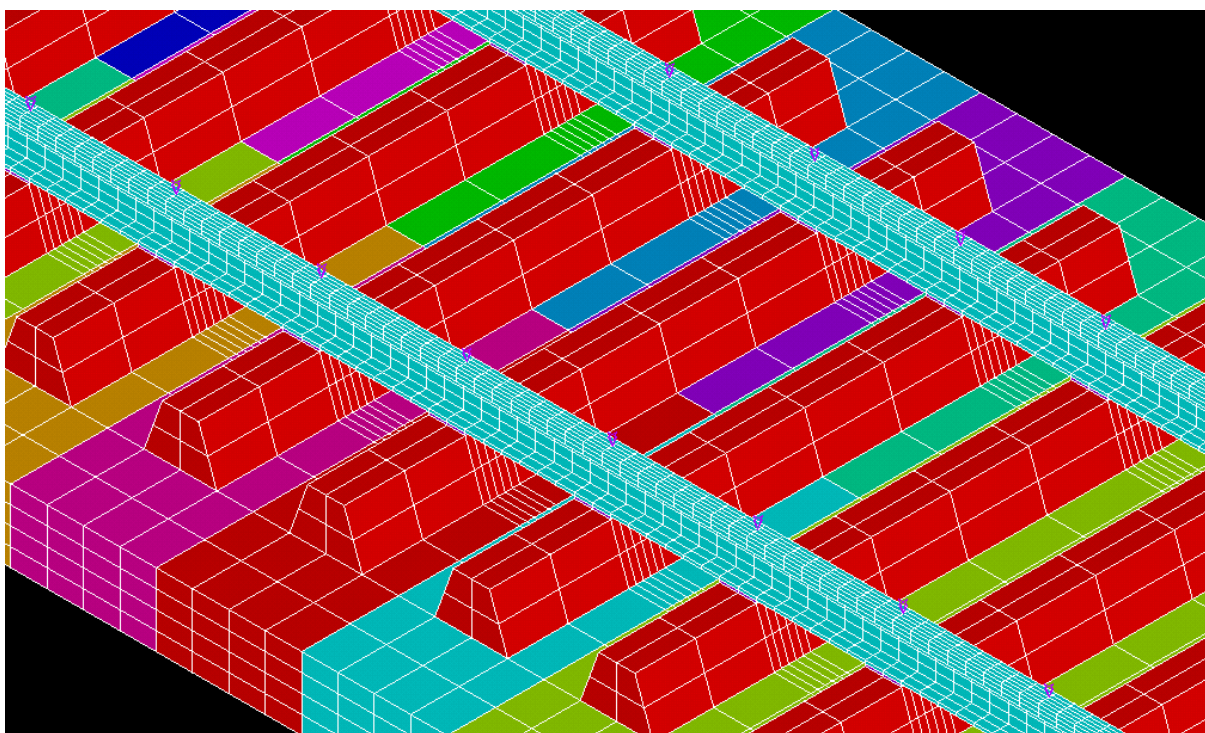


Figure 40 Illustration of the defined “Master node” in FEM model (Purple arrow)

The modal analysis of the condensed model is realized in the next step. From all the selected master nodes, only the eigenmodes in vertical direction are calculated, because the modes defining tilting and lateral movement are not required to be included in this research.

The representation of the track stiffness should rely on many different modes due to different stiffness setting under individual rail seat. Thus, for the best representation, the number of the included eigenmodes should be the same as the number of “Master node” itself (in this research about 150 eigen modes). The frequency variation of those eigenmodes is between 1300 (eigen frequency of mode 1) and 7500 Hz (eigen frequency of mode 150). This ensures the best representation of stiffness behaviors for the total measurement section. Figure 41 and Figure 42 show the first two eigenmodes using counter plots. The graphical and table list of all the included eigen modes can be found in appendices 28 to 30.

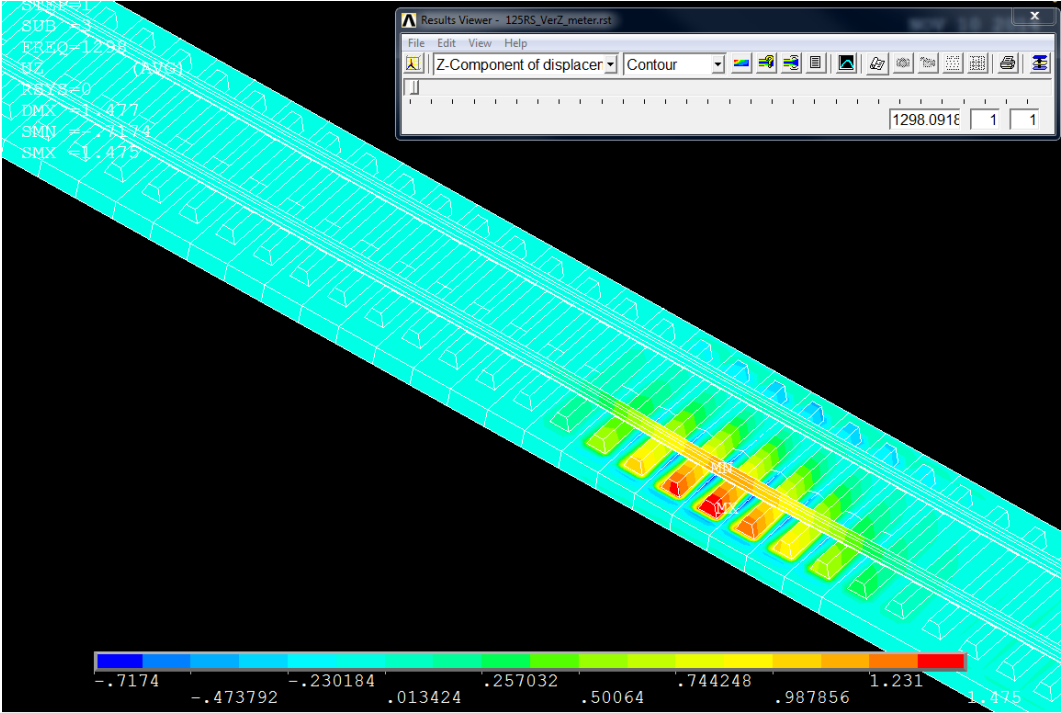


Figure 41 Illustration of eigen mode 1 ($f_0 = 1298$ Hz)

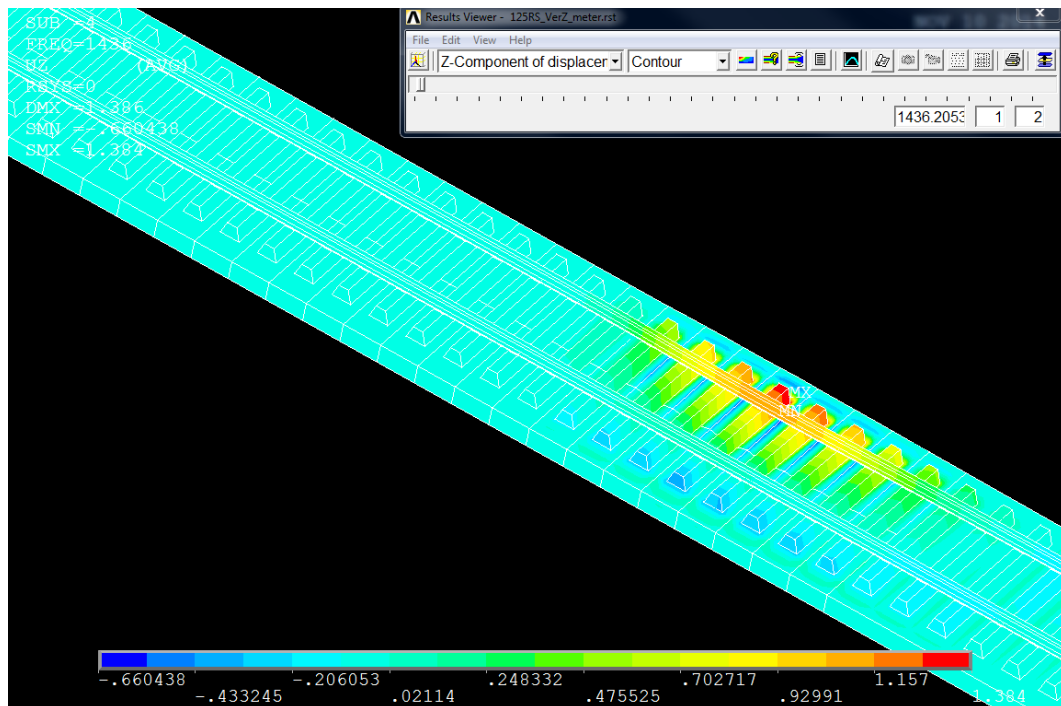


Figure 42 Illustration of eigen mode 2 ($f_0 = 1436$ Hz)

5.4.3. Adjustment of the vehicle model with contact markers and model calculation

The vehicle model is already described in section 5.3. Now, each wheel is bound together with the contact marker type “-96: Curve-curve 2D contact” in Simpack [31]. The contact geometry is “Cylinder” in wheel and “Prism” in track. For defining the elastic track, the condensed model and the results of eigenmodes are read into the Simpack. An “fbi” file is generated, which contains all the information from FEM model. The general view of the flexible track and the train is shown in Figure 43:

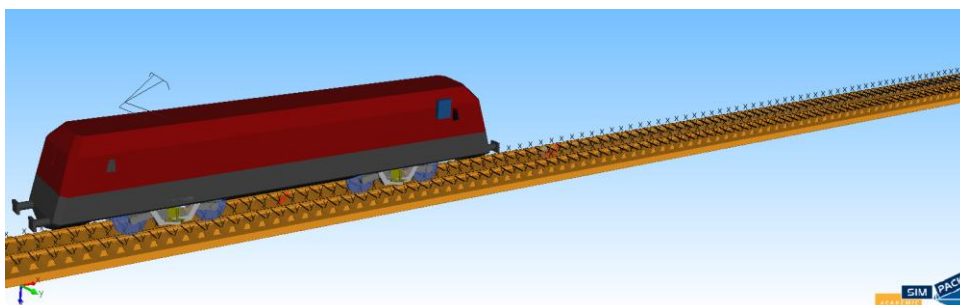


Figure 43 Simpack vehicle model with built-in flexible track structure

The output of the simulation run includes single deflection line at each predefined location, meaning that a visualization of the deflection at single point during the train runs is possible. The simulation runs are only performed under a quasi-static run with 1 m/s. This is used to calibrate the contact force element between wheel and rail.

5.4.4. Simulation results

The graphical representation under quasi-static run with 1 m/s is shown in Figure 44. The advanced Simpack postprocessor ensures a real-time illustration of the track displacement of the flexible body. Sample deflection curves of the passage of train under selected interview points are also attached. It can be seen from Figure 45 that the same axle load can cause a difference at the elastic deflection, which is identical with the model approach described in chapter 4.

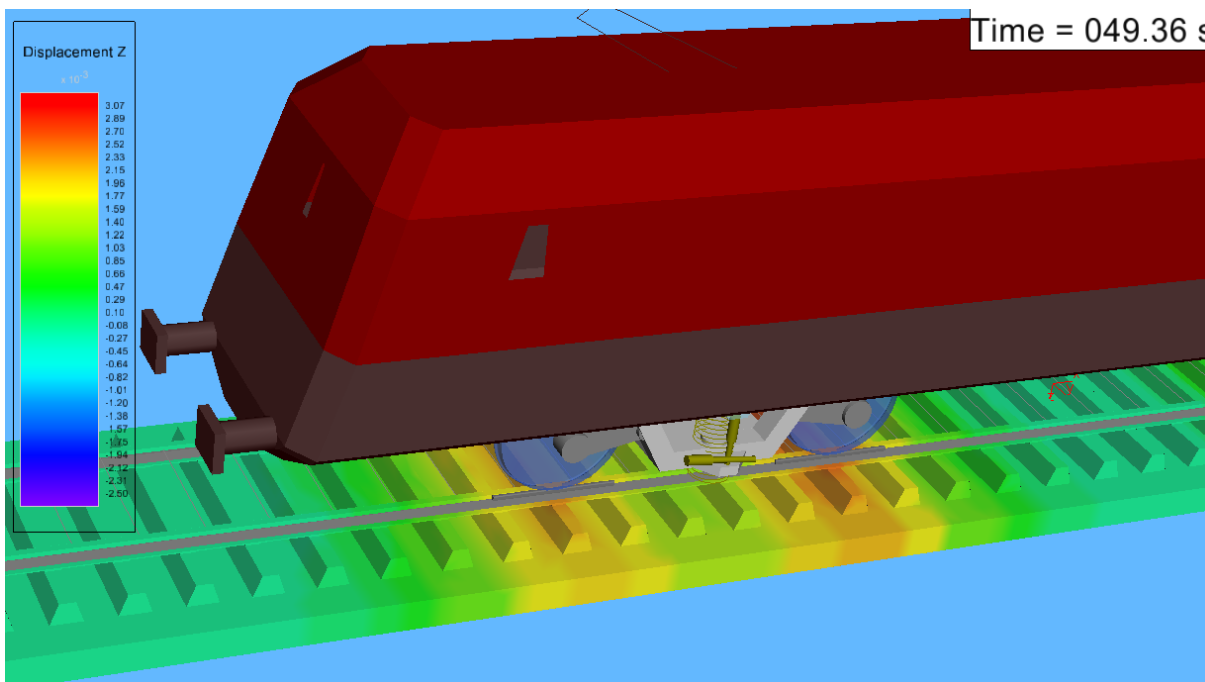


Figure 44 Graphical representation of elastic track deflection under wheel load

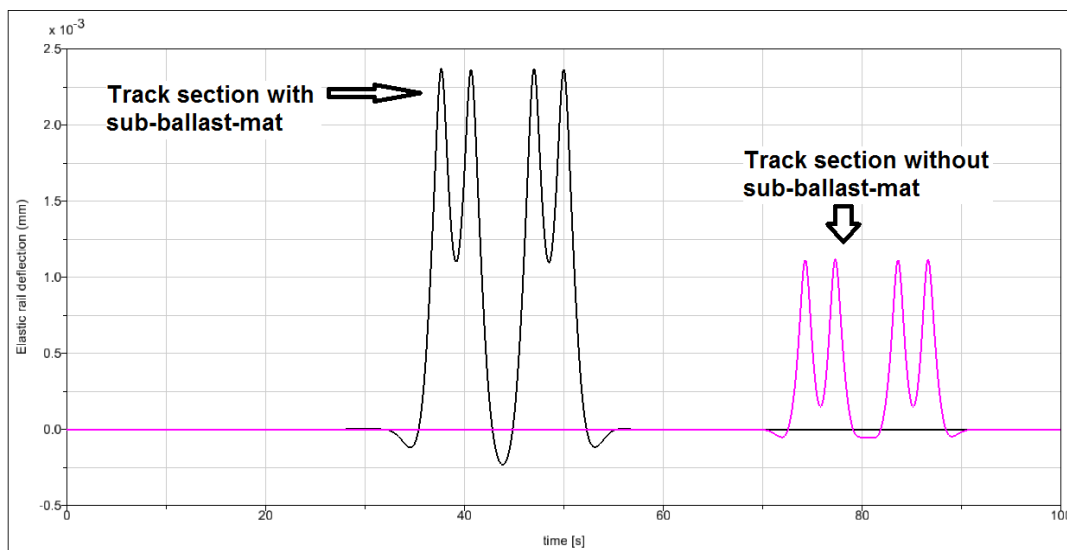


Figure 45 Elastic deflection under train passage at certain rail seats

5.5. Model 4 (Co-simulation with FEM and MBS) – Calculation of the dynamic wheel load under elastic track with irregularities ($V = 160 \text{ km/h}$)

5.5.1. Background and introduction

After the model calibration, the flexible track input is used for train runs with higher speed. The track geometry is also read and overlapped with the same location in which they were measured. In other words, this track is able to represent the real track, described in chapter 4, on behalf of geometry and stiffness. The track geometry was measured in 2012 and in 2014. The supposed minor change of track stiffness due to 1 year of operation is not measured in 2014 and the simulation runs for 2014 still use the track stiffness data from 2012.

An important factor which should be considered is the damping of the track. The modeling of the track stiffness relies on the modal analysis of the flexible system with built in modal damping. The damping is categorized as a number in percentage.

The selection of the modal damping should be dependent on the travel speed of the vehicle, since the modal analysis can only provide a linear damping approach, whereas the track damping in reality is mostly found to be nonlinear. It is defined under experience that a modal damping at about 5 % (inclusion of rubber rail pads) is required for the dynamic run with 160 km/h [35].

5.5.2. Simulation results

The calculated dynamic wheel load along the selected section is the best output parameter specifying the overall vehicle track interaction behavior, which directly specifies the content of vehicle track interaction. Since the time dependent curve shows stochastic behavior, advanced statistical analysis is applied for clarifying the values. Table 35 documents the results by the conventional statistical analysis. The major outputs of this section are the appearance of the track stiffness to the overall performance of vehicle track interaction.

Table 35: Statistical results of the simulated dynamic wheel loads (static wheel load of 105 kN)

| | Geometry measured in 2012 | | | Geometry measured in 2014 | | |
|------------------------------|---------------------------|---------------------|----------------|---------------------------|-----------------------------------|----------------|
| | Only Geometry | Geometry +Stiffness | Difference (%) | Only Geometry | Geometry +Stiffness ^{*)} | Difference (%) |
| Minimum (kN) | 86.4 | 88.6 | 2.5 | 86.8 | 87.2 | 0.5 |
| Maximum(kN) | 123.0 | 118.8 | -3.4 | 125.4 | 124.6 | -0.6 |
| Mean (kN) | 103.9 | 104.0 | 0.1 | 103.9 | 104.0 | 0.1 |
| Standard deviation (kN) | 7.24 | 6.19 | -14.5 | 7.60 | 7.40 | -2.6 |
| Coefficient of variation (%) | 7.0 | 6.0 | -14.3 | 7.3 | 7.1 | -2.7 |
| Dynamic load factor (%) | 18.3 | 14.3 | -21.9 | 20.7 | 19.9 | -3.9 |

^{*)}: Track stiffness data from measurement in 2012 due to lack of repeated measurement in 2014

Generally, the inclusion of track stiffness improves the vehicle track interaction performance. The reason is that the stiffness of the structure can compensate the effect of irregularity to a certain extent. A dynamic loading factor of approximately 20.0 % can be found under the travel speed at 160 km/h for scenario 2014, which is principally identical to the measurement results using strain gauges.

Since the track stiffness input for both scenarios remains the same, it is therefore to conclude, that the improvement of vehicle track interaction due to track stiffness is dependent on track geometry conditions. The column “Difference” in terms “Standard deviation, Coefficient of variation and Dynamic loading factor” shows much higher values for the scenario in 2012 than in 2014, where the track geometry level in 2012 is still smoother than in 2014. This proves that, the stiffness can compensate the excitation load better under better track geometry qualities. In other words, the effect of track stiffness in compensating the excitation from track geometry also decreases with the decrease of the quality of track. This effect is further investigated in the chapter 6.

The “Frequency distribution” curves in 2012 and in 2014 are attached in Figure 46 and Figure 47. The legend “Gm” refers to the simulation with only geometry variation and “GE” referred to the simulation with overlapped geometry and stiffness variations.

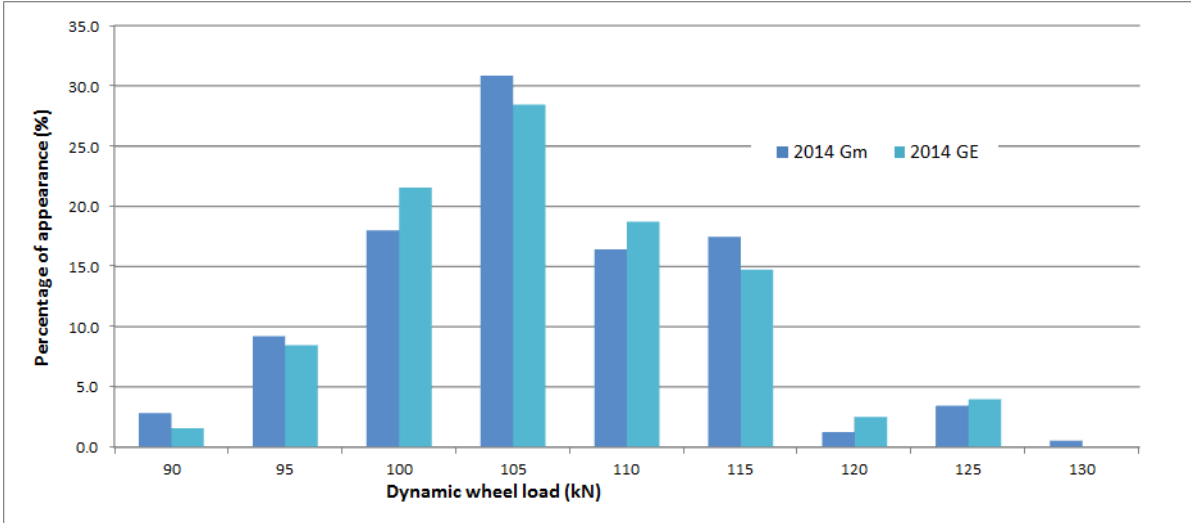


Figure 46 The statistical frequency distribution analysis of dynamic load (measurement in 2012, Section 4)

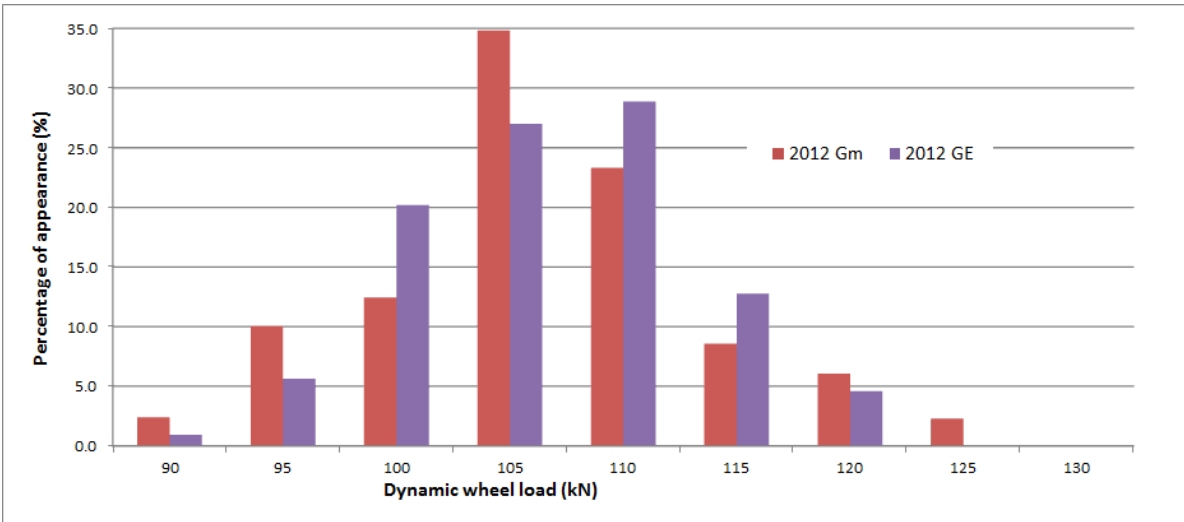


Figure 47 The statistical frequency distribution analysis of dynamic load (measurement in 2014, Section 4)

5.6. Conclusion and outcome

In this chapter, the innovative co-simulation is performed and illustrated. The approach of the co-simulation remains at the combination of ANSYS and Simpack, with Simpack as master program reading the modal represented elastic model from ANSYS. With the help of this innovative approach, a dynamic real-time simulation under fully elastic

track was realized. The model 4 described in the section 5.5 can fully integrate both the track geometry and stiffness, with exact overlapping of the both excitations. Therefore, this provides the best close to reality information of the interaction between vehicle and track, as well as their effects on the respective track superstructures.

6. FEEDBACK BETWEEN VEHICLE AND TRACK UNDER TRACK SIDED EXCITATIONS

In this chapter, the track sided influence factors on the dynamic vehicle track interactions (in short, “DVTI”) are studied. Since this research work focuses on the influence parameters of the track side, the only variable from the vehicle side is the travel speed and the vehicle model included here is the same with the one described in chapter 5. Various measurement results and data from the previous works of the institute are included. This chapter covers the following main contents:

- Categorizing and collecting the track geometry with different quality indexes;
- Categorizing and collecting the track stiffness with different quality indexes;
- Analyzing the vehicle track interaction parameters (from classic and innovative approach) under different speed level;

It should be noticed, that the values calculated here exclude the microscopic parameters like wheel and rail imperfection, which certainly could also influence the dynamic wheel rail interactions (already shown in Figure 24, subsection 4.4.2). Therefore, a direct comparison with the results from this model and the measurement data could not be realized and the values calculated in this part are purely due to the influence of speed, track geometry (minimum wave length of 0.5 m) and track stiffness.

6.1. The limitation of the existing method on evaluation of the track quality and preliminary studies

The modern track inspection car always measures the combined effect of track geometry and stiffness (integrated approach) with the movable chord approach. For the evaluation of the measurement data, the classic statistical analysis is used. Those methods are documented already in the railway standard EN 13848-5:2008 ^[36] and DB Richtlinie 821.2001 ^[37]. Both approaches calculate the statistical standard deviation of

the track geometry inside a certain length and provide guideline values for maintenance.

The classic statistical approach of evaluation of the track quality cannot consider the sequence of the appeared values. In other words, no inclusion of the shape of the excitation is assessed. By two track excitations with the same statistic values but different sequences (different wave length and wave amplitude), the appeared dynamic effect of the vehicle track interaction can vary.

Therefore, initial studies are performed. The following two simulations are taken from different two track geometry excitations with the same statistical values, but with different shape. The simulation result with same train and same speed level showed that the standard deviation of the dynamic load was different as well as the maximum dynamic load. This leads to the conclusion that the classic statistical analysis, which does not consider the shape of the excitation, is not able to consistently result in the effect of dynamic vehicle track interaction. The classic statistical approach of the evaluation of track quality should be renewed by numerical simulations for exact simulation of the real time vehicle track interaction. Table 36 shows the significant results. The shape of the excitation, as well as the PSD output, can be found in Figure 48 and Figure 49.

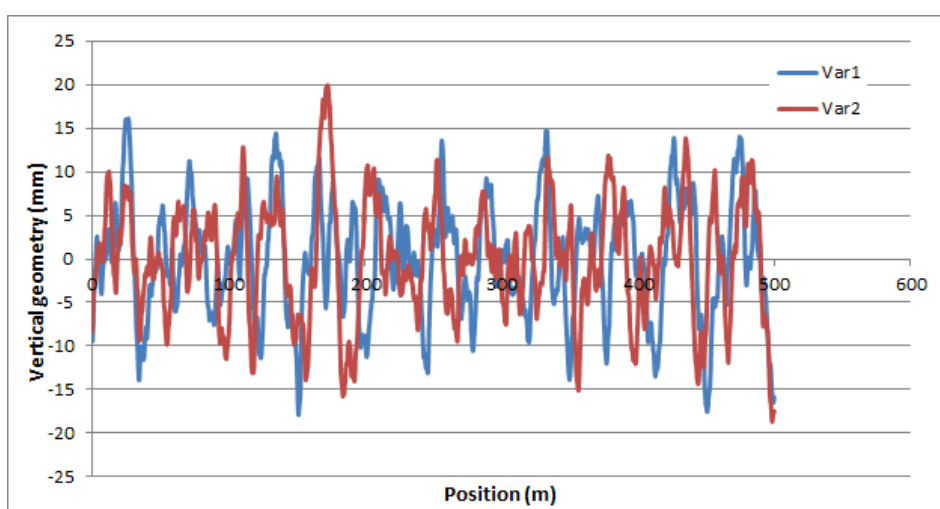


Figure 48 Track vertical geometry (Var1 and Var2)

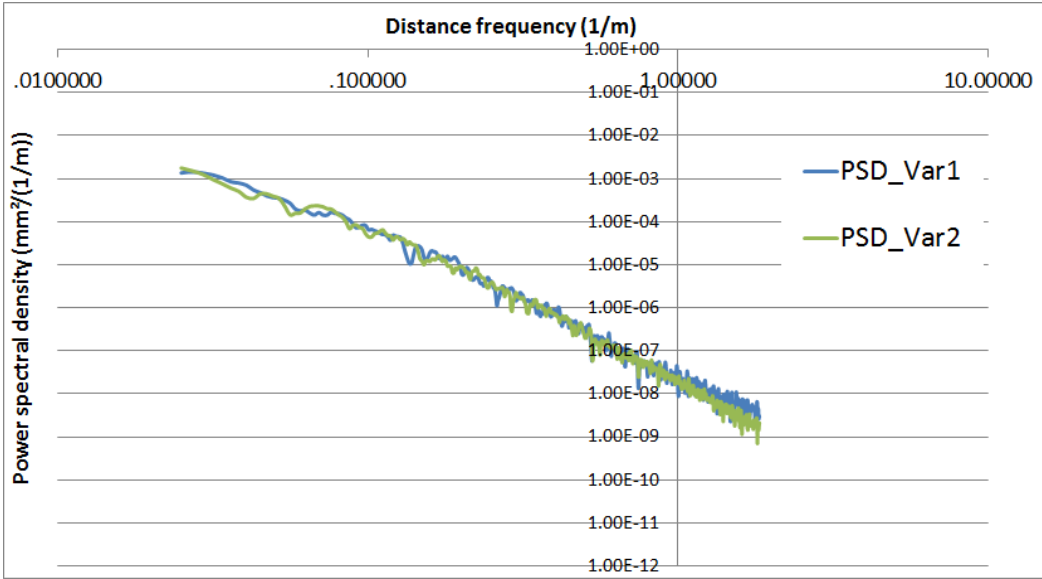


Figure 49 PSD output of the track vertical geometry (Var1 and Var2)

Table 36: The dynamic load under track geometry and speed variations (static wheel load of 105 kN)

| | Var1 | Var2 | Difference |
|---|-------|-------|------------|
| Length (m) | 500 | | 0 |
| Standard deviation over the total length (mm) | 6.6 | 6.6 | 0 |
| Vertical spread (mm) | 34.0 | 38.6 | 4.6 |
| Vehicle speed (km/h) | 80 | | 0 |
| Max. induced dynamic wheel load (kN) | 172.9 | 185.4 | 12.5 |
| Dynamic loading factor (%) | 66.2 | 77.2 | 11.0 |

6.2. The improvement of track quality evaluation method

The improvement of the classical approach is shown in this section. From the measurement side, since the vertical displacement, due to the change in track stiffness, is damped and due to track geometry, is undamped, these effects should be studied separately.

From the data evaluation side, since the real-time dynamic vehicle track interaction depends on the change in the track geometry along the track section, the classic

calculation of statistics should be exchanged for the evaluation of the output parameters by the modern numerical simulations with FEM and MBS.

The wheel dynamic load provides the best surface for the analysis of the DVTI. For this research, the dynamic wheel load is processed into three terms: “Dynamic loading factor”, “Energy Spectral Density” and “Statistical frequency distribution”. The term “Dynamic loading factor” defines the obvious leveling of the DVTI by seeing the proportion of the maximum dynamic loading to the static one. The other term “Energy Spectral Density” (ESD) describes the energy of the dynamic load contributing to the system, by a frequency, per unit frequency ^[38]. This generally holds the same calculation method of the “Power Spectral Density” (illustrated in chapter 2) but utilizes time signal of the dynamic wheel load as input. The processed ESD holds the x and y unit of Hz and kN²/Hz. This output is distributed in a frequency curve for every calculated dynamic wheel load. The “Statistical frequency distribution” is the same, as described in subsection 5.3.4.

All the results from this section are collected from the simulation output of Simpack. The built-up of the basic models are described in chapter 5.

6.3. Variation of the included influence parameters

As described before, the included parameters, which are studied, are the following three: the vehicle speed (specified as X), the track geometry (specified as Y) and the track stiffness (specified as Z). Therefore, for a better categorization, each simulation is given a three digits “index number” with X, Y and Z which are found as “DVTI_XYZ”. Table 37 shows the exact numbering of the X, Y and Z and their references.

In order to understand the track quality level, the classic statistical standard deviation (SR₁₀₀ for track geometry of DB 821.2001) is calculated as guidelines. But they cannot provide an accurate quality index concerning the effect of vehicle track interaction, due

to the aforementioned reasons. The measured track geometry has a total length of more than 500 m and the track stiffness includes 60 to 75 measured rail seats.

Table 37: Numbering of influence factors X, Y and Z and their values

| | Vehicle speed (km/h) | Standard deviation of track geometry SR ₁₀₀ (mm) > 500 m | Standard deviation of rail deflection (mm) 60 to 75 rail seats | Simulation frequency (Hz) |
|--------------|----------------------|---|--|---------------------------|
| Index number | X | Y | Z | |
| 0 | - | No excitation | No excitation | - |
| 1 | 80 | 0.20 mm (MG1) *) | 0.07 mm (ME1) *) | 250 |
| 2 | 120 | 0.82 mm (MG3) *) | 0.08 mm (ME3) *) | 400 |
| 3 | 160 | 1.77 mm (EG1) **) | 0.20 mm (EE2) **) | 500 |
| 4 | 200 | 3.18 mm (ERL) ***) | 0.75 mm (EE3) **) | 600 |
| 5 | 250 | 5.81 mm (ERH) ***) | | 700 |
| 6 | 300 | 0.91 mm (AKFF) ****) | | 800 |
| 7 | 350 | | | 1000 |

*) : symbol “MG1” and “ME1” refer to the data coming from measurement section 1 (“G” – Geometry; “E” - Stiffness)

**): symbol “EG” and “EE” refer to the external data source from previous measurement activities (data recording not included in this research. “G” – Geometry; “E” - Stiffness)

***): Definition of the track geometry through interpolation from PSD function specified by standard ORE B 176 [10]. The case “Y=5” could only be found in local railway lines where normally a maximum speed of less than 60 km/h was allowed.

****): Definition of track geometry through interpolation from PSD function specified by German railway standard “Anforderungskatalog zum Bau der Festen Fahrbahn – 4. Überarbeitete Auflage” [20]

According to this numbering strategy (see Table 37), the name with “DVTI_350” refers to a simulation under 160 km/h, with ERRI high excitation (“ERH”) and no track

stiffness input; the name with “DVTI_611” refers to a simulation under 300 km/h, with geometry excitation “MG1” and stiffness input “ME1”.

The travel speed of the vehicle should be also included as a major influence parameter. A minimum speed level is fixed at 80 km/h, because under this speed level, no significant dynamic effect should be expected. Moreover, because the ballastless track with design speed at 300 km/h is included, for purely academic reasons, a maximum speed of 350 km/h is fixed.

The studied track geometry and track stiffness scenarios have different quality indexes, in order to research the effect of the dynamic vehicle track interaction under different tracks. Their data were ranked in sequence, meaning that the scenario with the best quality always has smaller number in their index. All the studied data refer to tracks in straight alignment, without specific structures like bridge or tunnels.

With this allocation, there are scenarios like “DVTI_XY0” and “DVTI_X0Z” for the visualization of the effect of single excitation input. The vertical geometry and distribution of the maximum rail deflection of the external data are shown in appendices 31 to 32.

6.4. Distribution of dynamic wheel load according to standard track quality factors (Y = 6)

The German railway standard AKFF defines the limit for the power spectral density distribution of the vertical track geometry for ballastless tracks. Calculations of dynamic loading factor dependent on speed levels have been done using track models according to this track quality limit (PSD track geometry). The calculation is performed for the train type “Locomotive” (without wheel flats). This distribution can be seen in Figure 50.

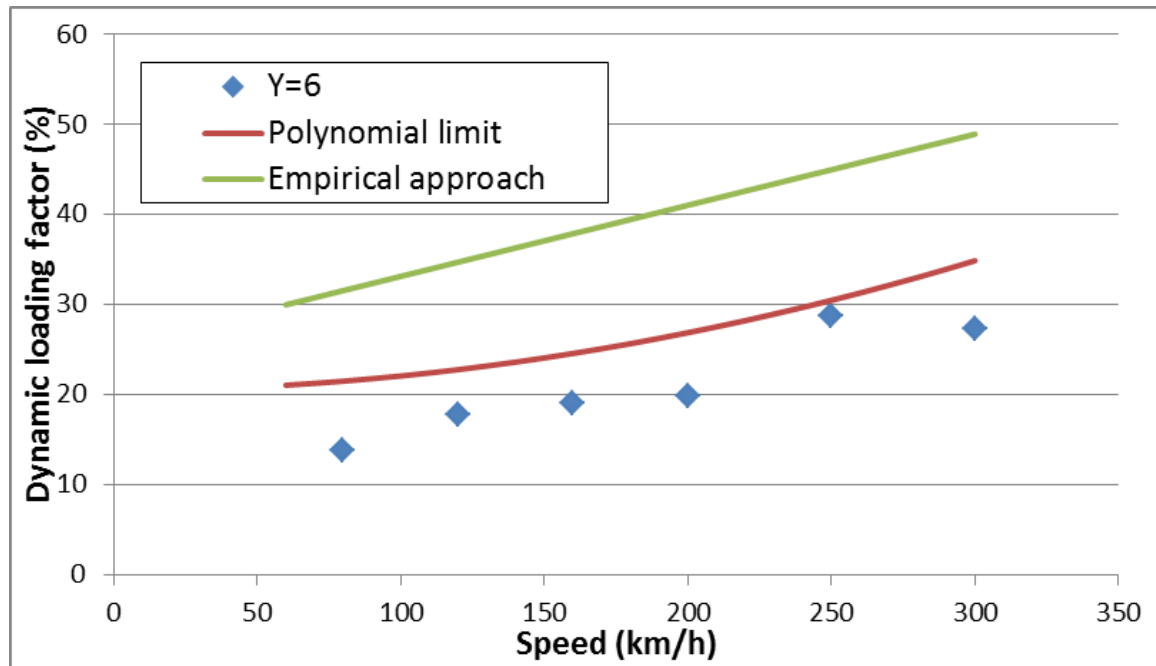


Figure 50 dynamic loading factor (percentage) according to speed (Y = 6)

The calculation based on the conventional empirical approach described in 2.3.1 is also given which gives the dynamic loading factor of 1.489 under the speed of 300 km/h. A “polynomial limit” curve can be interpolated, which is above all the calculated points. This limit could provide guideline values for the next generation design specifications. Till a maximum speed of 300 km/h (straight track with $V \geq 60$ km/h), the interpolated curve can be described by the following formula :

$$\max Q = Q_{\text{mean}} * \left(1 + \frac{V^2 + 128000}{625000} \right)$$

with V – vehicle speed (km/h)

Q_{mean} – static wheel load (kN)

$\max Q$ – maximum dynamic wheel load (kN)

A higher maximum loading factor under the speed of 250 km/h can be seen which can be explained by resonance effects from random allocation of the track geometry (the difference between 250 and 300 km/h runs is within 1.5 %). It can be concluded that

for the modeled locomotive, a dynamic loading factor of 1.35 will be sufficient for train runs up to 300 km/h if the track geometry condition fulfills the requirement defined by the PSD distribution in AKFF^[20].

6.5. Simulation results under purely track geometry variations (Z = 0)

The first simulation series refer to single input of track geometry variations. The PSD calculation on all the Y scenarios are performed and shown in Figure 51. These values include all the possible track quality level, which could be found nowadays in the network. All the included track geometry data are filtered between a wave length from 0.5 m to 50 m (distance frequency between 0.02 m⁻¹ and 2.0 m⁻¹).

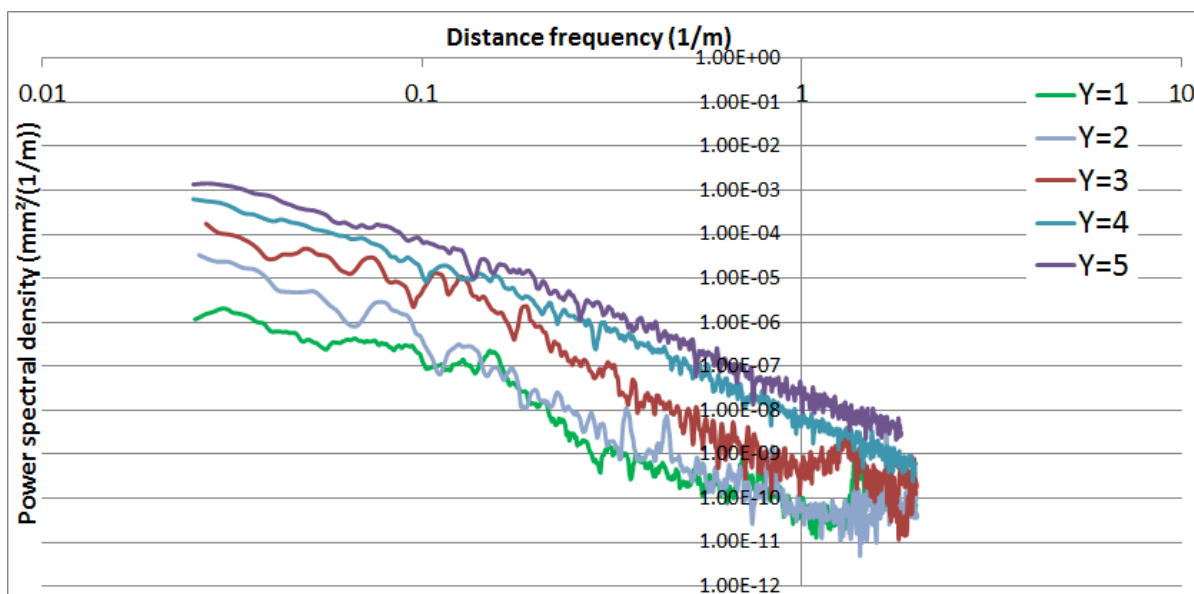


Figure 51 PSD output of the selected track geometry

Table 38 collects the dynamic loading factor after the simulation runs, which principally increases with the decrease of track quality and the increase of the travel speed for obvious reasons. The ESD output of selected combination is shown in appendix 33.

Table 38: The dynamic load under track geometry and speed variations

| | | Track geometry variation (index Y) | | | | |
|---------|--------------|------------------------------------|-------|-------|-------|-------|
| | | Y = 1 | Y = 2 | Y = 3 | Y = 4 | Y = 5 |
| Index X | Speed (km/h) | Dynamic loading factor (%) | | | | |
| 1 | 80 | - *) | 16.1 | 17.2 | 50.8 | 77.2 |
| 2 | 120 | - *) | 13.3 | 21.4 | 75.5 | 103.3 |
| 3 | 160 | - *) | 18.6 | 19.3 | 73.8 | - **) |
| 4 | 200 | 5.0 | 22.0 | 26.6 | 79.6 | - **) |
| 5 | 250 | 7.5 | 24.6 | 31.0 | 84.5 | - **) |
| 6 | 300 | 11.4 | 34.7 | 48.6 | - **) | - **) |
| 7 | 350 | 43.4 | 50.7 | 67.0 | - **) | - **) |

*) : Simulation not done due to expected insignificant value output

**) : Simulation not done due to too severe dynamic impacts

6.6. Simulation results under purely track stiffness variations (Y = 0)

The second simulation series concern single input of track stiffness variations. Both ballasted and ballastless tracks are studied. But because the ballastless track normally holds obvious non-linear stiffness behavior, which cannot be included in this approach, the calculated values (in scenario Z = 1) can be slightly different in reality.

Each selected data set contains 60 to 75 single measurements. Table 39 collects the dynamic loading factor from each simulation result, which principally increases with the increase of travel speed and reduction of the quality of track stiffness for obvious reasons. The ESD output of selected combination is shown in appendix 33.

Table 39: The dynamic load under track stiffness and speed variations

| | | Track stiffness variation (index Z) | | | |
|---------|--------------|-------------------------------------|-------|-------|-------|
| | | Z = 1 | Z = 2 | Z = 3 | Z = 4 |
| Index X | Speed (km/h) | Dynamic loading factor (%) | | | |
| 1 | 80 | 4.2 | 4.1 | 4.1 | 13.6 |
| 2 | 120 | 4.1 | 3.5 | 3.8 | 7.0 |
| 3 | 160 | 4.7 | 4.0 | 5.0 | 13.7 |
| 4 | 200 | 7.3 | 5.2 | 3.6 | 19.9 |
| 5 | 250 | 7.4 | 6.3 | 6.5 | 15.3 |
| 6 | 300 | 8.6 | 8.7 | 9.7 | 16.3 |
| 7 | 350 | 10.3 | 10.8 | 12.6 | 19.2 |

6.7. The “hybrid” simulations

In this section, the effect of combining the excitations from Y (geometry) and stiffness (Z) is studied. This can be realized by the so called “hybrid” simulation with combination of the factor of X, Y and Z (none with zero indexes).

Due to the free positioning of the overlapped excitations Y and Z, their effect in dynamic loading can be either amplified or compensated. A virtual simulation program can combine every X, Y and Z index together, but only a few of those combinations are close to the real situations. For scientific reasons, the maximum possible speed levels for each selected Y and Z combination is selected. Table 40 shows the realistic combination of X, Y and Z and the simulated dynamic loading factor. The maximum dynamic loading (max Q), based on the analytic method, described in subsection 2.3.1, is listed in Table 41 for comparison reasons. The reader is referred to Appendices 34 to 36 for the statistical frequency distribution analysis of the dynamic load.

Table 40: Realized combination of X, Y and Z and dynamic loading factor

| XYZ | Max. Speed limit (km/h) | Dynamic loading factor (%) | | |
|-----|-------------------------|----------------------------|-------|-------|
| | | Combined Y and Z | Z = 0 | Y = 0 |
| 611 | 300 | 11.1 | 11.4 | 8.6 |
| 522 | 250 | 25.2 | 24.6 | 6.3 |
| 333 | 160 | 19.5 | 19.3 | 5.0 |
| 244 | 120 | 74.6 | 75.5 | 7.0 |
| 154 | 80 | 76.7 | 77.2 | 13.6 |

Table 41: Analytical calculation of dynamic loading factor from classic formulas

| XYZ | Max. Speed limit (km/h) | t | n | φ | Dynamic loading factor (%) |
|-----|-------------------------|-----|------|-------|----------------------------|
| 611 | 300 | 3.0 | 0.10 | 1.632 | 49.0 |
| 522 | 250 | 3.0 | 0.10 | 1.500 | 45.0 |
| 333 | 160 | 3.0 | 0.15 | 1.263 | 56.9 |
| 244 | 120 | 3.0 | 0.20 | 1.158 | 69.5 |
| 154 | 80 | 3.0 | 0.25 | 1.053 | 79.0 |

It is proved that, the dynamic loading factor calculated by Simpack has good identity under the scenarios “154” and “244” (variation of both results inside 5 %). All the calculated values by Simpack are smaller than the empirical approach (see section 2.3.1). Under those cases, the track sided parameters are dominant, while the difference in vehicle design and vehicle performances is not significant for the variation of the results, due to the limited speed level ($v \leq 120$ km/h).

The significant difference of the values of the cases “611”, “522” and “333” can be due to the improvement of mechanical behavior of the vehicle (technology innovations from 1993 to 2010), which is also determinant for the overall vehicle track interaction. This contributes to the fact that, the formulas are designed to always stay at the safe side, which reserves space for the vehicle track interaction behavior under high speed levels ($V > 120$ km/h).

The modern high speed lines induce less dynamic effect between vehicle and track even under higher speed limit, due to improvement of the track geometry condition. The case “522” represents the high speed ballasted track after about 1 year of operation; this dynamic loading factor of 25.2 % is the best situation for ballasted track under this speed level. For a smoother track like the case “611” (dynamic loading factor

of only 11.1 %), it can be only realized by ballastless track allocation. Figure 52 shows the ESD calculation of the above mentioned combinations.

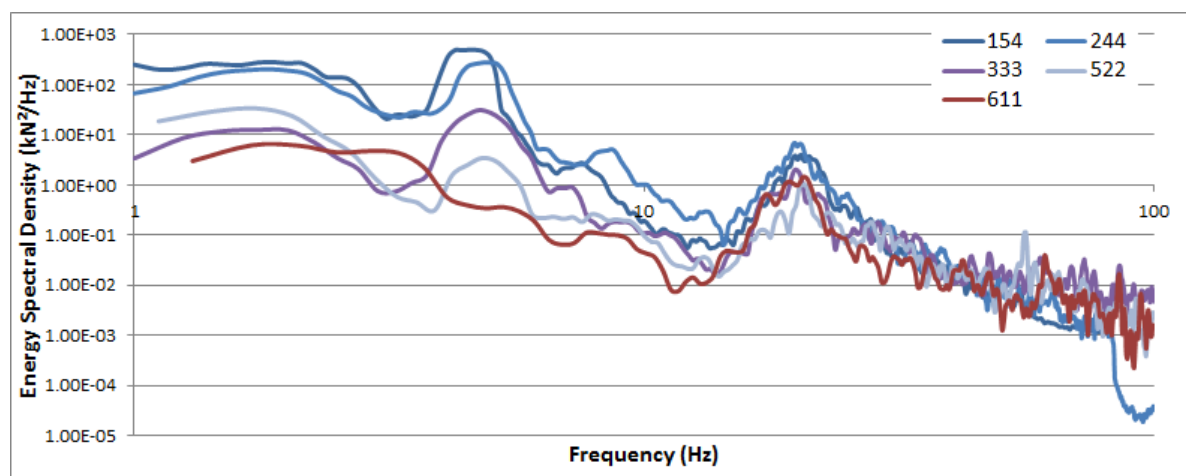


Figure 52 ESD output of selected X, Y and Z combinations

The distribution of ESD is dominantly decided by the design of the vehicle. Therefore, for same vehicle input, the shape of the ESD lines insignificantly change under different track sided influence parameters. There are two obvious peaks in the ESD distributions at the frequencies of 4.5 Hz and 20 Hz. Referring back to subsection 5.3.2 and to the vehicle design, those two peaks are caused by the bogie frame bounce and yaw, because they hold the same frequencies. Furthermore, the bounce and yaw motions of bogie frame are obvious influence parameters in the vehicle track interactions. According to the theory of ESD, those peaks mean that the dynamic wheel load under this frequency includes more energies than the surrounding frequencies and consequently, the track is severely excited under this frequency. Under certain travel speed, this might cause the so called “resonance effect”, when this wave length is typical also for track.

Since those characteristic frequencies remained the same for each speed level, they cause different characteristic wave lengths. Table 42 shows the wave length and the distance frequency at 20 Hz under different speed level.

Table 42: The wave length and distance frequency induced by the 20 Hz peak from the vehicle under different speed levels

| Frequency (Hz) | Speed (km/h) | Wave length (m) | Distance frequency (m^{-1}) |
|----------------|--------------|-----------------|---------------------------------|
| 4.5 | 80 | 4.94 | 0.20 |
| | 120 | 7.41 | 0.14 |
| | 160 | 9.88 | 0.10 |
| | 200 | 12.35 | 0.08 |
| | 250 | 15.43 | 0.06 |
| | 300 | 18.52 | 0.05 |
| | 350 | 21.60 | 0.05 |
| 20 | 80 | 1.11 | 0.90 |
| | 120 | 1.67 | 0.60 |
| | 160 | 2.20 | 0.45 |
| | 200 | 2.78 | 0.36 |
| | 250 | 3.47 | 0.29 |
| | 300 | 4.17 | 0.24 |
| | 350 | 4.86 | 0.21 |

An example of this effect could be found under the PSD output of the track vertical geometry of sections 3 and 4. Their PSD output of the track geometry was again shown in Figure 53 to Figure 54 (same as Figure 14 to Figure 15 in section 4.4.1). The maximum speed of the section is 160 km/h therefore, the peak at $0.45 m^{-1}$ should be considered as the consequence of the eigen frequency of 20 Hz of the locomotive (bogie frame bounce).

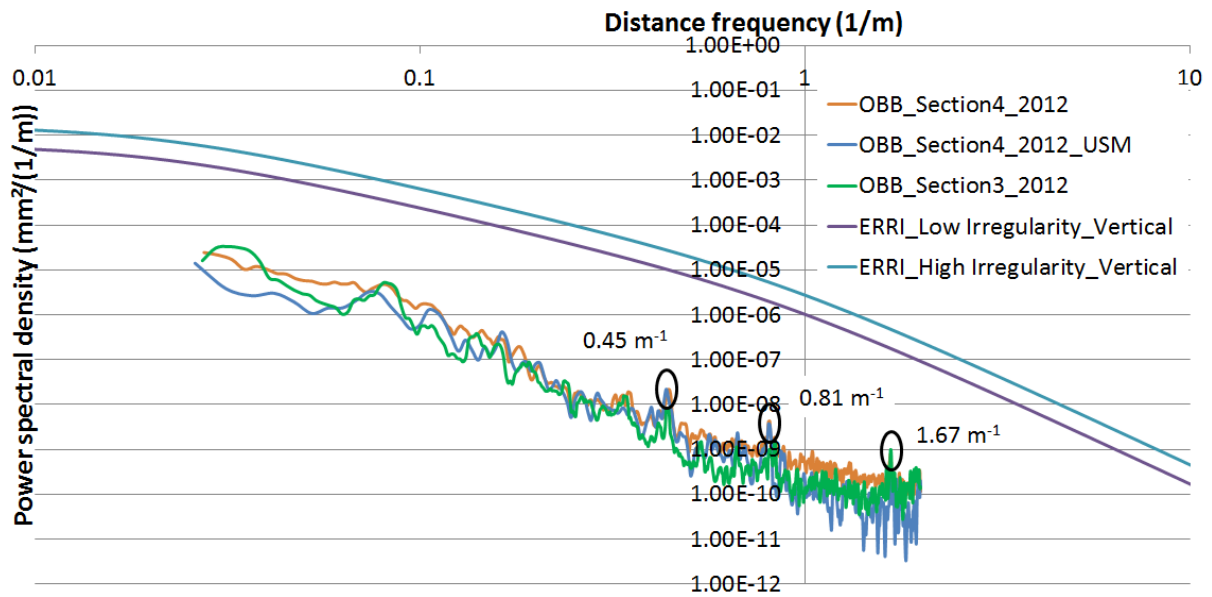


Figure 53: PSD analysis of measurement sections 3 and 4 (A-ÖBB)

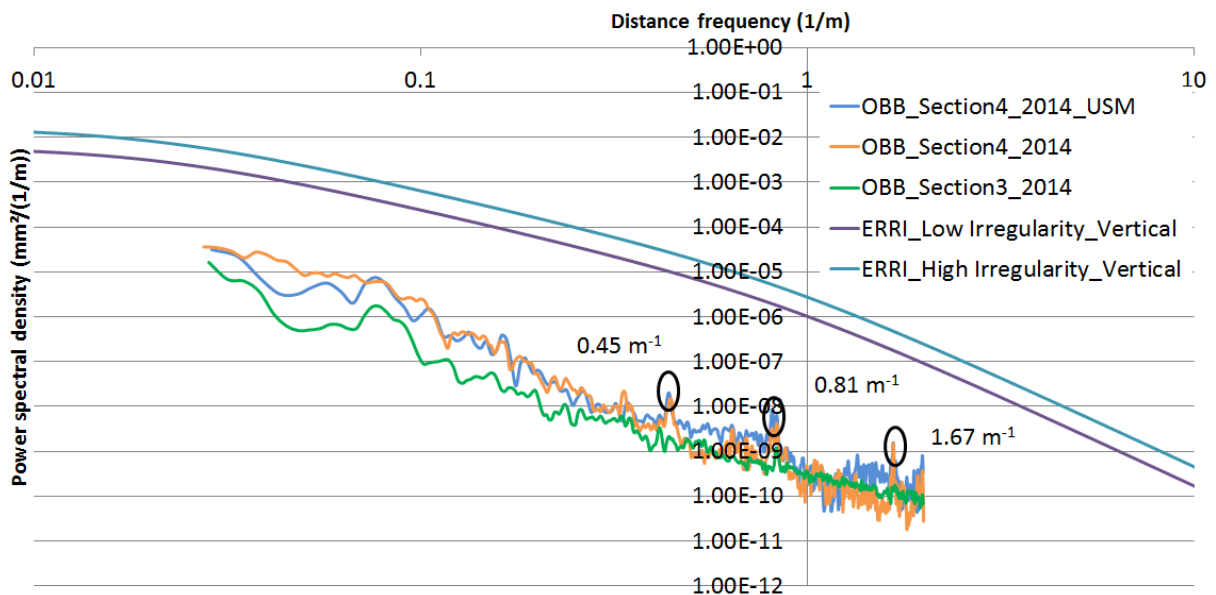


Figure 54: PSD analysis of measurement sections 3 and 4 (A-ÖBB)

6.8.ESD analysis and possibilities of improving existing track measures with track inspection car in high speed lines

It can be concluded from the above performed simulations that formal tracks have more geometrical variations than the stiffness variations. The control of the stiffness variation

can be simply realized by increasing the rigidity of the track bed, but this would counterproductively increase the deterioration rate of track geometry.

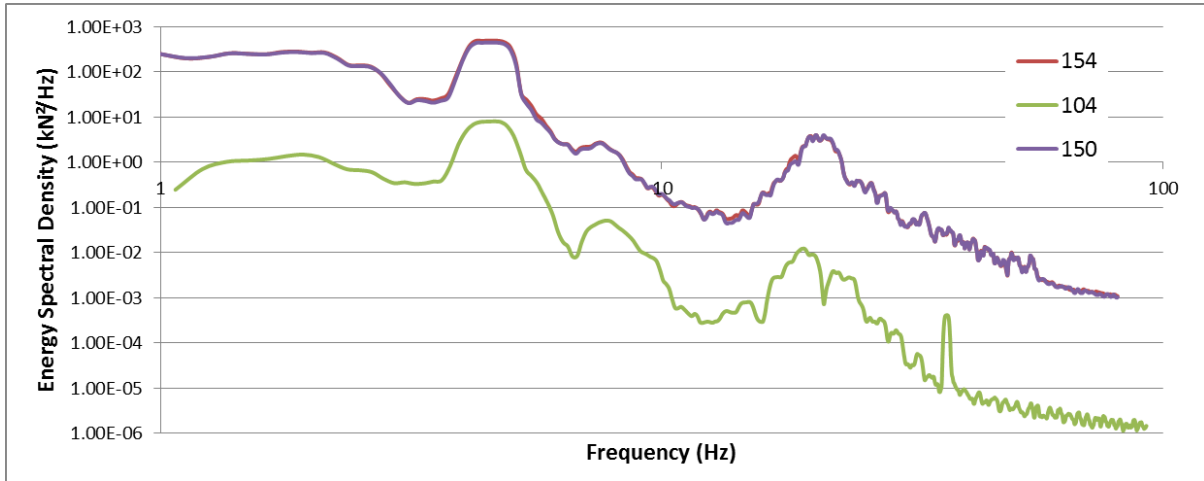


Figure 55 ESD output of 154, 150 and 104

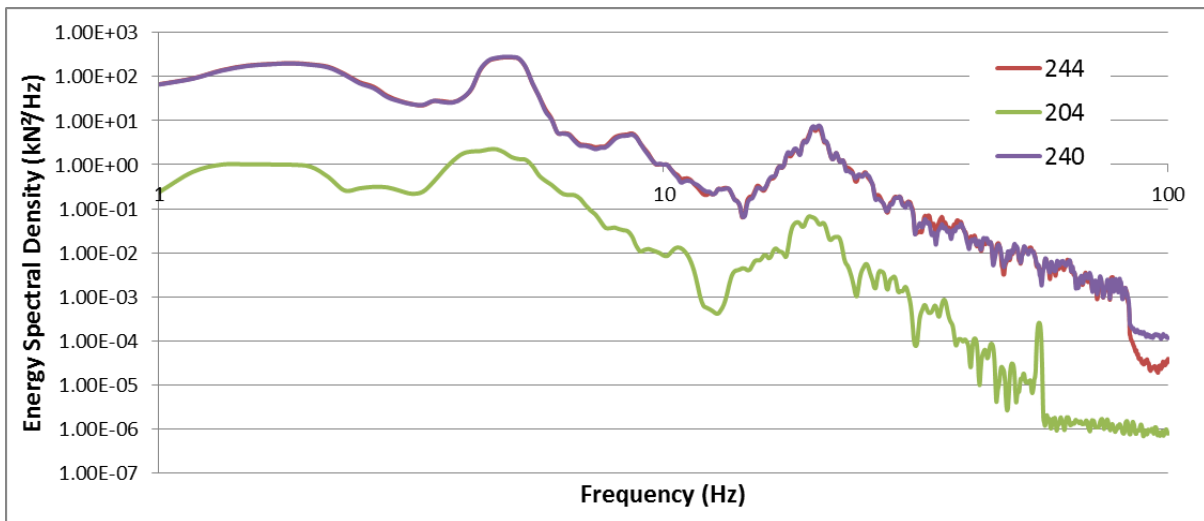


Figure 56 ESD output of 244, 240 and 204

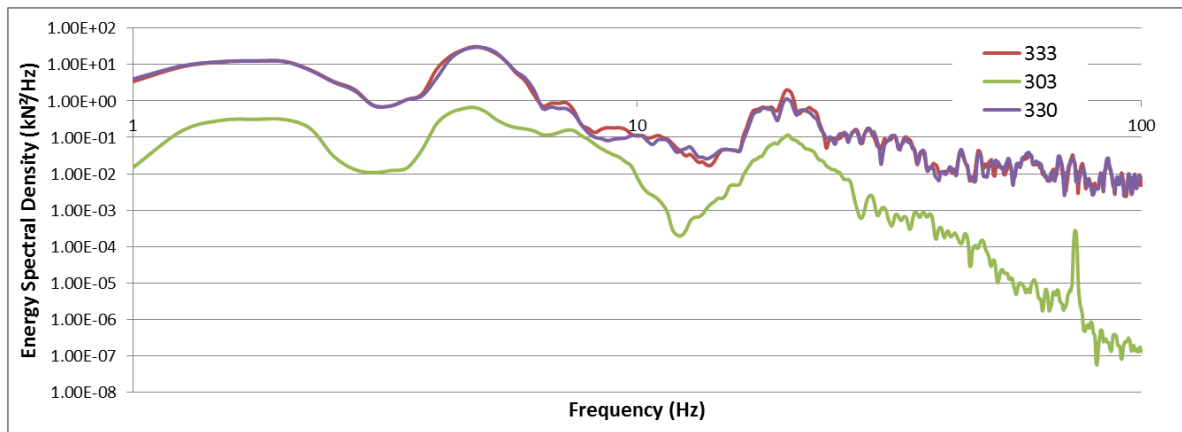


Figure 57 ESD output of 333, 330 and 303

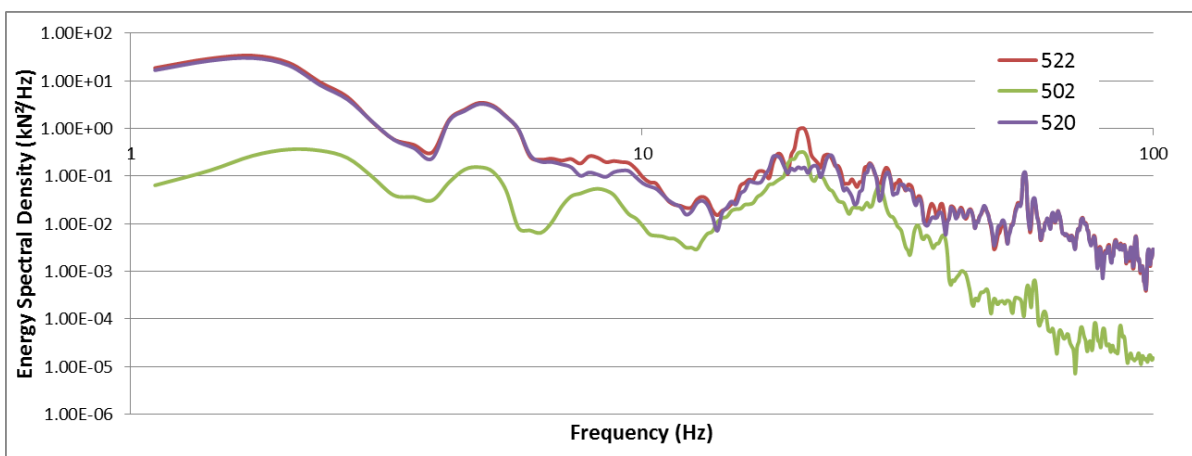


Figure 58 ESD output of 522, 520 and 502

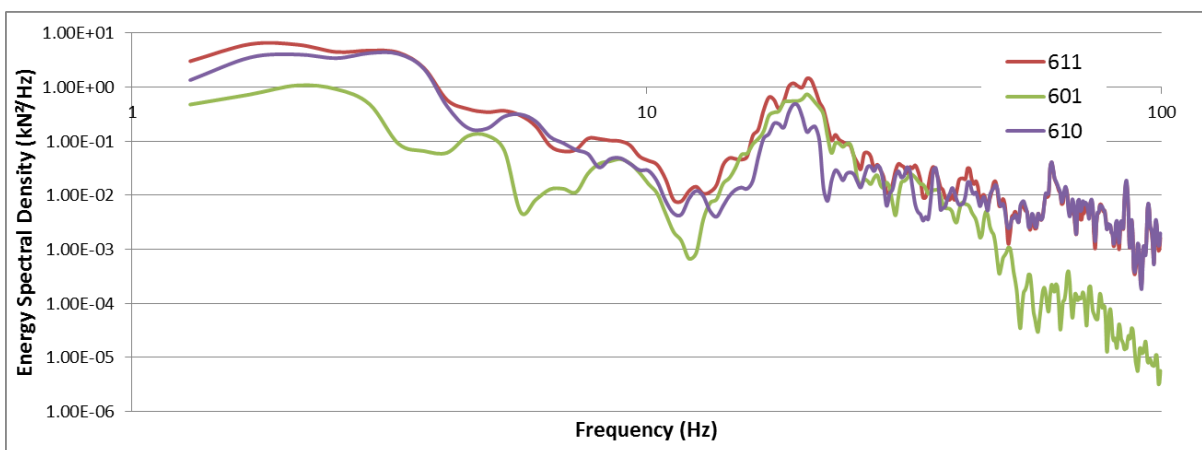


Figure 59 ESD output of 611, 610 and 601

Figure 55 to Figure 59 show the overlapped ESD curves due to single and combined excitations for each combination (the “Statistical frequency distribution” of the

scenarios can be found in appendices 34 to 36). The obvious peaks at 4.5 and 20 Hz are explained in the previous section by the bounce and yaw motion of the bogie frame. For ballasted track, with maximum design speed at under 160 km/h, the overall dynamic performance of vehicle track interaction is dominated by the variation caused by the track geometry (misalignment or settlement problem). This could be proved by observing the nearly overlapped curves of “154” and “150”, “244” and “240”, “333” and “330”. Nonetheless, the track stiffness also directly influences in the deterioration rate of the track geometry quality. Therefore, the general track quality is specified by the track geometrical condition and the variation of track stiffness can influence the track quality through an indirect way. Obvious peaks in “104”, “204” and “303” can be observed, which is identical to the sleeper spacing of the line.

This is not any longer the case while looking at the curve series of “522” and “520” as well as, “611” and “610”. Noticing that those series refer to the best modern high speed line (ballasted track or ballastless track) with very well maintained track geometry and compressively smaller superstructure stiffness than conventional tracks, the ESD output of the dynamic wheel load due to combined excitation is higher than due to track geometry excitation under certain frequencies. This frequency level is also larger in the case of “611” than “522”, because the ballastless track can achieve better track geometry quality but requires more elasticity in the superstructure. Therefore, for high speed lines with design speed at 300 km/h or higher, the variation of track stiffness becomes also the direct influence parameter.

The effect of the excitation to the track stiffness should also be studied by measuring the change of track elastic deflection separately from the track geometry. The measurements should include the following items:

- Track geometry under unloaded condition;
- Track elastic deflection under different speed levels (from quasi-static to max. operational speed). Continuous vehicle based measurement using Benkelman beam method (under construction).

Both values should be continuously measured on track. Only by gathering the above mentioned information, it is possible to dedicate the exact source of potential problems in high speed lines, where direct measures can be applied to every appeared situation.

7. SUMMARY AND CONCLUSIONS

7.1. Summary of the workflow

As the increase of train speed and axle load is the future trend in railway transportation, there will be higher requirements in technology in railway engineering field. Such requirements will focus more on ensuring the overall behavior of the rail system. In order to better understand the overall behavior of the system and to reduce the maintenance costs of the track quality (irregularity and stiffness level) in high speed lines, relative field side observations and computer simulations are applied. Field measurements provide useful data as an input, whereas the simulation can help to enlarge the sight of understanding the system's behavior. The results shown provide the evidence that such simulation tools are suitable to meet the respective requirements.

A systematic research work related to the influence of track quality, in terms of stiffness and geometry, on the performance of vehicle-track interaction and respective track quality changes, is carried out since January 2012. The research work is supported by the Karl-Vossloh funding (Project S047/10021/2011) and lasted for 3 years. This report includes the results from the activities realized in the work plan:

- Literature review, as well as collection of data (used as input for preliminary simulations and preparation of measurement strategies), results and experiences from previous works (covered in Chapter 2);
- Review of existing measures and developments of field measurements for selected pilot sections (covered in Chapter 3);
- Execution of four field measurements at four pilot sections in Germany and Austria, as well as the analysis and processing of the measurement data (covered in Chapter 4);
- Selection of the suitable numerical simulation algorithms with focus on Finite-Element-Method (FEM) and Multi-Body-Simulation (MBS) as well as co-simulations (covered in Chapter 5);

- Innovative solutions for measurement and simulation for retrieving the feedback of the dynamic interaction between vehicle and track (covered in Chapter 6).

The general procedure of the workflow follows the flip chart shown in Figure 60. The whole workflow can be divided into four blocks: measurement, data analysis, simulation and conclusion.

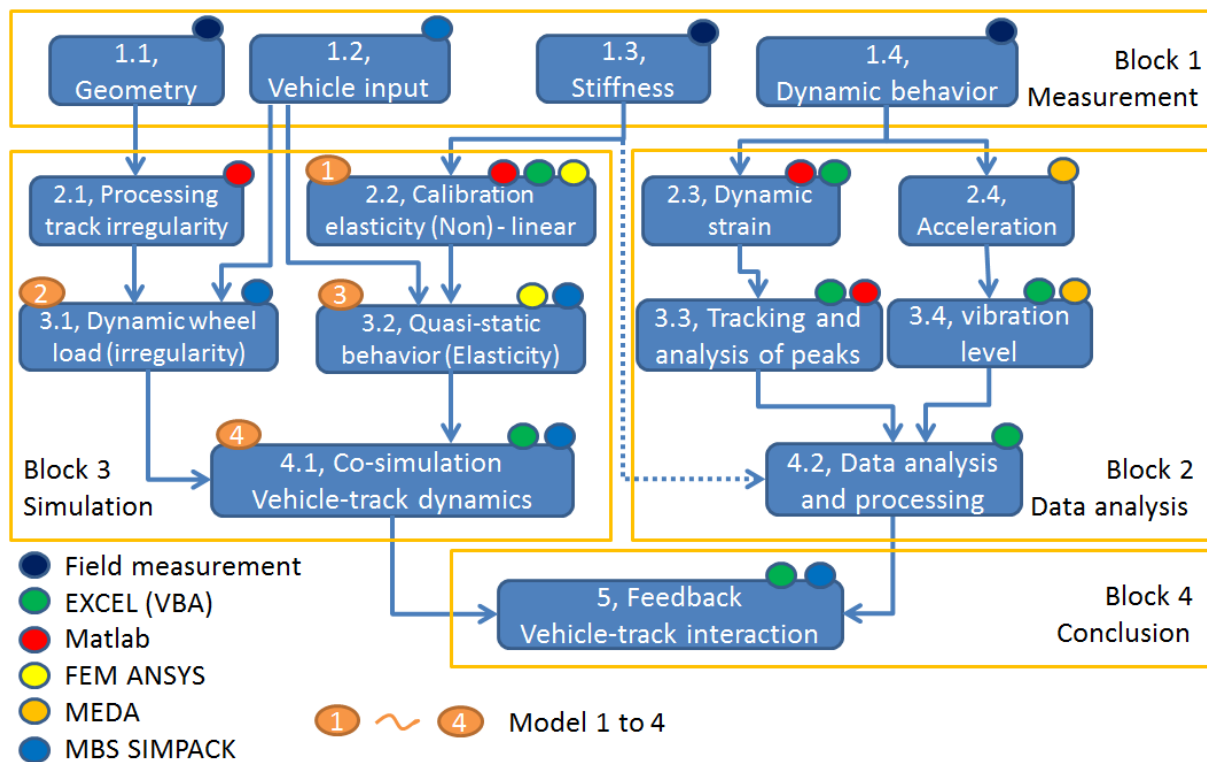


Figure 60 Illustration of the general workflow

Following measurement activities were performed in the pilot sections (**Block 1** and **Block 2**):

- Track geometry (track irregularities): A continuous 3D acquisition of the track geometry was achieved during the field measurement, including vertical, lateral, gauge and twist. A sufficient length of the sampling track (> 500 m) was recorded in order to conclude the necessary parameters for Power-Spectral-

Density functions, which is necessary for the comparison with the guideline values derived from various literatures.

- Track stiffness (static loading): The Benkelman beam measurement is actually the best tool to determine the change in track stiffness along the test section. It records the (quasi-)static rail deflection of selected individual rail seats. The methodology was applied by the field measurement on more than 400 rail seats (on both rails), in total. Respective measurement results are shown in Chapter 4.
- Calibration measurements using static axle load (quasi-static test runs): Test runs with limited speed level ($V < 15$ km/h) were performed in order to determine the actual axle load of the ballast wagon. These results also provide the information of the change in the rail foot strain due to the variation of track stiffness.
- Dynamic wheel load: Strain gauges are the most suitable measurement equipment as they provide accurate measurement data. Problem of discontinuous installation (at least every sleeper spacing) is solved by smart arrangement of allocations of strain gauges along the line (through linear estimation method). In total more than 250 strain gauges were installed in the measurement sections. The maximum measured speed of train passage is 300 km/h.
- Track vibration level: This test was done under two different approaches, namely the vibration level under singular impulse load and the vibration level under operational trains. It was found that this method could provide acceptable guidelines for observation of the track quality deterioration at the early stage. The overall vibration levels for all the measurement sections were calculated.

A better understanding of the influence of track geometry and track stiffness to the dynamic vehicle-track interaction can be achieved by applying modern numerical simulations (**Block 3**). The selection of the suitable numerical simulation methodologies relies on the specific target, as well as the experiences from previous works. Both Finite-Element-Method (FEM) and Multi-Body-Simulation (MBS) models are reviewed and their advantages as an auxiliary tool for the research work are summarized. The application of FEM and MBS, as well as the co-simulation between the both in this research is designed in the following ways:

- FEM: The stiffness of the track was simulated in the FEM models. Multi-elastic track superstructure models were built which were verified by the field measurement data. A condensation of the model by Substructural / Modal analysis was performed, which provides the possibility for time dependent simulations;
- MBS: A full-scaled vehicle model (in this research a locomotive), including detailed modeling of body and suspensions, was built. The wheel-rail contact was integrated in the MBS system with realistic wheel and rail head profiles. 3D track irregularity was included in the generation of the track sided excitation for the running vehicle, which was either derived from the measurement data or generated by the pre-given PSD curves;
- Co-simulation strategies (Off-line): The condensed FEM model with all the stiffness information was included into the MBS environment. Special contact elements were investigated and implemented for transmitting the wheel contact patch to the track. A full scale simulation of the running vehicle on real track with both the excitations of track stiffness and track irregularity was realized in the MBS interface.

Based on the developed technology, a better understanding of the influence mechanism of the track sided excitations on the behavior of vehicle track interaction could be achieved (**Block 4**). Varies inputs of track stiffness and irregularity which had different quality indexes were collected from previous measurement activities. In addition, large amount of simulations were performed under the influencing parameters of vehicle speed, track geometry and track stiffness input. The effect of the geometry and stiffness to the performance of vehicle track interaction due to the new method can now be separately analyzed, which previously was not possible.

7.2. Conclusions

The track sided key parameters of track geometry and track stiffness are determinant factors for the overall performance of the dynamic vehicle track interaction. A real-time representation of the dynamic vehicle track interaction under pre-defined vehicle and track sided parameters is realized by the co-simulation with FEM and MBS. For this research, the modeled vehicle is a modern electric locomotive with an axle load of 21.5 t.

The individual influencing parameters, like vehicle speed, track geometry and track stiffness, can be adjusted in the model easily from scenario to scenario. A wide selection of the values of the three influencing parameters and their simulations were performed. The selected scenarios are able to cover a wide spectrum of realistic track qualities from the local lines with strict speed limits to the branch lines with high speed operations.

One of the major advantages of numerical modeling is the rich output of simulation results. A direct output of the wheel dynamic load in time sequence is possible which is normally difficult to measure in a direct way. Dynamic loading factors are calculated and can be compared with the conventional factors used for coverage of dynamic effects by increasing the static wheel load e.g. for ballastless track design.

Energy Spectral Density (ESD) functions based on the dynamic wheel load are calculated. The ESD analyses of the output “dynamic wheel load” can provide the energy distribution of the vehicle passage under each frequency level. This is the precise output of the effect of the dynamic wheel load with respect to track quality deterioration and maintenance strategy (ballasted track). The vehicle and track sided eigen behavior (shown as peaks in the distribution) shows all the characteristic frequencies which shall not be overlapped e.g. due to change of passage speed, in order to avoid resonance effects. For this research, peaks in ESD distribution were found at 5 Hz and 20 Hz, which are identical to the bounce and yaw modes of the bogie frame of the modeled locomotive. This vehicle running under 160 km/h can cause due to the 20 Hz peak a wave length of 2.2 m, which can accelerate the deterioration rate

of the track geometry quality under this wave length (proved by the PSD distribution of vertical track geometry for sections 3 and 4).

It is found out from the plotted ESD curves under different scenarios that for design of ballasted track with stiff superstructure support, the effect of track stiffness to the overall behavior of the dynamic vehicle track interaction is much less than the effect of track irregularity. In this case, track measurement by track inspection car (TIC) can use the integrated measurement approach for specification of maintenance strategies. For high speed lines, especially with ballastless track, it is preferable to apply separate measurements for determination of track stiffness and track geometry since their effects, due to the improved track geometry level and low track stiffness, become comparable. These measures shall include the following items:

- Track geometry under unloaded condition;
- Track elastic deflection under different speed levels (from quasi-static to max. operational speed due to acquisition of track damping factors).

The second measure may rely on a new continuous vehicle based measurement using an advanced Benkelman beam method.

Finally it can be concluded from the aforementioned simulation results, that the conventional empirical approach for determination of the dynamic loading factor provides comparative results (less than 5 % of difference) under bad or very bad track quality and low speed level. E.g. the calculated dynamic loading factor for speed level 120 km/h is 1.70 vs 1.75, for 80 km/h is 1.79 vs 1.77 (conventional empirical approach vs simulation). However, the conventional approach will be too conservative under good or moderate track quality with higher speed level. This can be found at 300 km/h by 1.49 vs 1.11, at 250 km/h by 1.45 vs 1.25 and under 160 km/h by 1.57 and 1.19 (conventional empirical approach vs simulation). This effect is due to the strong contribution of track quality (if the quality is poor) to the results which overtakes the major effect coming from the vehicle design. Under good track quality conditions with improved mechanical design of the vehicle, the dynamic factors will be much smaller than those from the conventional empirical approach. Consequently, the empirical

method can always provide a rough estimation of the dynamic loading factor being on the safe side, but a more precise calculation is possible based on the developed co-simulation strategy and will give lower dynamic forces in case good track quality is maintained e.g. for ballastless track design. For modern locomotives without wheel flats (freight wagons are not considered here), a maximum dynamic loading factor of 1.35 will be sufficient if the track geometry condition fulfills the requirement of AKFF^[20] (defined using PSD distribution of vertical track geometry) when the travel speed is below 300 km/h corresponding to a modified calculation formula for straight track (speed higher than 60 km/h, compared to the factor 1.49 given by the conventional empirical approach):

$$\max Q = Q_{\text{mean}} * \left(1 + \frac{V^2 + 128000}{625000} \right)$$

Better track quality (with respect to track stiffness and geometry) of ballastless tracks provided and demonstrated by design and respective construction procedures could lead to reduced dynamic factors applied for next generation design specifications.

SOURCE OF REFERENCE

1. KAEWUNRUEN, S, REMENNIKOV, A.M. (2007), Response and Prediction of Dynamic Characteristics of Worn Rail Pads Under Static Preloads, University of Wollongong, Australia
2. ZIMMERMANN, H. (1888), Die Berechnung des Eisenbahnoberbaus, in German, Verlag von Ernst&Korn (Wihelm Ernst), Berlin, Germany.
3. VAN'T. ZAND. Ir. J. (1994), Assessment of dynamic characteristics of rail pads, Railway Engineering international edition Number 4
4. KNOTHE, KL, GRASSIE, S.L. (1993), Modelling of railway track and vehicle/track interaction at high frequencies, Volume 22, Issue 3-4, Vehicle system dynamics.
5. KUMARAN, G., MENON, D. and KRISHNAN, K. (2003), Dynamic Studies of Railtrack Sleepers in a Track Structure System, Journal of Sound and Vibration.
6. WOLTER, K., (2012), Rekonstruktion der originalen Gleislageabweichungen aus 3-Punkt-Signalen (Wandersehenmessverfahren) und Beurteilung hinsichtlich Amplitude, Fehlerwellenlänge sowie Fehlerform. In German. Berlin, Germany, 2012
7. OPPENHEIM, A.V, SCHAFER, R.W. (1999), Zeitdiskrete Signalverarbeitung, 3. Auflage. In German. Wien, Austria, 1999
8. DIRAC, P. (1958), The Principles of Quantum Mechanics (4th edition, 1958). Page 58. §15 The δ function
9. Intec GmbH (2008), SIMPACK Reference Guide, SIMPACK Release 8.9, Wessling, Germany
10. ORE B 176: Lastenheft für ein Drehgestell mit verbesserten Eigenschaften bei Fahrt im Bogen. Utrecht 1991
11. DE MAN, A. P. (2002), DYNATRACK - A survey of dynamic railway track properties and their quality, PhD, Technical University Delft, DUP Science, Delft University Press, Netherlands
12. LECHNER B. (2007), Modelling vertical loading, page 13 to 14, Lecture notes for rail design, Master of Transportation System, Technische Universitaet Muenchen, Germany

13. Intec GmbH (2008), SIMPACK Reference Guide, Page 19, SIMPACK Release 8.9, Wessling, Germany
14. ALBERS A. , HAEUSSLER P. (2005), Topology optimization of dynamic loaded parts using multibody simulation and durability analysis, University of Karlsruhe (TH), Karlsruhe, Germany
15. Intec GmbH (2008), SIMPACK Reference Guide, Page 17, SIMPACK Release 8.9, Wessling, Germany
16. DIETZ, S., et.al (2001), Interaction of vehicles and flexible tracks by co-simulation of Multibody vehicle systems and finite element track models, Vehicle system dynamics
17. WEIDEMANN, C. (2003), Air-springs in Simpack, SIMPACK news, Wessling, Germany, 2003.
18. Vogel&Plötscher (2010), Production catalog, MessReg CLS. www.vogelundploetscher.de
19. DIN 45672-2 (1995), Schwingungsmessung in der Umgebung von Schienenverkehrswegen - Teil 2: Auswerteverfahren (in German), Deutsches Institut für Normung e.V.
20. DB Netz AG / DB Systemtechnik (2002), Anforderungskatalog zum Bau der Festen Fahrbahn – 4. Überarbeitete Auflage – Stand 01.08.2002, in German.
21. LEYKAUF, G., LECHNER, B. (2006), research report No. 2253, Chair and institute of road, railway and airfield construction, TU-Muenchen, Germany.
22. LIU, J. (2007), Tragwirkung der elastische gelagerten Schiene unter exzentrischer vertikaler und horizontaler Belastung. Lehrstuhl und Prüfamnt für Verkehrswegebau der TU München. Diplomarbeit Nr. 805. In German. Munich, Germany. 2007.
23. MA, HC. (2013), Determination of the dynamic wheel load in vertical direction under running trains using Finite-Element-Method, Master's thesis No. 39 (not published), Chair and institute of road, railway and airfield construction, TU-Muenchen, Germany.
24. DING, L. (2014), Automatisierung eines Iterationsverfahrens für das FEM-Programm ANSYS durchgeführt mit MATLAB, Internship report (in German, not published), Chair and institute of road, railway and airfield construction, TU-Muenchen, Germany.

-
25. Manchester Metropolitan University (1998), The Manchester Benchmarks for rail vehicle simulation, Rail Technology unit.
 26. PANDEY, K. (2013), Study and numerical simulation of railway vehicle-track interaction based on vehicle side parameters using SIMPACK, Master's thesis No. 71 (not published), Chair and institute of road, railway and airfield construction, TU-Muenchen, Germany.
 27. KALKER, J.J. (1982), A Fast Algorithm for the Simplified Theory of Rolling Contact, Vehicle system dynamics 11 (1982), pp.1-13, Delft University of Technology, Delft, Netherlands
 28. Intec GmbH (2008), SIMPACK Track module, page 10.1-85, SIMPACK release 8.9, Wessling, Germany.
 29. SIMPACK AG (2013), SIMACK Documentation, D22.6.3 Track excitations, SIMPACK release 9.5, Wessling, Germany
 30. DIN EN 14363 (2005), Bahnanwendungen – Fahrtechnische Prüfung für die fahrtechnische Zulassung von Eisenbahnfahrzeugen – Prüfung des Fahrverhaltens und stationäre Versuche; Deutsche Fassung EN 14363:2005. In German. Berlin, Germany, 2005
 31. SIMPACK AG (2014), Curve-Curve 2D contact, Page D.15.5.-96, Simpack documentation release 9.7, Wessling, Germany.
 32. Intec GmbH (2008), SIMPACK Track module, page 11.3-107, SIMPACK release 8.9, Wessling, Germany.
 33. CHEN, KL. (2014), Dynamische Simulation eines Gleises unter Berücksichtigung der echtzeitigen Wechselwirkung zwischen Zug und Gleis basierend auf einem kombinierten Ansatz von FEM und MBS, Master's thesis No. 68 (in German, not published), Chair and institute of road, railway and airfield construction, TU-Muenchen, Germany.
 34. FREUDENSTEIN, S., LIU, D., LECHNER, B. (2014), Smart Maintenance and Analysis of Rail Infrastructure SMART Rail, Final report, work package 3.4 (7th Framework program), research report No. 3122, Chair and institute of road, railway and airfield construction, TU-Muenchen, Germany.
 35. SIMPACK AG (2011), Flexible Bodies Tutorial I, Page 82, Simpack documentation release 9.7, Wessling, Germany

Source of reference

36. EN 13848-5:2008+A1 (2010), Railway applications – Track – Track geometry quality – Part 5: Geometric quality levels – Plain line, European Committee for Standardization.
37. DB Richtlinien 821.2001 (2010), Prüfung der Gleisgeometrie mit Gleismessfahrzeugen, in German, Deutsche Bahn.
38. OPPENHEIM, A.V., VERGHESE, G.C. (2010), Signals, systems and inference, class notes for 6.011: Introduction to communication, control and signal processing, Massachusetts Institute of Technology

List of Figures

| | |
|---|----|
| Figure 1 Principle of the LTI system ^[07] | 5 |
| Figure 2 Typical railway superstructure and optional elastic elements | 7 |
| Figure 3 Typical deflection line calculated by Zimmermann Theory | 8 |
| Figure 4 Distribution of ballast pressure under soft and stiff pad allocations | 9 |
| Figure 5 Sample SIMPACK Model for railway vehicle ^[15] | 15 |
| Figure 6 Movable track recording wagon (Type CLS from company V&P) ^[18] ... | 21 |
| Figure 7 Benkelman beam for the measurement of track elastic deflection | 22 |
| Figure 8: Typical accelerometers and its internal design..... | 25 |
| Figure 10: Allocation of the measurement sensors | 26 |
| Figure 11: The processing of track geometry (GUI interface)..... | 33 |
| Figure 12: Sample PSD distribution in vertical direction (values derived from “ERRI” and “AKFF”)..... | 35 |
| Figure 13: PSD analysis of measurement sections 1 and 2 (vertical direction) . | 36 |
| Figure 14: Illustration of the analysis interval of section 4 (vertical direction) | 37 |
| Figure 15: PSD analysis of measurement sections 3 and 4 (vertical direction) . | 38 |
| Figure 16: PSD analysis of measurement sections 3 and 4 (vertical direction) . | 38 |
| Figure 17: Automatic peak selection (GUI interface)..... | 43 |
| Figure 18: CV of locomotive – Section 1 (passage speed of 200 ± 10 km/h) | 46 |
| Figure 19: CV of locomotive – Section 2 (passage speed of 200 ± 10 km/h) | 47 |
| Figure 20: CV of locomotive – Section 3 (passage speed of 160 ± 10 km/h) | 47 |
| Figure 21: CV of IC locomotive – Section 4 (passage speed of 160 ± 10 km/h) | 47 |
| Figure 22: Change of vertical track geometry in sections 3 and 4 (selection).... | 48 |
| Figure 23: Vibration velocity on rail under hammer excitation | 52 |
| Figure 24: Vibration velocity on sleeper under hammer excitation | 52 |
| Figure 25: Effect of trains with wheel flat (passage speed of approximately 80 km/h) | 54 |
| Figure 26: Distribution of vibration velocity – train type IC ($V = 160$ km/h) | 54 |
| Figure 27 General modeling process | 58 |
| Figure 28 Principle of the FEM model | 60 |
| Figure 29 Graphical representation of elements and system (ballasted track) .. | 61 |
| Figure 30 Graphical representation of elements and system (ballastless track) | 61 |
| Figure 31 Sample measurement and calculation results (Rail seats 10 and 12) | 63 |
| Figure 32 Measurement and calculation result after 6 th iteration (Rail seats 10 and 12)..... | 67 |
| Figure 33: Structure of the co-simulation program | 68 |
| Figure 34: Automatic calibration of ANSYS model (GUI interface)..... | 69 |
| Figure 35 Topology of the vehicle with two layers of suspensions | 71 |
| Figure 36 Modeled bogie and vehicle in Simpack | 71 |

List of figures and tables

Figure 37 Important eigen modes for vertical vehicle behavior 71

Figure 38 Contact between wheel and rail (Profile S1002 and 60E1) 72

Figure 39 The definition of 3D track excitation in MBS system ^{[28][29]}..... 73

Figure 40 The statistical frequency distribution analysis of dynamic load (Section 4)..... 75

Figure 41 Illustration of the defined “Master node” in FEM model (Purple arrow) 77

Figure 42 Illustration of eigen mode 1 ($f_0 = 1298$ Hz) 78

Figure 43 Illustration of eigen mode 2 ($f_0 = 1436$ Hz) 79

Figure 44 Simpack vehicle model with built-in flexible track structure 80

Figure 45 Graphical representation of elastic track deflection under wheel load 80

Figure 46 Elastic deflection under train passage at certain rail seats 81

Figure 47 The statistical frequency distribution analysis of dynamic load (measurement in 2012, Section 4) 84

Figure 48 The statistical frequency distribution analysis of dynamic load (measurement in 2014, Section 4) 84

Figure 49 Track vertical geometry (Var1 and Var2)..... 87

Figure 50 PSD output of the track vertical geometry (Var1 and Var2)..... 88

Figure 51 dynamic loading factor according to speed (track irregularity according to AKFF)..... 92

Figure 51 PSD output of the selected track geometry 93

Figure 52 ESD output of selected X, Y and Z combinations..... 97

Figure 53: PSD analysis of measurement sections 3 and 4 (A-ÖBB)..... 99

Figure 54: PSD analysis of measurement sections 3 and 4 (A-ÖBB)..... 99

Figure 55 ESD output of 154, 150 and 104 100

Figure 56 ESD output of 244, 240 and 204 100

Figure 57 ESD output of 333, 330 and 303 101

Figure 58 ESD output of 522, 520 and 502 101

Figure 59 ESD output of 611, 610 and 601 101

Figure 60 Illustration of the general workflow 105

List of Tables

| | |
|---|----|
| Table 1: Theoretical calculation with Zimmermann theory (Rail type 60E2)..... | 8 |
| Table 2: Determination of factors n and φ ^[12] | 12 |
| Table 3: General working process of FEM and MBS..... | 13 |
| Table 4: Comparison of FEM and MBS approach | 16 |
| Table 5: Selection of measurement sections..... | 19 |
| Table 6: Calculation of the minimum measurement length for geometry measurement | 20 |
| Table 7: Performance data of movable track recording wagon | 21 |
| Table 8: Data amplifier QuantumX | 24 |
| Table 9: Inter-City-Express, ICE 1 / ICE 2 (D-DB)..... | 28 |
| Table 10: Inter-City-Express, ICE 3 / ICE T (D-DB)..... | 29 |
| Table 11: The express trains IC / RE (D-DB) | 29 |
| Table 12: Electric Multiple Units KISS (A-ÖBB)..... | 30 |
| Table 13: Electric locomotives (A-ÖBB) | 31 |
| Table 14: Passenger wagons (A-ÖBB)..... | 31 |
| Table 15: Statistical analysis of vertical track geometry | 34 |
| Table 16: Statistical analysis of rail seat deflection at sections 1 and 2 ^{*)} | 40 |
| Table 17: Statistical analysis of rail seat deflection at sections 3 and 4 ^{*)} | 40 |
| Table 18: Statistical analysis of rail foot bending stress of the quasi-static test runs | 44 |
| Table 19: Frequent measured passage speed of all the train types | 45 |
| Table 20: Statistical analysis of the dynamic rail foot bending stress of the measured locomotive of type "IC" (static axle load of 21.5 t)..... | 46 |
| Table 20: Change of vertical track geometry in sections 3 and 4 | 48 |
| Table 21: Average and Max of CV of max rail bending stress for selected train types..... | 50 |
| Table 22: The measurement items and their functionalities for the numerical models..... | 56 |
| Table 23: Comparison of FEM and MBS approach | 58 |
| Table 24: Directions of motion for numerical models..... | 58 |
| Table 25: Parameters of the simplified rail model ^[22] | 59 |
| Table 26: Error analysis after initial condition ^{*)} | 63 |
| Table 27: Illustration of weighting factor | 64 |
| Table 28: Boundary condition; Diff. Deflection [mm], Iteration 6 – 5 (rounding applied) | 65 |
| Table 29: Number of difference over limitation | 66 |
| Table 30: Error analysis after 6 th iteration step ^{*)} | 66 |
| Table 31: Comparison of the calculation time with Excel and Matlab (Model 1) | 69 |
| Table 32: The eigen values of selected motion | 72 |

List of figures and tables

Table 33: Simulated dynamic wheel loads under track geometry variations(wheel load of 105 kN) 74

Table 34: Sstatistical results of the simulated dynamic wheel loads (static wheel load of 105 kN) 82

Table 35: The dynamic load under track geometry and speed variations (static wheel load of 105 kN)..... 88

Table 36: Numbering of influence factors X, Y and Z and their values 90

Table 37: The dynamic load under track geometry and speed variations 94

Table 38: The dynamic load under track stiffness and speed variations 95

Table 39: Realized combination of X, Y and Z and dynamic loading factor 96

Table 40: Analytical calculation of dynamic loading factor from classic formulas 96

Table 41: The wave length and distance frequency induced by the 20 Hz peak from the vehicle under different speed levels 98

Appendices

This document included all the appendices. They were numbered from 1 to 36.

Deutsche Bahn – NIM – Mess 1

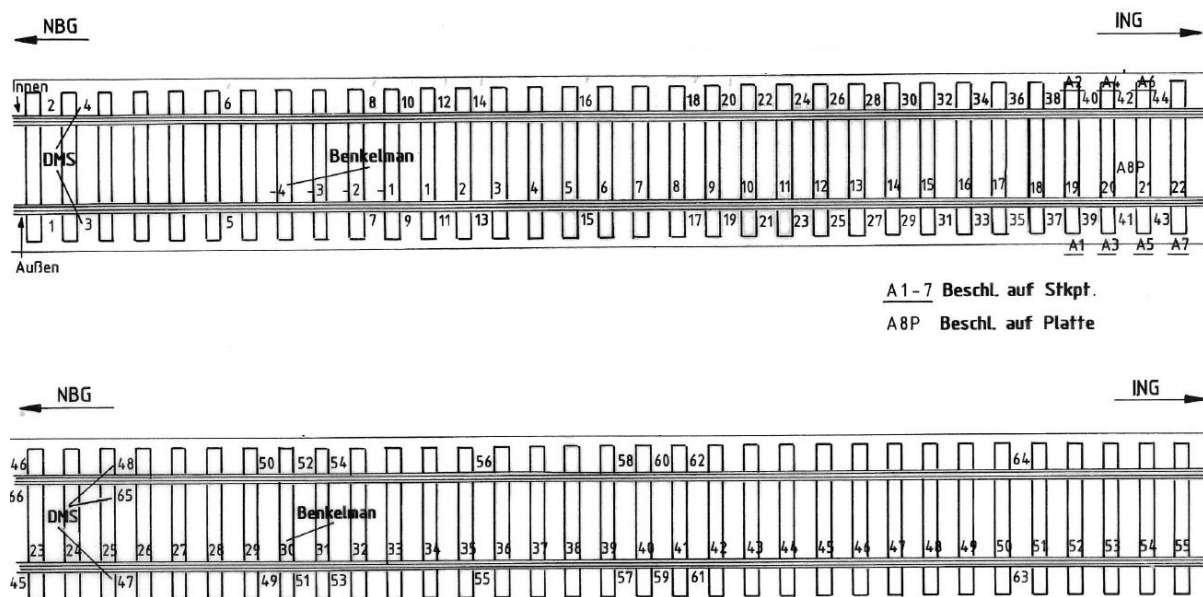


Figure: Section plan and installation of test sensors (section 1)

Table: Pilot section 1 in the German railway network (DB)

| Item | Description |
|-----------------------------------|--------------------------|
| Location between | Nuremberg and Ingolstadt |
| Art of superstructure | Ballastless track type 1 |
| Rail fastening | Vossloh 300-1 |
| Design speed (km/h) | 300 |
| Design axle load (t) | 25.0 |
| Alignment horizontal | $R = \infty$ |
| Installed number of strain gauges | 64 |
| Measured Benkelman points | 120 (60 on each rail) |
| Measured train runs (high speed) | 17 |

Appendix 2

Deutsche Bahn - NIM - Mess 2

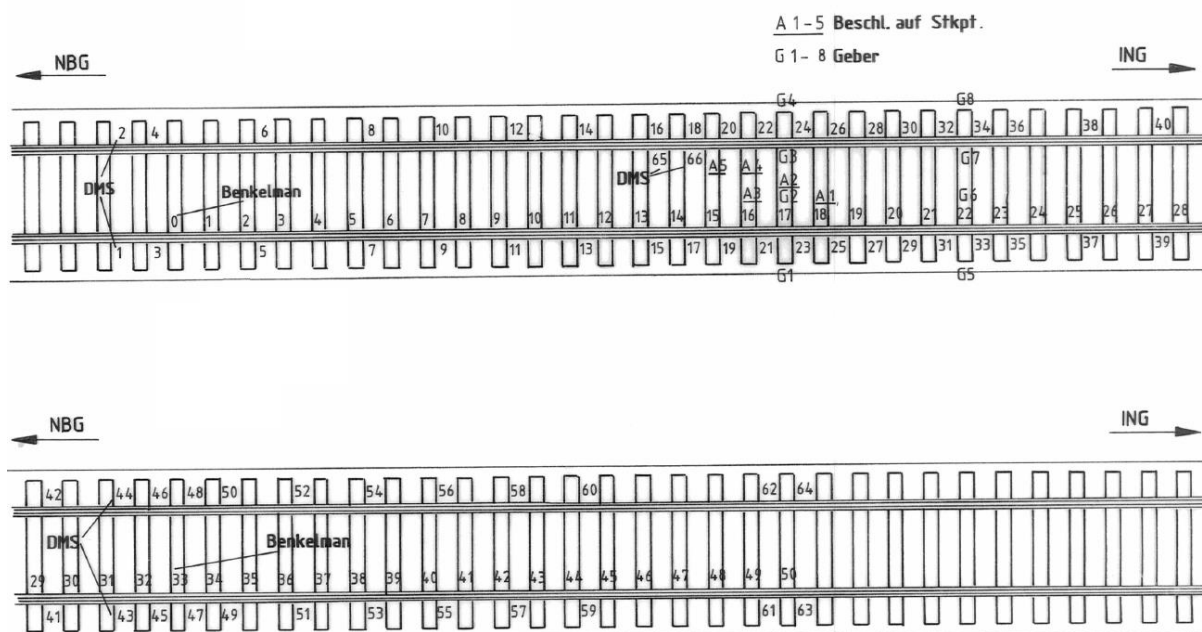


Figure: Section plan and installation of test sensors (section 2)

Table: Pilot section 2 in the German railway network (DB)

| Item | Description |
|-----------------------------------|---------------------------------|
| Location between | Nuremberg and Ingolstadt |
| Art of superstructure | Ballastless track type 2 |
| Rail fastening | Vossloh 300-1 |
| Design speed (km/h) | 300 |
| Design axle load (t) | 25.0 |
| Alignment horizontal | $R = \infty$ |
| Installed number of strain gauges | 64 |
| Measured Benkelman points | 50 (only at field side rail) |
| Measured train runs (high speed) | 12 |

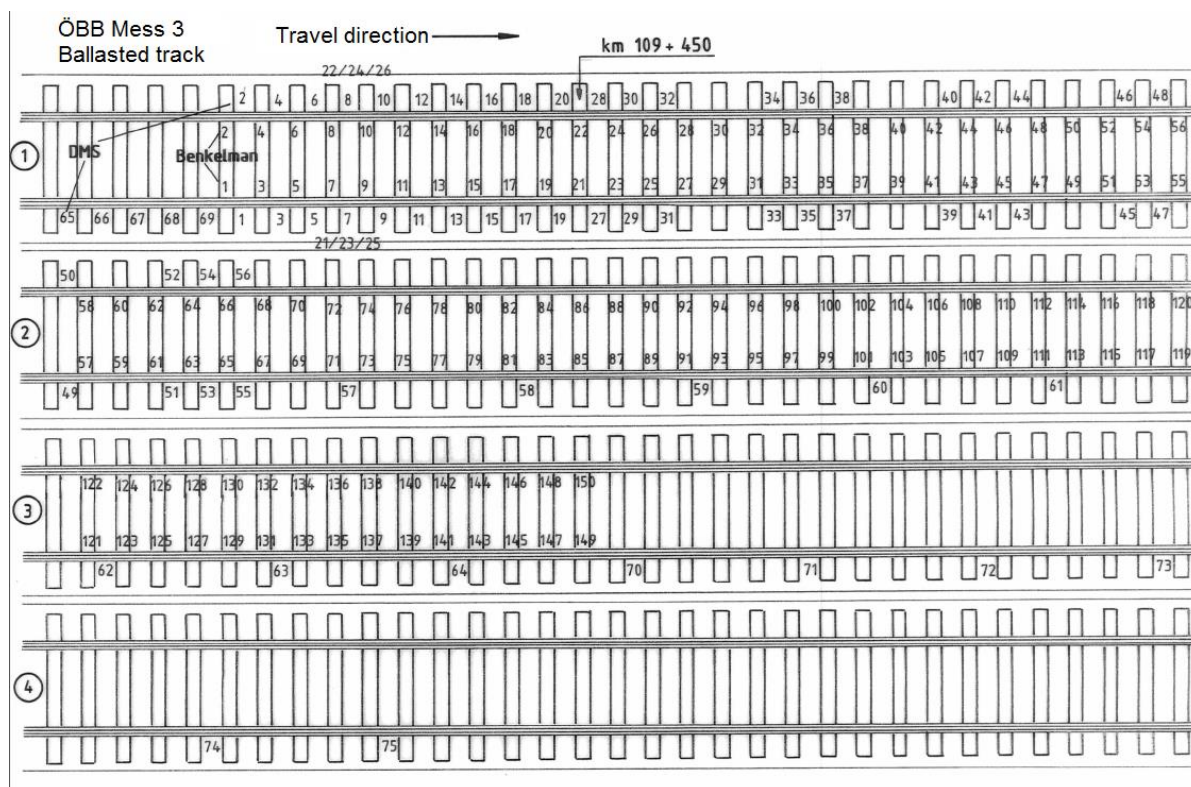


Figure: Section plan and installation of test sensors (section 3)

Table: Pilot section 3 in the Austrian railway network (ÖBB)

| Item | Description |
|-----------------------------------|---|
| Location between | Ybbs and Amstetten |
| Milepost between | km 109+400 and km 109+500 |
| Art of Superstructure | Ballasted |
| Rail fastening | Vossloh Zw700+SkI21 |
| Sleeper and USP | K1 + SLB3007G |
| Design speed (km/h) | 250 |
| Design axle load (t) | 25.0 |
| Alignment horizontal | $R = \infty$ |
| Alignment vertical (slope) | +3.3‰ to -2.4‰ |
| Slope change at milepost | km 109+450 |
| Installed number of strain gauges | 75 |
| Measured Benkelman points | 150 (75 points on each rail) |
| Measured train runs | 3 (quasi-static for calibration) 30 (passenger and freight with regular speed level) |

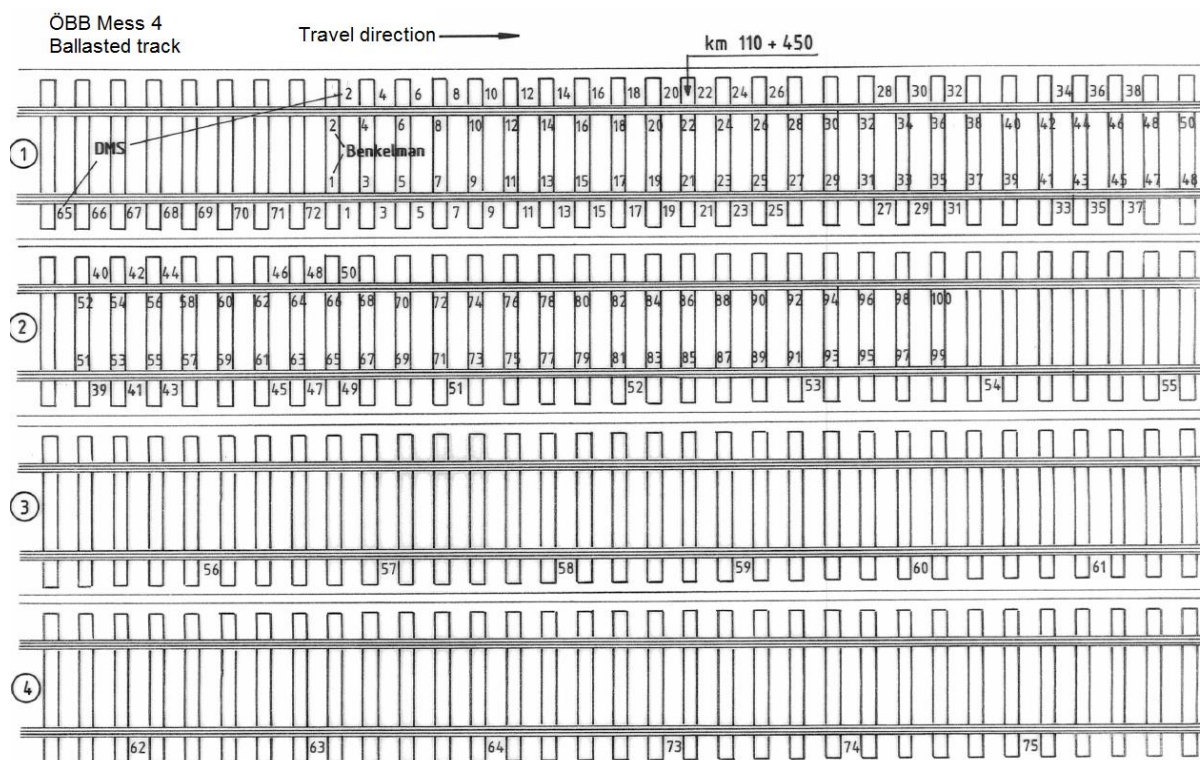


Figure: Section plan and installation of test sensors (section 4)

Table: Pilot section 4 in the Austrian railway network (ÖBB)

| Item | Description |
|------------------------------------|---|
| Location between | Ybbs and Amstetten |
| Milepost between | km 110+400 and km 110+500 |
| Special super structure design | Sub-ballast-mat installed between km 110+450 and km 110+500 |
| Art of superstructure | Ballasted |
| Rail fastening | Vossloh Zw700+Sk121 |
| Sleeper and USP | K1 + SLB3007G |
| Design speed (km/h) | 250 |
| Design axle load (t) | 25.0 |
| Alignment horizontal | $R = \infty$ |
| Alignment vertical (slope) | +4.5‰ constant |
| Installed Sub-ballast-mat between | km 110+450 and 110+500 |
| Elasticity change at milepost | km 110+450 |
| Installed number of strain gauges | 75 |
| Measured Benkelman points | 80 (50 points on field side rail and 30 on inside rail) |
| Measured train runs (quasi-static) | 4 quasi-static for calibration |

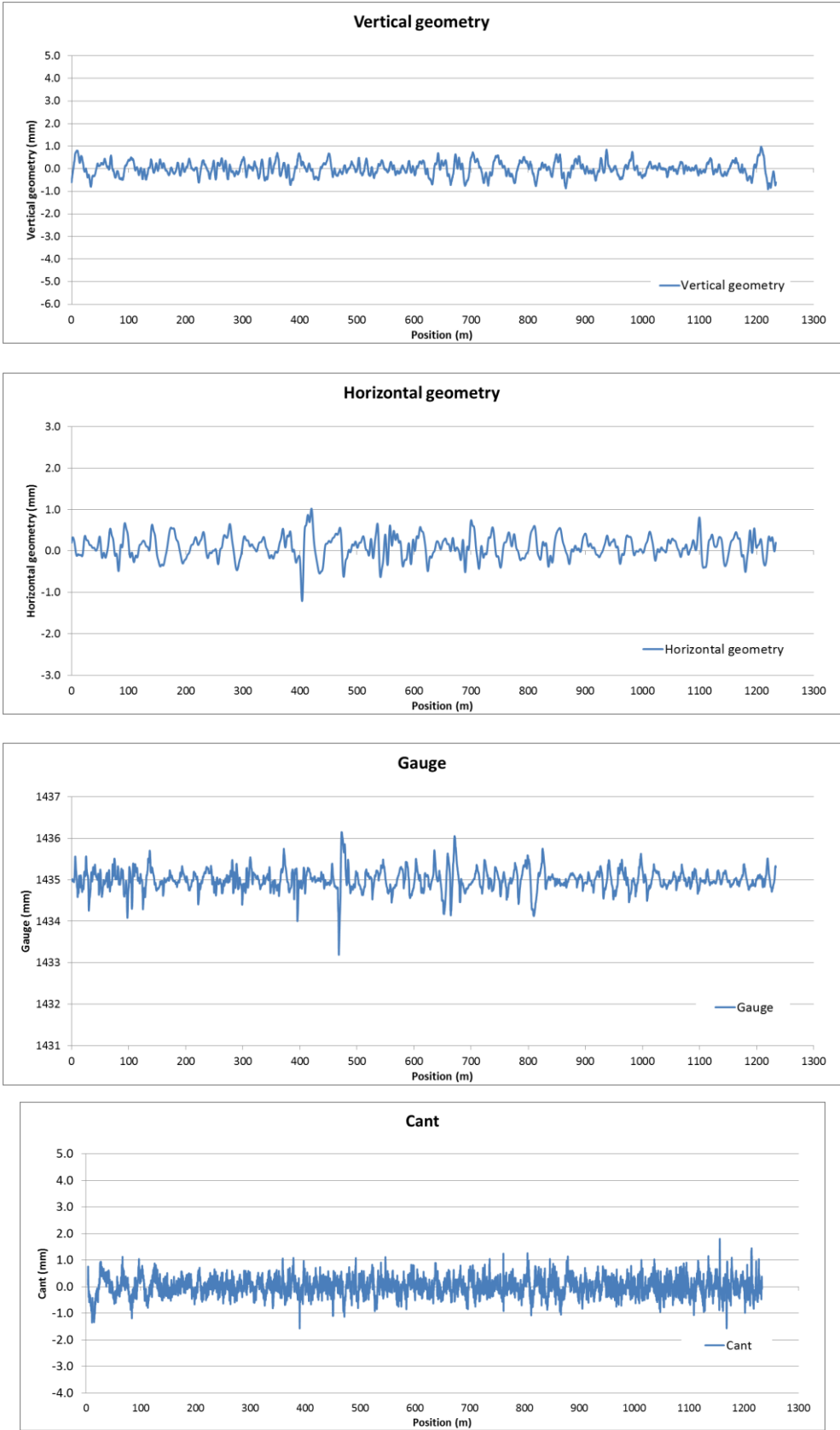


Figure: 3D track geometry (Section 1, 2013)

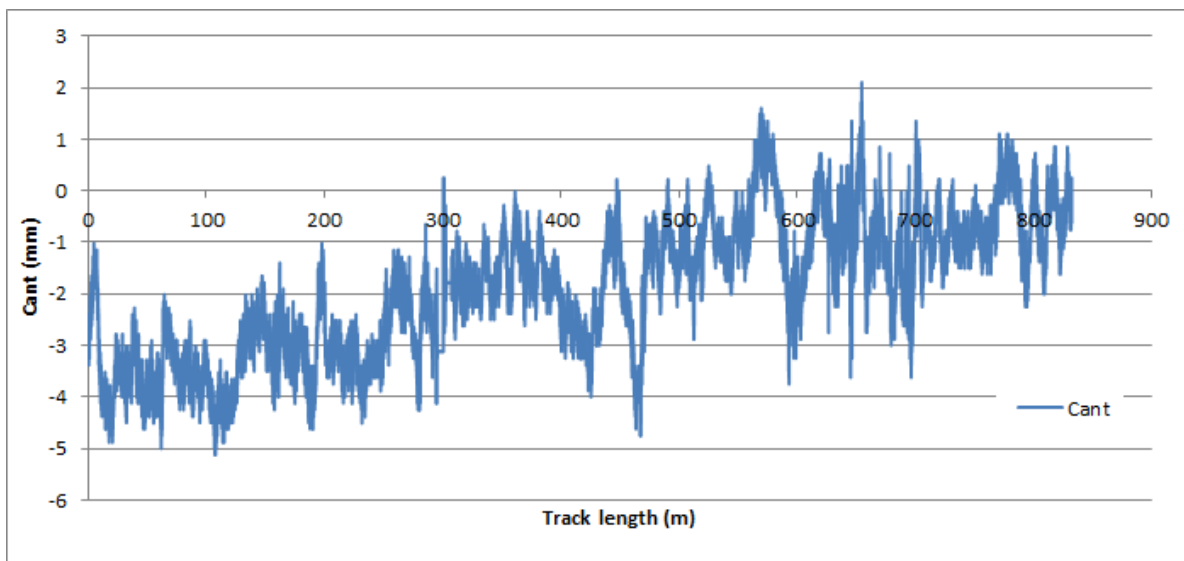
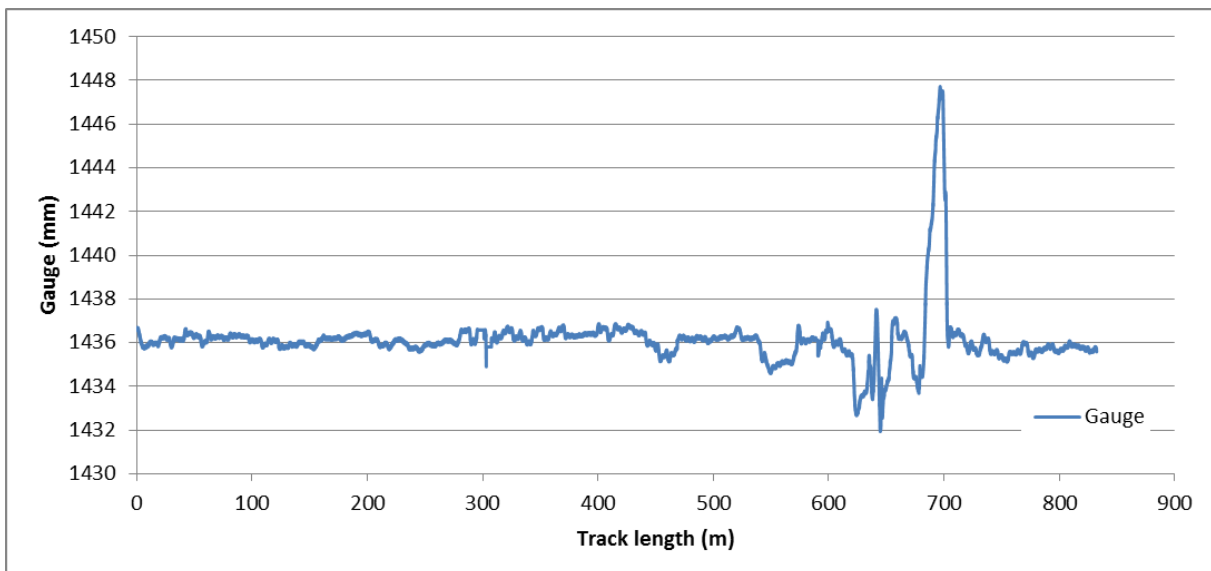
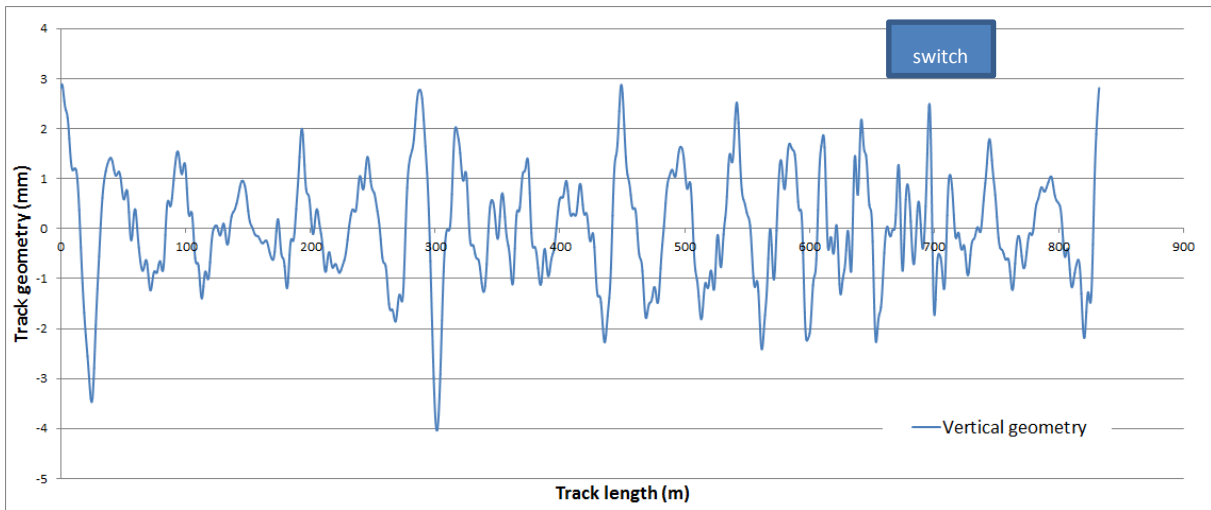


Figure: 3D track geometry (Section 2, 2013)

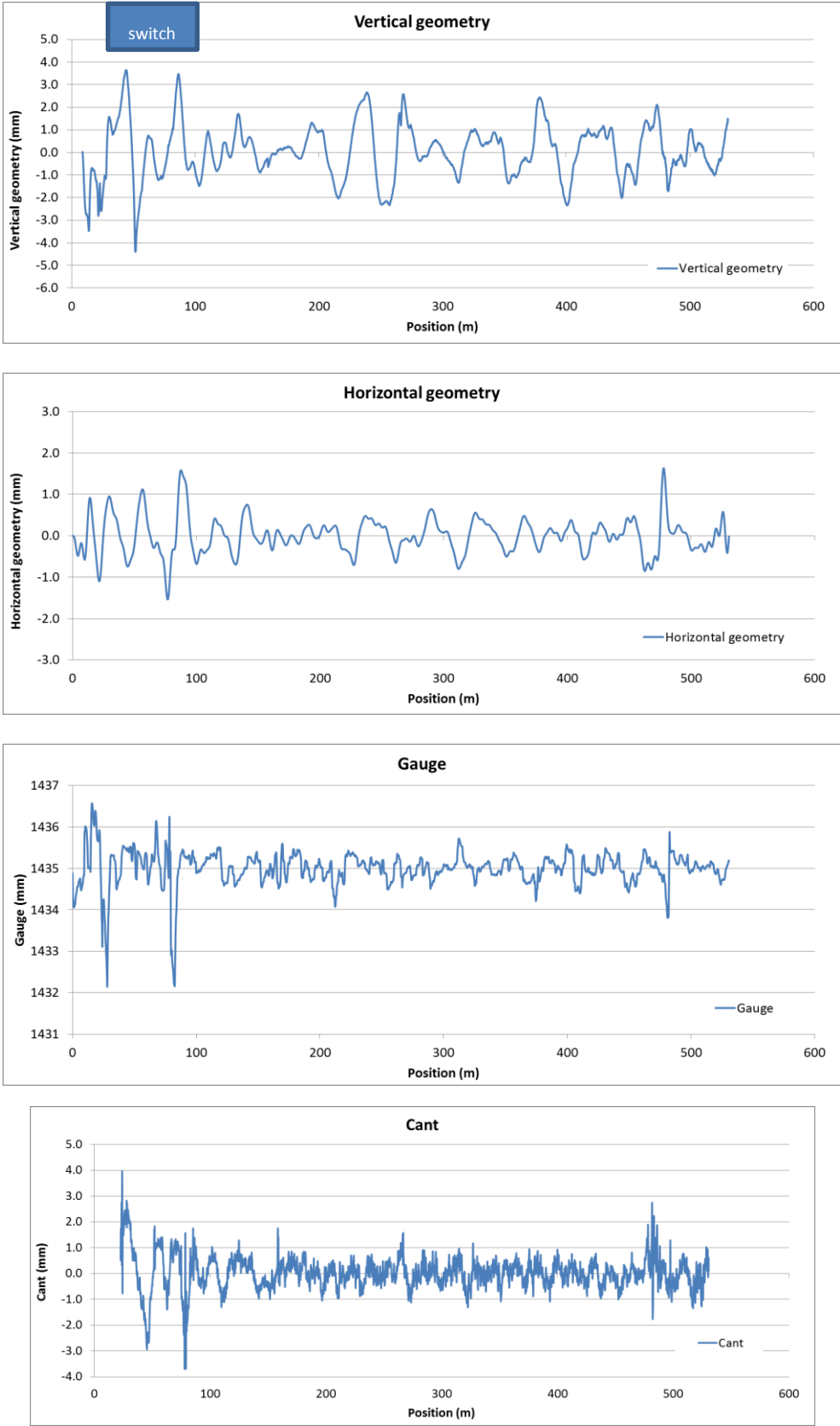


Figure: 3D track geometry (Section 3, 2012)

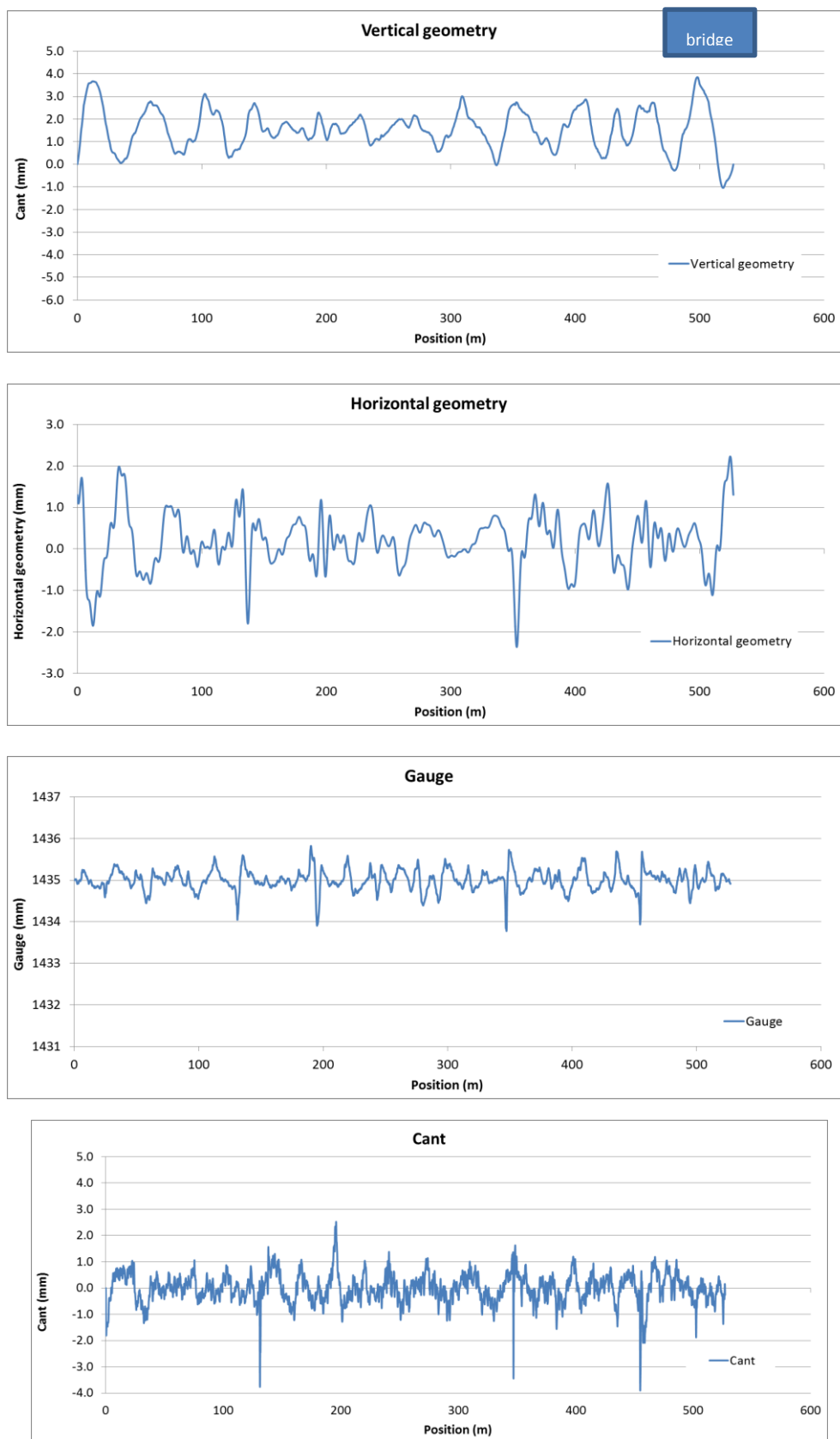


Figure: 3D track geometry (Section 3, 2014)

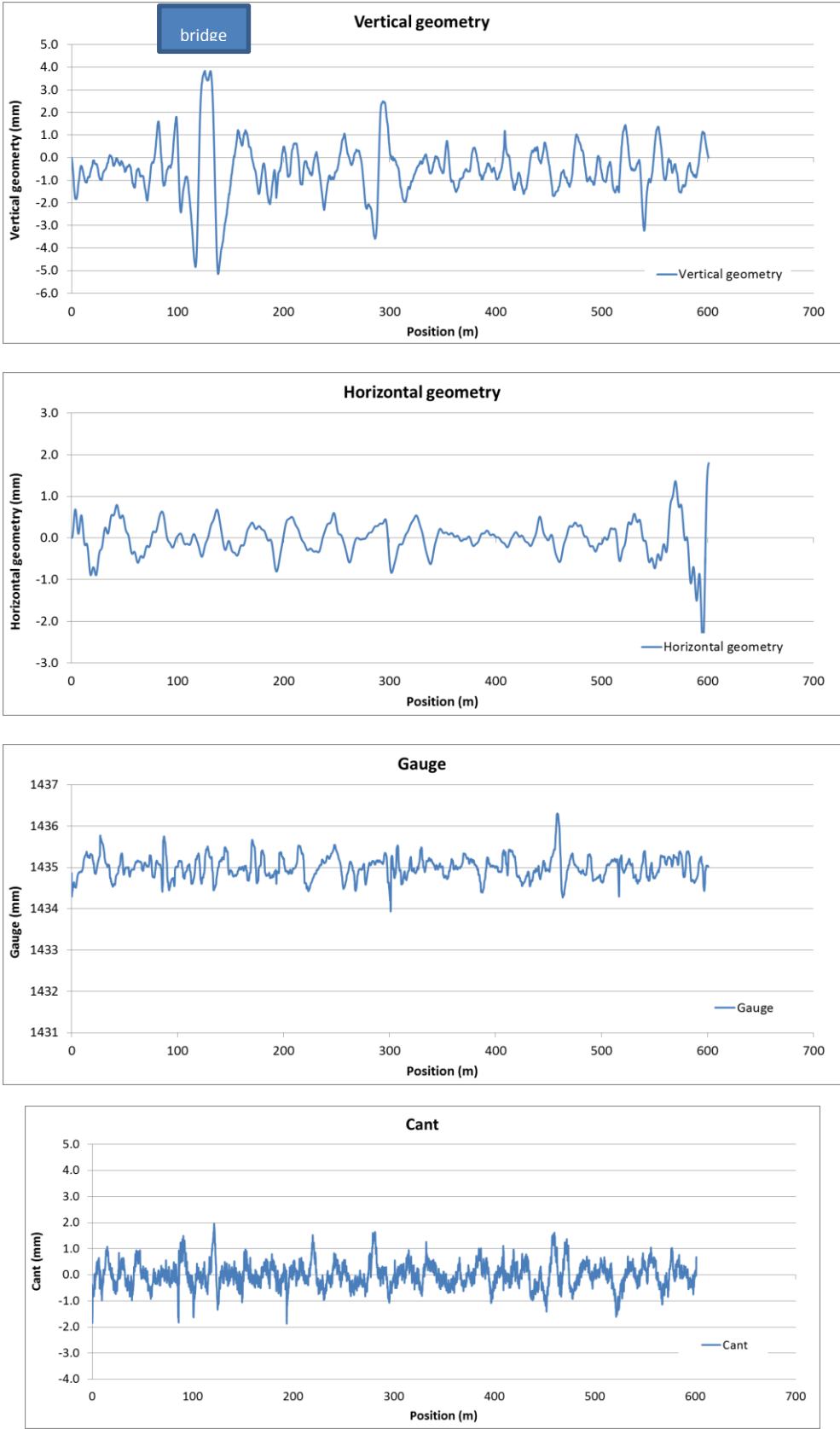


Figure: 3D track geometry (Section 4, 2012)

Appendix 10

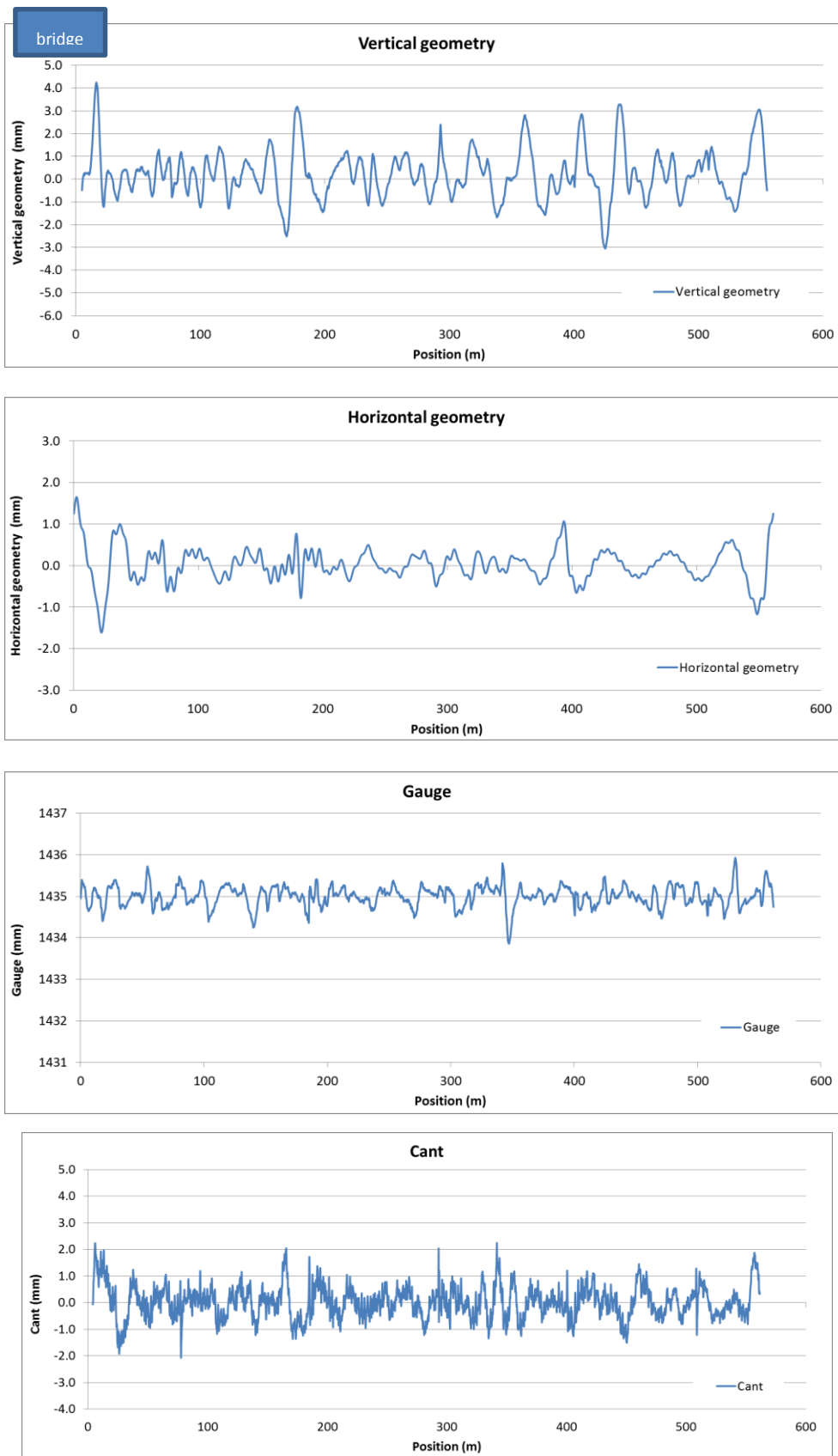


Figure: 3D track geometry (Section 4, 2014)

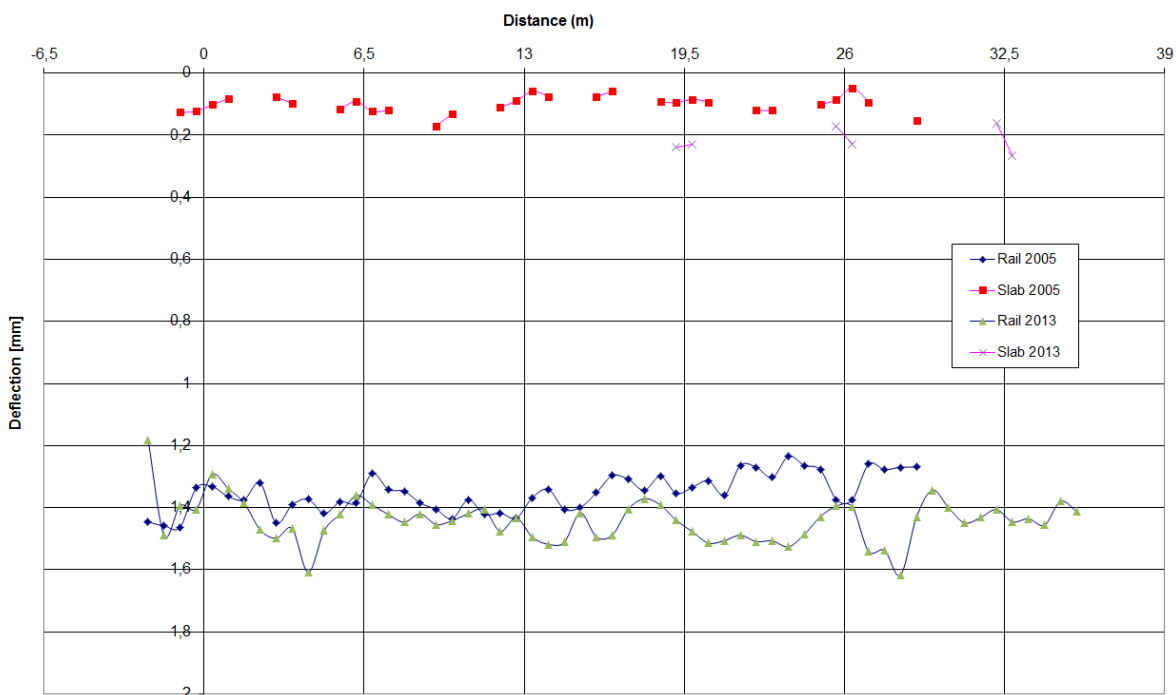


Figure: Measured maximum rail and slab deflection (Section 1, 2005 and 2013)

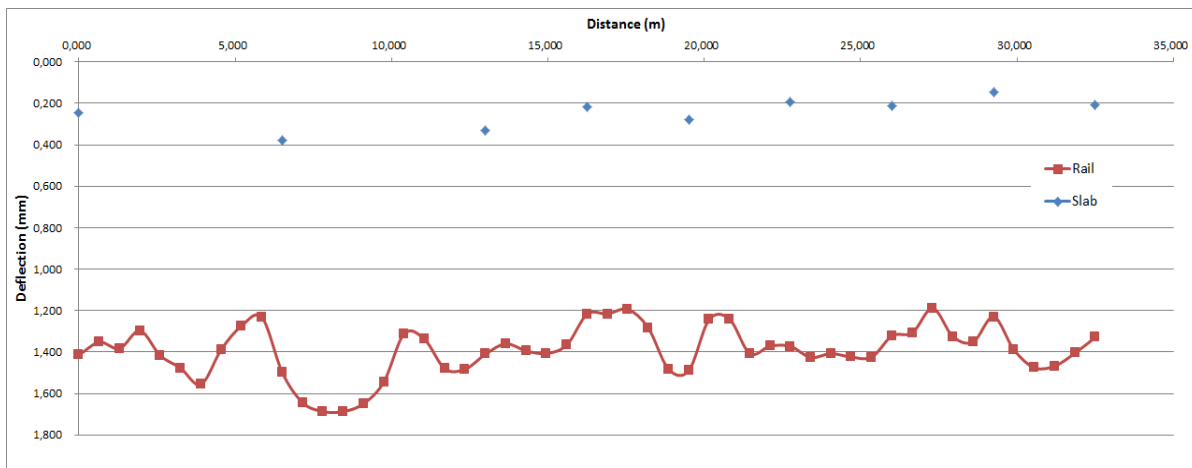


Figure: Measured maximum rail and slab deflection (Section 2, 2013)

Appendix 12

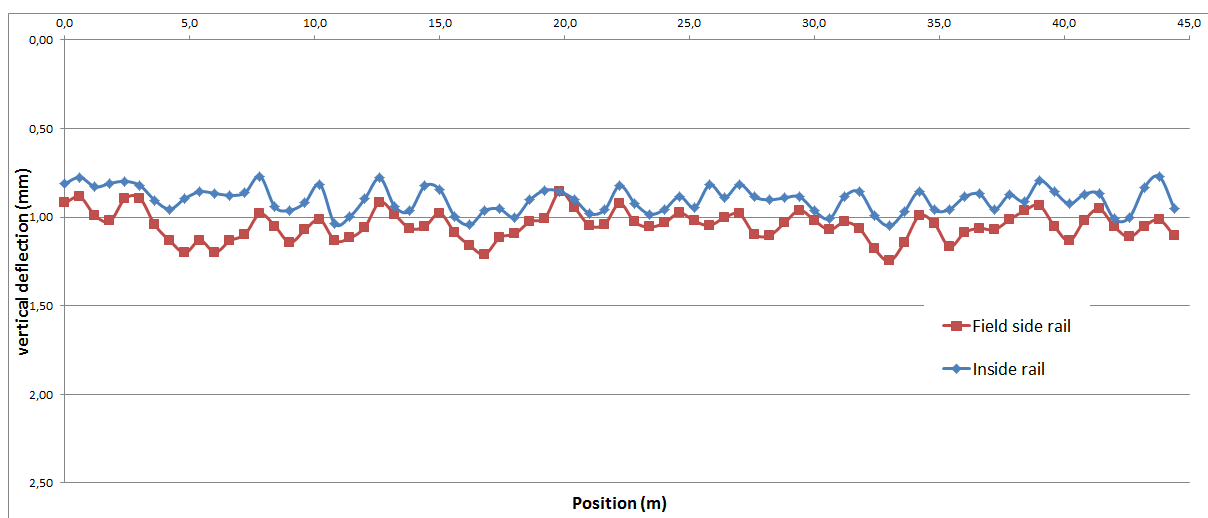


Figure: Measured maximum rail and slab deflection (Section 3, 2012)

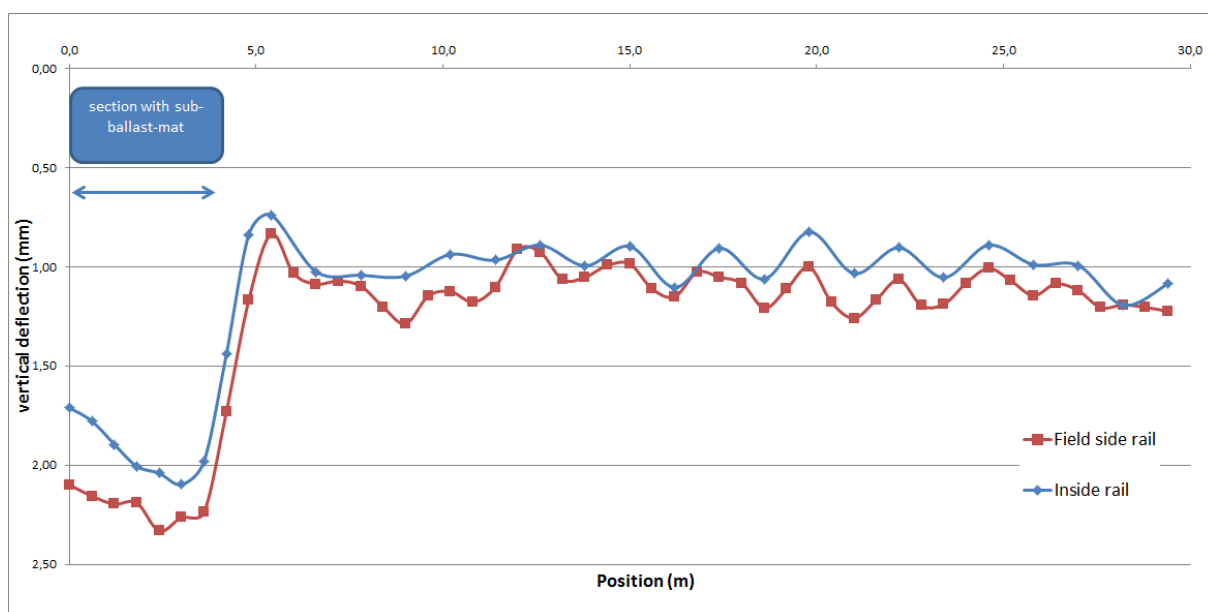


Figure: Measured maximum rail and slab deflection (Section 4, 2012)

Table: Calculated deflection line (Section 3, field side rail)

| | RS1 | RS2 | RS3 | RS4 | RS5 | RS6 | RS7 | RS8 | RS9 |
|-----|------|-------|-------|-------|-------|-------|-------|-------|-------|
| | 0 m | 0.6 m | 1.2 m | 1.8 m | 2.4 m | 3 m | 3.6 m | 4.2 m | 4.8 m |
| Z1 | 0.92 | | | | | | | | |
| Z3 | 0.89 | 0.62 | | | | | | | |
| Z5 | 0.99 | 0.53 | 0.22 | | | | | | |
| Z7 | 1.02 | 0.59 | 0.21 | 0.02 | | | | | |
| Z9 | 0.90 | 0.64 | 0.25 | 0.03 | -0.02 | | | | |
| Z11 | 0.89 | 0.50 | 0.19 | 0.03 | -0.01 | -0.01 | | | |
| Z13 | 1.04 | 0.58 | 0.10 | -0.02 | -0.05 | 0.00 | 0.00 | | |
| Z15 | 1.13 | 0.72 | 0.20 | -0.05 | -0.04 | -0.03 | 0.00 | 0.01 | |
| Z17 | 1.20 | 0.72 | 0.32 | 0.01 | -0.08 | -0.01 | -0.01 | 0.00 | 0.01 |
| Z19 | 1.13 | 0.77 | 0.24 | 0.07 | -0.01 | -0.06 | -0.01 | 0.00 | 0.00 |
| Z21 | 1.20 | 0.81 | 0.30 | 0.00 | -0.02 | -0.01 | -0.04 | 0.00 | 0.00 |
| Z23 | 1.13 | 0.86 | 0.32 | 0.04 | -0.07 | -0.03 | 0.00 | -0.03 | 0.00 |
| Z25 | 1.10 | 0.65 | 0.35 | 0.04 | -0.04 | -0.07 | -0.02 | 0.00 | -0.03 |
| Z27 | 0.98 | 0.70 | 0.15 | 0.04 | -0.04 | -0.05 | -0.03 | 0.00 | 0.00 |
| Z29 | 1.05 | 0.67 | 0.25 | -0.01 | -0.08 | -0.05 | -0.02 | -0.02 | 0.00 |
| Z31 | 1.14 | 0.73 | 0.28 | 0.02 | -0.08 | -0.08 | -0.03 | -0.01 | -0.01 |
| Z33 | 1.07 | 0.76 | 0.31 | 0.06 | -0.03 | -0.05 | -0.03 | -0.01 | 0.00 |
| Z35 | 1.01 | 0.59 | 0.23 | 0.02 | -0.02 | 0.00 | 0.01 | -0.01 | 0.00 |
| Z37 | 1.13 | 0.73 | 0.16 | 0.01 | -0.06 | -0.04 | 0.00 | 0.01 | -0.01 |
| Z39 | 1.12 | 0.79 | 0.31 | -0.03 | -0.05 | -0.07 | -0.02 | 0.00 | 0.01 |
| Z41 | 1.06 | 0.75 | 0.36 | 0.09 | -0.06 | -0.04 | -0.04 | -0.01 | -0.01 |
| Z43 | 0.92 | 0.59 | 0.27 | 0.08 | 0.00 | -0.04 | -0.01 | 0.00 | 0.00 |
| Z45 | 0.99 | 0.57 | 0.14 | -0.01 | -0.07 | -0.04 | -0.02 | 0.01 | 0.00 |
| Z47 | 1.06 | 0.60 | 0.18 | -0.05 | -0.08 | -0.07 | -0.03 | -0.02 | 0.01 |
| Z49 | 1.05 | 0.67 | 0.22 | -0.02 | -0.06 | -0.07 | -0.05 | -0.02 | -0.01 |
| Z51 | 0.98 | 0.67 | 0.20 | 0.00 | -0.05 | -0.03 | -0.03 | -0.03 | 0.00 |
| Z53 | 1.09 | 0.66 | 0.21 | -0.03 | -0.08 | -0.05 | -0.01 | -0.03 | 0.00 |
| Z55 | 1.16 | 0.68 | 0.27 | -0.02 | -0.05 | -0.06 | -0.03 | -0.01 | 0.01 |
| Z57 | 1.21 | 0.76 | 0.27 | 0.01 | -0.06 | -0.03 | -0.04 | -0.01 | -0.01 |
| Z59 | 1.11 | 0.72 | 0.26 | 0.04 | 0.00 | -0.03 | 0.00 | -0.01 | -0.01 |
| Z61 | 1.10 | 0.82 | 0.24 | 0.00 | 0.00 | 0.00 | -0.01 | 0.00 | 0.00 |
| Z63 | 1.03 | 0.75 | 0.34 | -0.01 | -0.08 | 0.00 | 0.00 | -0.01 | 0.00 |
| Z65 | 1.01 | 0.67 | 0.26 | 0.07 | -0.04 | -0.07 | 0.01 | 0.00 | 0.00 |
| Z67 | 0.86 | 0.63 | 0.16 | 0.03 | -0.03 | -0.01 | -0.06 | 0.01 | 0.00 |
| Z69 | 0.95 | 0.58 | 0.19 | -0.06 | -0.03 | -0.03 | 0.00 | -0.04 | 0.01 |
| Z71 | 1.05 | 0.56 | 0.17 | 0.01 | -0.07 | -0.01 | -0.02 | 0.01 | -0.01 |

| | | | | | | | | | |
|------|------|------|------|-------|-------|-------|-------|-------|-------|
| Z73 | 1.04 | 0.72 | 0.15 | 0.00 | 0.01 | -0.05 | 0.00 | -0.01 | 0.01 |
| Z75 | 0.92 | 0.64 | 0.30 | -0.01 | -0.03 | 0.01 | -0.01 | 0.00 | -0.01 |
| Z77 | 1.03 | 0.65 | 0.21 | 0.05 | -0.02 | -0.03 | 0.01 | -0.01 | 0.01 |
| Z79 | 1.06 | 0.67 | 0.28 | 0.01 | -0.03 | -0.01 | -0.01 | 0.01 | 0.00 |
| Z81 | 1.03 | 0.75 | 0.25 | 0.05 | -0.04 | -0.01 | 0.00 | 0.00 | 0.01 |
| Z83 | 0.98 | 0.71 | 0.24 | 0.01 | -0.03 | -0.04 | 0.00 | 0.00 | 0.00 |
| Z85 | 1.02 | 0.60 | 0.27 | -0.01 | -0.06 | -0.05 | -0.02 | 0.00 | 0.00 |
| Z87 | 1.05 | 0.66 | 0.22 | 0.01 | -0.04 | -0.04 | -0.03 | 0.00 | 0.01 |
| Z89 | 1.00 | 0.76 | 0.24 | 0.02 | -0.02 | -0.01 | -0.04 | -0.01 | 0.01 |
| Z91 | 0.98 | 0.63 | 0.28 | 0.01 | -0.04 | -0.03 | 0.00 | -0.02 | -0.01 |
| Z93 | 1.10 | 0.64 | 0.21 | 0.03 | -0.07 | -0.04 | -0.02 | 0.00 | -0.01 |
| Z95 | 1.10 | 0.71 | 0.27 | 0.01 | -0.03 | -0.06 | -0.02 | -0.01 | 0.00 |
| Z97 | 1.03 | 0.78 | 0.30 | 0.08 | -0.01 | -0.01 | -0.03 | -0.01 | -0.01 |
| Z99 | 0.96 | 0.72 | 0.30 | 0.06 | -0.01 | -0.02 | 0.00 | 0.00 | 0.00 |
| Z101 | 1.02 | 0.59 | 0.22 | 0.01 | -0.03 | -0.02 | 0.00 | 0.01 | 0.00 |
| Z103 | 1.07 | 0.67 | 0.23 | 0.00 | -0.04 | -0.02 | 0.00 | 0.00 | 0.01 |
| Z105 | 1.03 | 0.69 | 0.25 | 0.02 | -0.01 | -0.02 | 0.00 | 0.00 | 0.01 |
| Z107 | 1.07 | 0.69 | 0.22 | 0.02 | -0.04 | 0.00 | 0.00 | 0.00 | 0.00 |
| Z109 | 1.18 | 0.79 | 0.23 | 0.00 | -0.04 | -0.03 | 0.00 | 0.00 | 0.00 |
| Z111 | 1.25 | 0.85 | 0.35 | 0.01 | -0.05 | -0.04 | -0.02 | 0.01 | 0.00 |
| Z113 | 1.14 | 0.82 | 0.36 | 0.10 | -0.03 | -0.04 | -0.02 | -0.01 | 0.01 |
| Z115 | 0.99 | 0.68 | 0.28 | 0.05 | 0.00 | -0.03 | -0.02 | 0.00 | 0.00 |
| Z117 | 1.04 | 0.62 | 0.21 | -0.02 | -0.05 | -0.03 | -0.02 | -0.01 | 0.01 |
| Z119 | 1.17 | 0.66 | 0.25 | -0.02 | -0.06 | -0.05 | -0.01 | 0.00 | 0.00 |
| Z121 | 1.09 | 0.76 | 0.25 | 0.02 | -0.03 | -0.03 | -0.03 | 0.00 | 0.01 |
| Z123 | 1.06 | 0.69 | 0.30 | 0.03 | -0.02 | -0.01 | 0.00 | 0.00 | 0.00 |
| Z125 | 1.07 | 0.64 | 0.20 | 0.03 | -0.06 | -0.02 | 0.00 | 0.00 | 0.00 |
| Z127 | 1.01 | 0.76 | 0.20 | -0.02 | -0.04 | -0.05 | -0.01 | 0.00 | 0.00 |
| Z129 | 0.96 | 0.70 | 0.29 | 0.01 | -0.04 | -0.03 | -0.03 | -0.01 | 0.00 |
| Z131 | 0.93 | 0.62 | 0.20 | 0.04 | -0.02 | -0.02 | 0.00 | -0.01 | -0.01 |
| Z133 | 1.05 | 0.63 | 0.20 | -0.02 | -0.04 | -0.02 | -0.01 | 0.00 | 0.00 |
| Z135 | 1.13 | 0.72 | 0.23 | 0.01 | -0.07 | 0.00 | 0.00 | 0.00 | 0.00 |
| Z137 | 1.02 | 0.72 | 0.29 | 0.04 | -0.04 | -0.05 | 0.00 | 0.00 | 0.00 |
| Z139 | 0.95 | 0.62 | 0.26 | 0.03 | -0.02 | -0.03 | -0.02 | 0.01 | 0.00 |
| Z141 | 1.05 | 0.62 | 0.19 | 0.02 | -0.03 | -0.02 | -0.01 | -0.02 | 0.01 |
| Z143 | 1.11 | 0.71 | 0.23 | 0.00 | -0.03 | -0.03 | -0.02 | 0.00 | 0.00 |
| Z145 | 1.05 | 0.70 | 0.23 | 0.00 | -0.07 | -0.02 | -0.02 | 0.00 | -0.02 |
| Z147 | 1.01 | 0.65 | 0.22 | 0.02 | -0.02 | -0.04 | 0.00 | 0.00 | 0.00 |
| Z149 | 1.10 | 0.72 | 0.24 | 0.01 | -0.05 | -0.02 | -0.02 | 0.00 | 0.00 |

Table: Calculated deflection line (Section 3, inside rail)

| | RS1 | RS2 | RS3 | RS4 | RS5 | RS6 | RS7 | RS8 | RS9 |
|-----|------|-------|-------|-------|-------|-------|-------|-------|-------|
| | 0 m | 0.6 m | 1.2 m | 1.8 m | 2.4 m | 3 m | 3.6 m | 4.2 m | 4.8 m |
| Z2 | 0.81 | 0.50 | 0.19 | -0.01 | -0.02 | -0.02 | -0.02 | -0.01 | 0.00 |
| Z4 | 0.77 | 0.53 | 0.17 | 0.03 | -0.03 | -0.02 | 0.00 | -0.01 | 0.01 |
| Z6 | 0.83 | 0.52 | 0.21 | 0.02 | -0.03 | -0.03 | -0.03 | 0.01 | -0.01 |
| Z8 | 0.81 | 0.53 | 0.18 | 0.01 | -0.04 | -0.03 | 0.00 | -0.01 | 0.00 |
| Z10 | 0.80 | 0.54 | 0.17 | 0.03 | -0.03 | -0.01 | -0.01 | -0.01 | 0.00 |
| Z12 | 0.82 | 0.55 | 0.29 | 0.03 | 0.00 | -0.02 | -0.02 | 0.00 | -0.01 |
| Z14 | 0.91 | 0.69 | 0.28 | 0.06 | -0.04 | -0.05 | -0.02 | 0.03 | 0.05 |
| Z16 | 0.95 | 0.64 | 0.23 | 0.00 | -0.05 | -0.03 | 0.02 | 0.07 | -0.01 |
| Z18 | 0.89 | 0.58 | 0.17 | 0.00 | -0.04 | -0.02 | -0.06 | -0.02 | -0.02 |
| Z20 | 0.86 | 0.53 | 0.19 | 0.03 | -0.05 | -0.12 | -0.06 | -0.01 | 0.00 |
| Z22 | 0.87 | 0.59 | 0.22 | 0.00 | -0.03 | -0.05 | -0.03 | 0.00 | 0.00 |
| Z24 | 0.88 | 0.57 | 0.14 | -0.06 | -0.08 | -0.04 | -0.03 | -0.01 | 0.00 |
| Z26 | 0.86 | 0.50 | 0.15 | 0.01 | -0.04 | -0.05 | -0.02 | -0.04 | -0.01 |
| Z28 | 0.77 | 0.54 | 0.23 | 0.01 | -0.05 | -0.02 | -0.04 | -0.03 | 0.01 |
| Z30 | 0.94 | 0.63 | 0.24 | 0.01 | -0.03 | -0.04 | -0.03 | 0.00 | 0.01 |
| Z32 | 0.96 | 0.67 | 0.21 | 0.02 | -0.06 | -0.04 | -0.01 | 0.01 | 0.01 |
| Z34 | 0.92 | 0.52 | 0.22 | 0.00 | -0.04 | -0.03 | -0.01 | 0.00 | 0.00 |
| Z36 | 0.82 | 0.68 | 0.20 | 0.01 | -0.02 | -0.05 | 0.00 | -0.01 | 0.02 |
| Z38 | 1.04 | 0.68 | 0.24 | 0.03 | -0.07 | -0.04 | -0.02 | 0.01 | -0.01 |
| Z40 | 1.00 | 0.62 | 0.19 | 0.01 | -0.03 | -0.04 | 0.00 | -0.03 | 0.00 |
| Z42 | 0.90 | 0.52 | 0.23 | 0.01 | -0.01 | -0.02 | -0.02 | -0.02 | 0.00 |
| Z44 | 0.78 | 0.64 | 0.23 | 0.02 | 0.01 | -0.09 | -0.01 | 0.01 | 0.01 |
| Z46 | 0.94 | 0.62 | 0.16 | 0.04 | -0.06 | -0.03 | 0.01 | 0.01 | -0.01 |
| Z48 | 0.97 | 0.52 | 0.18 | -0.02 | -0.04 | -0.01 | 0.00 | 0.00 | 0.02 |
| Z50 | 0.82 | 0.54 | 0.22 | 0.10 | 0.00 | 0.00 | -0.01 | -0.01 | 0.01 |
| Z52 | 0.84 | 0.66 | 0.29 | 0.06 | 0.02 | -0.02 | -0.10 | -0.01 | -0.02 |
| Z54 | 1.00 | 0.78 | 0.28 | 0.11 | -0.02 | -0.07 | -0.02 | -0.01 | 0.00 |
| Z56 | 1.04 | 0.63 | 0.27 | 0.03 | -0.15 | -0.03 | 0.00 | 0.00 | -0.01 |
| Z58 | 0.96 | 0.65 | 0.21 | 0.03 | -0.02 | -0.02 | -0.01 | 0.03 | -0.02 |
| Z60 | 0.95 | 0.62 | 0.27 | 0.05 | -0.02 | -0.03 | 0.02 | -0.01 | 0.00 |
| Z62 | 1.00 | 0.59 | 0.24 | 0.02 | -0.04 | 0.00 | -0.01 | -0.01 | -0.03 |
| Z64 | 0.90 | 0.59 | 0.17 | -0.01 | -0.01 | -0.01 | -0.02 | -0.04 | -0.03 |
| Z66 | 0.85 | 0.52 | 0.15 | 0.06 | -0.02 | -0.03 | -0.04 | -0.02 | 0.01 |
| Z68 | 0.86 | 0.51 | 0.26 | 0.03 | -0.02 | -0.05 | -0.01 | 0.00 | 0.00 |
| Z70 | 0.90 | 0.68 | 0.27 | 0.01 | -0.07 | -0.05 | -0.04 | 0.00 | 0.01 |

| | | | | | | | | | |
|------|------|------|------|-------|-------|-------|-------|-------|-------|
| Z72 | 0.98 | 0.62 | 0.17 | -0.04 | -0.09 | -0.05 | 0.00 | 0.00 | -0.04 |
| Z74 | 0.96 | 0.51 | 0.14 | -0.05 | -0.04 | -0.02 | -0.01 | -0.01 | 0.01 |
| Z76 | 0.82 | 0.53 | 0.13 | 0.06 | -0.01 | -0.01 | 0.00 | 0.00 | 0.00 |
| Z78 | 0.92 | 0.59 | 0.28 | 0.05 | -0.01 | 0.00 | -0.02 | -0.01 | 0.00 |
| Z80 | 0.98 | 0.66 | 0.24 | 0.05 | 0.00 | -0.04 | -0.01 | 0.00 | 0.01 |
| Z82 | 0.96 | 0.60 | 0.24 | -0.01 | -0.03 | -0.02 | -0.01 | 0.04 | 0.03 |
| Z84 | 0.88 | 0.63 | 0.12 | 0.03 | -0.02 | -0.01 | 0.03 | 0.03 | 0.02 |
| Z86 | 0.95 | 0.52 | 0.22 | 0.02 | -0.01 | 0.01 | 0.00 | 0.02 | 0.02 |
| Z88 | 0.82 | 0.56 | 0.20 | 0.04 | -0.04 | 0.00 | 0.00 | 0.01 | -0.01 |
| Z90 | 0.89 | 0.53 | 0.19 | 0.00 | 0.00 | 0.00 | 0.01 | 0.00 | -0.01 |
| Z92 | 0.81 | 0.55 | 0.20 | 0.05 | -0.01 | 0.00 | -0.02 | 0.01 | 0.01 |
| Z94 | 0.89 | 0.57 | 0.23 | 0.05 | -0.03 | -0.04 | -0.01 | 0.01 | 0.00 |
| Z96 | 0.90 | 0.53 | 0.25 | -0.01 | -0.06 | -0.02 | 0.00 | 0.00 | 0.01 |
| Z98 | 0.89 | 0.60 | 0.14 | -0.04 | -0.03 | -0.01 | -0.02 | 0.02 | 0.03 |
| Z100 | 0.88 | 0.49 | 0.23 | 0.02 | -0.01 | -0.03 | 0.03 | 0.01 | 0.00 |
| Z102 | 0.96 | 0.66 | 0.22 | 0.03 | -0.04 | 0.01 | -0.02 | -0.01 | 0.04 |
| Z104 | 1.01 | 0.61 | 0.23 | 0.01 | -0.01 | -0.05 | -0.01 | 0.03 | 0.01 |
| Z106 | 0.88 | 0.56 | 0.23 | 0.05 | -0.02 | -0.01 | 0.01 | 0.01 | -0.01 |
| Z108 | 0.86 | 0.69 | 0.30 | 0.04 | -0.02 | 0.00 | 0.00 | -0.01 | -0.01 |
| Z110 | 0.99 | 0.75 | 0.24 | 0.03 | 0.00 | -0.01 | -0.02 | -0.01 | 0.03 |
| Z112 | 1.05 | 0.61 | 0.21 | 0.06 | -0.03 | -0.03 | -0.03 | 0.04 | 0.01 |
| Z114 | 0.97 | 0.54 | 0.29 | 0.00 | -0.04 | -0.04 | 0.03 | 0.01 | 0.01 |
| Z116 | 0.85 | 0.67 | 0.25 | 0.01 | -0.04 | 0.02 | 0.00 | 0.00 | 0.00 |
| Z118 | 0.96 | 0.66 | 0.21 | 0.00 | 0.00 | -0.03 | -0.02 | 0.00 | 0.00 |
| Z120 | 0.96 | 0.57 | 0.17 | 0.02 | -0.05 | -0.04 | -0.01 | 0.00 | 0.01 |
| Z122 | 0.89 | 0.52 | 0.18 | 0.01 | -0.03 | -0.01 | 0.00 | 0.01 | 0.00 |
| Z124 | 0.87 | 0.61 | 0.20 | 0.05 | -0.01 | -0.02 | 0.01 | 0.00 | 0.01 |
| Z126 | 0.96 | 0.59 | 0.30 | 0.01 | -0.04 | 0.00 | 0.00 | 0.00 | 0.00 |
| Z128 | 0.88 | 0.65 | 0.18 | 0.00 | -0.02 | -0.01 | 0.00 | 0.00 | 0.02 |
| Z130 | 0.91 | 0.53 | 0.15 | 0.00 | -0.02 | -0.02 | -0.01 | 0.01 | 0.00 |
| Z132 | 0.80 | 0.52 | 0.20 | -0.01 | -0.03 | -0.01 | 0.00 | 0.00 | 0.00 |
| Z134 | 0.86 | 0.62 | 0.16 | 0.00 | -0.02 | -0.04 | 0.00 | 0.00 | 0.00 |
| Z136 | 0.92 | 0.55 | 0.16 | -0.01 | -0.05 | -0.03 | 0.00 | 0.01 | |
| Z138 | 0.87 | 0.52 | 0.21 | 0.00 | -0.03 | 0.00 | -0.01 | | |
| Z140 | 0.87 | 0.63 | 0.24 | 0.04 | -0.01 | -0.03 | | | |
| Z142 | 1.01 | 0.67 | 0.25 | 0.00 | -0.05 | | | | |
| Z144 | 1.00 | 0.60 | 0.12 | -0.01 | | | | | |
| Z146 | 0.83 | 0.44 | 0.14 | | | | | | |
| Z148 | 0.77 | 0.56 | | | | | | | |
| Z150 | 0.95 | | | | | | | | |

Table: Calculated deflection line (Section 4, field side rail)

| | RS1 | RS2 | RS3 | RS4 | RS5 | RS6 | RS7 | RS8 | RS9 |
|-----|------|-------|-------|-------|-------|-------|-------|-------|-------|
| | 0 m | 0.6 m | 1.2 m | 1.8 m | 2.4 m | 3 m | 3.6 m | 4.2 m | 4.8 m |
| Z1 | 2.10 | | | | | | | | |
| Z3 | 2.16 | 1.50 | | | | | | | |
| Z5 | 2.20 | 1.62 | 0.81 | | | | | | |
| Z7 | 2.19 | 1.75 | 0.85 | 0.31 | | | | | |
| Z9 | 2.33 | 1.84 | 1.04 | 0.35 | 0.03 | | | | |
| Z11 | 2.26 | 1.78 | 1.08 | 0.46 | 0.07 | -0.07 | | | |
| Z13 | 2.24 | 1.85 | 1.00 | 0.48 | 0.15 | -0.05 | -0.08 | | |
| Z15 | 1.73 | 1.66 | 1.07 | 0.44 | 0.14 | 0.02 | -0.05 | -0.04 | |
| Z17 | 1.17 | 0.84 | 0.80 | 0.40 | 0.10 | 0.00 | -0.02 | -0.03 | -0.01 |
| Z19 | 0.84 | 0.85 | 0.20 | 0.18 | 0.02 | -0.05 | -0.05 | -0.02 | -0.02 |
| Z21 | 1.03 | 0.53 | 0.30 | -0.10 | -0.09 | -0.09 | -0.08 | -0.05 | -0.01 |
| Z23 | 1.09 | 0.71 | 0.21 | 0.02 | -0.12 | -0.12 | -0.05 | -0.06 | -0.03 |
| Z25 | 1.07 | 0.67 | 0.27 | 0.03 | -0.04 | -0.06 | -0.05 | 0.00 | -0.03 |
| Z27 | 1.10 | 0.63 | 0.23 | 0.03 | -0.01 | -0.04 | -0.02 | -0.01 | 0.01 |
| Z29 | 1.20 | 0.72 | 0.24 | 0.00 | -0.02 | -0.02 | -0.01 | -0.01 | 0.00 |
| Z31 | 1.29 | 0.85 | 0.30 | 0.02 | -0.05 | -0.02 | -0.01 | 0.00 | -0.01 |
| Z33 | 1.15 | 0.88 | 0.35 | 0.07 | -0.02 | -0.02 | 0.00 | 0.00 | 0.02 |
| Z35 | 1.12 | 0.78 | 0.36 | 0.07 | -0.01 | -0.01 | 0.00 | 0.02 | 0.00 |
| Z37 | 1.18 | 0.77 | 0.30 | 0.07 | -0.04 | -0.02 | -0.01 | 0.00 | 0.03 |
| Z39 | 1.10 | 0.74 | 0.33 | 0.04 | -0.03 | -0.04 | 0.01 | 0.00 | 0.00 |
| Z41 | 0.91 | 0.61 | 0.28 | 0.08 | -0.02 | -0.03 | -0.02 | 0.00 | 0.00 |
| Z43 | 0.93 | 0.55 | 0.20 | 0.02 | 0.01 | -0.03 | -0.03 | 0.00 | 0.02 |
| Z45 | 1.06 | 0.58 | 0.17 | -0.01 | -0.04 | -0.02 | -0.01 | -0.02 | 0.01 |
| Z47 | 1.05 | 0.73 | 0.27 | -0.01 | -0.04 | -0.04 | 0.00 | 0.00 | -0.01 |
| Z49 | 0.99 | 0.71 | 0.30 | 0.06 | -0.06 | -0.02 | -0.01 | 0.00 | 0.00 |
| Z51 | 0.99 | 0.61 | 0.25 | 0.05 | 0.01 | -0.07 | 0.00 | 0.01 | 0.02 |
| Z53 | 1.11 | 0.71 | 0.23 | 0.01 | -0.03 | -0.01 | -0.07 | 0.00 | 0.01 |
| Z55 | 1.15 | 0.78 | 0.32 | 0.04 | -0.03 | -0.02 | -0.01 | -0.06 | 0.00 |
| Z57 | 1.03 | 0.80 | 0.32 | 0.08 | 0.00 | -0.01 | 0.00 | -0.01 | -0.04 |
| Z59 | 1.05 | 0.65 | 0.30 | 0.05 | -0.01 | 0.00 | 0.00 | 0.00 | 0.02 |
| Z61 | 1.08 | 0.69 | 0.24 | 0.04 | -0.04 | -0.02 | 0.00 | 0.01 | 0.00 |
| Z63 | 1.21 | 0.70 | 0.26 | 0.02 | -0.01 | -0.04 | -0.01 | 0.00 | 0.01 |
| Z65 | 1.11 | 0.78 | 0.23 | 0.01 | -0.02 | 0.00 | -0.01 | 0.00 | 0.00 |
| Z67 | 1.00 | 0.77 | 0.29 | -0.01 | -0.02 | -0.01 | 0.01 | -0.01 | 0.00 |
| Z69 | 1.18 | 0.70 | 0.29 | 0.03 | -0.06 | 0.01 | 0.00 | 0.00 | 0.00 |

| | | | | | | | | | |
|-----|------|------|------|------|-------|-------|-------|-------|-------|
| Z71 | 1.26 | 0.82 | 0.32 | 0.04 | -0.03 | -0.03 | 0.00 | 0.00 | -0.01 |
| Z73 | 1.17 | 0.83 | 0.35 | 0.08 | -0.02 | -0.01 | 0.00 | -0.01 | 0.01 |
| Z75 | 1.06 | 0.75 | 0.32 | 0.06 | -0.01 | -0.02 | 0.00 | 0.02 | -0.07 |
| Z77 | 1.19 | 0.71 | 0.28 | 0.03 | -0.01 | -0.01 | -0.02 | 0.01 | -0.01 |
| Z79 | 1.19 | 0.80 | 0.30 | 0.04 | -0.02 | -0.01 | -0.01 | 0.00 | 0.00 |
| Z81 | 1.08 | 0.80 | 0.30 | 0.06 | -0.01 | -0.01 | 0.00 | 0.01 | 0.01 |
| Z83 | 1.01 | 0.65 | 0.28 | 0.03 | 0.00 | -0.01 | 0.00 | 0.00 | 0.01 |
| Z85 | 1.07 | 0.66 | 0.22 | 0.01 | -0.04 | -0.01 | 0.00 | 0.01 | 0.00 |
| Z87 | 1.14 | 0.67 | 0.28 | 0.01 | -0.03 | -0.04 | 0.00 | 0.00 | 0.00 |
| Z89 | 1.09 | 0.74 | 0.23 | 0.07 | -0.02 | -0.03 | -0.02 | 0.00 | 0.00 |
| Z91 | 1.12 | 0.72 | 0.27 | 0.03 | 0.02 | -0.02 | -0.02 | -0.01 | 0.00 |
| Z93 | 1.21 | 0.81 | 0.28 | 0.04 | -0.02 | 0.02 | -0.02 | 0.00 | 0.00 |
| Z95 | 1.19 | 0.78 | 0.36 | 0.05 | -0.01 | -0.01 | 0.02 | -0.02 | 0.00 |
| Z97 | 1.20 | 0.76 | 0.31 | 0.10 | -0.01 | -0.01 | 0.00 | 0.03 | -0.02 |
| Z99 | 1.22 | 0.79 | 0.25 | 0.06 | 0.01 | 0.00 | 0.01 | 0.00 | 0.04 |

Table: Calculated deflection line (Section 4, inside rail)

| | RS1 | RS2 | RS3 | RS4 | RS5 | RS6 | RS7 | RS8 | RS9 |
|-----|------|-------|-------|-------|-------|-------|-------|-------|-------|
| | 0 m | 0.6 m | 1.2 m | 1.8 m | 2.4 m | 3 m | 3.6 m | 4.2 m | 4.8 m |
| Z2 | 1.71 | 1.24 | 0.65 | 0.21 | -0.02 | -0.06 | -0.06 | -0.06 | 0.00 |
| Z4 | 1.78 | 1.37 | 0.73 | 0.32 | 0.10 | -0.04 | -0.04 | 0.00 | -0.02 |
| Z6 | 1.90 | 1.46 | 0.89 | 0.49 | 0.10 | -0.01 | 0.00 | -0.02 | |
| Z8 | 2.01 | 1.64 | 1.08 | 0.40 | 0.08 | 0.01 | -0.02 | | -0.02 |
| Z10 | 2.04 | 1.80 | 0.89 | 0.28 | 0.06 | -0.02 | | -0.02 | |
| Z12 | 2.10 | 1.54 | 0.68 | 0.19 | -0.02 | | -0.04 | | 0.00 |
| Z14 | 1.98 | 1.14 | 0.40 | 0.02 | | -0.09 | | 0.00 | |
| Z16 | 1.44 | 0.65 | 0.18 | | -0.09 | | -0.01 | | 0.00 |
| Z18 | 0.84 | 0.46 | | -0.02 | | -0.02 | | 0.00 | |
| Z20 | 0.74 | | 0.18 | | -0.02 | | 0.00 | | 0.00 |
| Z22 | | 0.65 | | 0.03 | | -0.02 | | 0.00 | |
| Z24 | 1.02 | | 0.21 | | -0.03 | | 0.00 | | 0.02 |
| Z26 | | 0.60 | | 0.02 | | -0.01 | | 0.01 | |
| Z28 | 1.04 | | 0.22 | | -0.02 | | 0.00 | | 0.00 |
| Z30 | | 0.65 | | 0.00 | | -0.01 | | 0.00 | |
| Z32 | 1.05 | | 0.12 | | -0.03 | | -0.01 | | 0.00 |
| Z34 | | 0.54 | | 0.02 | | -0.02 | | 0.00 | |
| Z36 | 0.94 | | 0.24 | | -0.03 | | 0.00 | | 0.00 |
| Z38 | | 0.66 | | 0.00 | | -0.02 | | 0.00 | |
| Z40 | 0.97 | | 0.19 | | -0.02 | | -0.02 | | 0.01 |
| Z42 | | 0.56 | | 0.01 | | -0.02 | | 0.02 | |
| Z44 | 0.89 | | 0.20 | | -0.04 | | 0.01 | | 0.01 |
| Z46 | | 0.56 | | 0.02 | | -0.01 | | 0.00 | |
| Z48 | 0.99 | | 0.22 | | -0.01 | | 0.00 | | -0.01 |
| Z50 | | 0.61 | | 0.04 | | 0.00 | | -0.02 | |
| Z52 | 0.90 | | 0.25 | | 0.00 | | 0.00 | | 0.00 |
| Z54 | | 0.72 | | 0.03 | | -0.01 | | 0.00 | |
| Z56 | 1.10 | | 0.22 | | -0.02 | | 0.00 | | 0.02 |
| Z58 | | 0.56 | | 0.02 | | 0.00 | | 0.02 | |
| Z60 | 0.91 | | 0.23 | | 0.00 | | 0.02 | | 0.00 |
| Z62 | | 0.66 | | 0.03 | | 0.00 | | -0.01 | |
| Z64 | 1.06 | | 0.19 | | -0.01 | | 0.00 | | 0.01 |
| Z66 | | 0.52 | | 0.03 | | -0.01 | | 0.01 | |
| Z68 | 0.82 | | 0.24 | | -0.01 | | 0.01 | | 0.00 |
| Z70 | | 0.65 | | 0.03 | | 0.01 | | 0.00 | |

| | | | | | | | | | |
|------|------|------|------|------|-------|-------|-------|-------|-------|
| Z72 | 1.03 | | 0.23 | | 0.00 | | 0.00 | | -0.01 |
| Z74 | | 0.62 | | 0.05 | | -0.01 | | -0.01 | |
| Z76 | 0.90 | | 0.31 | | 0.00 | | -0.01 | | 0.01 |
| Z78 | | 0.75 | | 0.03 | | -0.02 | | 0.00 | |
| Z80 | 1.05 | | 0.22 | | -0.02 | | -0.02 | | -0.01 |
| Z82 | | 0.58 | | 0.01 | | -0.03 | | -0.01 | |
| Z84 | 0.89 | | 0.18 | | -0.03 | | -0.01 | | 0.00 |
| Z86 | | 0.58 | | 0.03 | | -0.02 | | 0.00 | |
| Z88 | 0.99 | | 0.25 | | -0.04 | | -0.01 | | |
| Z90 | | 0.61 | | 0.05 | | -0.01 | | | |
| Z92 | 0.99 | | 0.35 | | -0.01 | | | | |
| Z94 | | 0.85 | | 0.04 | | | | | |
| Z96 | 1.19 | | 0.29 | | | | | | |
| Z98 | | 0.70 | | | | | | | |
| Z100 | 1.09 | | | | | | | | |

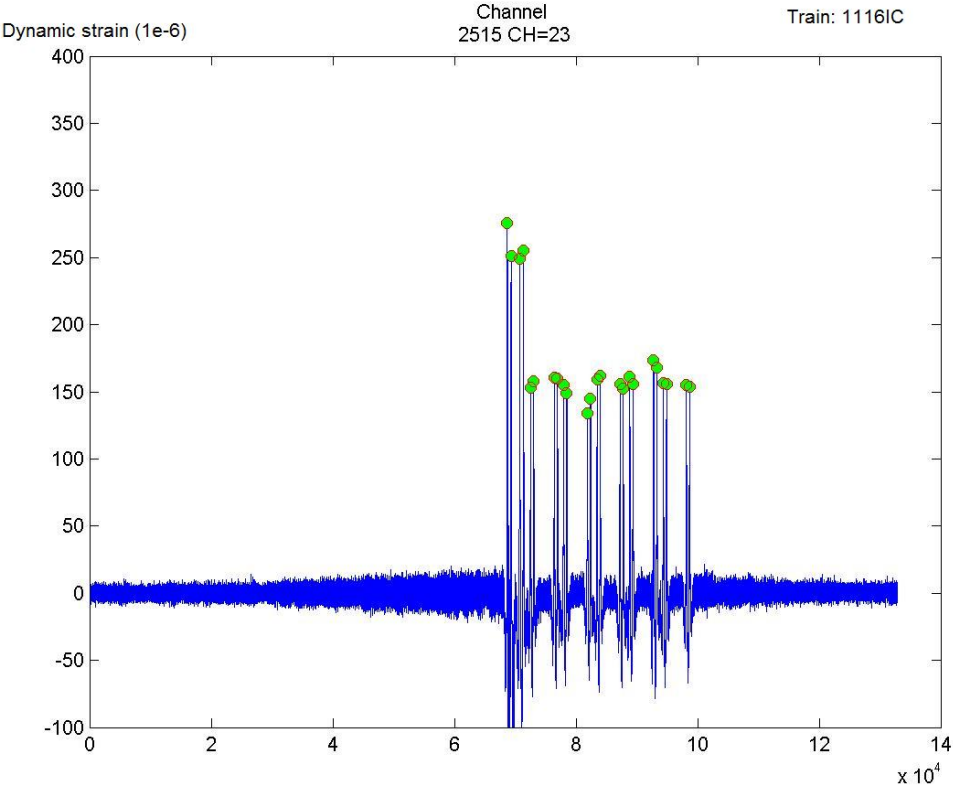


Figure: Measured dynamic strain under train passage (1116IC, Section 3)

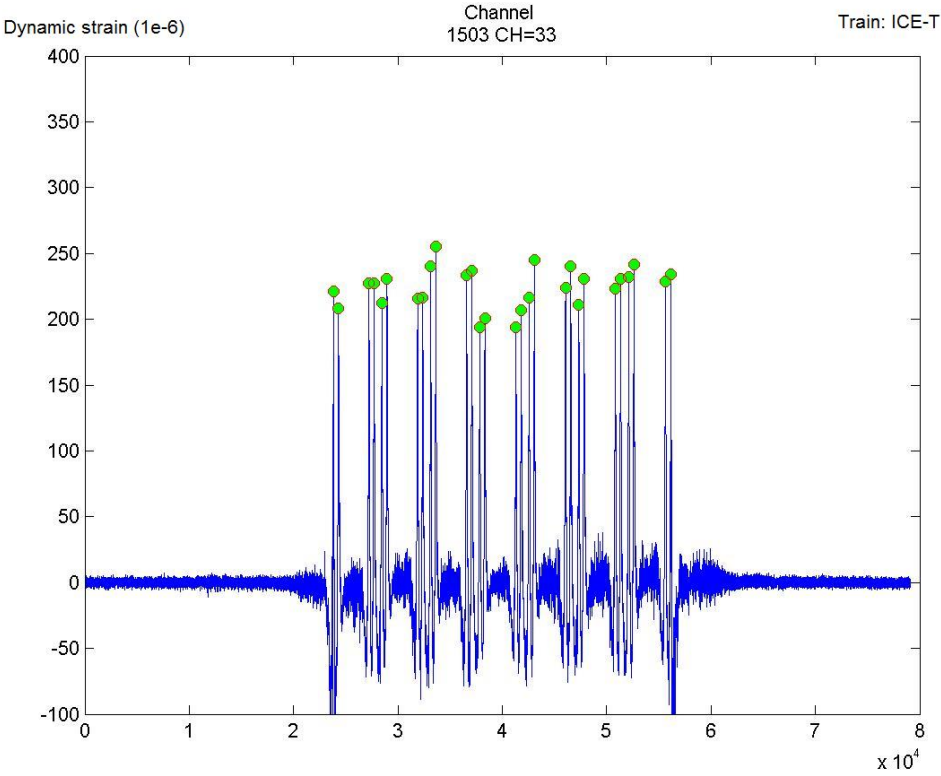


Figure: Measured dynamic strain under train passage (ICE-T, Section 4)

Appendix 18

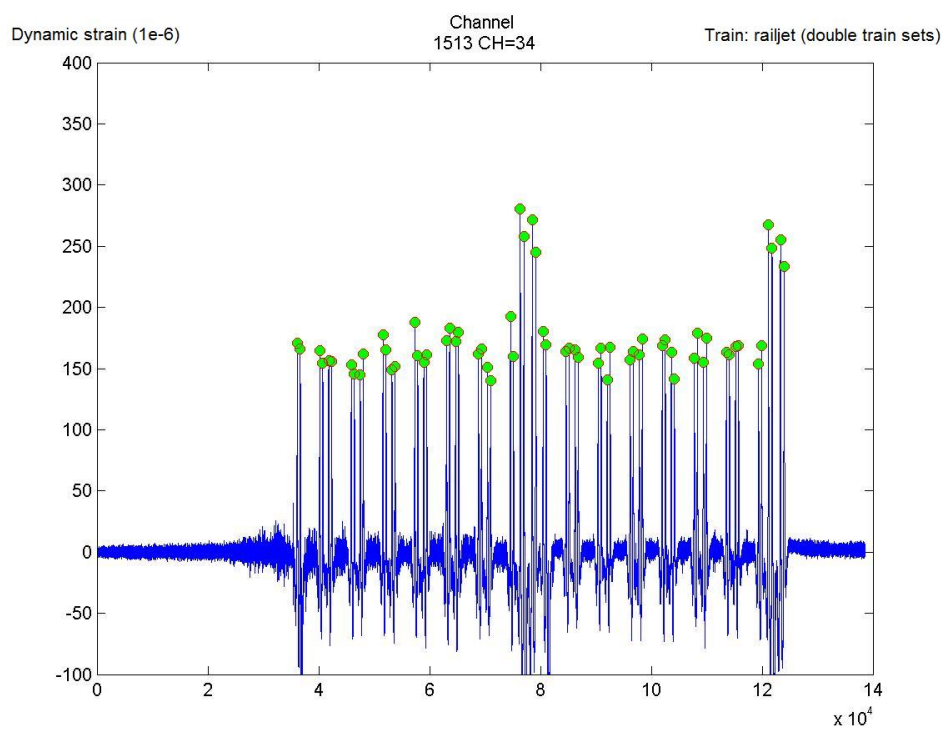


Figure: Measured dynamic strain under train passage (Railjet, Section 3)

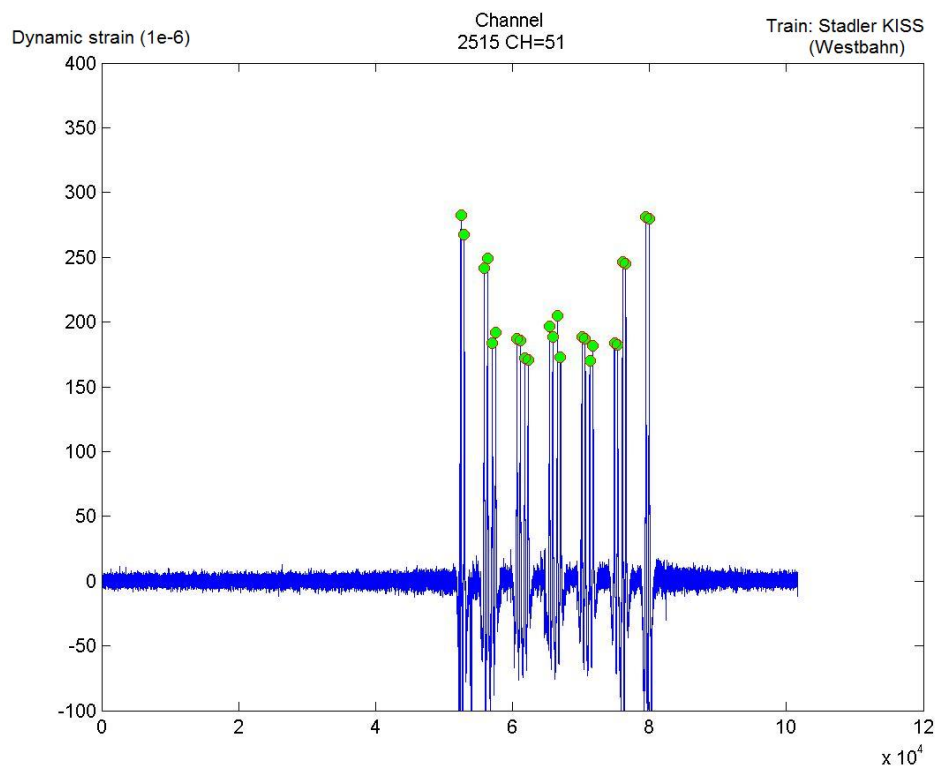


Figure: Measured dynamic strain under train passage (Stadler KISS, Section 4)

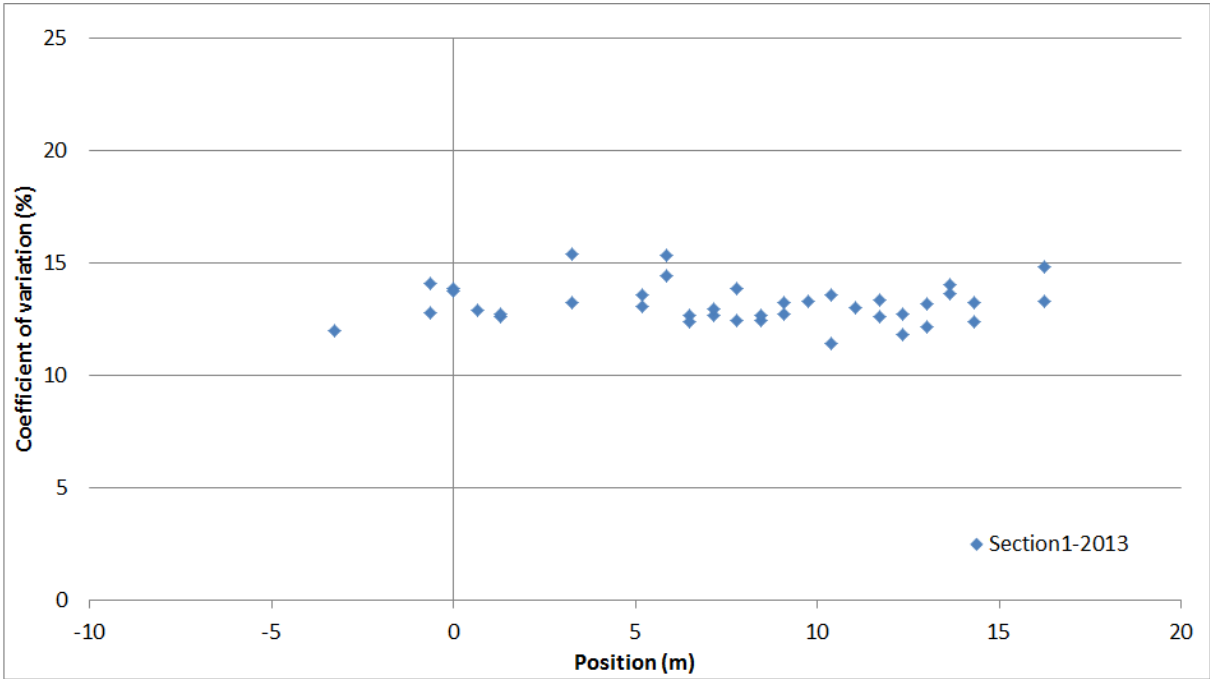


Figure: CV of passenger wagon (Section 1, V = 200 ± 10 km/h)

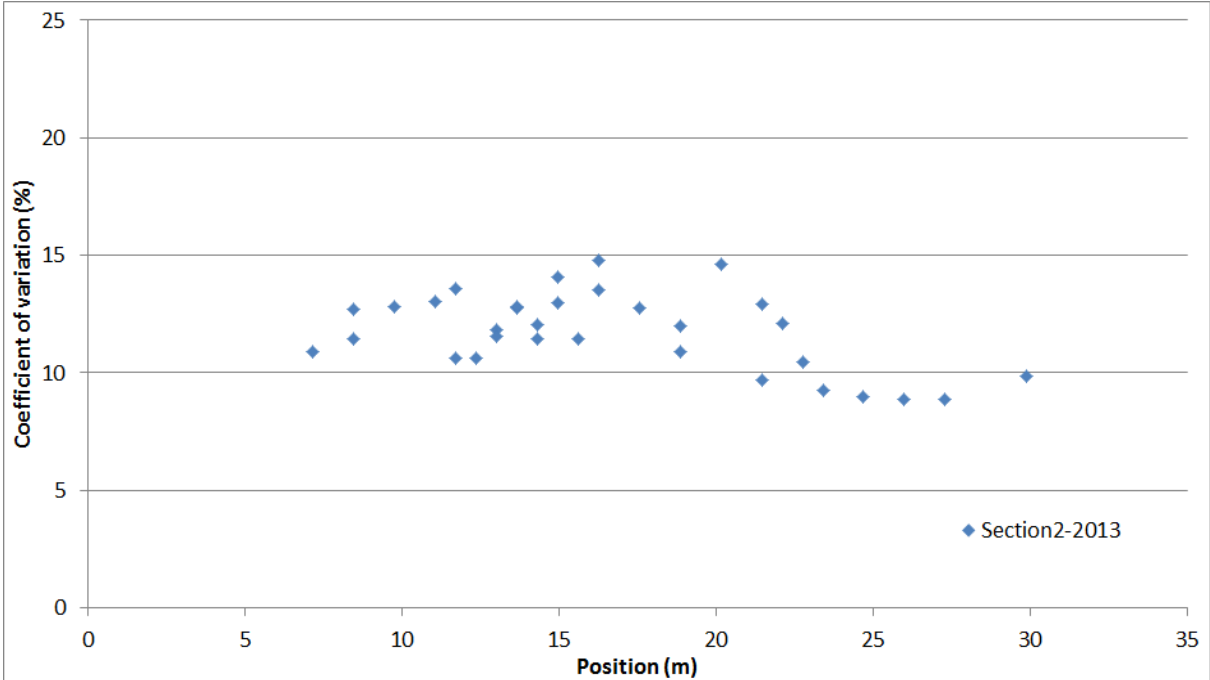


Figure: CV of passenger wagon (Section 2, V = 200 ± 10 km/h)

Appendix 20

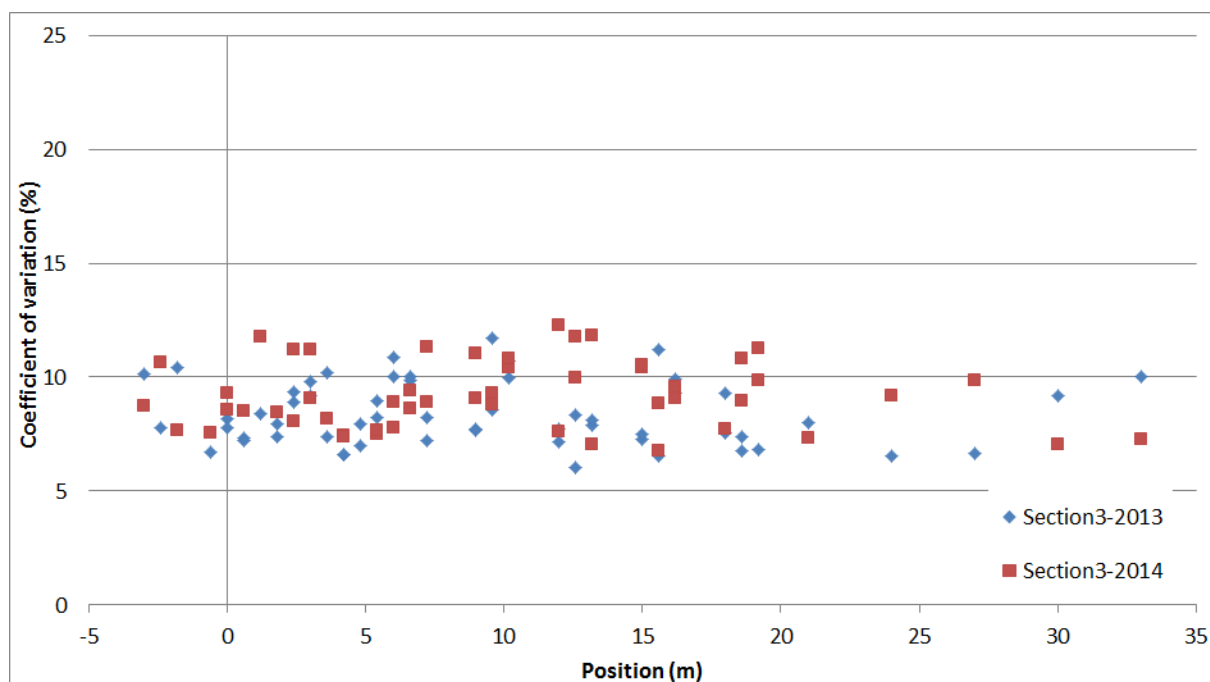


Figure: CV of passenger wagon (Section 3, $V = 160 \pm 10$ km/h)

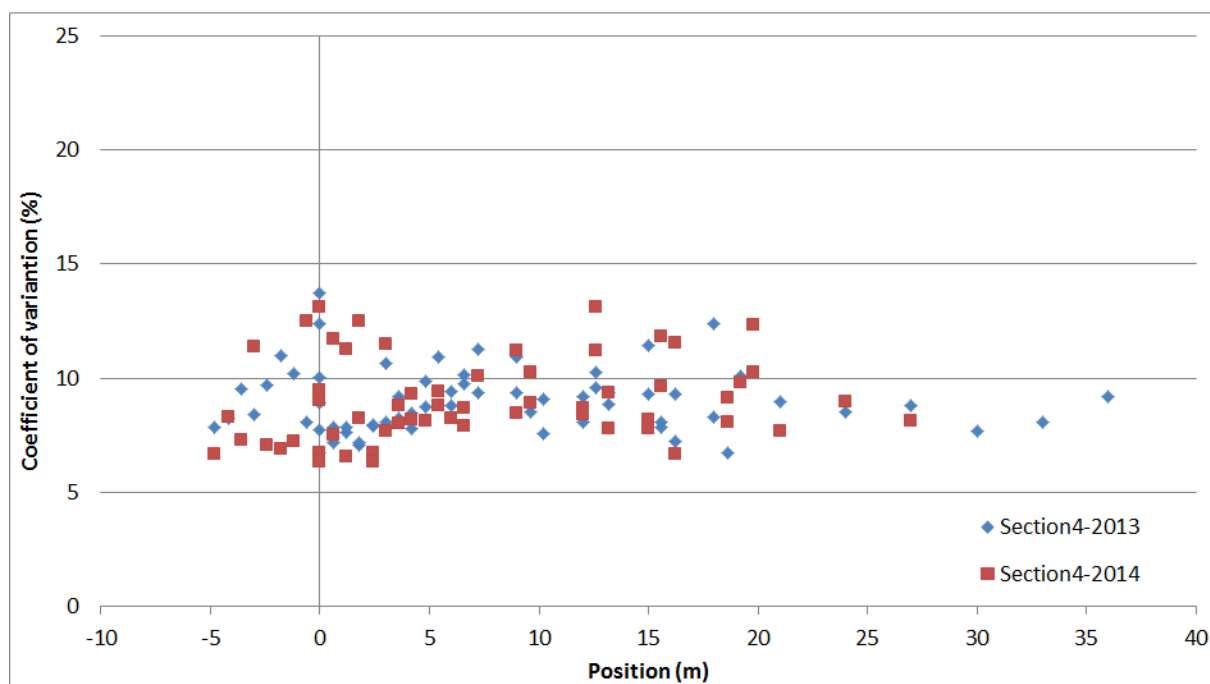


Figure: CV of passenger wagon (Section 4, $V = 160 \pm 10$ km/h)

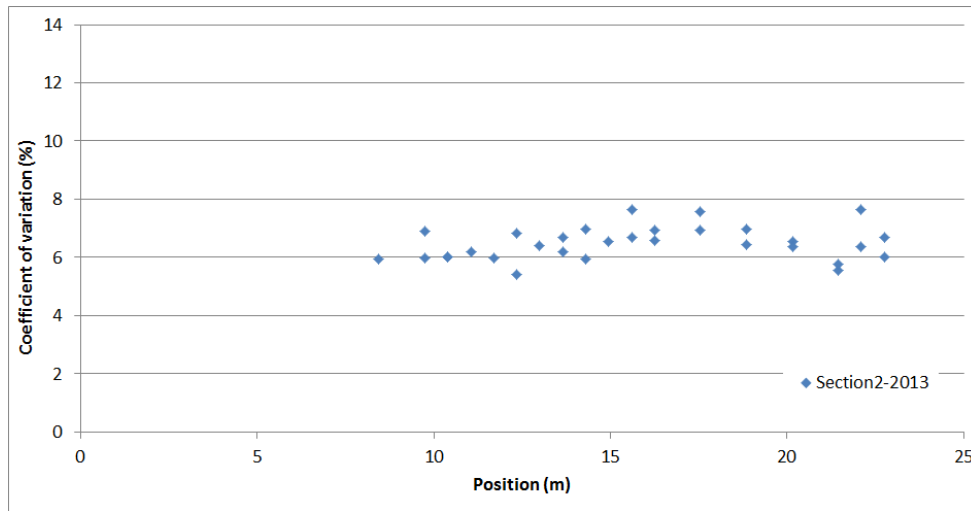


Figure: CV of ICE-T (Section 2, $V = 230 \pm 10$ km/h)

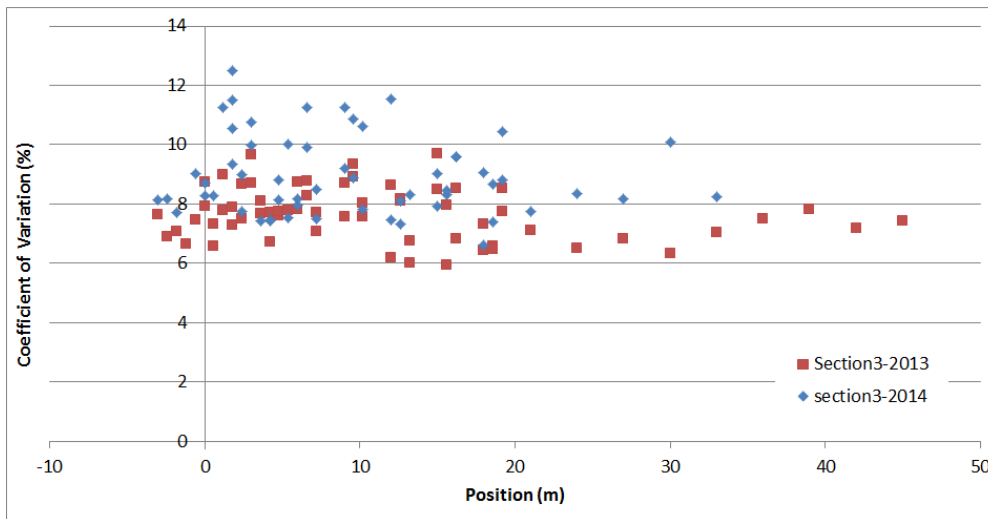


Figure: CV of ICE-T (Section 3, $V = 160 \pm 10$ km/h)

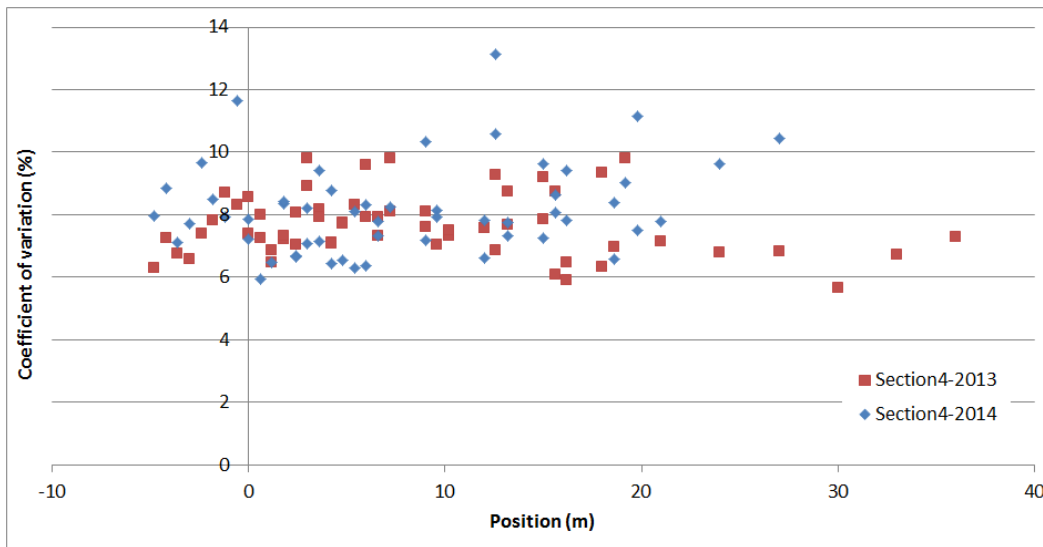


Figure: CV of ICE-T (Section 4, $V = 160 \pm 10$ km/h)

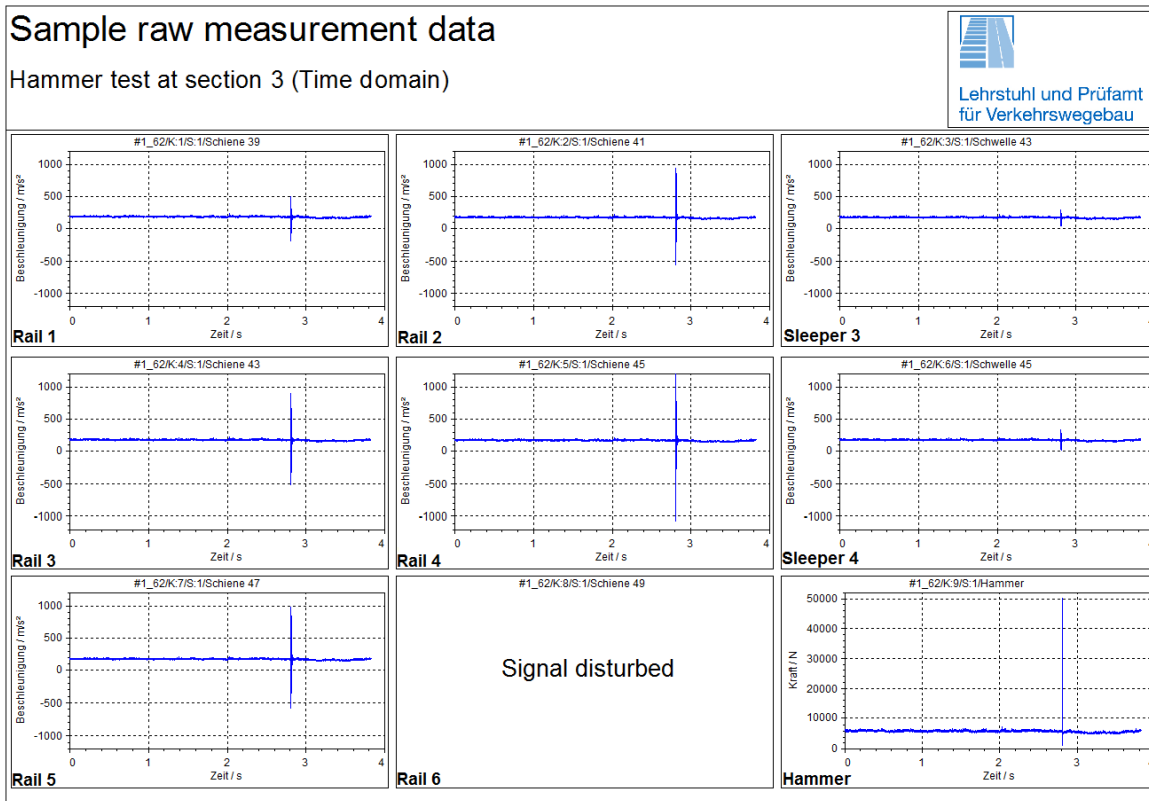


Figure: Sample raw measurement data in time domain under impact load

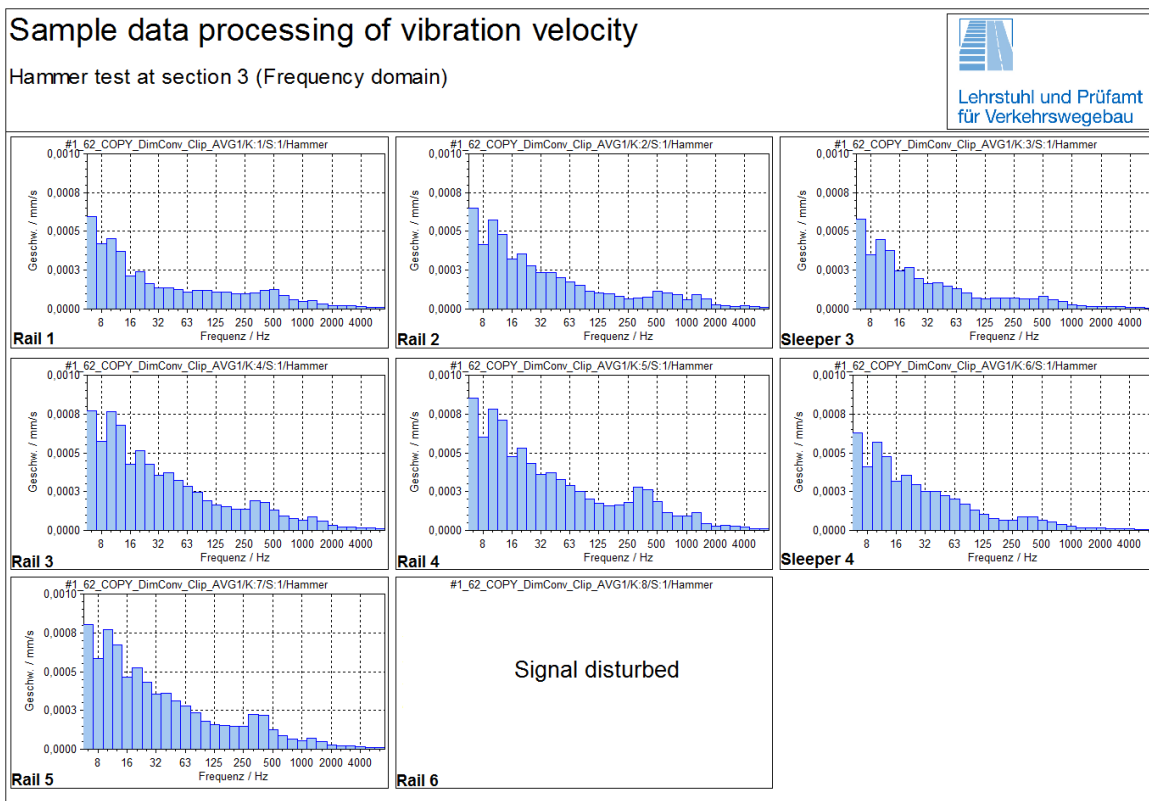


Figure: Sample processed data in frequency domain under impact load

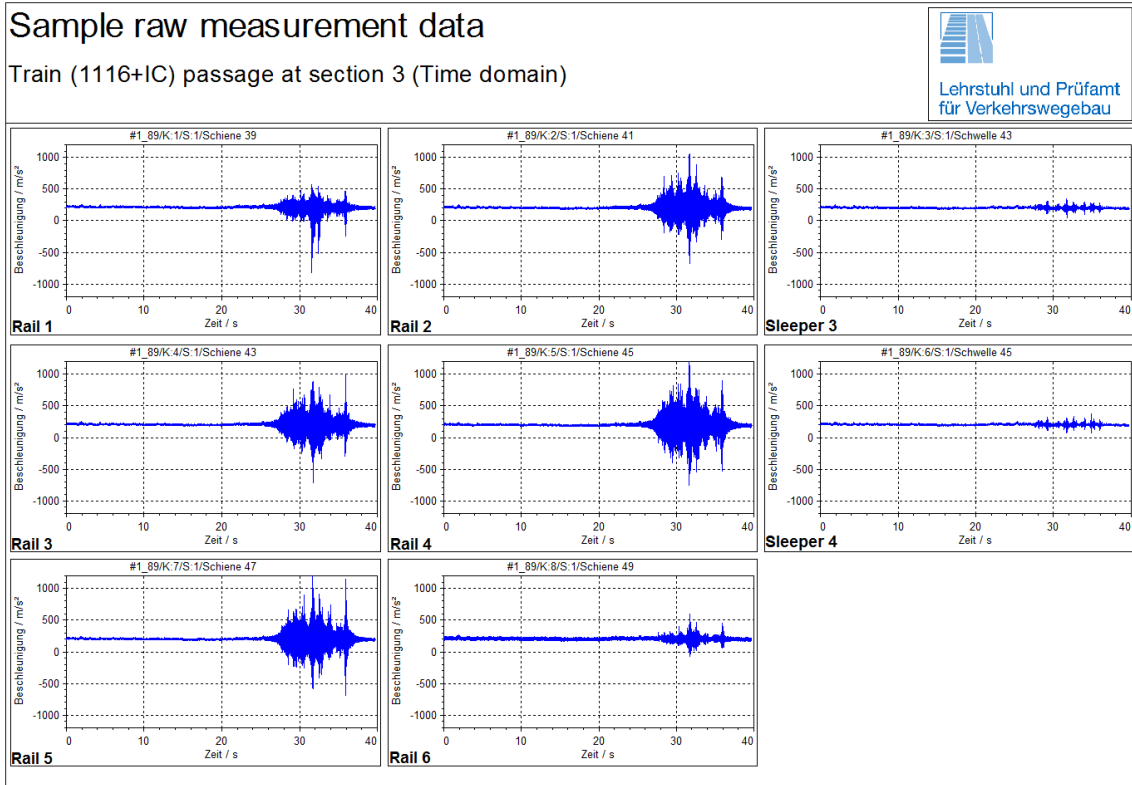


Figure: Sample raw measurement data in time domain under impact load

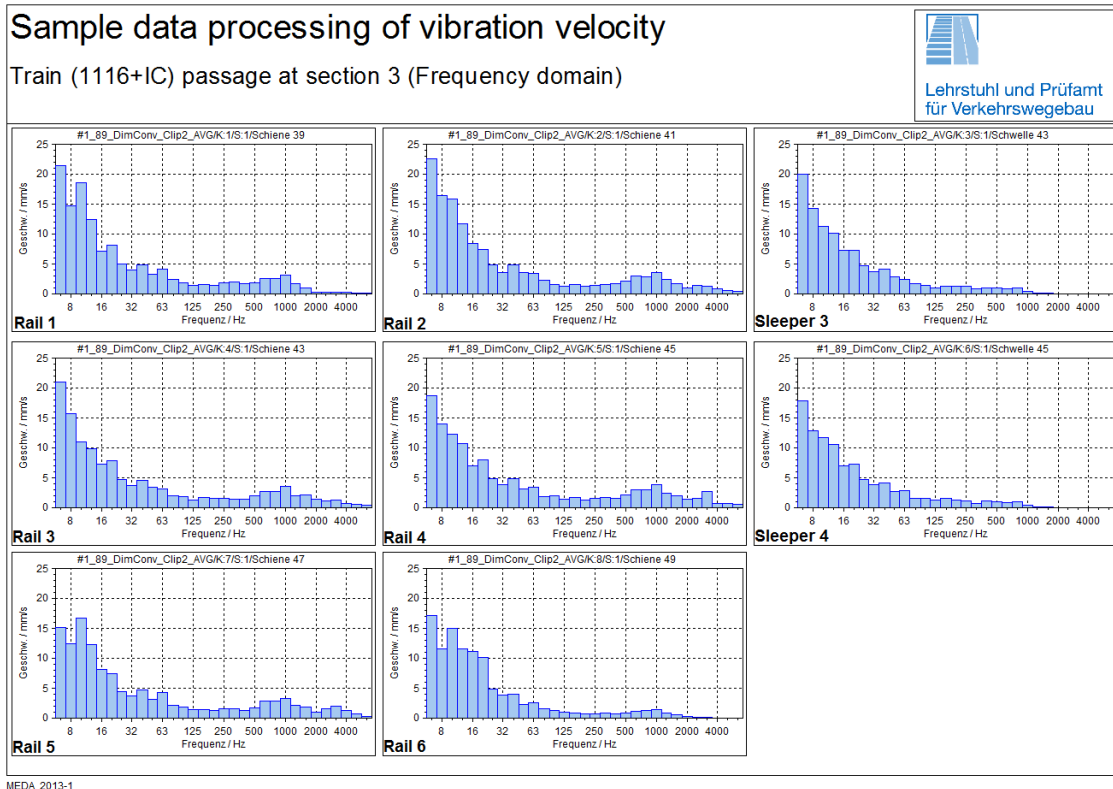


Figure: Sample raw measurement data in time domain under impact load

Appendix 24

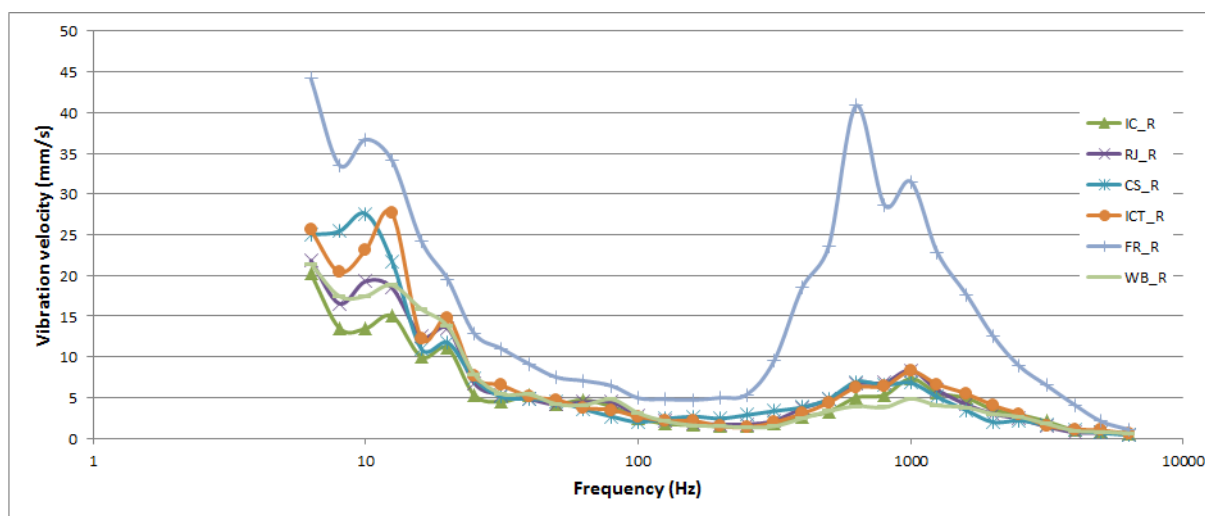


Figure: Distribution of vibration velocity on rail (section 3, 2013)

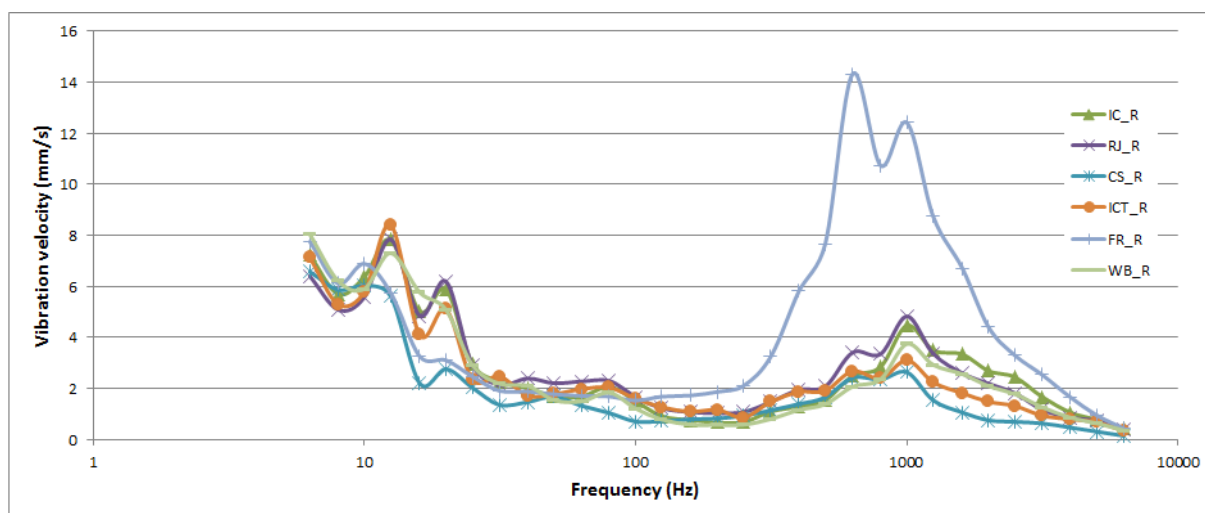


Figure: Distribution of vibration velocity on rail (section 3, 2014)

Table: Explanation of the legends

| Symbol | Train type |
|--------|-------------------------|
| IC | 1116 + IC (Inter city) |
| RJ | Railjet (Inter city) |
| CS | City shuttle (regional) |
| ICT | ICE-T (high speed EMU) |
| FR | Freight train |
| WB | Stadler KISS (Westbahn) |

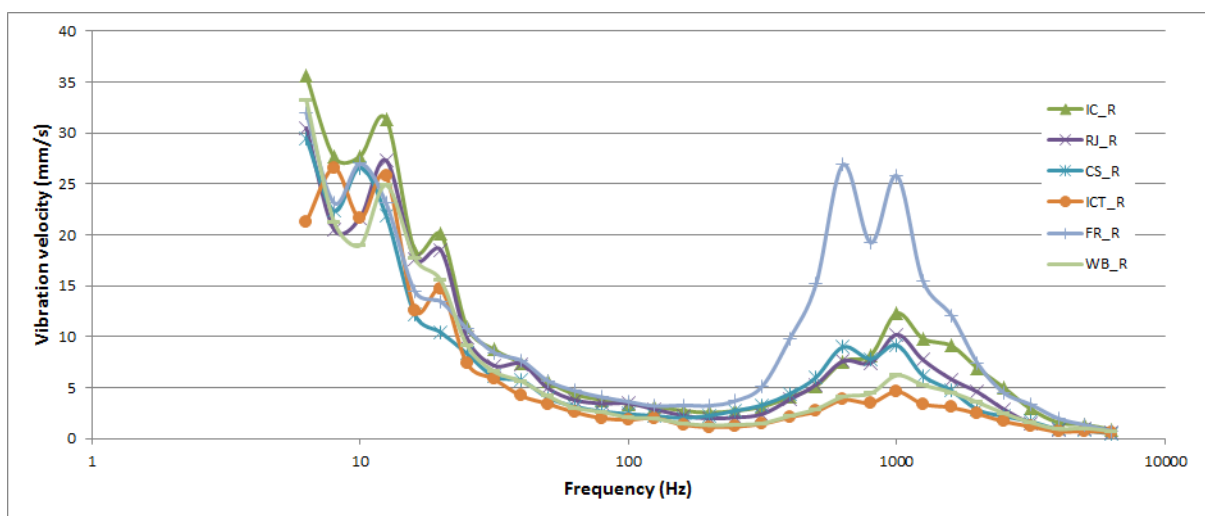


Figure: Distribution of vibration velocity on rail (section 4, 2013)

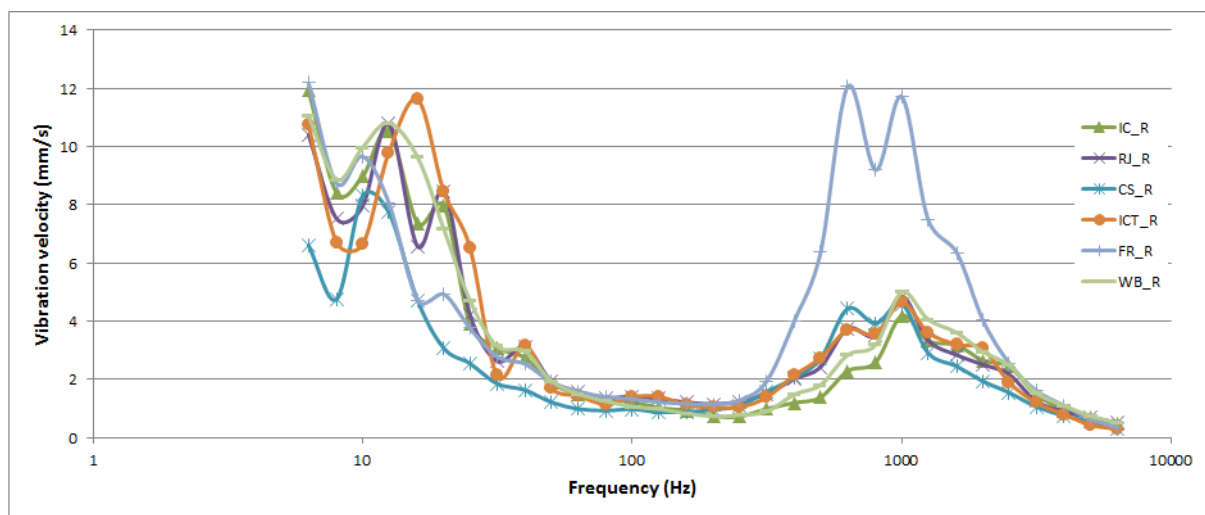


Figure: Distribution of vibration velocity on rail (section 4, 2014)

Table: Explanation of the legends

| Symbol | Train type |
|--------|-------------------------|
| IC | 1116 + IC (Inter city) |
| RJ | Railjet (Inter city) |
| CS | City shuttle (regional) |
| ICT | ICE-T (high speed EMU) |
| FR | Freight train |
| WB | Stadler KISS (Westbahn) |

Appendix 26

Table: Inertia parameters for the built vehicle

| Rigid body | Mass (kg) | Moment of inertia | | |
|------------|-----------|-------------------------------|-------------------------------|-------------------------------|
| | | I_{xx} (kg-m ²) | I_{yy} (Kg-m ²) | I_{zz} (Kg-m ²) |
| Car body | 48000 | 89998 | 2397000 | 2397000 |
| Bogie | 14800 | 14992.409 | 28364.739 | 42325.46 |
| Wheelset | 1500 | 1446.011 | 74 | 1446.011 |

Table: Suspension parameters for the built vehicle

| Suspension level | Type of stiffness/damping | Representation | Value |
|--|--------------------------------------|----------------|---|
| Primary Suspension/ (Rubber spring and primary vertical damper) | Translational serial stiffness (x) | KS_{px} | 6.0e7 N/m |
| | Translational serial stiffness (y) | KS_{py} | 7.5e6 N/m |
| | Translational serial stiffness (z) | KS_{pz} | 0 |
| | Translational serial damping (x) | CS_{px} | 3.0e4 Ns/m |
| | Translational serial damping (y) | CS_{py} | 5.0e3 Ns/m |
| | Translational serial damping (z) | CS_{pz} | 0 |
| | Translational parallel stiffness (x) | KP_{px} | 4.1e7 N/m |
| | Translational parallel stiffness (y) | KP_{py} | 4.5e6 N/m |
| | Translational parallel stiffness (z) | KP_{pz} | 2.5e6 N/m |
| | Primary vertical damper | C_{pz} | Non-linear behavior given by input function |
| Primary Suspension/ (Bushing stiffness) | Bushing translational stiffness (x) | K_{bx} | 1.8e7 N/m |
| | Bushing translational stiffness (y) | K_{by} | 6.0e6 N/m |
| | Bushing translational stiffness (z) | K_{bz} | 1.8e7 N/m |
| | Bushing translational damping (x) | C_{bx} | 1.0e4 Ns/m |
| | Bushing translational damping (y) | C_{by} | 1.0e4Ns/m |

Appendices

| | | | |
|---|--|-----------|---|
| | Bushing translational damping (z) | C_{bz} | 3.0e3 Ns/m |
| | Bushing rotational stiffness (al) | K_{bal} | 2.3e3 N/m |
| | Bushing rotational stiffness (be) | K_{bbe} | 3.0e3 N/m |
| | Bushing rotational stiffness (ga) | K_{bga} | 2.8e3N/m |
| | Bushing rotational damping (al) | C_{bal} | 70 Ns/m |
| | Bushing rotational damping (be) | C_{bbe} | 50 Ns/m |
| | Bushing rotational damping (ga) | C_{bga} | 90 Ns/m |
| Secondary suspension (Secondary shear spring and damping elements) | Longitudinal Shear stiffness | K_{sx} | 2.5e5 N/m |
| | Lateral shear stiffness | K_{sy} | 2.5e5 N/m |
| | Vertical stiffness | K_{sz} | 8.91e6 N/m |
| | Roll bending stiffness | K_r | 1.05e4 N/m |
| | Pitch bending stiffness | K_p | 1.05e4 N/m |
| | Torsion stiffness | K_t | 0 |
| | Secondary vertical damper (mounting stiffness) | K_m | 6.0e6 N/m |
| | Secondary vertical damper (damping) | C_{sz} | 4.5e4 Ns/m |
| | Secondary horizontal (or lateral) damper | C_{sy} | Non-linear behavior given by input function |
| | Secondary longitudinal or yaw damping | C_{sx} | Non-linear behavior given by input function |
| Anti-roll bar | Stiffness | K | 9.4e5 Nm/rad |
| Traction rod | Stiffness | K | 5.0e6 N/m |
| | Damping | C | 2.5e4 Ns/m |
| Bump Stop | Stiffness | K | Non-linear behavior given by input function |

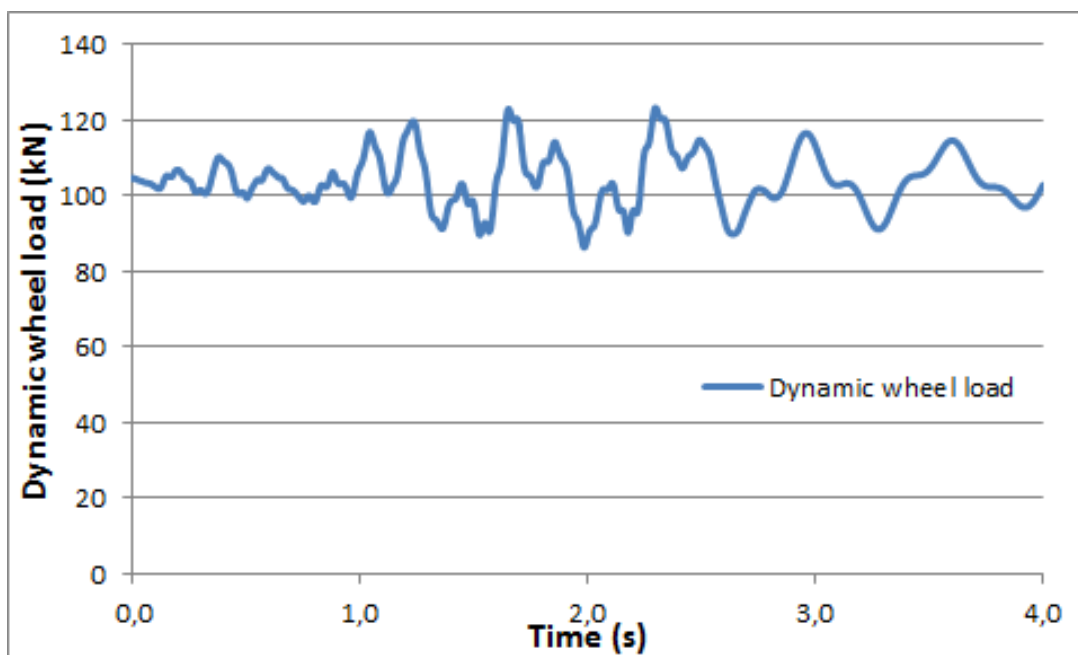


Figure: Distribution of dynamic wheel load under track geometry excitation (Simpack simulation, Section 4, 2012)

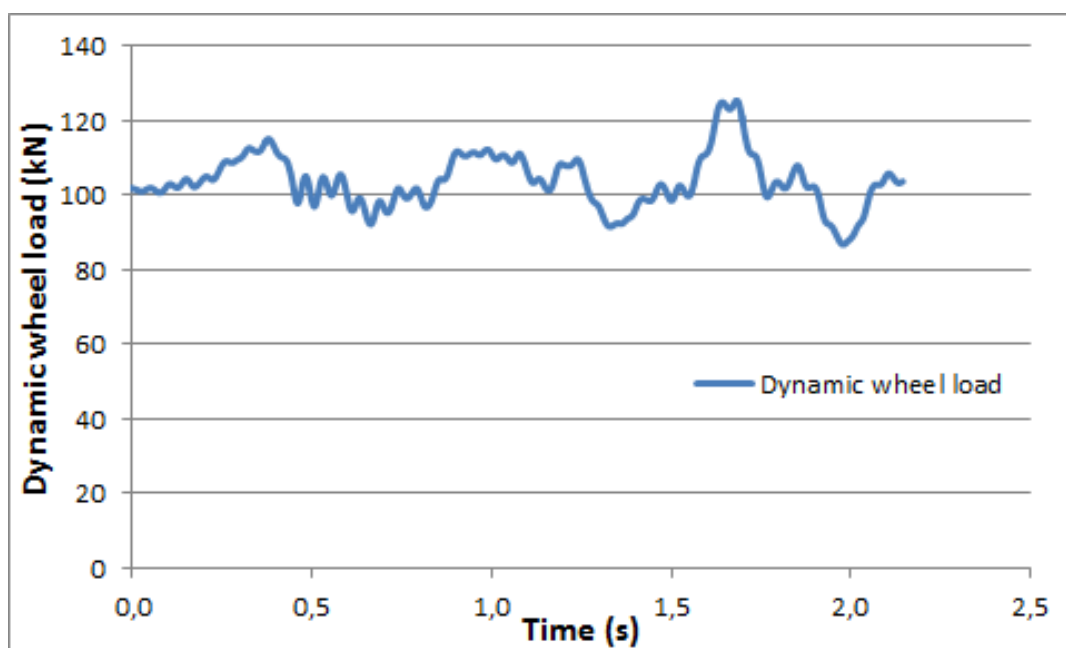


Figure: Distribution of dynamic wheel load under track geometry excitation (Simpack simulation, Section 4, 2014)

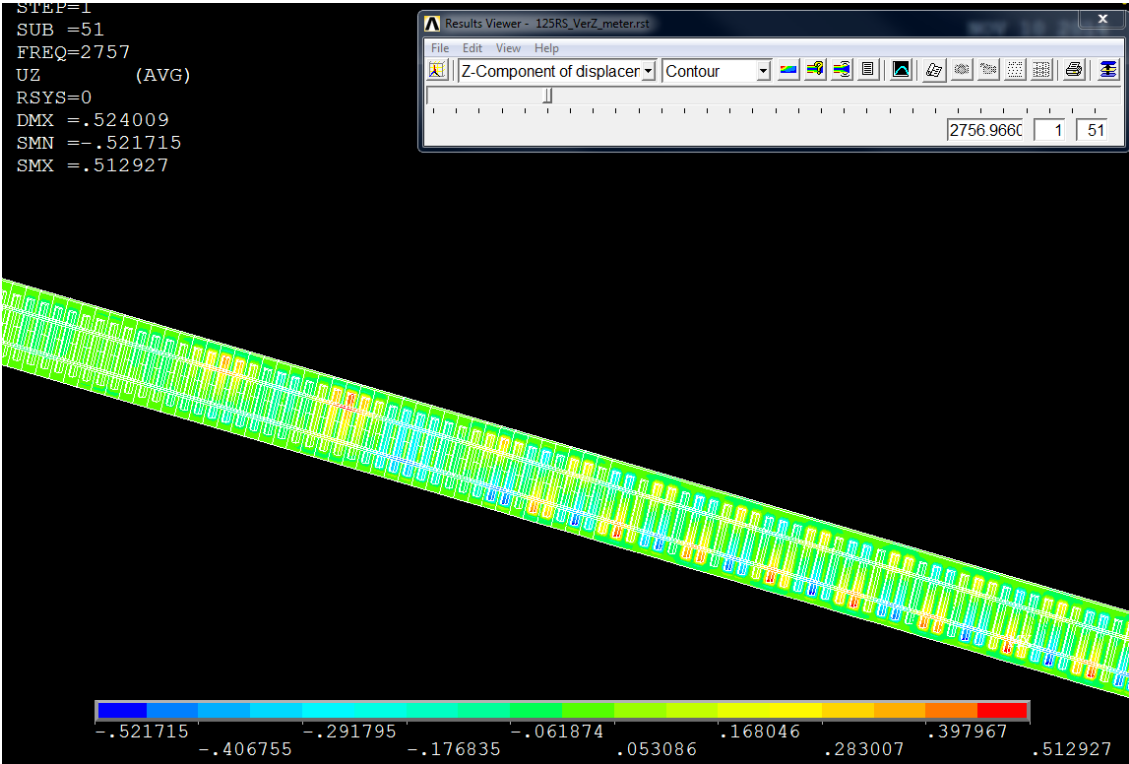


Figure: Illustration of eigen mode 51 ($f_0 = 2757$ Hz)

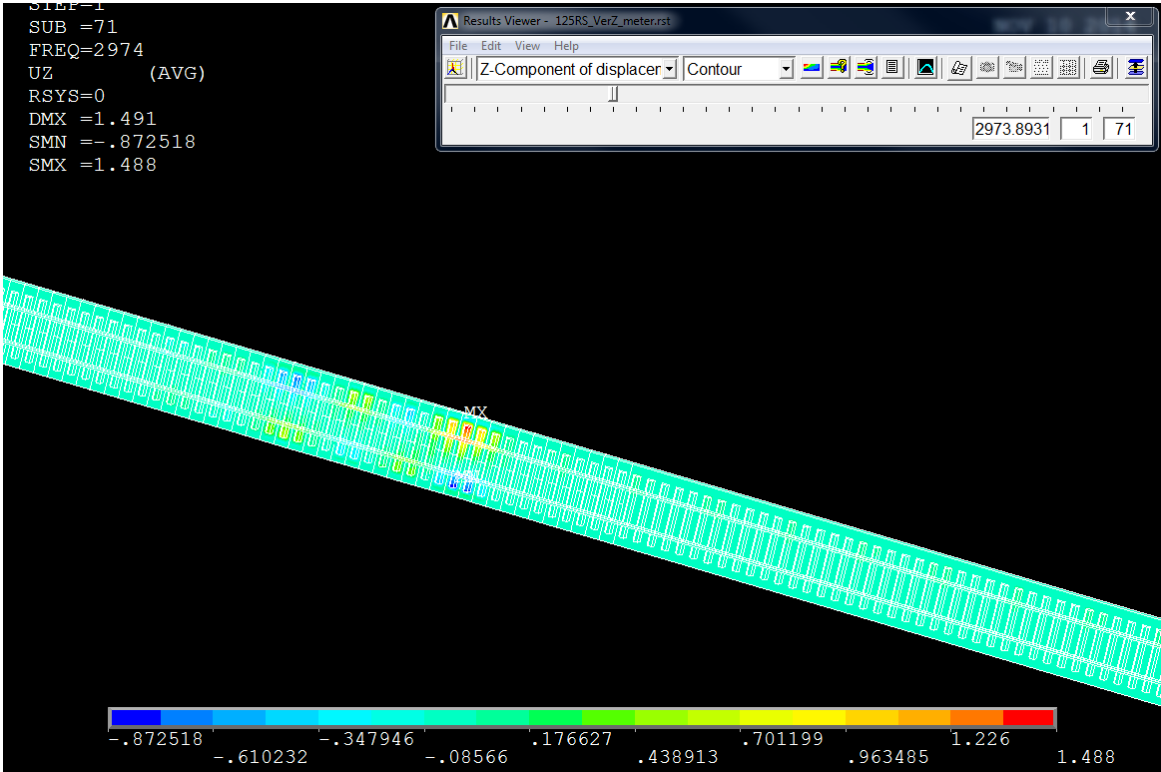


Figure: Illustration of eigen mode 71 ($f_0 = 2974$ Hz)

Appendix 29

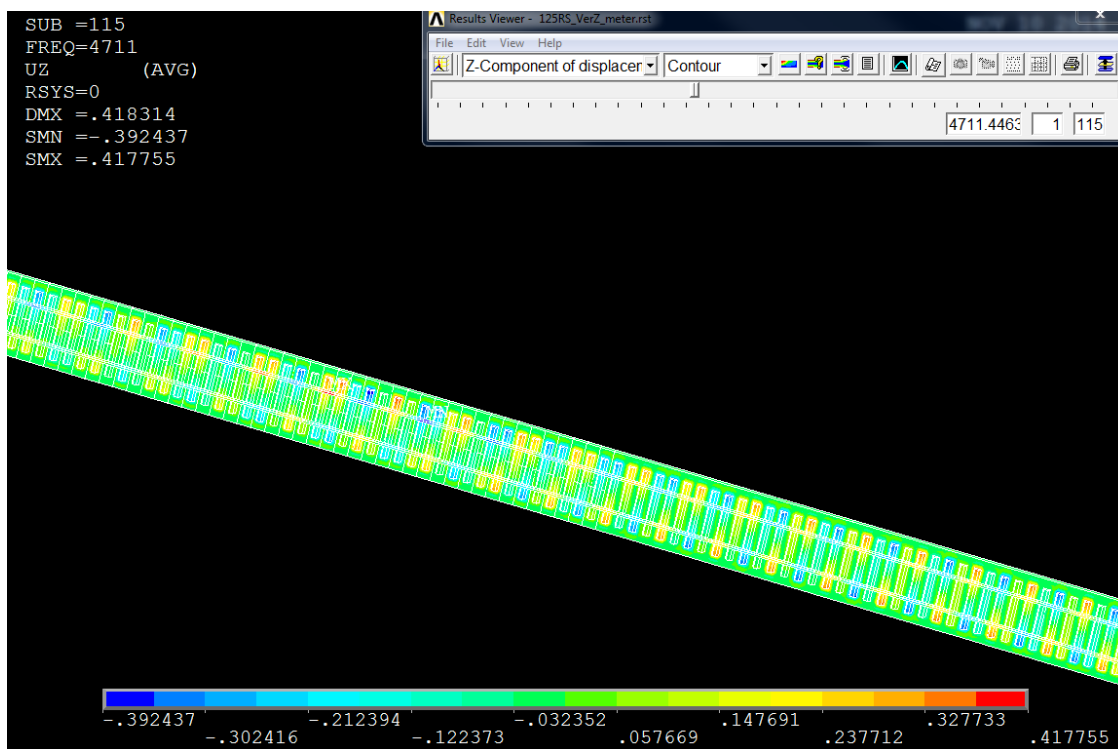


Figure: Illustration of eigen mode 115 ($f_0 = 4711$ Hz)

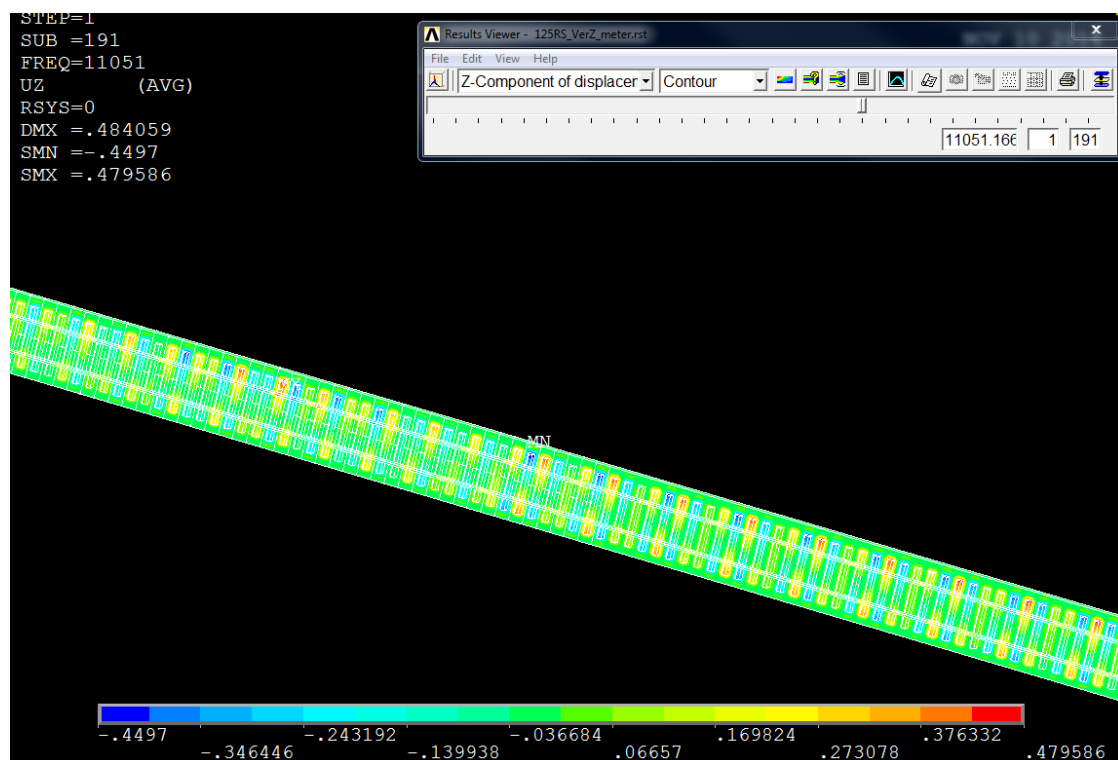


Figure: Illustration of eigen mode 191 ($f_0 = 11051$ Hz)

| Eigen mode | Frequenc y (Hz) | Eigen mode | Frequenc y (Hz) | Eigen mode | Frequenc y (Hz) | Eigen mode | Frequenc y (Hz) |
|------------|-----------------|------------|-----------------|------------|-----------------|------------|-----------------|
| 1 | 1298.1 | 41 | 2652.6 | 81 | 3379.3 | 121 | 5393.1 |
| 2 | 1436.2 | 42 | 2679.5 | 82 | 3421.1 | 122 | 5416.1 |
| 3 | 1456.2 | 43 | 2686.4 | 83 | 3468.4 | 123 | 5545.1 |
| 4 | 1456.6 | 44 | 2689.8 | 84 | 3476.5 | 124 | 5584.5 |
| 5 | 1457.8 | 45 | 2712.6 | 85 | 3499.4 | 125 | 5632.2 |
| 6 | 1462.8 | 46 | 2730.6 | 86 | 3518.0 | 126 | 5731.5 |
| 7 | 1463.6 | 47 | 2758.5 | 87 | 3529.6 | 127 | 5792.5 |
| 8 | 1464.3 | 48 | 2760.6 | 88 | 3545.8 | 128 | 5843.2 |
| 9 | 1467.6 | 49 | 2767.3 | 89 | 3641.3 | 129 | 5953.2 |
| 10 | 1469.6 | 50 | 2786.3 | 90 | 3658.1 | 130 | 6003.9 |
| 11 | 1472.6 | 51 | 2796.9 | 91 | 3694.4 | 131 | 6143.7 |
| 12 | 1478.4 | 52 | 2803.0 | 92 | 3771.5 | 132 | 6150.4 |
| 13 | 1490.9 | 53 | 2806.7 | 93 | 3803.1 | 133 | 6178.6 |
| 14 | 1503.6 | 54 | 2830.2 | 94 | 3859.4 | 134 | 6303.4 |
| 15 | 1524.0 | 55 | 2863.2 | 95 | 3887.6 | 135 | 6357.3 |
| 16 | 1543.2 | 56 | 2864.0 | 96 | 3923.4 | 136 | 6474.4 |
| 17 | 1574.5 | 57 | 2873.1 | 97 | 3968.1 | 137 | 6570.6 |
| 18 | 1599.0 | 58 | 2874.6 | 98 | 4039.2 | 138 | 6620.6 |
| 19 | 1643.3 | 59 | 2897.4 | 99 | 4074.6 | 139 | 6766.3 |
| 20 | 1672.5 | 60 | 2911.2 | 100 | 4114.8 | 140 | 6816.3 |
| 21 | 1732.2 | 61 | 2914.2 | 101 | 4191.9 | 141 | 6921.6 |
| 22 | 1765.8 | 62 | 2928.5 | 102 | 4215.5 | 142 | 6979.8 |
| 23 | 1841.1 | 63 | 2935.4 | 103 | 4306.4 | 143 | 6995.0 |
| 24 | 1879.7 | 64 | 2948.1 | 104 | 4320.4 | 144 | 7124.9 |
| 25 | 1971.9 | 65 | 2954.4 | 105 | 4381.5 | 145 | 7235.2 |
| 26 | 2015.6 | 66 | 2964.4 | 106 | 4415.7 | 146 | 7297.7 |
| 27 | 2122.7 | 67 | 2974.0 | 107 | 4518.3 | 147 | 7435.8 |
| 28 | 2171.6 | 68 | 2989.5 | 108 | 4561.1 | 148 | 7464.2 |
| 29 | 2294.2 | 69 | 3001.3 | 109 | 4596.4 | | |
| 30 | 2348.2 | 70 | 3011.8 | 110 | 4648.1 | | |
| 31 | 2393.1 | 71 | 3042.2 | 111 | 4715.8 | | |
| 32 | 2483.2 | 72 | 3089.4 | 112 | 4763.0 | | |
| 33 | 2528.6 | 73 | 3123.4 | 113 | 4880.4 | | |
| 34 | 2542.0 | 74 | 3150.8 | 114 | 4911.1 | | |
| 35 | 2546.8 | 75 | 3206.7 | 115 | 5014.3 | | |
| 36 | 2551.5 | 76 | 3225.2 | 116 | 5045.1 | | |
| 37 | 2581.7 | 77 | 3234.9 | 117 | 5099.4 | | |

| | | | | | | | |
|----|--------|----|--------|-----|--------|--|--|
| 38 | 2592.5 | 78 | 3263.1 | 118 | 5184.0 | | |
| 39 | 2598.7 | 79 | 3308.6 | 119 | 5224.7 | | |
| 40 | 2630.4 | 80 | 3322.5 | 120 | 5282.9 | | |

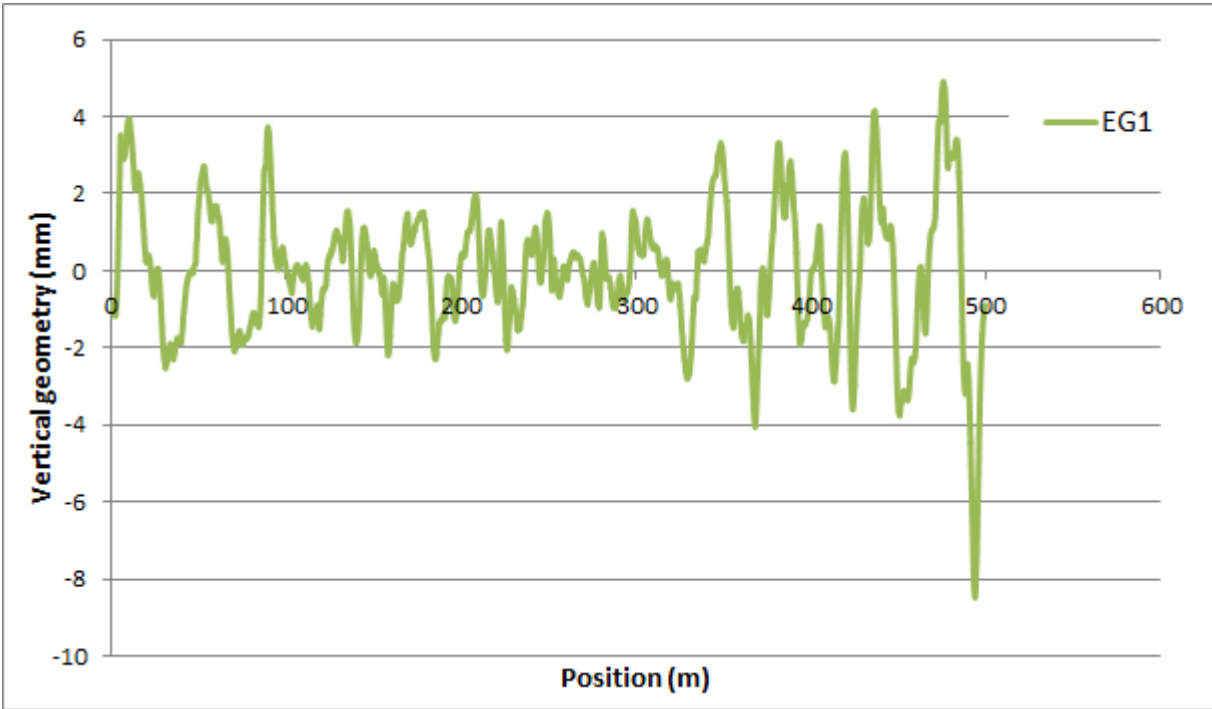


Figure: Vertical geometry – EG1 (Y = 3)

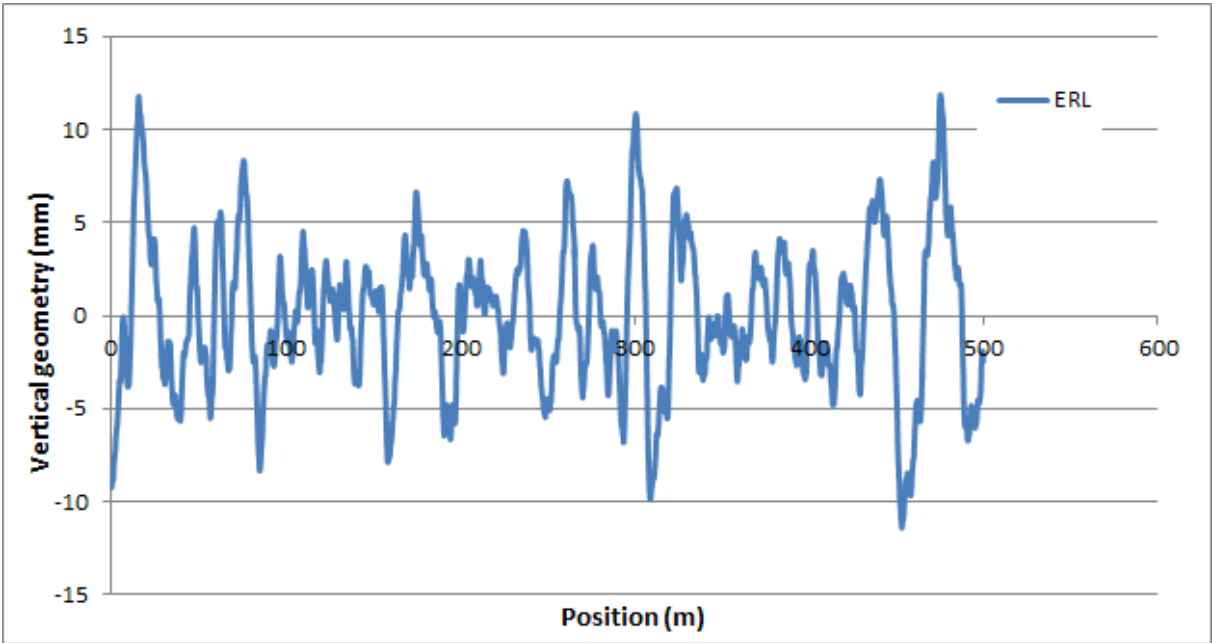


Figure: Vertical geometry – ERL (Y = 4)

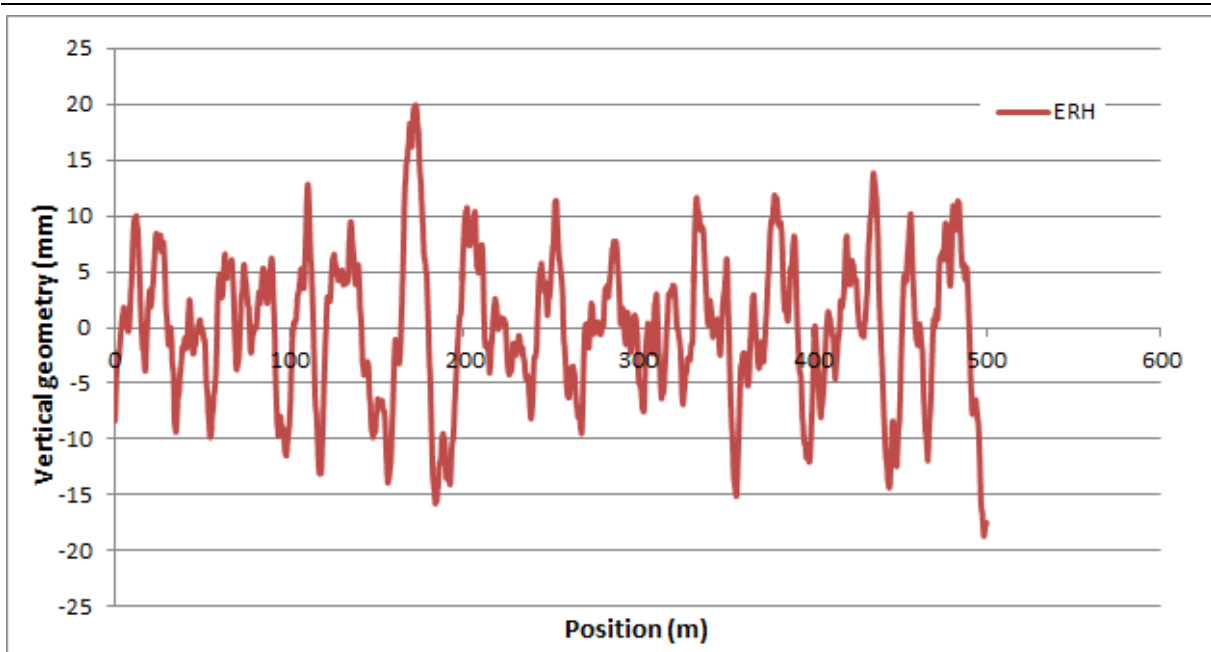


Figure: Vertical geometry – ERH (Y = 5)

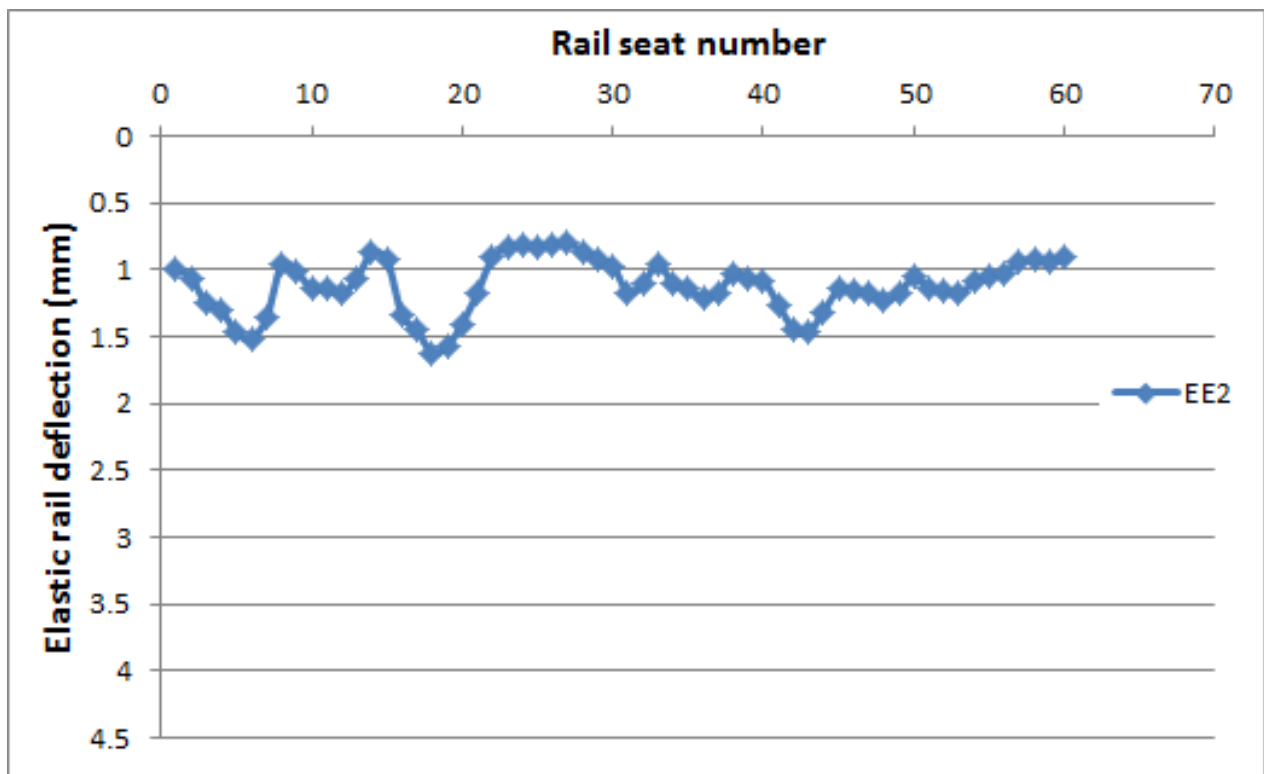


Figure: Elastic rail deflection – EE2 (Z = 3)

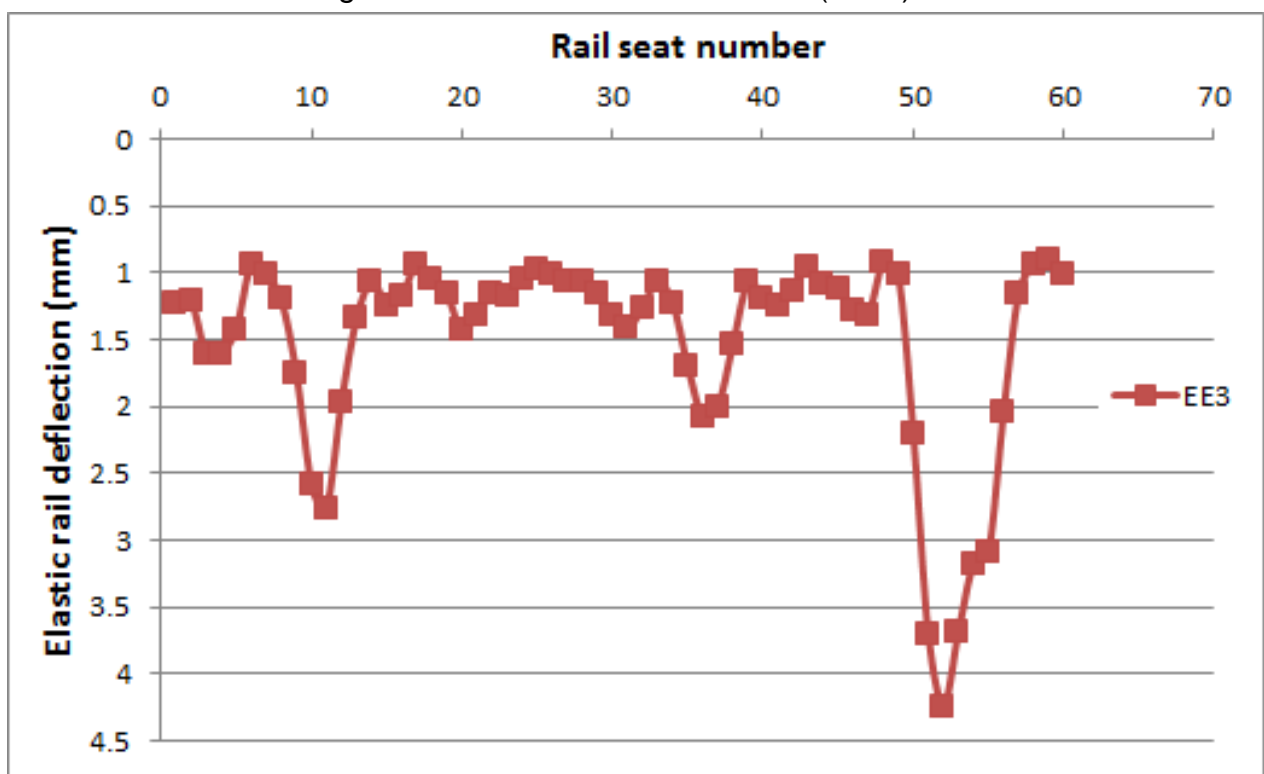


Figure: Elastic rail deflection – EE3 (Z = 4)

Appendix 33

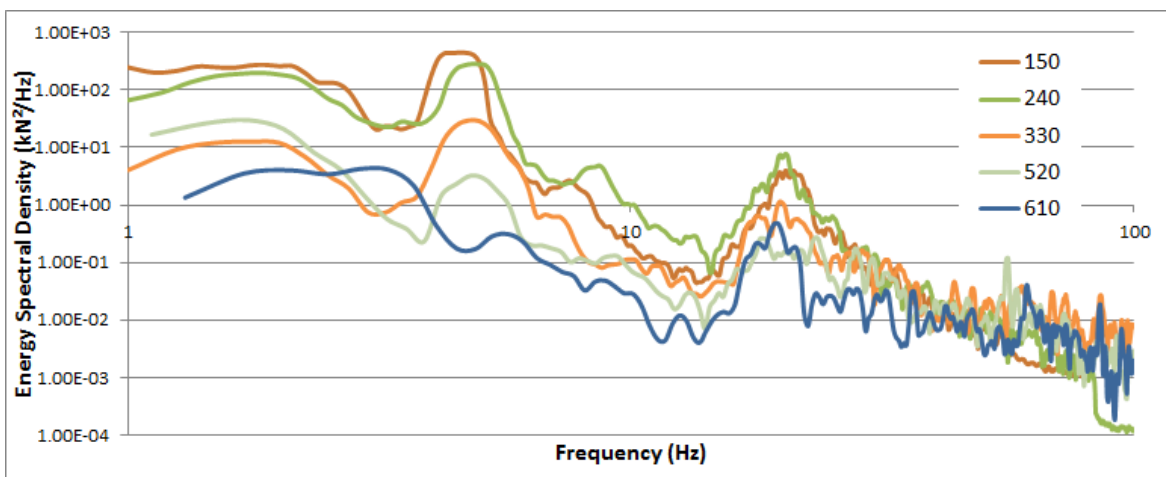


Figure: ESD output of selected X and Y combinations (Z = 0)

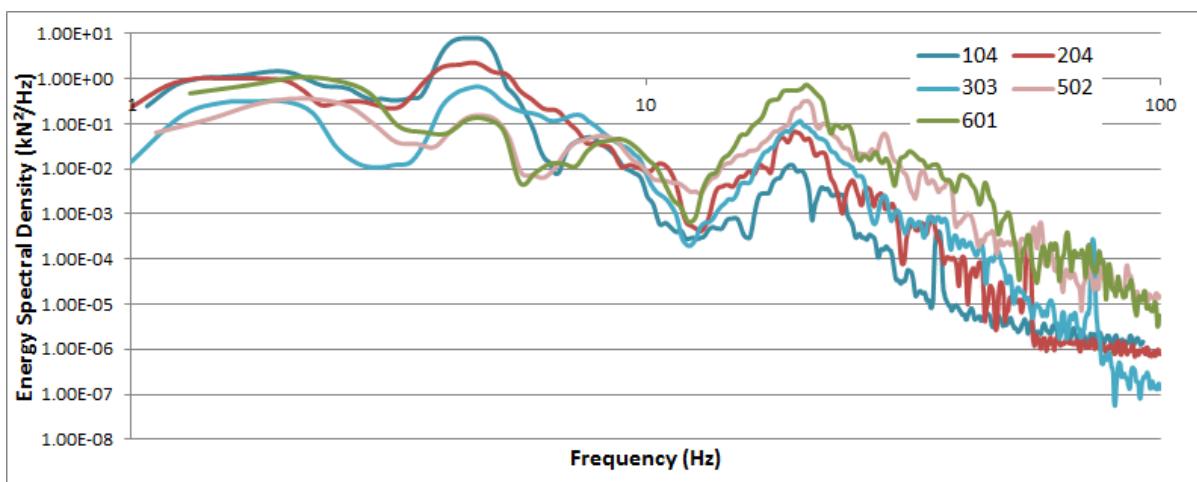


Figure: ESD output of selected X and Z combinations

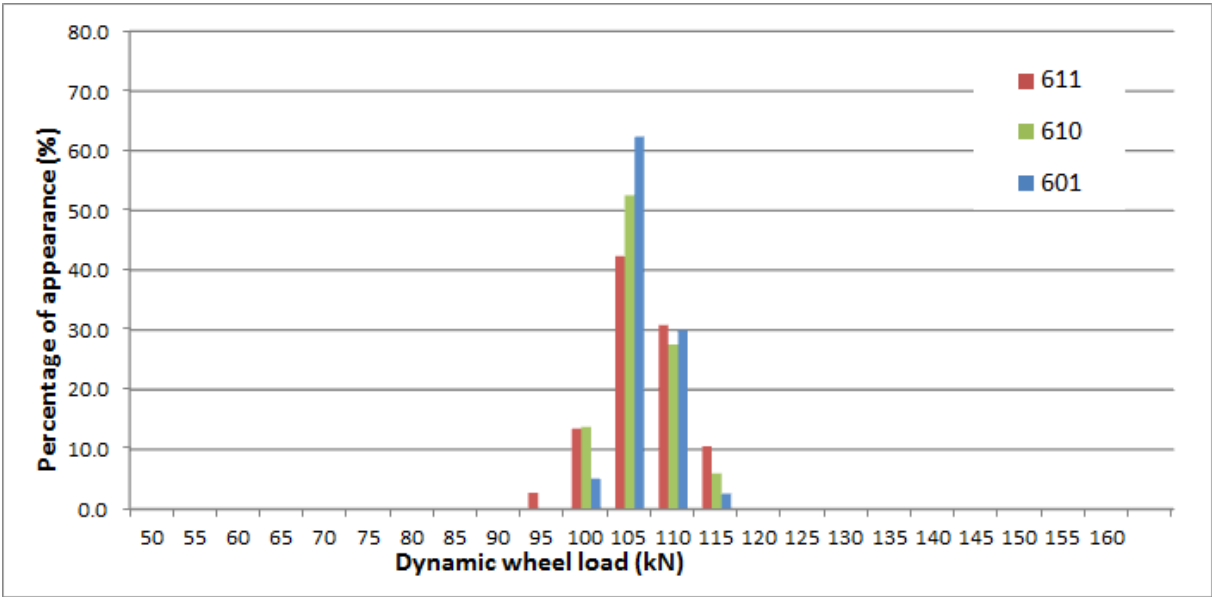


Figure: The statistical frequency distribution analysis of dynamic load (Combination 611, 610 and 601, V = 300km/h)

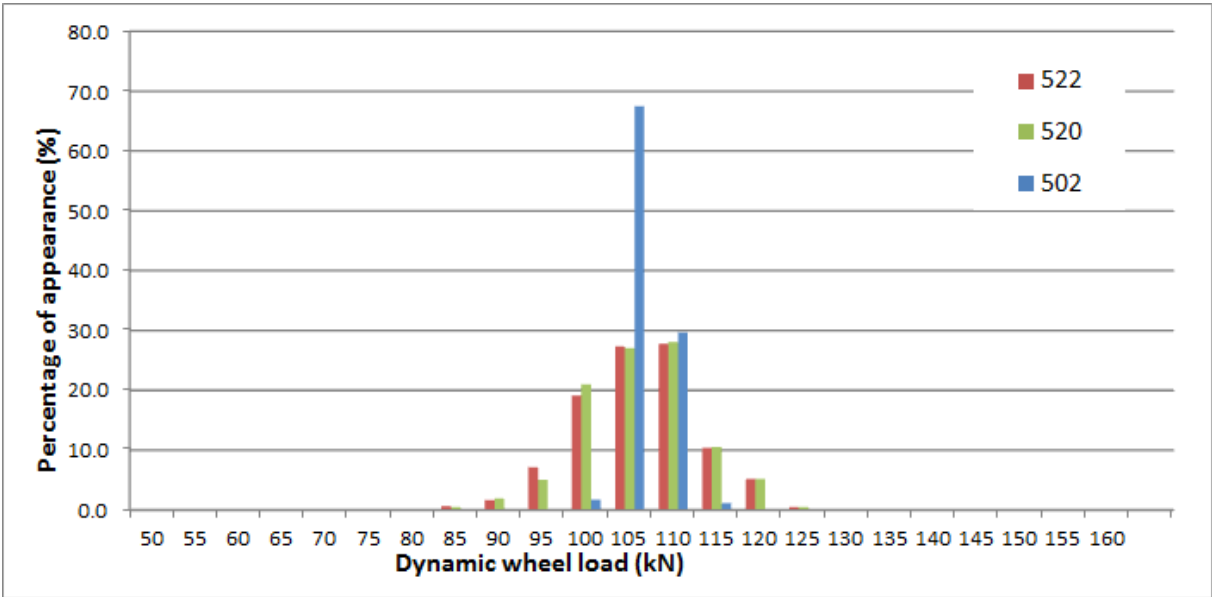


Figure: The statistical frequency distribution analysis of dynamic load (Combination 522, 520 and 502, V = 250km/h)

Appendix 35

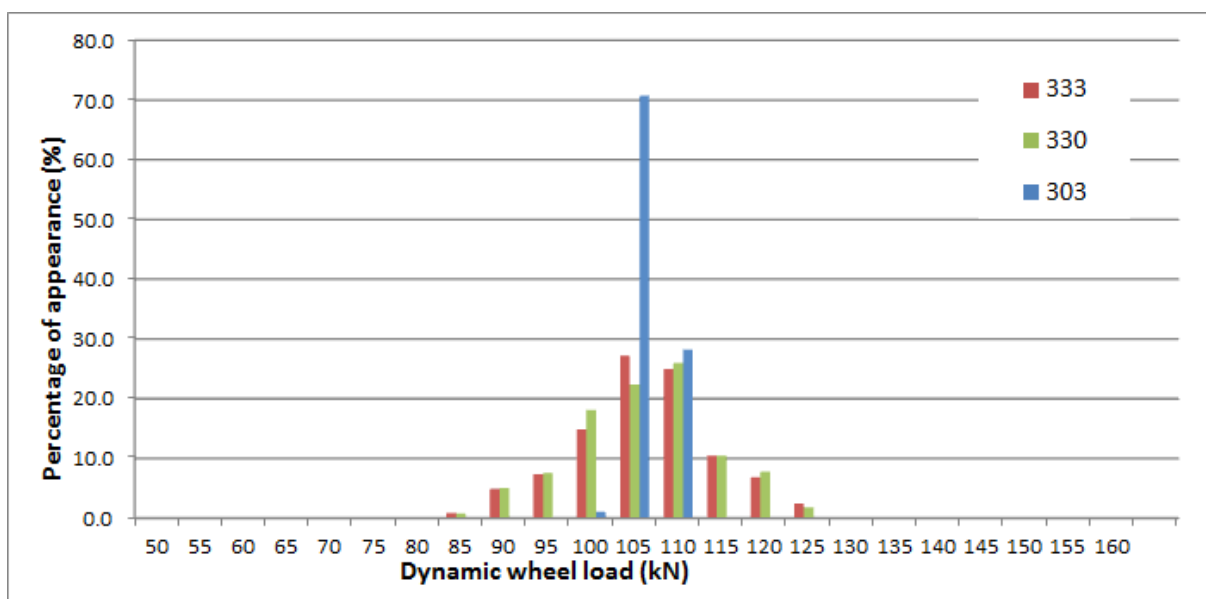


Figure: The statistical frequency distribution analysis of dynamic load (Combination 333, 330 and 303, V = 160km/h)

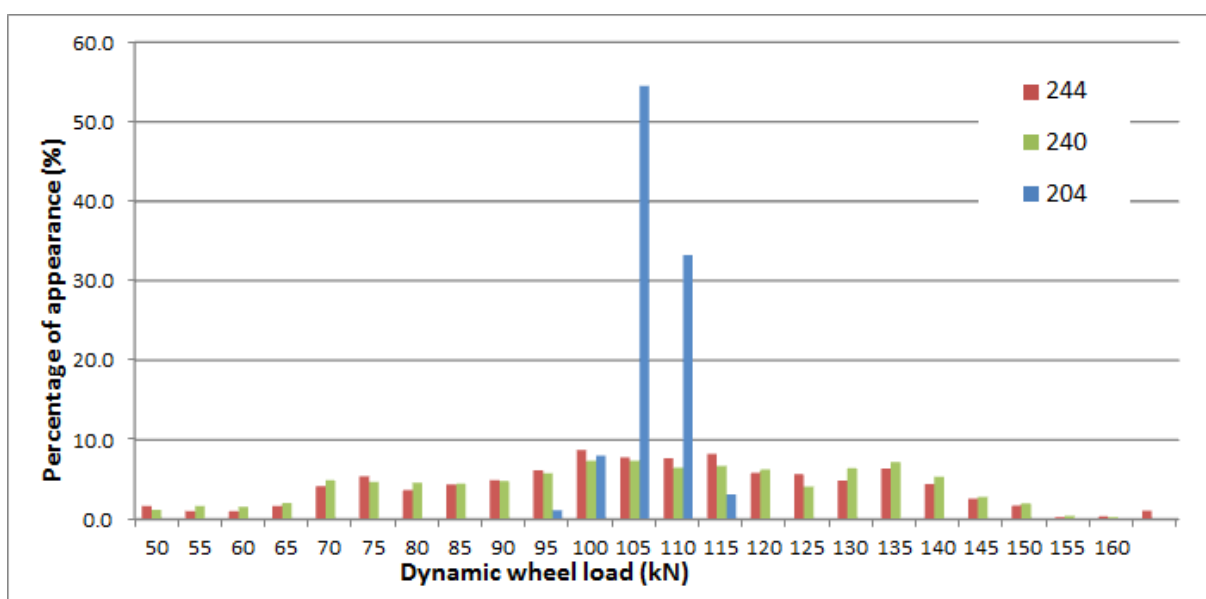


Figure: The statistical frequency distribution analysis of dynamic load (Combination 244, 240 and 204, V = 120km/h)

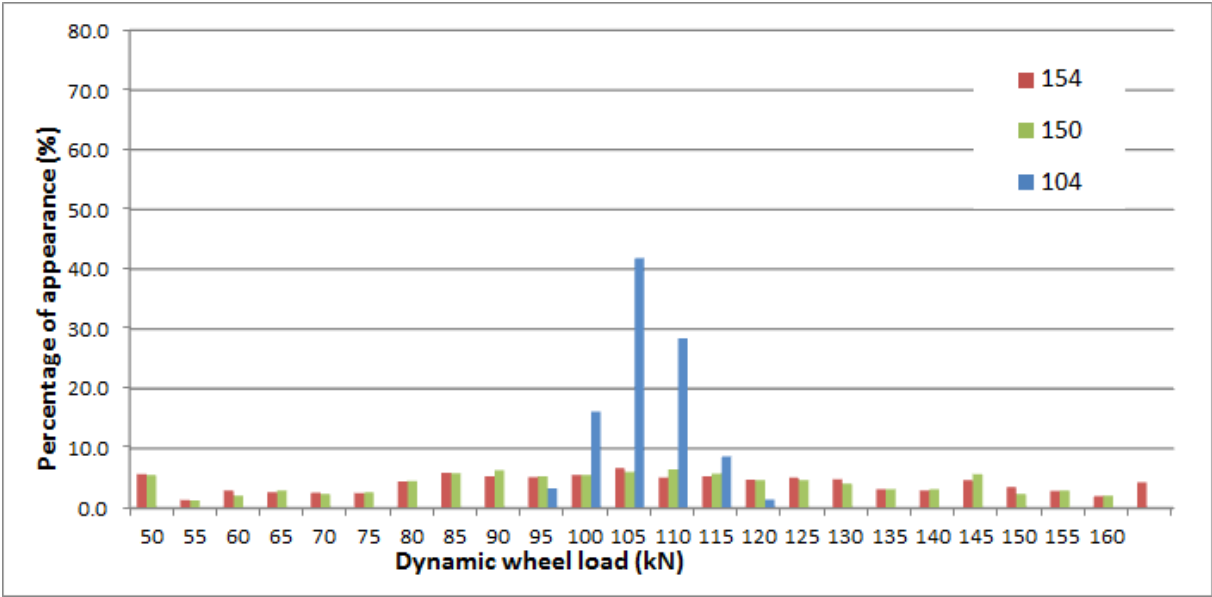


Figure: The statistical frequency distribution analysis of dynamic load (Combination 154, 150 and 104, V = 80km/h)

Annexes and user instructions

List of annexes and user instructions

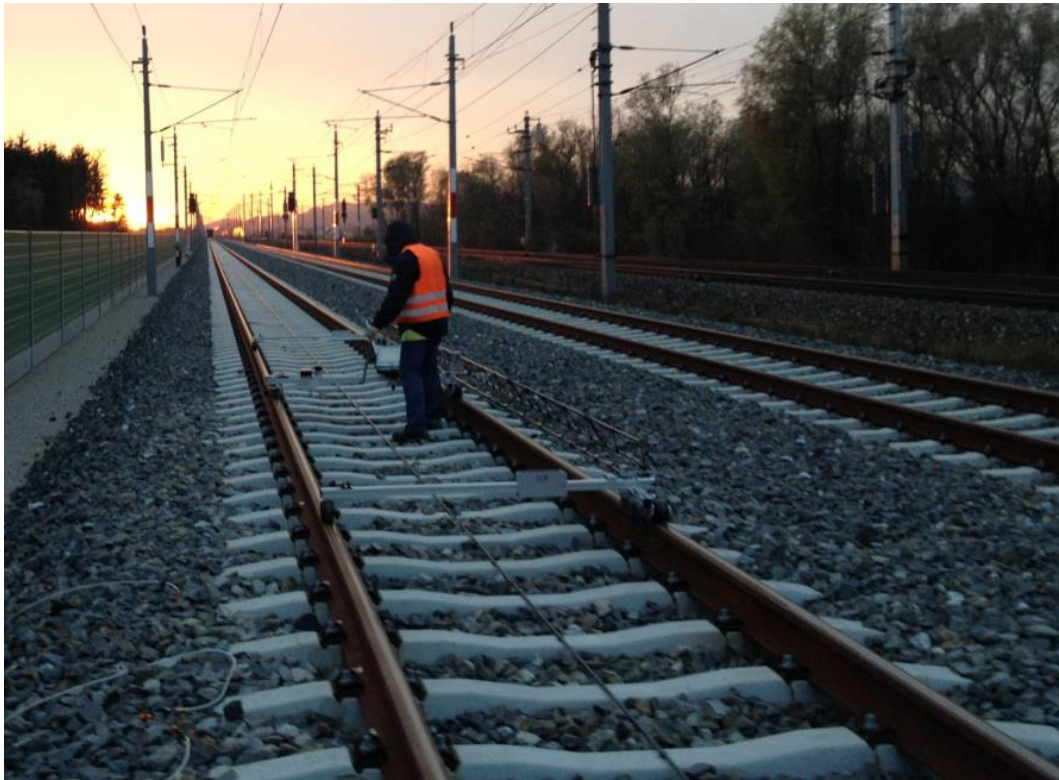
| Item | Page |
|--------------------|------|
| Annex 1 | 163 |
| Annex 2 | 164 |
| Annex 3 | 165 |
| Annex 4 | 166 |
| Annex 5 | 167 |
| Annex 6 | 168 |
| Annex 7 | 169 |
| User instruction 1 | 170 |
| User instruction 2 | 172 |
| User instruction 3 | 174 |



Pic 1: Overview of measurement section 3 (Ballasted track A-ÖBB)



Pic 2: Overview of measurement section 4 (Ballasted track with/without sub-ballast-mat A-ÖBB)



Pic 3: Recording of track geometry by track recording wagon



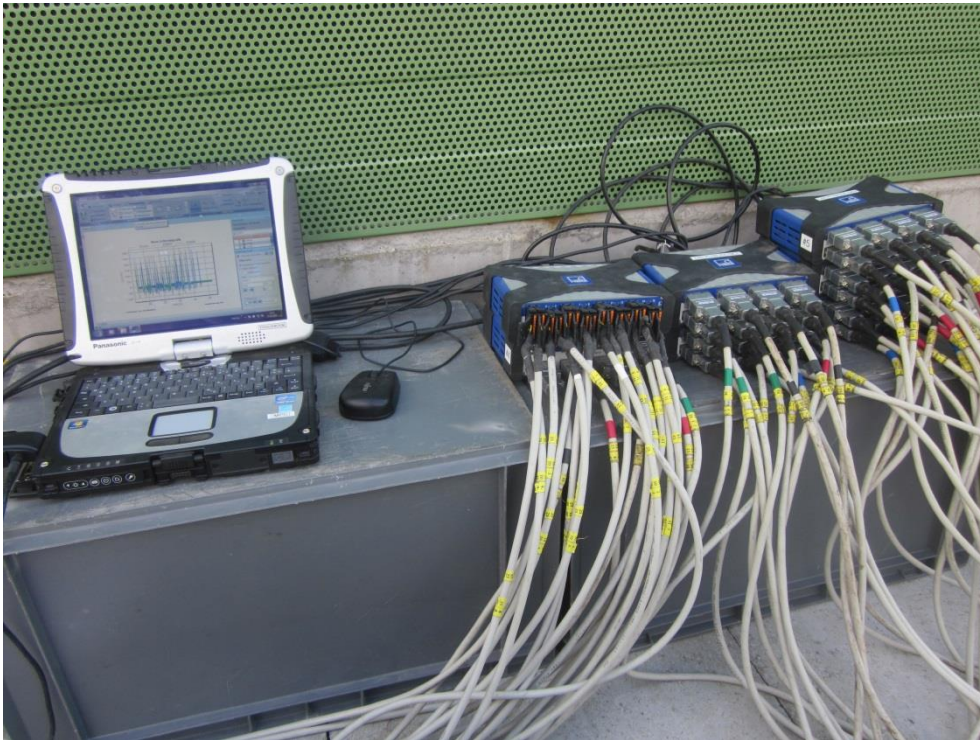
Pic 4: Ballast wagon for test of Benkelman beam and quasi-static test runs



Pic 5: Benkelman beam test for elastic rail deflection (ballastless track)



Pic 6: Installation of accelerometers



Pic 7: Synchronized measurement of rail foot strains (48 channels)



Pic 8: Protection of data amplifiers against raining



Pic 9: Built work station and data amplifiers for vibration measurement



Pic 10: Train passage in section 3 and 4 (Type Railjet)



Pic 11: Train passage in section 3 and 4 (Type freight trains)

Level compensation in section 2 due to irregular settlement

Due to the fact of local, irregular settlement of the sub-structure (here: earthworks), level compensation was done at the measurement section 2. The total height of shims used for vertical rail adjustment varies from about 6 mm up to about 16 mm, which has major consequences to the track level as well as track deflection in vertical directions. Consequently the change of track quality is not related to the performance of the slab track system but to the sub-structure performance. The figure shows the measured track deflection and geometry.

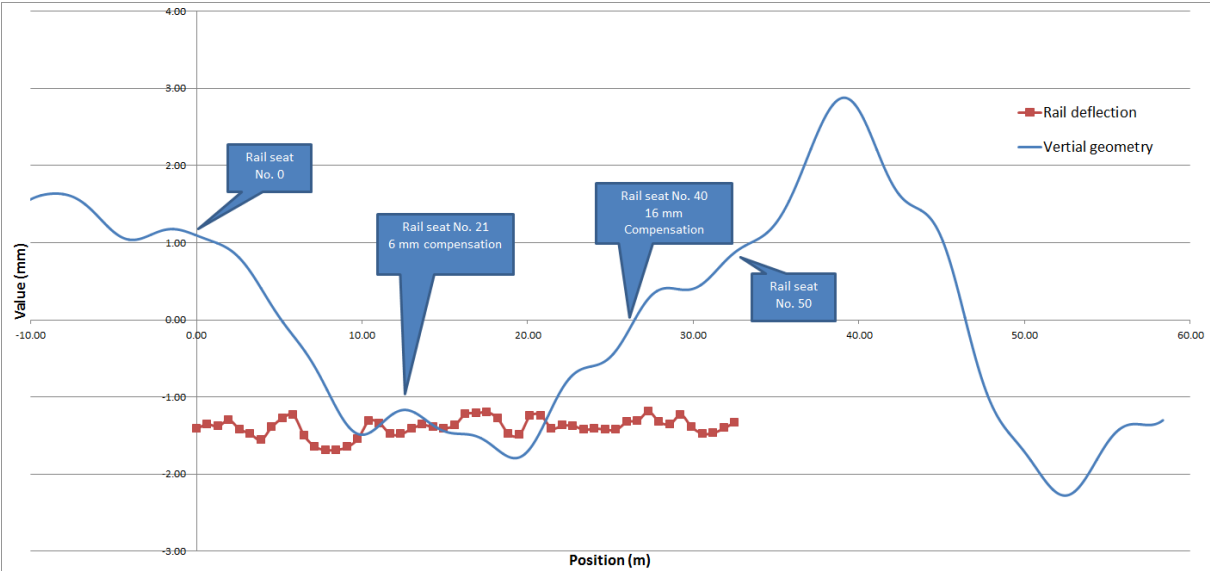
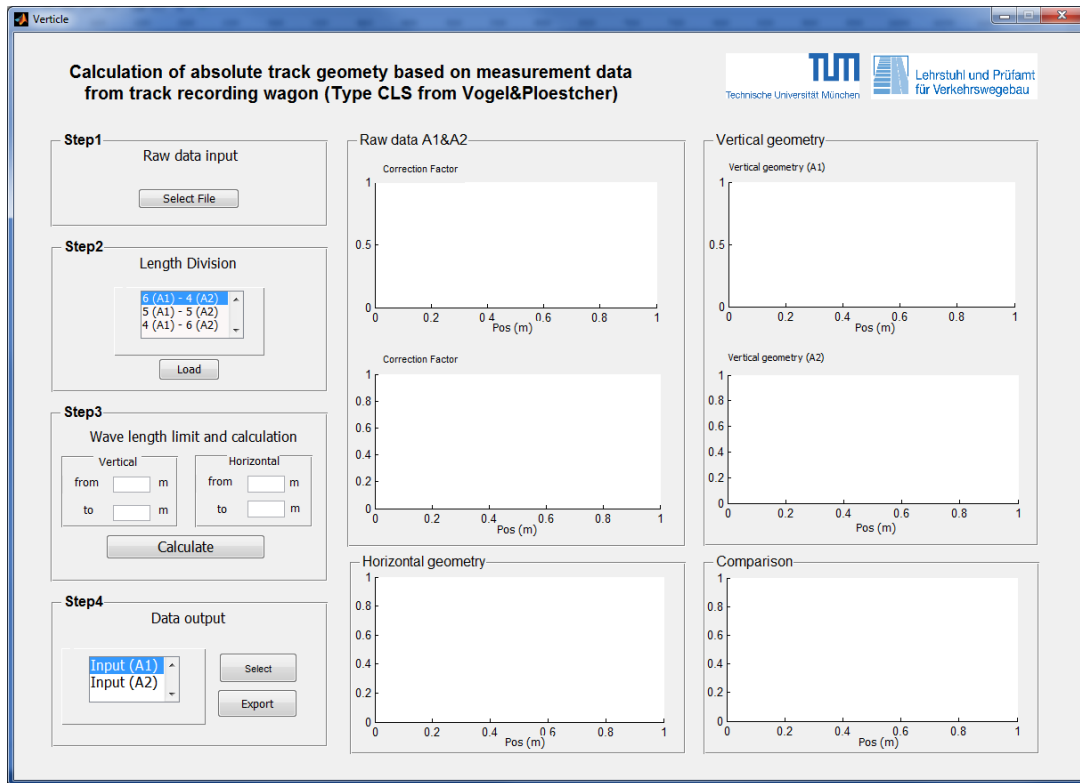


Figure: Measured maximum rail deflection and vertical track geometry (Section 2)

User Instruction 1

Calculation of absolute track geometry in vertical and horizontal direction based on measurement data from track recording wagon (Type CLS from Vogel&Ploetscher)

Specify working directory of the work; Open Matlab program and GUI window



Step 1, Adjust respect measurement results to required position and load file

| | A | B | C | D | E | F | G | H | I | J |
|----|--------------|------------|-----------|--------------------------|----------|------------|-------|------|----------|--------|
| 1 | Datei | C:\Program | Files | (x86)\VP\Data\obb11r.CLS | | | | | | |
| 2 | Gleis | Leftrail | | | | | | | | |
| 3 | Zeit | 0.36850694 | | | | | | | | |
| 4 | Datum | 22.07.2014 | | | | | | | | |
| 5 | Bediener | Liu | | | | | | | | |
| 6 | Start-KM | 0 | | | | | | | | |
| 7 | Kilometriert | 0 | | | | | | | | |
| 8 | Gleisbezug | 0 | | | | | | | | |
| 9 | | | | | | | | | | |
| 10 | | | | | | | | | | |
| 11 | | | | | | | | | | |
| 12 | 15446 | Position | Pfeilhöhe | Spur | Querhöhe | Verwindung | A1 | A2 | Gradient | Radius |
| 13 | @ | | | | | | | | | |
| 14 | 1 | 0 | -1.68 | 1436.57 | 2.88 | 0.26 | -29.5 | 30.5 | 0.546 | >5000 |
| 15 | 2 | 0.01 | -3.65 | 1436.39 | 2.75 | 0.15 | -28 | 24.4 | -1.97 | 3425 |
| 16 | 3 | 0.02 | -3.64 | 1436.38 | 3.25 | 0.75 | -28 | 24.4 | -1.97 | 3432 |
| 17 | 4 | 0.03 | -3.64 | 1436.38 | 3.62 | 1.12 | -28 | 24.4 | -1.97 | 3432 |
| 18 | 5 | 0.04 | -3.63 | 1436.38 | 3.38 | 1 | -28 | 25.3 | -1.47 | 3440 |
| 19 | 6 | 0.05 | -3.63 | 1436.38 | 2.88 | 0.38 | -28 | 25.5 | -1.37 | 3440 |
| 20 | 7 | 0.06 | -3.62 | 1436.39 | 2.5 | 0 | -28 | 26.4 | -0.874 | 3448 |
| 21 | 8 | 0.07 | -3.62 | 1436.39 | 2.75 | 0.13 | -28 | 27.5 | -0.273 | 3448 |
| 22 | 9 | 0.08 | -3.62 | 1436.39 | 2.88 | 0.16 | -28 | 27.4 | 0.270 | 3448 |

Annexes and user instructions (UI)

| Direction | Legend | In Column | Direction | Legend | In Column |
|------------|-----------|-----------|-----------|-----------|-----------|
| Position | Pos. | B | Gauge | Spurweite | D |
| Vertical | A1/A2 | G,H | Cant | Querhöhe | E |
| Horizontal | Pfeilhöhe | C | | | |

Step 2, 3, Parameter selection (Length division, Wave length for vertical and horizontal) and calculation

Step 4, Result output based on selected vertical channel (A1 or A2)

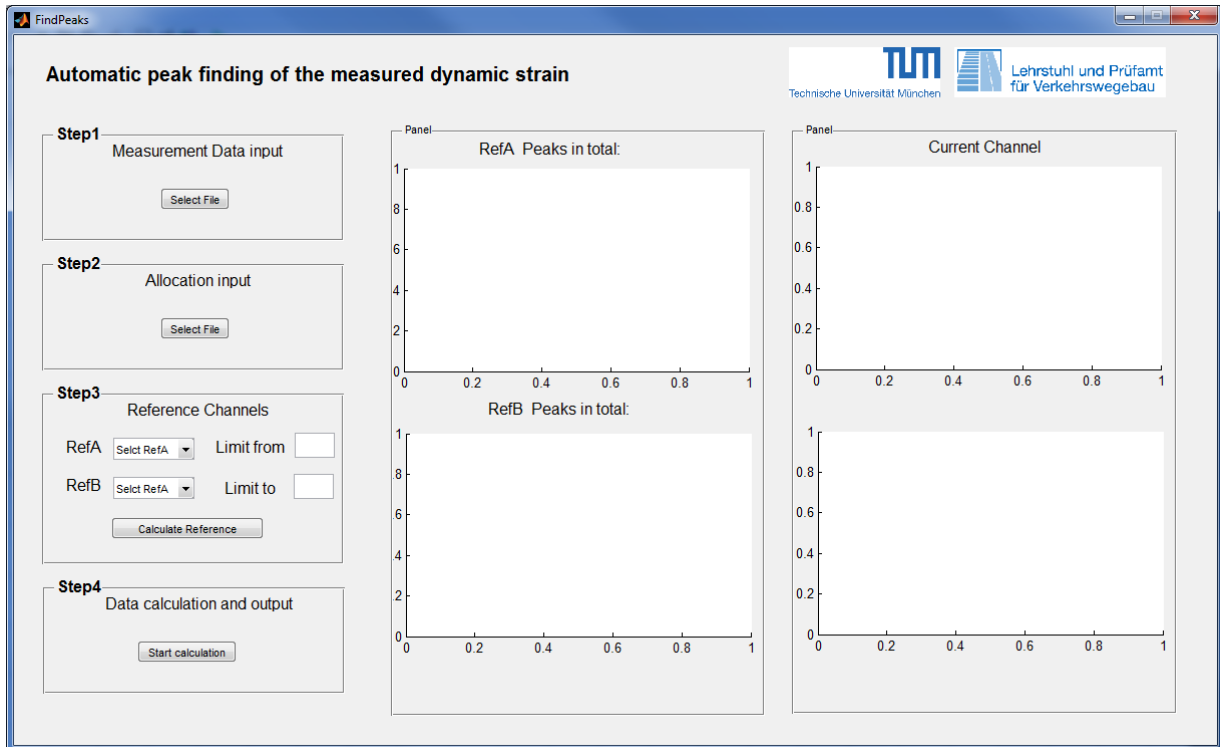
The result EXCEL sheet should be like the following (Direct importable as track geometry excitation into Simpack):

| | A | B | C | D | E |
|----|--------------------|-------------|------------|------------|---------|
| 1 | header.begin | | | | |
| 2 | data.type=1 | | | | |
| 3 | data.par(1)=1.0 | | | | |
| 4 | data.par(2)=1000.0 | | | | |
| 5 | data.par(3)=1000.0 | | | | |
| 6 | data.par(4)=1.0 | | | | |
| 7 | data.par(5)=1000.0 | | | | |
| 8 | data.par(6)=1.0 | | | | |
| 9 | header.end | | | | |
| 10 | | | | | |
| 11 | | | | | |
| 12 | | | | | |
| 13 | | | | | |
| 14 | !S | Delta-y | Delta-z | Delta-phi | Delta-g |
| 15 | 0 | 0 | 0 | 0 | 0 |
| 16 | 0.01 | -0.00025889 | 0.00678842 | 0.00191452 | -0.18 |
| 17 | 0.02 | -0.00053079 | 0.01360917 | 0.00226263 | -0.19 |
| 18 | 0.03 | -0.00081565 | 0.02041826 | 0.00252022 | -0.19 |
| 19 | 0.04 | -0.00111343 | 0.02716989 | 0.00235314 | -0.19 |
| 20 | 0.05 | -0.0014241 | 0.03381682 | 0.00200504 | -0.19 |
| 21 | 0.06 | -0.00174759 | 0.04031085 | 0.00174047 | -0.18 |
| 22 | 0.07 | -0.00208388 | 0.04660324 | 0.00191452 | -0.18 |
| 23 | 0.08 | -0.0024329 | 0.05264523 | 0.00200503 | -0.18 |
| 24 | 0.09 | -0.0027946 | 0.05838848 | 0.00191452 | -0.18 |
| 25 | 0.1 | -0.00316894 | 0.06378558 | 0.00182402 | -0.18 |
| 26 | 0.11 | -0.00355587 | 0.06879051 | 0.00174046 | -0.17 |
| 27 | 0.12 | -0.00395531 | 0.07335913 | 0.001824 | -0.17 |
| 28 | 0.13 | -0.00436723 | 0.07744961 | 0.00174046 | -0.17 |
| 29 | 0.14 | -0.00479156 | 0.08102287 | 0.00174047 | -0.18 |
| 30 | 0.15 | -0.00522823 | 0.08404302 | 0.00165693 | -0.18 |

User Instruction 2

Automatic peak finding of the measured dynamic strain with Matlab

Specify working directory of the work; Open Matlab program and GUI window



Step 1, Adjust respect measurement results to required position and load file

| Item | Legend | Position |
|--------------|-------------------|----------|
| Time | Zeit | Column A |
| Channel info | 2512 CH = 6, etc. | Row 9 |

Step 2, Load allocation file (See following screen shot for location information)

| | A | B | C | D | E | F | G | H | I |
|----|-------------|-----------|----------|-----------|------------|---------|-----------|------|------|
| 1 | 1 | 2 | 3 | 4 | 5 | 6 | 7 | 8 | 9 |
| 2 | Line number | Number | Position | DMS/Geber | Left/Right | Minimum | RS Number | | |
| 3 | | | 1 | | | | | | |
| 4 | 1 | 2510 CH=2 | 2 | 1.8 D | L | | | 8 | 3 |
| 5 | 2 | G36 CH=3 | 3 | 12.3 G | R | M | | 39 | 20.5 |
| 6 | 3 | G34 CH=4 | 4 | 12.3 G | R | M | | 3901 | 20.5 |
| 7 | 4 | G35 CH=5 | 5 | 15.3 G | R | M | | 45 | 25.5 |
| 8 | 5 | 2512 CH=6 | 6 | 19.2 D | L | | | 56 | 32 |
| 9 | 6 | 1504 CH=7 | 7 | 7.2 D | L | | | 32 | 12 |
| 10 | 7 | 2507 CH=8 | 8 | 9.6 D | L | | | 36 | 16 |
| 11 | 8 | 2509 CH=9 | 9 | 1.8 D | R | | | 7 | 3 |
| 12 | | | 10 | | | | | | |
| 13 | 9 | G07 CH=11 | 11 | 0.3 G | R | M | | 0 | 0.5 |
| 14 | 10 | G23 CH=12 | 12 | 12.3 G | R | | | 3902 | 20.5 |

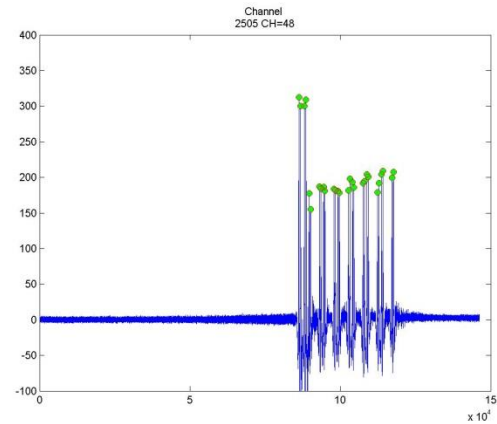
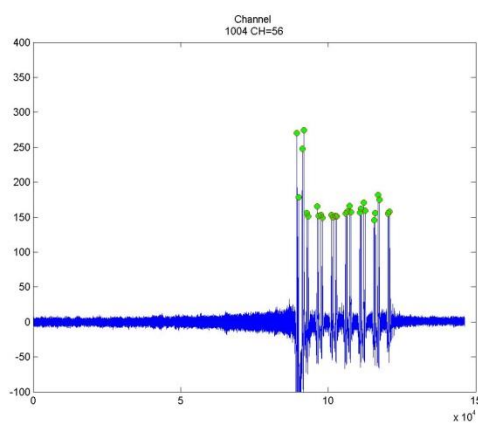
Annexes and user instructions (UI)

Step 3, Specify reference channel by drop-down window and calculation parameters;
Find the peaks for both selected reference channels

Step 4, Redo step 3 until acceptable results coming out; Find the peaks for all the rest channels based on the number and time information from the both reference channels

The result EXCEL sheet and figure outputs should be like the following:

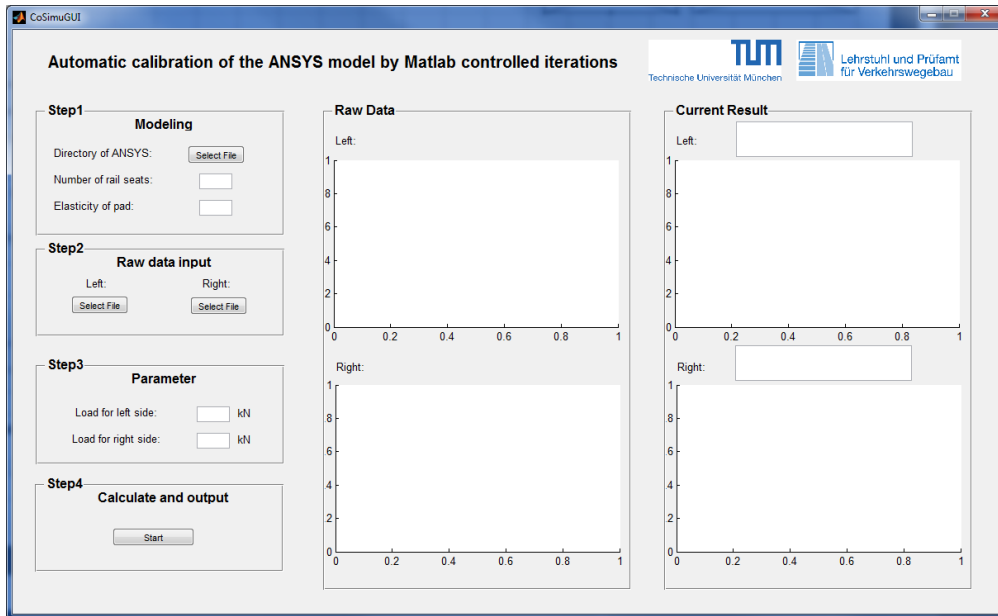
| | A | B | C | D | E | F | G | H | I | J | K | L | M | N |
|----|---|-------------|-----------|------------|------|------------|------------|------------|------------|------------|------------|------------|------------|----------|
| 1 | | 21_1216.xls | m/s | km/h | | | | | | | | | | |
| 2 | | | 52.084051 | 187.502584 | | | | | | | | | | |
| 3 | | Right Rail | | | | 1 | 2 | 3 | 4 | 5 | 6 | 7 | 8 | |
| 4 | | 25102 CH=68 | 65 | -8 | -4.8 | 253.1728 | 258.3528 | 253.4028 | 251.8528 | 151.4428 | 140.8128 | 159.3728 | 149.8228 | 151.29 |
| 5 | | 2505 CH=48 | 66 | -7 | -4.2 | 312.23607 | 300.08607 | 300.34607 | 309.16607 | 177.71607 | 155.03607 | 187.00607 | 184.43607 | 186.396 |
| 6 | | 2515 CH=51 | 67 | -6 | -3.6 | 315.52987 | 323.56987 | 310.87987 | 323.21987 | 222.71987 | 182.97987 | 199.76987 | 193.31987 | 182.239 |
| 7 | | 2501 CH=50 | 68 | -5 | -3 | 285.265446 | 276.255446 | 284.805446 | 281.025446 | 161.945446 | 159.835446 | 166.515446 | 170.805446 | 163.4554 |
| 8 | | 2509 CH=43 | 69 | -4 | -2.4 | 324.54153 | 307.41153 | 311.30153 | 307.28153 | 186.97153 | 180.36153 | 198.62153 | 184.10153 | 202.681 |
| 9 | | 2518 CH=53 | 70 | -3 | -1.8 | 325.39824 | 301.73824 | 334.70824 | 309.14824 | 175.92824 | 167.75824 | 216.86824 | 194.26824 | 196.368 |
| 10 | | 2516 CH=44 | 71 | -2 | -1.2 | 353.6312 | 188.6812 | 191.9812 | 186.2912 | 108.0512 | 101.6012 | 115.6112 | 114.1912 | 110.43 |
| 11 | | 2503 CH=39 | 72 | -1 | -0.6 | 175.567542 | 175.397542 | 172.477542 | 184.867542 | 114.257542 | 94.647542 | 92.817542 | 104.877542 | 111.8275 |
| 12 | | 2511 CH=52 | 1 | 0 | 0 | 334.51057 | 332.38057 | 339.60057 | 335.41057 | 190.39057 | 183.59057 | 203.43057 | 199.94057 | 191.960 |
| 13 | | 2502 CH=45 | 3 | 1 | 0.6 | 133.1696 | 122.0696 | 120.5296 | 108.6996 | 75.3696 | 66.1896 | 80.6296 | 71.3196 | 72.66 |
| 14 | | 25108 CH=66 | 5 | 2 | 1.2 | 0 | 400.70315 | 0 | 0 | 419.17315 | 326.02315 | 318.66315 | 390.85315 | 322.673 |
| 15 | | 2514 CH=42 | 7 | 3 | 1.8 | 0 | 335.985165 | 338.565165 | 336.765165 | 190.095165 | 181.525165 | 199.335165 | 205.505165 | 187.3051 |
| 16 | | 2517 CH=49 | 9 | 4 | 2.4 | 343.72985 | 348.22985 | 392.33985 | 344.82985 | 192.85985 | 186.08985 | 188.45985 | 195.81985 | 199.489 |



User Instruction 3

Automatic calibration of the ANSYS model by Matlab controlled iterations (Co-simulation with Matlab and ANSYS)

Specify working directory of the work; Open Matlab program and GUI window



Step 1, Specification of basic information for the co-simulation (Directory of ANSYS program, number of rail seats for calibration, pad elasticity in N/mm^2)

Step 2, Adjust respect measurement results to required position and load file (File for left and right rail being loaded separately)

| Item | Position |
|---|----------------------|
| Rail seat number | Column A |
| Max. elastic deflection | Column B |
| Elastic deflection in 0.6, 1.2, 1.8 m, etc. | Columns C, D, E, ... |

Step 3, Provision of calculation parameters (applied wheel load in measurement for left and right rail)

Step 4, Calculation and data output

The result EXCEL sheet and figure outputs should be like the following:

1, Output of max. rail deflection after each iteration step

| | A | B | C | D | E | F | G | H |
|----|---------------|------------------|-------|-------|-------|-------|-------|------|
| 1 | Rail seat No. | Iteration number | | | | | | |
| 2 | | 1 | 2 | 3 | 4 | 5 | 6 | 7 |
| 3 | 1 | 1.247 | 1.206 | 1.202 | 1.205 | 1.209 | 1.213 | 1.21 |
| 4 | 2 | 1.328 | 1.285 | 1.262 | 1.246 | 1.235 | 1.23 | 1.21 |
| 5 | 3 | 1.486 | 1.518 | 1.537 | 1.546 | 1.551 | 1.556 | 1.55 |
| 6 | 4 | 1.503 | 1.561 | 1.604 | 1.625 | 1.634 | 1.639 | 1.63 |
| 7 | 5 | 1.319 | 1.314 | 1.34 | 1.353 | 1.362 | 1.368 | 1.36 |
| 8 | 6 | 1.077 | 0.97 | 0.957 | 0.949 | 0.944 | 0.942 | 0.94 |
| 9 | 7 | 1.074 | 0.975 | 0.976 | 0.979 | 0.984 | 0.99 | 0.99 |
| 10 | 8 | 1.306 | 1.226 | 1.219 | 1.209 | 1.204 | 1.201 | 1.19 |
| 11 | 9 | 1.752 | 1.765 | 1.784 | 1.781 | 1.776 | 1.771 | 1.76 |
| 12 | 10 | 2.188 | 2.333 | 2.416 | 2.453 | 2.475 | 2.489 | 2.48 |
| 13 | 11 | 2.259 | 2.422 | 2.517 | 2.566 | 2.594 | 2.612 | 2.61 |
| 14 | 12 | 1.905 | 1.94 | 1.976 | 1.992 | 1.999 | 2.002 | 2.00 |

2, Calculated elasticity of the ballast for each rail seat (direct importable into ANSYS for Substructuring and modal analysis)

| | A | B | C | D |
|----|---|---|------|--------|
| 1 | E | | 9 = | 14.000 |
| 2 | E | | 11 = | 14.000 |
| 3 | E | | 13 = | 7.264 |
| 4 | E | | 15 = | 16.087 |
| 5 | E | | 17 = | 2.285 |
| 6 | E | | 19 = | 6.407 |
| 7 | E | | 21 = | 2.933 |
| 8 | E | | 23 = | 35.900 |
| 9 | E | | 25 = | 9.189 |
| 10 | E | | 27 = | 12.342 |
| 11 | E | | 29 = | 5.624 |
| 12 | E | | 31 = | 1.144 |
| 13 | E | | 33 = | 0.833 |
| 14 | E | | 35 = | 4.541 |
| 15 | E | | 37 = | 7.170 |

3, Overlapped results of the raw data and the calculated results from the last iteration step

